Searching optimum equation of states of neutron stars with internal magnetic fields
(内部磁場を持つ中性子星における最適な状態方程式の探索)

19DS005 Chinatsu Watanabe

Thesis for the degree of Doctor of Science

Department of Physics
Graduate school of Science and Engineering
Saitama University
Supervisor : Professor Naotaka Yoshinaga

March, 2022

Abstract

On August 17 in 2017, a gravitational wave signal from a binary neutron star spiral was observed at various wavelengths (GW170817). Now, observation of the gravitational waves together with ordinary light and X-rays from pulsars and magnetars (neutron stars with magnetic field strength of $B \sim 10^{15}$ G) are being searched for throughout the world. Gravitational waves together with electromagnetic sources have opened an era of multi-messenger astrophysics, which provides a powerful means for the precise information on neutron stars and magnetars.

Recently, neutron star PSR J1614−2230 making a binary system with a white dwarf has been discovered to have the mass of $1.97 \pm 0.04\,M_\odot$. In 2013, mass of the neutron star PSR J0348+0432 was measured as $2.01 \pm 0.04\,M_\odot$. Furthermore, in 2019, PSR J0740+6620 was observed by NICER and XMM−Newton and mass was measured as $2.072^{+0.067}_{-0.066}\,M_\odot$. Existence of neutron stars with mass around twice the solar mass has been now established. Such very heavy neutron stars give strong constraints on equations of state (EoS) for nuclear matter.

In this thesis, mass and radius of a neutron star are calculated for twelve EoSs based on the relativistic mean field (RMF) theory, and mass-radius relations (MR relations) are obtained with or without strong internal magnetic fields. For different choices of the observed constraints, we investigate which EoS is optimum in describing the structure of a neutron star.

As the first constraints for EoSs, the observed maximum mass of $2.072\,M_\odot$ (PSR J0740+6620), the upper limit radius of 13.76 km at $1.4\,M_\odot$, and radius $12.39^{+1.30}_{-0.98}$ km at $2.072\,M_\odot$ are considered. Here two EoSs with strong internal magnetic fields meet the requirements of observations. As the second constraints for EoSs, the observed masses and radii of two pulsars are considered for the following neutron stars: PSR J0030+0451 ($R = 13.02^{+1.24}_{-1.06}$ km at $M = 1.44^{+0.15}_{-0.14}\,M_\odot$) and PSR J0740+6620. Here three EoSs with strong internal magnetic fields meet the requirements of observations.

Furthermore, in this thesis, to search for a proper EoS with strong internal magnetic fields, we have made an attempt to vary the strength B_0 at the center, the strength B_s at the surface, and two other shape parameters of the internal magnetic field, which is a smooth function of the baryon number density. Consequently, mass and radius of a neutron star take various values. We investigate which EoS is optimum in the sense that mass and radius determined by a certain EoS are within the proper range of the observed masses and radii.

Contents

1 Introduction **5**
- 1.1 Neutron stars . . . 5
- 1.2 Problems concerning neutron stars . . . 6
- 1.3 What are done in this thesis . . . 7

2 Nuclear physics and nuclear matter **8**
- 2.1 Nuclear physics . . . 8
- 2.2 Nuclear matter . . . 9
- 2.3 Equation of State . . . 11
- 2.4 Neutron star with quark matter . . . 13
  - 2.4.1 MIT Bag model . . . 13

3 Observation **17**
- 3.1 Rotating Neutron Stars . . . 17
- 3.2 Magnetic fields in Neutron Star . . . 20
- 3.3 Gravitational waves . . . 21
  - 3.3.1 Gravitational wave observation . . . 21
  - 3.3.2 Gravitational waves from GW170817 . . . 22
- 3.4 Mass and Radius of Neutron star . . . 25
  - 3.4.1 Masses around 2 $M_\odot$ . . . 25
  - 3.4.2 Radius of neutron star . . . 25
  - 3.4.3 Both mass and radius observation of Neutron star . . . 29

4 Formalism **30**
- 4.1 Metric . . . 30
- 4.2 Lagrangian . . . 30
- 4.3 RMF Theory . . . 32
- 4.4 Baym-Pethick-Sutherland (BPS) EoS . . . 34
- 4.5 Tolman Oppenheimer-Volkoff equation . . . 34
- 4.6 Hartle Equations . . . 35
- 4.7 Magnetic field . . . 35
  - 4.7.1 EoS of hadronic matter with magnetic fields . . . 37
  - 4.7.2 Landau diamagnetism . . . 37

4.8 Eccentricity of neutron star . . . 38

5 Results **39**
5.1 MR relations of EoSs . . . 39
5.2 MR relation of EoS with rotation . . . 41
5.3 MR relations of EoSs with internal magnetic fields . . . 43
5.4 MR relation of EoS with rotation and magnetic fields . . . 48

6 Discussion **52**
6.1 Two-solar-mass problem . . . 52
6.2 Radius at 1.4 $M_\odot$ . . . 53
6.3 Radius at 2.072 $M_\odot$ . . . 54
6.4 Constraining masses and radii from two observed pulsars . . . 55
6.5 Comparison of the case with/without hyperons with magnetic fields . . . 56
6.6 Magnetic fields with different forms . . . 57
6.6.1 Change of α and γ in magnetic fields . . . 57
6.6.2 Searching optimum α and γ in magnetic fields for each EoS . . . 62
6.7 Particle populations of neutron star with magnetic fields . . . 68

7 Summary **72**
7.1 Searching EoS in rotating magnetized neutron star . . . 72
7.2 Searching α and γ of magnetic fields . . . 73
7.3 Summary of summary . . . 73

Appendices **83**

A Relativistic mean field **84**
A.1 RMF without and with magnetic fields . . . 84

B Landau level **88**
B.1 Zero temperature . . . 88
B.2 BPS with magnetic fields . . . 89

C TOV equation **91**
C.1 Derivation of TOV equation . . . 91

D Units **94**
D.1 Gravitational unit and Natural unit . . . 94
D.1.1 Gravitational unit . . . 94
D.1.2 Natural unit . . . 95

E Hartle equations **96**

F Energy levels in a strong magnetic field **100**

G Original results by changing α and γ for neutron star with magnetic fields ($B_s = 10^{12}$ G) 103

H Original resutls by changing α and γ for neutron star with magnetic fields ($B_s = 10^{15}$ G) 128

Chapter 1

Introduction

The neutron star is one of the possible evolutionary end points of massive stars. In this chapter, we take a brief look at a neutron star, for which we now know how it was discovered and how the internal structure looks like to some extent.

1.1 Neutron stars

A pulsar that emits radio waves periodically was observed in 1967 by a graduate student, Susan Jocelyn Bell Burnell and her supervisor Antony Hewish. The pulsar is thought to be a remnant of a supernova explosion at the evolutionary end point of a massive star. It is thought to be a star almost made of neutrons, making highest-density material observed in space. It has the typical mass of 1.4 times the solar mass ($M_\odot$) and the maximum mass is around $2\,M_\odot$, but its radius is very small, from 10 to 15 km. Therefore, central density becomes highest to reach several times of the nuclear saturation density. The shortest rotational period is as short as 1ms. The details of the internal structure are yet mysterious, although the surface of a neutron star is composed of neutron rich nuclei and electrons. It is thought that nuclei begin melting as one goes inside and a uniform substance is formed in terms of baryons and leptons. We can consider a neutron star as a huge atomic nucleus with radius about 10 km. Thus, knowledge of nuclear physics is indispensable in understanding a neutron star.

Recently the possibility is suggested that R-process elements (elements synthesized in the process of capturing neutrons rapidly) such as gold, platinum, rare earth, etc. were created during the merger of neutron stars [1]. It has been found that R-process elements can be explained without contradiction if they were created at the time of coalescence of neutron stars.

In 2015, gravitational waves were observed for the very first time by LIGO collaboration [2]. LIGO is abbreviation of Laser Interferometer Gravitational-Wave Observatory. These gravitational waves were produced by the merger of two black holes and the event was named as GW150914. In August 2017, for the first time, gravitational waves and simultaneously various wavelengths of light are observed from the same event, namely, a merger of two neutron stars, GW170817 [3, 4]. This observation marks the beginnings

of 'multi-messenger astronomy'. In this event, R-process elements such as gold was produced [1]. Now, researchers start working on understanding fundamental physics of neutron star interiors with the merger of two neutron stars.

The possible range of values for mass and radius of a neutron star has been one of the main themes in the study of neutron stars since their discovery. In 1933, Fritz Zwicky and Walter Baade proposed the model that neutron stars are made by a supernova explosion [5]. In 1939, Oppenheimer and Volkoff (and, independently, Tolman) applied the Einstein equation to a neutron star and calculated numerically its mass in a non-interacting, strongly degenerate relativistic gas of neutrons. They calculated its mass to show that stable static neutron stars have a maximum mass of $M_{max} \sim 0.71 M_{\odot}$; the so-called the Oppenheimer-Volkoff mass limit. A star was believed to become a black hole when it surpasses this limit.

Cameron showed that the inclusion of the nuclear force can considerably stiffen the equation of state (EoS) [6]. This inclusion can increase the maximum mass of the Oppenheimer-Volkoff limit to about $2\,M_{\odot}$. The Brueckner–Bethe–Goldstone (BBG) theory, formulated in 1954–1965, is a successful application of field-theoretical methods to strongly interacting many-body systems. Strong repulsive nuclear forces (two- or three-body) have been found to be necessary to explain maximum masses of neutron stars within the nucleon's degrees of freedom. Recently, some advanced studies use microscopic EoSs based on the Brueckner–Hartree–Fock (BHF) many-body theory with realistic two- or three-body nucleonic forces [7, 8] and also those EoSs based on lowest order constrained variational (LOCV) many-body theory [9].

1.2 Problems concerning neutron stars

Discoveries of neutron stars with masses around twice the solar mass have made a strong impact on nuclear physics community, who had once believed that the maximum mass of a neutron star should not exceed 1.56 $M_{\odot}$ [10, 11]. Indeed, neutron stars with around $2M_{\odot}$ have been confirmed since 2010. The neutron star PSR J1614-2230 has the observed mass of $1.97 \pm 0.04\,M_{\odot}$ [12] and the NS PSR J0348+0432 has mass of $2.01 \pm 0.04\,M_{\odot}$ [13]. Moreover, mass of the millisecond-pulsar (MSP) J0740+6620 was measured to be $2.14^{+0.10}_{-0.09}$ $M_{\odot}$ in 2019 [14], and with additional observation with the XMM-Newton, a more exact value $2.072^{+0.067}_{-0.066}\,M_{\odot}$ was determined in 2021 [15]. If neutron star matter consists of only nucleons with strong two or three body repulsive forces, massive neutron stars more than $2M_{\odot}$ can be easily described. However, hyperons are energetically favorable when the baryon chemical potential is large enough in the inner core of a neutron star. This leads to a reduction of the Fermi pressure to soften the EoS and to a reduction of the predicted maximum mass less than $2M_{\odot}$. This is called the hyperon puzzle. Since discoveries of massive neutron stars, many people have searched for the optimal EoSs that can achieve masses over twice the solar mass.

There are some characteristic neutron stars: millisecond-pulsar which has a short rotational period of less than 10 milliseconds, and magnetar that has a powerful magnetic field on its surface. As a part of external conditions to support over the $2M_{\odot}$, the

extremely rapid rotation and powerful magnetic field should be considered in the EoS study. In our recent study [16], EoSs for the rapid rotational neutron star with some deformation and with the internal magnetic field have been investigated. Although an unrealistic rotational frequency can modify the neutron star mass from $1.89M_\odot$ to $2M_\odot$, rotational effects on the mass increase are not significant for the realistic frequency range of the observed millisecond-pulsars.

Neutron stars that have strong magnetic fields on the surface, are called magnetars. Recently, up to 30 magnetars have been observed [17, 18]. Maximumly, about 10^{15} G of the magnetic field on the surface has been found by the observation [17], but we do not yet know the generation mechanism of the strong magnetic fields where and how they come from.

Another constraint on the EoS comes from the NS radius. From the observation of the GW170817 gravitational wave event, the upper limit radius is 13.6 km [19] at the mass of $M = 1.4\,M_\odot$. Moreover, another reports the upper limit radius 13.76 km [20] at $M = 1.4\,M_\odot$. The lower limit radius was reported as $10.68^{+0.15}_{-0.04}$ km [21] at $M = 1.6\,M_\odot$. From the observations by NICER for PSR J0030+0451, mass and radius was measured to be $13.02^{+1.24}_{-1.06}$ km at $M = 1.44^{+0.15}_{-0.14}\,M_\odot$ [22]. Also, the radius and mass of the pulsar PSR J0740 + 6620 observed by NICER and XMM-Newton is $12.39^{+1.30}_{-0.98}$ at $M = 2.072^{+0.067}_{-0.066}\ M_\odot$ [15].

1.3 What are done in this thesis

In this thesis, we use the relativistic mean field (RMF) theory including hyperons, which provide us with 12 different EoSs [23, 24, 25, 26, 27] depending on the different coupling constants between baryons and mesons.

We will deal with the topics as follows. First, as will be given in Sect. 5, we show the results of MR-relations in 4 different cases: (1) MR-relation of 12 EoSs, (2) with rotation, (3) with magnetic field, (4) with rotation and magnetic field.

Next, as in Sect. 6, we discuss MR-relations by considering maximum masses of neutron stars, upper limits of radius at 1.4 $M_\odot$, and radius at 2.072 $M_\odot$, which are the constraints from observation. We also consider another constraint, the observed masses and radii of two pulsars, PSR J0030 + 0451 and PSR J0740 + 6620 within 1 σ error.

Finally, we discuss the internal structure and mass and radius relation (MR-relation) of a neutron star including hyperons by changing the form of the magnetic fields.

This thesis is organized as follows. In Section 2, nuclear physics and matter is given. The details of observations are given in Section 3. The formulation of the calculation is given in Section 4, and the results and discussions are given in Section 5 and Section 6, respectively. Finally, summary is given in Section 7.

Chapter 2

Nuclear physics and nuclear matter

2.1 Nuclear physics

Our universe consists of various elements from hydrogen to uranium. An element was made by a nuclear reaction in a process of the evolution of universe. For example, the generation of carbon, the important element for a living creature, was enabled by exquisite balance of the nucleus structure. In this way, the nucleus is a main component of the universe. The radius of nucleus is about a few fm (fm=10^{-15} m) and it has a number of protons and neutrons (collectively called the nucleon). A nucleon is united with 'nuclear force', one of the strong interactions. From the lightest nucleus, hydrogen (1 proton) to uranium nucleus, which the atomic number (= proton number Z) is 92, about 270 kinds of stable nuclei exist. Among nuclides, there are short life unstable nuclides, which do not exist in nature. Theoretically, about 6,000 unstable nuclides are said to exist, but at present only about 3,000 have been identified experimentally.

Study of unstable nucleus has advanced by the progress of the recent accelerator technology rapidly. An interesting phenomenon is found to turn over common concepts of the conventional nuclear physics, such as abnormality of the magic numbers and halo nuclei. For most unstable nuclides, they conceivably exist in the combustion process of the star, particularly in a supernova explosion or a binary neutron star merger. This gives one of the keys to understand a nucleosynthesis process of the universe. It is important in understanding the high-density object "neutron star", which is said to be a huge atomic nucleus.

2.2 Nuclear matter

The binding energy of a nucleus with mass $A(= N + Z)$ is given by

$$\begin{aligned} B(A,Z) &\equiv Zm_p + (A-Z)m_n - M(A,Z) \\ &= a_{vol}A - a_{surf}A^{2/3} - a_{coul}\frac{Z^2}{A^{1/3}} - a_{sym}\frac{(N-Z)^2}{A} + \delta(A). \end{aligned} \tag{2.1}$$

This equation is based on the liquid-drop model of nuclei, called Bethe-Weizsäcker formula. In the right-hand side of Eq. (2.1), the first term is called volume energy and shows the condensation energy of the liquid-drop. The second term is called surface energy and shows the surface tension of liquid-drop. The third term is the Coulomb energy by the proton in the atomic nucleus, and it is provided by supposing that electric charge Ze is distributed over the nucleus inside the radius R uniformly. The fourth term is called symmetric energy and to expresses the isospin symmetry of the nucleon. The fifth term comes from the pairing interaction and is given from experiment as follows,

$$\delta(A) = \begin{cases} \Delta = \frac{12}{\sqrt{A}}\ \text{MeV} & (\text{even} - \text{even}) \\ 0 & (\text{odd}) \\ -\Delta = -\frac{12}{\sqrt{A}}\ \text{MeV} & (\text{odd} - \text{odd}) \quad . \end{cases} \tag{2.2}$$

The coefficient of each term in equation (2.1) is fitted to experimental binding energies, and the adopted coefficients are given in Table 2.1.

Table 2.1: The coefficients in Bethe-Weizsäcker formula [28].

a_{vol} (MeV)	a_{surf}(MeV)	a_{coul}(MeV)	a_{sym}(MeV)
16.2	19.0	0.76	23.5

Here the formula is adapted to nuclear matter, where mass number A becomes infinity in nuclear matter. We can ignore the contributions except the volume energy and the symmetry energy. Then the binding energy per nucleon for the symmetric matter ($N = Z$) is constant,

$$B(A,Z)/A = a_{vol} = 16.2\ \text{MeV}. \tag{2.3}$$

Moreover, for the stable atomic nucleus, the approximate radius is

$$\begin{aligned} R &= r_0 A^{1/3}, \\ r_0 &= 1.16\ \text{fm}. \end{aligned} \tag{2.4}$$

If we assume a nucleus to be spherical, the number density of the nucleus is given as follows.

$$\rho = \frac{A}{\frac{4}{3}\pi R^3} = 0.153\ \text{nucleons fm}^{-3}. \tag{2.5}$$

As shown from this equation, the nucleon number density of finite nuclei is approximately constant irrespective of the mass number. We call this property the density saturation.

Neutron star matter has to be neutral electrically. This shows that neutron star matter is a pure neutron matter in the first approximation. The energy per nucleon is given by

$$\frac{\varepsilon}{\rho} = \frac{M}{A} = m_n\, a_{vol} + a_{sym}\left(\frac{\rho_n - \rho_p}{\rho}\right)^2. \tag{2.6}$$

Therefore, taking $t = (\rho_n - \rho_p)/\rho$, the symmetric energy coefficient a_{sym} is

$$a_{sym} = \frac{1}{2}\left(\frac{\partial^2}{\partial t^2}\frac{\varepsilon}{\rho}\right)_{\rho=\rho_0}. \tag{2.7}$$

Incompressibility K is one of the important quantities which express the behavior of the equation of state at high density, and defined as follows.

$$K = \left[k^2\frac{d^2}{dk^2}\left(\frac{\varepsilon}{\rho}\right)\right]_{k=k_F} = 9\left[\rho^2\frac{d^2}{d\rho^2}\left(\frac{\varepsilon}{\rho}\right)\right]_{\rho=\rho_0}. \tag{2.8}$$

As shown from this equation, incompressibility is a quantity to express curvature of the energy of the nuclear matter at the saturation density. This value does not influence an equation of state at the normal density, but becomes influential at high density, and the equation of state gets stiffer as the value gets larger.

Nucleon effective mass m^* of saturation density is also one of the important quantities of high density nuclear matter, and from neutron scattering off the ^{208}Pb nucleus, following value is suggested,

$$m_S^*/m = 0.76 \text{ to } 0.82. \tag{2.9}$$

However, this m_S^* is non-relativistic effective mass and is given by the relations with Landau effective mass m_L^* and Dirac effective mass m^* as follows.

$$\begin{aligned} m_S^* \simeq m_L^* &= \left.\frac{k}{\partial\varepsilon(k)/\partial k}\right|_{k=k_F}, \\ &= \sqrt{m^{*2} + k_F^2}. \end{aligned} \tag{2.10}$$

From equation (2.10), Dirac effective mass is,

$$m^*/m \simeq 0.7 \text{ to } 0.8. \tag{2.11}$$

Slope parameter L and curvature of the nuclear symmetry energy K_{sym} characterize the density dependence of the nuclear symmetry energy around normal nuclear matter density and thus provide important information on the properties of nuclear symmetry energy at both high and low densities.

An isospin asymmetry δ and density ρ, for neutron-rich nucleonic matter of neutron density (ρ_n) and proton density (ρ_p), can be given as

$$\delta = \frac{\rho_n - \rho_p}{\rho}, \tag{2.12}$$

$$\rho = \rho_n + \rho_p. \tag{2.13}$$

Its EoS can be written as [29]

$$E(\rho, \delta) = E_0(\rho) + E_{sym}(\rho)\delta^2 + O(\delta^4) \tag{2.14}$$

in terms of the energy per nucleon $E_0(\rho) \equiv E(\rho, \delta = 0)$ in symmetric nuclear matter and the nuclear symmetry energy $E_{sym}(\rho)$ at nuclear density ρ. For a given EoS $E(\rho, \delta)$ from a nuclear many-body theory, it is customary to Taylor expand both the $E_0(\rho)$ and $E_{sym}(\rho)$ as functions of

$$\frac{\rho - \rho_0}{3\rho_0}, \tag{2.15}$$

with coefficients given by their density derivatives at the nuclear matter saturation density ρ_0 [30].

$E_{sym}(\rho)$ at ρ can be expanded around ρ_0 as [31]

$$E_{sym}(\rho) = E_{sym}(\rho_0) + L\left(\frac{\rho - \rho_0}{3\rho_0}\right) + \frac{K_{sym}}{2}\left(\frac{\rho - \rho_0}{3\rho_0}\right)^2, \tag{2.16}$$

where L and K_{sym} are the slope parameter and curvature of the nuclear symmetry energy at ρ_0. The first term of Eq. (2.16), $E_{sym}(\rho_0)$, is equal to a_{sym}. L and K_{sym} can be written as

$$L = 3\rho_0 \left.\frac{\partial E_{sym}(\rho)}{\partial \rho}\right|_{\rho=\rho_0}, \tag{2.17}$$

$$K_{sym} = 9\rho_0^2 \left.\frac{\partial^2 E_{sym}(\rho)}{\partial^2 \rho}\right|_{\rho=\rho_0}. \tag{2.18}$$

As for J, it is the same as

$$J = a_{sym} = E_{sym}(\rho_0). \tag{2.19}$$

2.3 Equation of State

There are various equations of state (EoSs) describing the internal structure of neutron stars. Figure 2.1 shows one example of mass-radius relations (MR relations) for non-rotating mass versus physical radius using various kinds of EoSs [12]. As for the blue solid lines, EoSs are described only by nucleons, by nucleons and also hyperons in pink, and by strange quark matter in green. The horizontal bands show the observed mass

of PSR J1614−2230 ($1.97 \pm 0.04\, M_{\odot}$), similar measurements for two other millisecond pulsars and, the range of observed masses for double-neutron-star binaries.

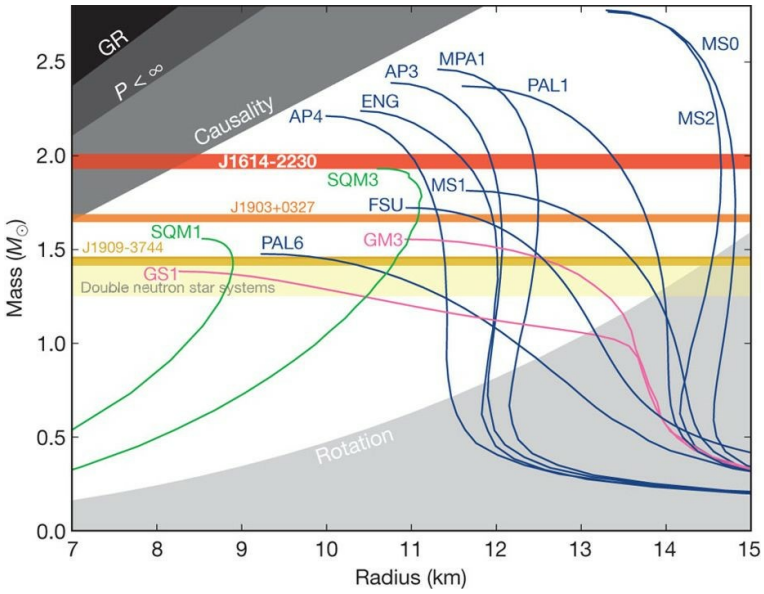

Figure 2.1: MR-relations using various kinds of EoSs [12].

For some other examples of EoSs, their basic properties and characteristics of the models in relativistic mean field theory are shown in Table 2.2 and 2.3.

The characteristics of each EoS is shown in Table 2.3. GM1 and GM3 EoSs have a non-linear self-interaction of σ mesons, which was made in 2000. TM1 EoS was made in 1994, oldest here, contains self-interacting terms for both σ and ω mesons. TM2-$\omega\rho$ EoS was made in 2017, which is stiffer than TM1 EoS and nonlinear ω, ρ term is added. NL3 EoS has non-linear self-interaction of σ mesons, which was made in 1997. NL3$\omega\rho$ EoS is containing self-interaction of σ mesons and coupling between ω and ρ mesons, which was made in 2001. DDME2 EoS, which was made in 2005, has the coupling parameters which are density dependent.

Table 2.2: Properties of various EoSs

EoS	B/A (MeV)	ρ (fm^{-3})	a_{sym} (MeV)	K (MeV)	m^*/m
GM1 [23, 24]	−16.3	0.153	32.5	300	0.70
GM3 [23, 24]	−16.3	0.153	32.5	240	0.76
TM1 [25]	−16.3	0.146	36.9	281.2	0.634
TM2-$\omega\rho$ [25]	−16.4	0.146	32.1	281.7	0.63
NL3 [26]	−16.299	0.148	37.4	271.76	0.60
NL3$\omega\rho$ [26]	−16.280	0.149	37.7	272.15	0.59
DDME2 [27]	−16.14	0.152	32.3	250.89	0.572

Table 2.3: EoS characteristics.

EoS	characteristics
GM1,GM3	Non-linear self-interaction of σ-mesons.
TM1	Self-interacting terms for both σ and ω mesons.
TM2-$\omega\rho$	Stiffer than TM1, plus nonlinear ω, ρ term.
NL3	Non-linear self-interaction of σ-mesons.
NL3$\omega\rho$	Containing self-interaction of σ mesons and coupling between ω and ρ mesons.
DDME2	Coupling parameters are density dependent.

2.4 Neutron star with quark matter

There may be such a neutron star containing quark matter. If there is a neutron star with only quark matter, it will be a quark star. The quark star is an object made of quark matter. The hypothesis about the quark star was first given by Soviet physicists, D. D. Ivanenko and D. F. Kurdgelaidze [32] in 1965.

The existence of a quark star was confirmed neither theoretically nor astronomically. Like the transition temperature between the hadron substance and the quark substance, the EoS of the quark substance is uncertain. Theoretical uncertainty precludes making predictions from the first principle. Experimentally, the properties of the quark substance are actively studied in the particle collision type accelerator, and it is the size of the nucleus that can produce hot quark-gluon plasma matter.

2.4.1 MIT Bag model

MIT bag model is used to obtain an equation of state commonly used to describe a quark star. MIT bag model is one of the models describing the properties of hadrons, which was proposed in 1974 by a group of researchers in the MIT (Massachusetts Institute of Technology).

The Lagrangian density for the bag is written as [33]

$$\mathcal{L} = \left[\frac{i}{2}\left(\overline{\psi}\gamma^{\mu}\partial_{\mu}\psi - (\partial_{\mu}\overline{\psi})\gamma^{\mu}\psi\right) - B\right]\theta_v(x) - \frac{1}{2}\overline{\psi}(x)\psi(x)\Delta_s, \tag{2.20}$$

where Δ_s is the surface delta-function, B is the bag constant. In the static spherical case, one has,

$$\theta_v = \theta(R-r), \quad \Delta_s = \delta(R-r). \tag{2.21}$$

The energy density, the pressure, and the quark density are given by [34]

$$\mathcal{E} = 3\times 2\sum_{q=u,d,s}\int \frac{d^3p}{(2\pi)^3}\sqrt{\mathrm{p}^2+{m_q}^2}(f_{q+}+f_{q-}) + B, \tag{2.22}$$

$$P = \frac{1}{\pi^2}\sum_q \int d^3p \frac{p^4}{\sqrt{p^2+{m_q}^2}}(f_{q+}+f_{q-}) - B, \tag{2.23}$$

$$\rho_q = 3\times 2\int \frac{d^3p}{(2\pi)^3}(f_{q+}-f_{q-}), \tag{2.24}$$

where 3 stands for the number of colors, and 2 for the spin degeneracy, and m_q for the quark masses. B represents the bag pressure and the distribution functions for the quarks and antiquarks are the Fermi distributions

$$f_{q\pm} = \left\{1+\exp[(\epsilon \mp \mu_q)/T]\right\}^{-1}, \tag{2.25}$$

with μ_q being the chemical potential for quarks and antiquarks of type q and

$$\epsilon = \sqrt{p^2+m_q^2}. \tag{2.26}$$

Quark EoS with strong magnetic fields

For a description of the magnetized quark matter, we adopt the MIT bag model [35]. NSs in the quark matter in the MIT bag model was studied in Ref. [36, 37].

In this work u, d, s quarks and electrons (e) are introduced. The effective mass $\bar{m}_i$ of a relativistic free charged particle of mass m_i and charge q_i ($i = u, d, s, e$) in the constant magnetic field with strength B can be written as

$$\bar{m}_i = \sqrt{m_i^2 + 2\nu\,|q_i|\,B} - s\kappa_i B. \tag{2.27}$$

Here $\nu = n + \frac{1}{2} - \mathrm{sqn}\,(q)\,\frac{s}{2}$ where $n = 0, 1, 2, \ldots$. Here κ_i is the anomalous magnetic moment (AMM) with spin s ($s = \pm 1$). For a positive charged particle, one starts from

$\nu = 1$ in the spin down ($s = -1$) case. For a negative charged particle, one starts from $\nu = 1$ in the spin up ($s = 1$) case. Here ν can take the maximum value

$$\nu^i_{\max} = \left[\frac{(\mu_i + s\kappa_i B)^2 - m_i^2}{2\,|q_i|\,B} \right], \tag{2.28}$$

where μ_i is the chemical potential of each particle and [ ] is the floor function.

The relation between Fermi momentum $k^i_{F,\nu}$ and the chemical potential μ_i can be given as

$$k^i_{F,\nu} = \sqrt{(\mu_i)^2 - \bar{m}_i^2}. \tag{2.29}$$

The thermodynamic potential for each particle at zero temperature is

$$\Omega_i = -\sum_{s=-1}^{+1} \sum_{\nu}^{\nu^i_{\max}} \frac{g_i\,|q_i|\,B}{4\pi^2} \left\{ \mu_i k^i_{F,\nu} - \bar{m}_i^2 \ln\left(\frac{\mu_i + k^i_{F,\nu}}{\bar{m}_i} \right) \right\}. \tag{2.30}$$

Here $g_i = 3$ for quarks and $g_i = 1$ for electrons. The total thermodynamic potential is

$$\Omega = \sum_{i=u,d,s,e} \Omega_i. \tag{2.31}$$

The total energy density ε can be given with a Bag constant B_{Bag} as,

$$\varepsilon = \Omega + \sum_{i=u,d,s,e} \mu_i \rho_i + \frac{B^2}{2} + B_{Bag}, \tag{2.32}$$

where the number density ρ_i for each particle is

$$\rho_i = \frac{g_i\,|q_i|\,B}{2\pi^2} \sum_{s=-1}^{+1} \sum_{\nu}^{\nu^i_{\max}} k^i_{F,\nu}. \tag{2.33}$$

Then quark EoS is obtained by imposing neutrality condition and beta stability condition for a fixed baryon number density ρ_B.

The neutrality and the beta stability conditions are

$$\frac{2}{3}\rho_u = \frac{1}{3}\rho_d + \frac{1}{3}\rho_s + \rho_e, \tag{2.34}$$

$$\mu_u + \mu_e = \mu_d = \mu_s. \tag{2.35}$$

The pressures of parallel and perpendicular to the magnetic fields are respectively given as

$$\begin{aligned} P_{\parallel} &= -\Omega - \frac{B^2}{2} - B_{Bag} \\ &= \sum_{i=u,d,s,e} \mu_i \rho_i - \varepsilon, \end{aligned} \tag{2.36}$$

and

$$\begin{aligned} P_{\perp} &= -\Omega - MB + \frac{B^2}{2} - B_{Bag} \\ &= \sum_{i=u,d,s,e} \mu_i \rho_i - \varepsilon + B^2 - MB. \end{aligned} \tag{2.37}$$

Here magnetization M is

$$M = -\frac{\partial \Omega}{\partial B} = \sum_{i=u,d,s,e} M_i \tag{2.38}$$

with

$$M_i = -\frac{\partial \Omega_i}{\partial B}. \tag{2.39}$$

In this work $P_{\perp}$ is considered as pressure for the EoS because we assume the spherically symmetric magnetic pressure. For the AMM, we take $\kappa_e = 0.00116\ \mu_B$, $\kappa_u = 1.85\ \mu_N$, $\kappa_d = -0.97\ \mu_N$, $\kappa_s = -0.58\ \mu_N$, where μ_N is the nuclear magneton and μ_B, Bohr magneton.

Chapter 3

Observation

3.1 Rotating Neutron Stars

Pulsars are rotating neutron stars. The pulsar is an object that radiates periodic pulses of the electromagnetic waves such as radio and X-rays. To have a short period, the star is expected to rotate at a very high frequency. The motion of a surface particle with mass m satisfies the following equation, assuming the surface speed v of the rotating object m on the surface of rigid material of mass M and radius R,

$$m\frac{v^2}{R} = \frac{GmM}{R^2}. \tag{3.1}$$

Here,

$$v = \sqrt{\frac{GM}{R}}, \tag{3.2}$$

where the maximum velocity in equation (3.2) is called Kepler velocity, and the matter cannot stay on the star if it rotates much faster than this velocity. Then, period P is

$$P = \frac{2\pi R}{v} = 2\pi\sqrt{\frac{R^3}{GM}}. \tag{3.3}$$

Here, mass M is

$$M = \frac{4\pi}{3}R^3\rho, \tag{3.4}$$

and substituting this into the equation (3.3),

$$P = 2\pi\sqrt{\frac{R^3}{G}\frac{3}{4\pi R^3\rho}} = \sqrt{\frac{3\pi}{G\rho}} = 1.2\,\mathrm{ms}\left(\frac{10^{14}\,\mathrm{g/cm^3}}{\rho}\right)^{1/2}, \tag{3.5}$$

where ρ is the average density.

If the rotating period of the object is 1 ms,

$$\begin{aligned}\rho &= 1.2^2 \mathrm{ms}^2 \times 10^{14}\,\mathrm{g/cm}^3 \times \frac{1}{1^2 \mathrm{ms}^2} \\ &= 1.44 \times 10^{14}\,\mathrm{g/cm}^3. \end{aligned} \tag{3.6}$$

Therefore, average density of 1 ms periodic object becomes about the nuclear matter density ($\rho_0 \sim 10^{14}$ g/cm^3). Thus pulsar is thought to be a neutron star.

For pulsars, Figure 3.1 shows the measurements of neutron star masses [38]. The dots show double neutron stars (magenta), recycled pulsars (gold), bursters (purple), and slow pulsars (cyan). It is seen from this Figure, masses of pulsars have a broad range, namely from ≈ 1.1 to $2M_\odot$. Also from Figure 3.2, it is found that the top population of masses is around 1.4 $M_\odot$.

Up to now, about 3300 pulsars have been observed [39]. The largest measured rotational frequency is 716 Hz [40].

If we define the angular velocity Ω, velocity of rotation v (Kepler velocity), and orbital radius R, the relation is $\Omega = v/R$. We can say that from this equation, velocity v will not be higher than the limit of Kepler velocity $v = c$ (c is the speed of light), therefore,

$$\Omega \leqq \frac{c}{R} = \frac{3 \times 10^5\,(\mathrm{km/s})}{10\,(\mathrm{km})} = 3 \times 10^4\,(\mathrm{Hz}), \tag{3.7}$$

assuming the radius of neutron star as 10 km. Accordingly, the upper limit of Ω is 3×10^4 Hz.

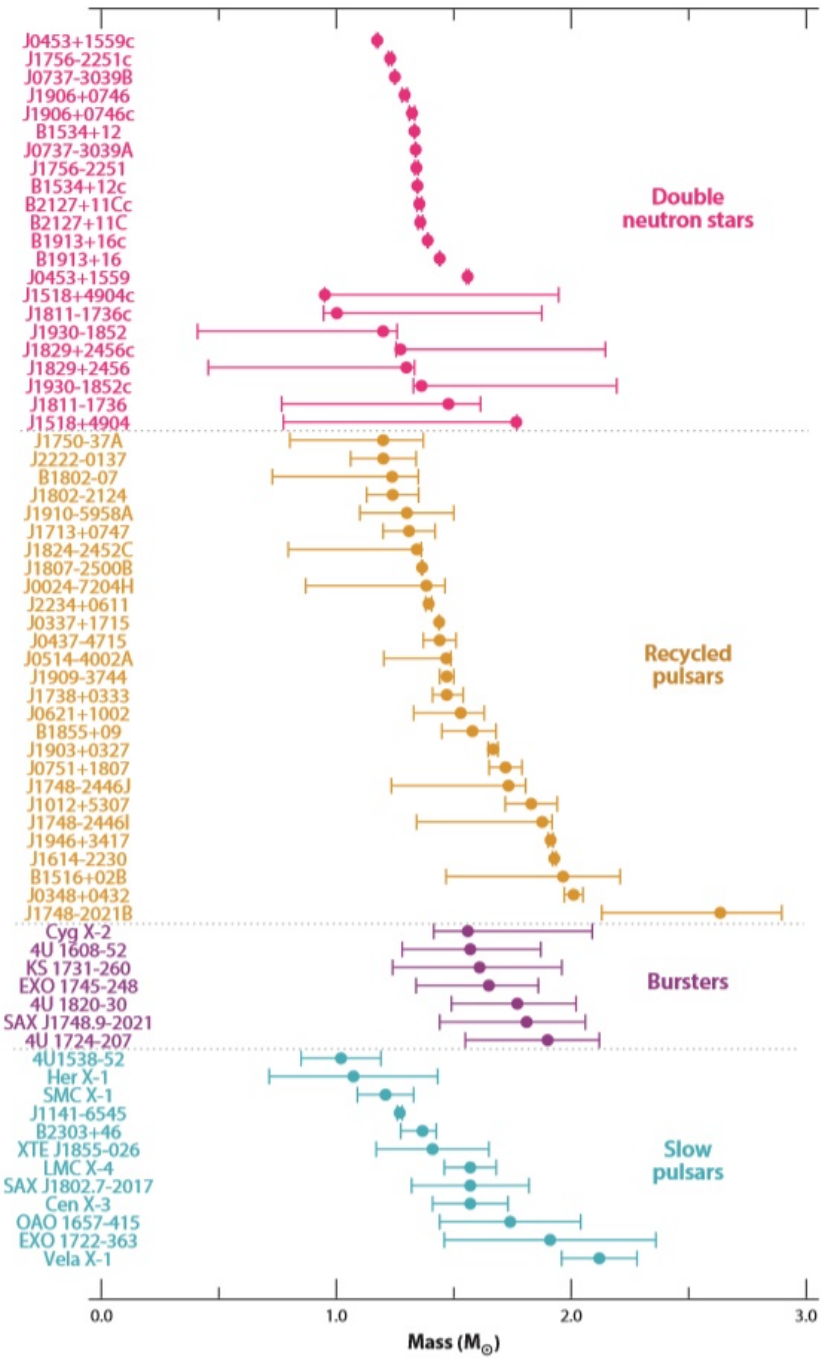

Figure 3.1: The measurements of neutron-star masses [38].

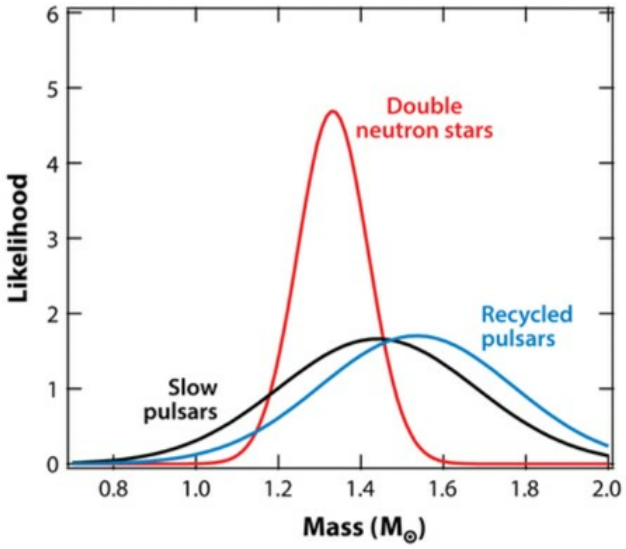

Figure 3.2: The inferred mass distributions for the different populations of neutron stars [38].

3.2 Magnetic fields in Neutron Star

The magnetic fields in neutron stars have been observed since the 1970's. The so-called P-$\dot{\text{P}}$ diagram is shown in Figure 3.3. This Figure shows measured P and $\dot{\text{P}}$ using the X-ray emission observation. Figure 3.3 gives all known radio pulsars in 2014. Pulsars are shown in gray or blue dots. X-ray isolated neutron stars are plotted in yellow squares, and magnetars in red stars. These magnetars have up to about 10^{15} gauss on the surface.

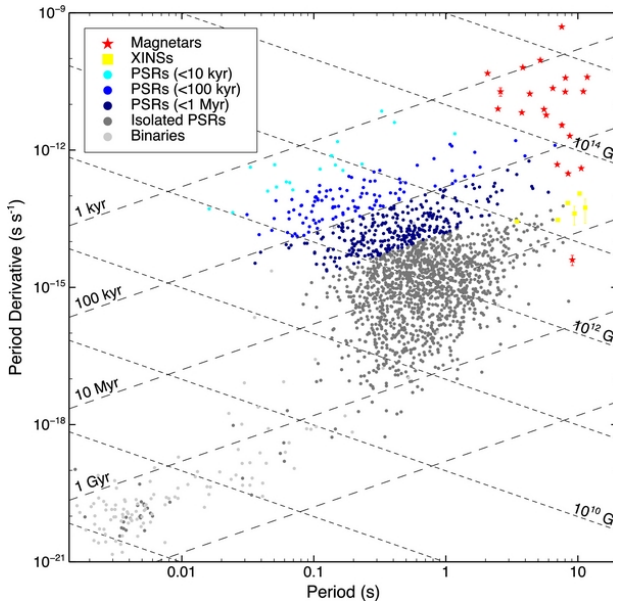

Figure 3.3: P-$\dot{\text{P}}$ diagram for radio pulsars (gray or blue dots as indicated), X-ray Isolated Neutron Stars (yellow squares), and magnetars (red stars) [41].

3.3 Gravitational waves

The gravitational wave is that of gravity itself, which was suggested by Einstein's general relativity. In general relativity, gravity is curvature of space, that is, distortion. If there is a heavy object, the space around the object will be distorted. When two heavy objects rotate around each other, space-time distortion spreads out to the surroundings as waves.

3.3.1 Gravitational wave observation

In recent years, at least 6 gravitational wave events were detected.

The first observation was in September 14, 2015. The LIGO collaboration directly observed gravitational waves from the black hole binary GW150914 for the first time. The masses of initial black holes are $36^{+5}_{-4}M_{\odot}$ and $29 \pm 4M_{\odot}$, and the final black hole mass is $62 \pm 4M_{\odot}$, with $3.0 \pm 0.5\text{M}_{\odot}\text{c}^2$ being radiated in gravitational waves [42].

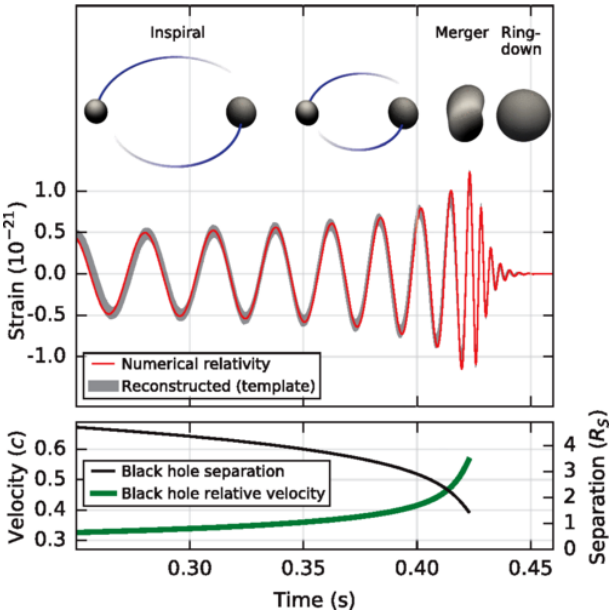

Figure 3.4: *Top* : Estimated gravitational-wave strain amplitude from GW150914 projected onto the LIGO Hanford (H1). This shows the full bandwidth of the waveforms. The inset images show numerical relativity models of the black hole horizons as the black holes coalesce. *Bottom* : The Keplerian effective black hole separation in units of Schwarzschild radii ($R_S = 2GM/c^2$) and the effective relative velocity given by the post-Newtonian parameter $v/c = (GM\pi f/c^3)^{1/3}$, where f is the gravitational-wave frequency calculated with numerical relativity and M is the total mass [42].

The second observation of gravitational waves was made on December 26, 2015, and the Letter was published in June 17, 2016. The masses of initial black holes are $14.2^{+8.3}_{-3.7}M_\odot$ and $7.5 \pm 2.3M_\odot$, and the final black hole mass is $20.8^{+6.1}_{-1.7}M_\odot$ [43]. Barry Barish, Kip Thorne and Rainer Weiss were awarded the 2017 Nobel Prize in Physics for leading this work.

The third, fourth, and fifth black hole binary merger gravitational wave observation was made on January 4, 2017 [44], June 8, 2017 [45], and August 14, 2017 [46]. The fourth detection of gravitational wave was the most lightweight black hole merger ever observed before 2018, that the masses are $12^{+7}_{-2}M_\odot$ and $7^{+2}_{-2}M_\odot$ [45].

The sixth observation was made on August 17, 2017 and it was the neutron star merger.

3.3.2 Gravitational waves from GW170817

One of the detected gravitational waves was from the double neutron star binary merger. On August 17, 2017, the Advanced LIGO and Advanced Virgo gravitational-wave detectors made their first observation of binary neutron stars in spiral. The signal, GW170817,

was detected with a combined signal-to-noise ratio (S/N) of 32.4. A false-alarm-rate estimate of less than $1/(8.0 \times 10^4)$ years [3]. The measured masses of two components lie between 1.00 and 1.89 $M_\odot$, and between 1.16 and 1.60 $M_\odot$ [47].

From a gravitational wave signal, not only the masses of two neutron stars are estimated, but also tidal deformability of neutron stars gives a strong limit to the equation of state.

Fortunately, gravitational wave and multi-bands of electronic waves from GW170817 were observed. Fermi telescope detected approximately two-second contiguous gamma ray burst signal 1.7 seconds later after the merger[4]. Two facilities of LIGO, and Virgo detected the gravitational wave signal. Due to its orientation with respect to the source at the time of detection, Virgo recovered a small signal; combined with the signal sizes and timing in the LIGO detectors, this allowed scientists to precisely triangulate the position in the sky to 30 square degrees. The correspondence object of the gravitational wave was identified optically in galaxy NGC4993 in the distance of about 40 MPc, 11 hours after the gravitational wave detection due to the result that telescopes all over the world explored the region. Figure 3.5 shows the time scale measured by gravitational wave, gamma ray, X-ray, ultra violet (UV), Optical, infrared (IR), and Radio.

When neutron stars were merged, some matter was released in the outer space, and it was thought that an early neutron capture reaction (r-process) occurred in the matter. It should be optical and IR emission, because the new composed elements made by r-process heat up the emitted matter. Such a phenomenon is expected in theory and it is called a kilonova. When lanthanoid elements (atomic number 57 to 71) are synthesized by r-process, the kilonova is bright in IR emission than optical emission and had been brightly longer than expected [48]. This is because an electron starts entering in the 4f orbit in lanthanoid elements, and energy levels are more densely stuffed than elements such as iron. This is caused by efficiently absorbing and emitting IR rays by bound transitions.

It continues emitting IR brightly for around two weeks while it becomes suddenly dark optically and this strongly suggested that the elements including the lanthanoid elements were synthesized by the neutron star merger. Also, in r-process in GW170817, lanthanoid elements were found and lighter elements were synthesized widely [49].

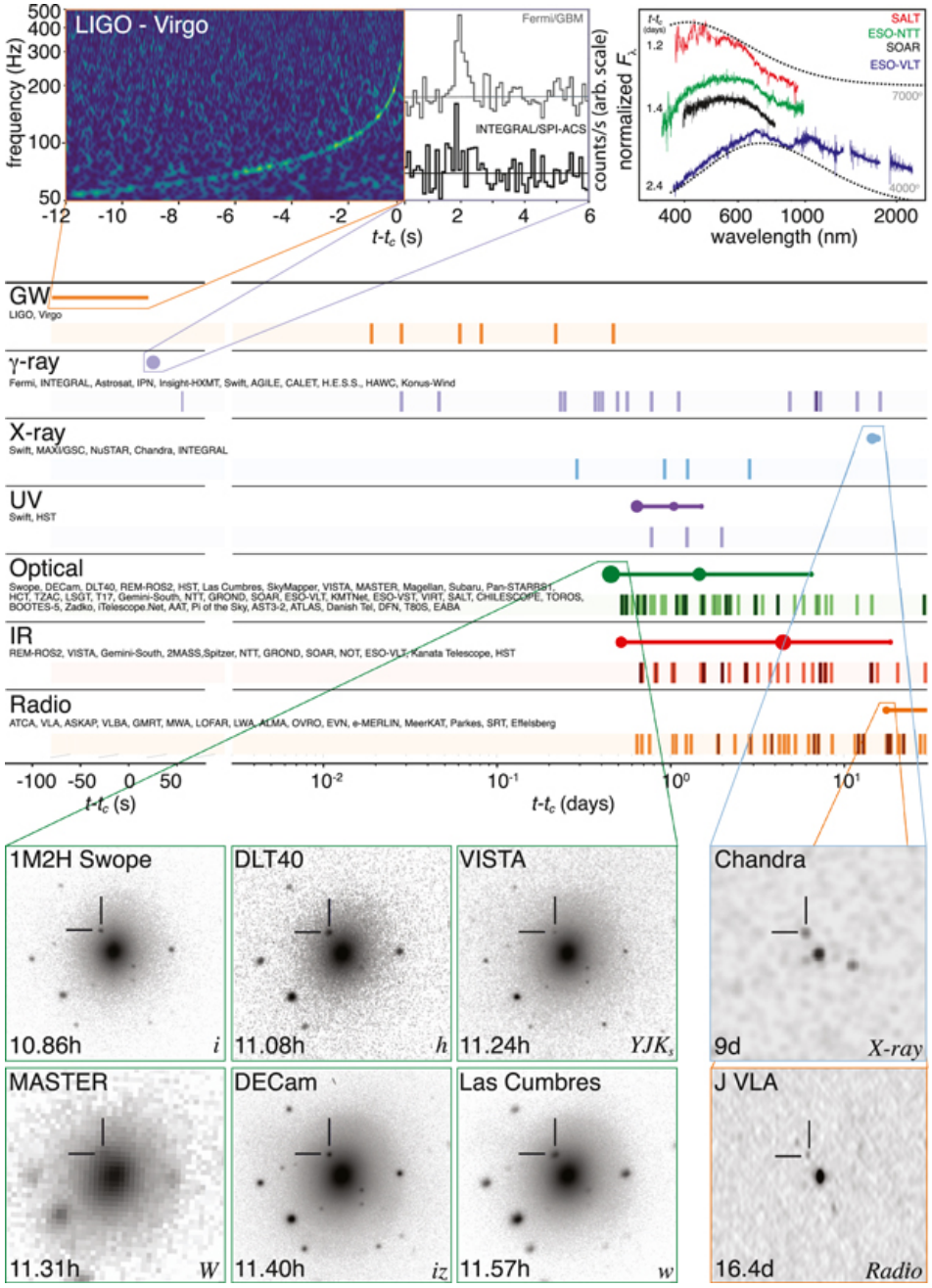

Figure 3.5: Timeline of the discovery of GW170817 (by LIGO and Advanced Virgo detectors), GRB 170817A (by the Fermi Gamma-ray Burst Monitor), SSS17a/AT 2017gfo (by the electromagnetic spectrum leading to the discovery of a bright optical transient), and the follow-up observations are shown by messenger and wavelength relative to the time t_c of the gravitational-wave event. Two types of information are shown for each band/messenger. First, the shaded dashes represent the times when information was reported in a GCN Circular. The names of the relevant instruments, facilities, or observing teams are collected at the beginning of the row. Second, representative observations in each band are shown as solid circles with their areas approximately scaled by brightness; the solid lines indicate when the source was detectable by at least one telescope [4].

3.4 Mass and Radius of Neutron star

3.4.1 Masses around 2 $M_\odot$

Table 3.1: Masses of heavy neutron stars from observation

neutron star	mass ($M_\odot$)	method
PSR J1614 − 2230	1.97 ± 0.04	Shapiro delay [12]
PSR J0348 + 0432	2.01 ± 0.04	Shapiro delay [13]
PSR J0740 + 6620	$2.072^{+0.067}_{-0.066}$	Bayesian estimation of pulse-profile modeling [14, 15, 50, 51]

The neutron star is an object of radius about 10 km, and most have masses of approximately 1.4 times the solar mass.

The observed masses of heavy neutron stars are shown in Table 3.1. In 2010, a strong Shapiro delay signature from the binary millisecond PSR J1614−2230 was observed (radio-timing observations) [12]. Neutron star PSR J0348+0432 with mass of $2.01 \pm 0.04\,M_\odot$ was measured with radio-timing observations in 2013 [13]. In 2019, millisecond pulsar PSR J0740+6620 was observed with mass of $2.072^{+0.067}_{-0.066}\,M_\odot$ using pulse-profile modeling and radio-timing measurements of X-ray data [15].

Existence of neutron stars with masses twice the solar mass is now established beyond doubt. Such a very heavy neutron star gives a strong limit on equations of state for hadronic matter.

3.4.2 Radius of neutron star

Observed radii of neutron stars are summarized as follows. Here we show the upper and lower limits of the radii in Table 3.2. From Table 3.2, (1) and (3) is obtain as lower limits for radius. (2) , (4), and (5) is the upper limit for radius.

In this thesis, we used (5) the upper limit from observed gravitational waves from merger.

Table 3.2: Radii of neutron stars from observation

	mass ($M_\odot$)	radius (km)	method
(1)	$0.86 - 2.42$	$7.6 - 10.4$ (lower limit)	Black body radiation from surface [52]
(2)	$1.2 - 1.7$	$< 9.0 - 13.2$ (upper limit)	Eddington limit [53]
(3)	1.4	> 6.6 (lower limit)	Red shift of the absorption line [54]
(4)	1.4	≤ 13.6 (upper limit)	Gravitational waves from merger [19]
(5)	1.4	< 13.76 (upper limit)	Gravitational waves from merger [20]

The details of method for each upper and lower limits in Table 3.2 are written in follows.

(1) Black body radiation from surface

One of the methods to measure radius of a neutron star is by black body radiation from the surface. Assuming Stephane-Boltzmann law, we can estimate the radius of the neutron star from total luminosity, temperature, and distance from X-ray energy (cf. Guillot et al.(2013) [52]).

Total luminosity L and observed flux F are given by,

$$L = 4\pi R_\infty^2 \sigma_{SB} T^4, \tag{3.8}$$

$$F = \frac{L}{4\pi D^2}. \tag{3.9}$$

where R_∞ is the radius of the neutron star observed at infinity, and D is the distance between the star and the observer, and σ_{SB} is Stephan-Boltzmann constant. From these equations, we obtain the radius R_{NS},

$$\begin{aligned} R_{NS} =& \sqrt{\frac{FD^2}{\sigma_{SB}T^4}}\left(1 - \frac{2GM_{NS}}{R_{NS}c^2}\right)^{1/2}, \\ R_\infty =& R_{NS}\left(1 - \frac{2GM_{NS}}{R_{NS}c^2}\right)^{-1/2}. \end{aligned} \tag{3.10}$$

From the above equation (3.10), we obtain R_{NS}.

(2) Eddington limit

Another method to measure radius of a neutron star is using the Eddington limit [55]. Eddington limit is given when the radiation pressure is balanced against the force of gravity. The observed luminosity L_∞, effective temperature T_∞ and apparent NS radius R_∞ are related with the luminosity at the NS surface L, the effective temperature measured at the surface T_{eff}, and the NS circumferential radius R_{NS} and mass M_{NS}

by the following relations (Lewin et al. 1993 [56])

$$L_\infty = \frac{L}{(1+z)^2}, \quad T_\infty = \frac{T_{eff}}{1+z}, \quad R_\infty = R_{NS}(1+z), \tag{3.11}$$

with the redshift factor $1+z = (1-2GM_{NS}/R_{NS}c^2)^{-1/2}$. The gravitational acceleration g on the NS surface is larger in comparison with the Newtonian one due to general relativity effects

$$g = \frac{GM_{NS}}{R^2}(1+z). \tag{3.12}$$

Therefore, the Eddington luminosity is also large:

$$\begin{aligned} L_{Edd} &= \frac{4\pi GM_{NS}c}{\kappa_e}(1+z) \\ &= 4\pi R_{NS}^2 \sigma_{SB} T_{Edd}^4. \end{aligned} \tag{3.13}$$

Here T_{Edd} is the maximum possible effective temperature on the NS surface, $\kappa_e = 0.2(1+X)$ cm^{2}g^{-1} is the electron (Thomson) scattering opacity, and X is hydrogen mass fraction. If the radiation pressure is larger than the force of gravity, the matter of the star will scatter, so,

$$\frac{4\pi GM_{NS}c}{\kappa_e}(1+z) > 4\pi R_{NS}^2 \sigma_{SB} T_{Edd}^4. \tag{3.14}$$

We must take the smaller radiation pressure than the force of gravity.

Now, we can get

$$R_{NS} < \sqrt{\frac{GM_{NS}c(1+z)}{\kappa_e \sigma_{SB} T_{Edd}^4}}. \tag{3.15}$$

This gives the upper limit of the radius.

(3) Red shift of the absorption line

The other method to measure radius is to see the red shift of the absorption line [54]. Surface of a neutron star contains iron. The red shift of absorption line of the iron is similar to the direct observation of R_{NS}/M_{NS}. Thus,

$$E_{obs} = E_{surf}\sqrt{1 - \frac{2GM}{Rc^2}}. \tag{3.16}$$

Due to Waki et al.(1984), the neutron star radius was only about 1.6 times the Schwarzschild radius.

(4) Gravitational waves from merger

All tidal deformabilities are observed to follow the empirical function

$$\Lambda(R_{NS}) = 2.88 \times 10^{-6}(R_{NS}/\mathrm{km})^{7.5}. \tag{3.17}$$

Because of the correlation between R_{NS} and Λ, the LIGO & Virgo measurement leads to a strong constraint on the possible radii of NSs: the 90% limit of $\Lambda(1.4M_\odot) < 800$ is directly translated into an upper limit of $R(1.4M_\odot) < 13.6$ km as we can see from Figure 3.6.

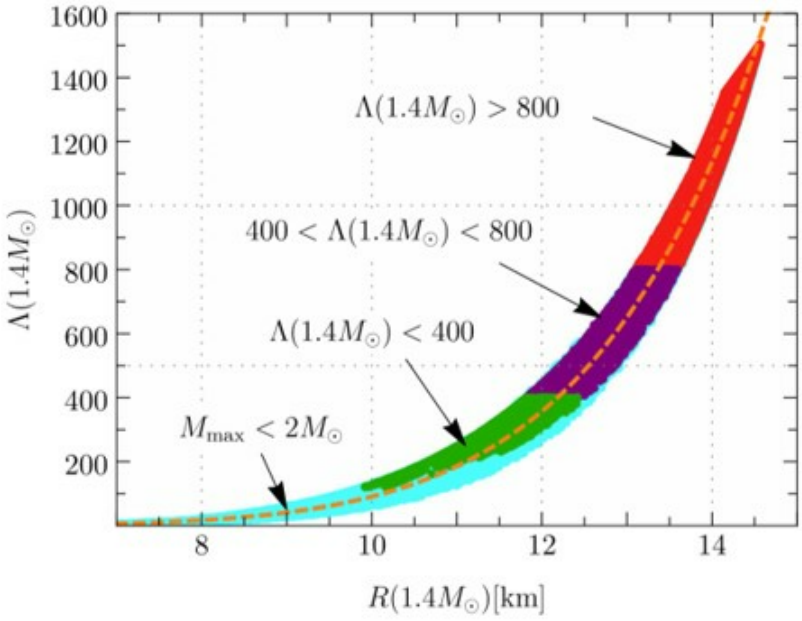

Figure 3.6: The Λ for stars with M=1.4$M_\odot$ as functions of the corresponding radius [19].

(5) Gravitational waves from merger

They model the EoS using RMF, namely 'FSUGold2 family' in Fattoyev et al. (2018) [20]. While, the FSUGold2 family provides the flexibility to generate a continuum of realistic models with varying neutron skins, the models span a fairly narrow range of neutron-star radii. They use 10 representative set of RMF models to alleviate this problem. By using figure, $\Lambda_{1.4}$ a function of the radius of a 1.4 $M_\odot$ neutron star for ten RMF models. Also using the experiment model (PREX) at the Jefferson Laboratory in favor of a neutron-rich skin in ^{208}Pb [57, 58]: $R_{skin}^{208} = 0.33^{+0.16}_{-0.18}$ fm and $\Lambda_{1.4} \leq 800$ limit deduced from GW170817 [3], they have estimate, stellar radius of a 1.4 $M_\odot$ neutron star of

$$R_{1.4} < 13.76 \text{ km}. \tag{3.18}$$

3.4.3 Both mass and radius observation of Neutron star

The observed mass and radius of two pulsars are shown in Table 3.3. There are two pulsars, PSR J0030 + 0451 and PSR J0740 + 6620, which both mass and radius are measured.

Table 3.3: Mass and radius of neutron stars from observation

neutron star	mass ($M_\odot$)	radius (km)	method
PSR J0030 + 0451	$1.44^{+0.15}_{-0.14}$	$13.02^{+1.24}_{-1.06}$	gravitational light-bending [22]
PSR J0740 + 6620	$2.072^{+0.067}_{-0.066}$	$12.39^{+1.30}_{-0.98}$	Bayesian estimation of pulse-profile modeling [14, 15, 50, 51]

Chapter 4

Formalism

4.1 Metric

We use the following metric in general relativity for a slowly rotating neutron star with axial deformation [59, 60, 61, 62],. This formulation was first given by J. B. Hartle. He perturbatively treated the metric with up to second order of Ω, which is the angular velocity,

$$\begin{aligned} ds^2 = & -e^{2\nu_0}\left[1-2h_0\left(r\right)+2h_2\left(r\right)P_2\left(\cos\theta\right)\right] \\ & + e^{2\lambda_0}\left\{1+\frac{e^{2\lambda_0}}{r}\left[2m_0\left(r\right)+2m_2\left(r\right)P_2\left(\cos\theta\right)\right]\right\}dr^2 \\ & + r^2\left[1+2k_2\left(r\right)P_2\left(\cos\theta\right)\right]\left\{d\theta^2+\left[d\phi-\omega\left(r\right)dt\right]^2\sin^2\theta\right\}. \end{aligned} \tag{4.1}$$

Here $\omega(r)$ is the rotational frequency at r. In this metric $P_2\left(\cos\theta\right)$ denotes Legendre polynomial of second order and h_0, h_2, m_0, m_2 and k_2 are quantities of order Ω^2. ω has a radial dependence of order Ω. Here m_0 is the mass increased by deformation.

4.2 Lagrangian

We employ the relativistic mean field (RMF) theory to give EoSs for hadronic matter. We use the following Lagrangian which includes interactions between baryon octet and σ, ω, and ρ mesons in the presence of magnetic fields. Occasionally σ^* and φ mesons of hidden strangeness are included. We determine some parameters in the model so that the basic properties at nuclear saturation density are reproduced.

Table 4.1: Baryon octet (Mass, anomalous magnetic moment from [63], others from [23]).

	mass (MeV)	charge	isospin	strangeness	anomalous magnetic moment (μ_N)
p	938.27	1	1/2	0	2.79
n	939.57	0	−1/2	0	−1.91
Λ	1115.68	0	0	−1	−0.613
Σ^+	1189.37	1	1	−1	1.67
Σ^0	1192.64	0	0	−1	1.61
Σ^-	1197.45	−1	−1	−1	−0.376
Ξ^0	1314.83	0	1/2	−2	−1.25
Ξ^-	1321.31	−1	−1/2	−2	0.0531

Table 4.2: Mesons (Mass from [25], others from [23]).

	mass (MeV)	charge	spin	isospin	strangeness	flavor
σ	511	0	0	0	0	u, d
ω	783	0	1	0	0	u, d
ρ	770	−1,0,1	1	1	0	u, d
σ^*	975	0	0	0	0	s
ϕ	1020	0	1	0	0	s

Table 4.3: Leptons

	mass (MeV)	charge
e	0.510999	−1
μ	105.658	−1
τ	1776.86	−1

In Table 4.1, unit of anomalous magnetic moment μ_N is called nuclear magneton. The Lagrangian for the GM1 EoS is given in terms of σ, ρ and ω as,

$$\begin{aligned}\mathcal{L} = &\sum_b \bar{\psi}_b \left(i\gamma_\mu \partial^\mu - m_b + g_{\sigma b}\sigma - g_{\omega b}\gamma_\mu \omega^\mu - g_{\rho b}\gamma_\mu \boldsymbol{\tau}\cdot\boldsymbol{\rho}^\mu\right)\psi_b \\ &+ \frac{1}{2}\left(\partial_\mu\sigma\partial^\mu\sigma - {m_\sigma}^2\sigma^2\right) - \frac{1}{4}\omega_{\mu\nu}\omega^{\mu\nu} + \frac{1}{2}{m_\omega}^2\omega_\mu\omega^\mu \\ &- \frac{1}{4}\rho_{\mu\nu}\cdot\rho^{\mu\nu} + \frac{1}{2}{m_\rho}^2\rho_\mu\cdot\rho^\mu - \frac{1}{3}bm_n(g_\sigma\sigma)^3 - \frac{1}{4}c(g_\sigma\sigma)^4. \end{aligned} \tag{4.2}$$

Here, $\boldsymbol{\tau}$ is isospin operator.

In other cases we add terms of magnetic fields and other meson fields in the La-

grangian. In this case the Lagrangian is as follows:

$$\mathcal{L} = \sum_b \mathcal{L}_b + \mathcal{L}_m + \sum_l \mathcal{L}_l + \mathcal{L}_{\rm em}, \tag{4.3}$$

where,

$$\begin{aligned}
\mathcal{L}_b &= \overline{\psi}_b \left(i\gamma_\mu \partial^\mu - m_b + g_{\sigma b}\sigma + g_{\sigma^* b}\sigma^* - g_{\omega b}\gamma_\mu \omega^\mu - g_{\phi b}\gamma_\mu \phi^\mu - g_{\rho b}\gamma_\mu \boldsymbol{\tau}\cdot\boldsymbol{\rho}^\mu \right. \\
&\qquad \left. - q_b \gamma_\mu A^\mu - \kappa_b \sigma_{\mu\nu} F^{\mu\nu} \right) \psi_b, \qquad (4.4) \\
\mathcal{L}_m &= \frac{1}{2}\left(\partial_\mu \sigma \partial^\mu \sigma - m_\sigma^2 \sigma^2\right) + \frac{1}{2}\left(\partial_\mu \sigma^* \partial^\mu \sigma^* - m_{\sigma^*}^2 \sigma^{*2}\right) \\
&\quad + \frac{1}{2} m_\omega^2 \omega_\mu \omega^\mu - \frac{1}{4}\Omega_{\mu\nu}\Omega^{\mu\nu} + \frac{1}{2} m_\phi^2 \phi_\mu \phi^\mu - \frac{1}{4}\Phi_{\mu\nu}\Phi^{\mu\nu} \\
&\quad + \frac{1}{2} m_\rho^2 \boldsymbol{\rho}_\mu \cdot \boldsymbol{\rho}^\mu - \frac{1}{4}\boldsymbol{P}^{\mu\nu}\cdot\boldsymbol{P}_{\mu\nu} \\
&\quad - \frac{1}{3} b m_n (g_\sigma \sigma)^3 - \frac{1}{4} c (g_\sigma \sigma)^4 + \frac{1}{4!}\xi \left(g_\omega^2 \omega_\mu \omega^\mu\right)^2 + \Lambda_\omega \left(g_\omega^2 \omega_\mu \omega^\mu\right)\left(g_\rho^2 \boldsymbol{\rho}_\mu \cdot \boldsymbol{\rho}^\mu\right), \qquad (4.5) \\
\mathcal{L}_l &= \overline{\psi}_l \left(i\gamma_\mu \partial^\mu - q_l \gamma_\mu A^\mu - m_l \right) \psi_l, \qquad (4.6) \\
\mathcal{L}_{\rm em} &= -\frac{1}{4} F^{\mu\nu} F_{\mu\nu}. \qquad (4.7)
\end{aligned}$$

Here $b, m, l,$ em indicate baryons, mesons, leptons, and photons, respectively. The field strengths are explicitly given as

$$\begin{aligned}
F_{\mu\nu} &= \partial_\mu A_\nu - \partial_\nu A_\mu, \qquad (4.8) \\
\Omega_{\mu\nu} &= \partial_\mu \omega_\nu - \partial_\nu \omega_\mu, \qquad (4.9) \\
\Phi_{\mu\nu} &= \partial_\mu \phi_\nu - \partial_\nu \phi_\mu, \qquad (4.10) \\
\boldsymbol{P}_{\mu\nu} &= \partial_\mu \boldsymbol{\rho}_\nu - \partial_\nu \boldsymbol{\rho}_\mu - g_\rho \boldsymbol{\rho}_\mu \times \boldsymbol{\rho}_\nu. \qquad (4.11)
\end{aligned}$$

4.3 RMF Theory

In chapter 5, we will employ various kinds of equations of state (EoS) (GM1, GM3, TM1-a, TM1-b, TM2$\omega\rho$-a, TM2$\omega\rho$-b, NL3-a, NL3-b, NL3$\omega\rho$-a, NL3$\omega\rho$-b DDME2-a and DDME2-b), whose parameters are listed in Table 4.4. As for the EoS, We use relativistic mean field (RMF) Theory. RMF Theories are used to give EoSs for hadronic matter. See Appendix A.
Here, g_σ is the coupling constant of nucleons with the scalar-meson σ, g_ω is the coupling constant of nucleons with the vector-meson ω , g_ρ is the coupling constant of nucleons with the vector-isovector-meson ρ. The masses of these mesons are listed in Table 4.5.

Table 4.4: EoS parameters

EoS	g_σ	g_ω	g_ρ	$b \times 10^3$	$c \times 10^3$	ξ	Λ_ω
GM1	8.895	10.61	8.195	2.947	-1.070	0	0
GM3	8.162	8.712	8.541	8.659	-2.421	0	0
TM1	10.03	12.61	4.632	1.508	0.061	0.0169	0
TM2$\omega\rho$	9.998	12.50	11.30	1.763	-0.790	0.0113	0.03
NL3	10.22	12.87	8.948	1.028	-0.442	0	0
NL3$\omega\rho$	10.22	12.87	11.28	1.028	-0.442	0	0.03
DDME2	10.54	13.02	7.367	0	0	0	0

Table 4.5: mesons and masses

meson	mass(MeV)
m_σ	511.198
m_ω	783.0
m_ρ	770.0
$m_\sigma*$	975
m_ϕ	1020

In the GM1 parameter set,

$$R_{\sigma h} = g_{\sigma h}/g_{\sigma N} = 0.6, \tag{4.12}$$
$$R_{\omega h} = g_{\omega h}/g_{\omega N} = 0.653, \tag{4.13}$$
$$R_{\rho h} = g_{\rho h}/g_{\rho N} = 0.6, \tag{4.14}$$

are adopted. For GM3 parameter sets,

$$R_{\sigma h} = g_{\sigma h}/g_{\sigma N} = 0.6, \tag{4.15}$$
$$R_{\omega h} = g_{\omega h}/g_{\omega N} = 0.568, \tag{4.16}$$
$$R_{\rho h} = g_{\rho h}/g_{\rho N} = 0.6, \tag{4.17}$$

are adopted. As for other couplings of hyperons with the vector and the vector-isovector mesons, the SU(6) values are adopted in the a-parameter sets (TM1-a, TM2$\omega\rho$-a, NL3-a, NL3$\omega\rho$-a and DDME2-a):

$$R_{\omega\Lambda} = \frac{2}{3}, \quad R_{\omega\Sigma} = \frac{2}{3}, \quad R_{\omega\Xi} = \frac{1}{3}, \tag{4.18}$$
$$R_{\rho\Sigma} = 2, \quad R_{\rho\Xi} = 1, \tag{4.19}$$
$$R_{\phi\Lambda} = -\frac{\sqrt{2}}{3}, \quad R_{\phi\Sigma} = -\frac{\sqrt{2}}{3}, \quad R_{\phi\Xi} = -\frac{2\sqrt{2}}{3}. \tag{4.20}$$

In the b-parameter sets (TM1-b, TM2$\omega\rho$-b, NL3-b, NL$\omega\rho$-b and DDME2-b), we adopted same parameter sets as a-parameter sets except

$$R_{\omega\Lambda} = 1, \tag{4.21}$$

which corresponds to the symmetry breaking of SU(6) symmetry.

The basic properties reproduced by various EoSs are shown in Table 4.6 [23, 24, 25, 64, 65]. These components suggest saturation number density ρ, binding energy B/A, incompressibility K, symmetry energy J, its slope parameter L, and curvature K_{sym} at the saturation point of uniform symmetric nuclear matter.

Table 4.6: Properties of various EoSs

EoS	ρ (fm^{-3})	B/A (MeV)	K (MeV)	J (MeV)	L (MeV)	K_{sym} (MeV)
GM1	0.153	−16.3	300.7	32.5	94.4	18.1
GM3	0.153	−16.3	240	32.5	89.7	−6.5
TM1	0.146	−16.3	281.2	36.9	111.2	33.8
TM2$\omega\rho$	0.146	−16.4	281.7	32.1	54.8	−70.5
NL3	0.148	−16.3	271.8	37.4	118.9	101.6
NL3$\omega\rho$	0.148	−16.3	271.8	31.7	55.5	−7.6
DDME2	0.152	−16.14	250.9	32.3	51.2	−87.1

4.4 Baym-Pethick-Sutherland (BPS) EoS

In order to describe the lower density region, the Baym-Pethick-Sutherland (BPS) EoS is used [66] with the atomic masses given in Ame2012 [67, 68] and HFB-24 [69]. The equations for obtaining EoSs in the presence of strong magnetic fields are summarized in the Appendix B.2.

4.5 Tolman Oppenheimer-Volkoff equation

Here, we introduce differential equations so that structure of a relativistic star with spherical symmetry can be calculated in the static frame.

Here we have the following equation, which is so-called Tolman Oppenheimer-Volkoff (TOV) equation (see Appendix C for derivation),

$$\frac{dp}{dr} = -\frac{\left[p(r)+\varepsilon(r)\right]\left[M(r)+4\pi r^3 p(r)\right]}{r\left[r-2M(r)\right]}, \tag{4.22}$$

$$\frac{dM}{dr} = 4\pi\varepsilon(r)r^2. \tag{4.23}$$

Here, pressure p and energy density ε are defined in Appendix C.

For calculating TOV equation, we use gravitational unit. See Appendix D.

4.6 Hartle Equations

A theoretical method in a perturbative way to calculate additional masses and eccentricities of axially deformed objects due to rotation was first introduced by J. B. Hartle and others in Refs. [59, 60, 61, 62] in the framework of General Relativity. In the gravitational unit ($G = c = 1$), the metric can be written as

$$\begin{aligned} ds^2 = & -e^{\nu}\left[1 + 2\left\{h_0 + h_2 P_2(\cos\theta)\right\}\right] dt^2 \\ & + e^{\lambda}\left[1 + \frac{2e^{\lambda}}{r}\left\{m_0 + m_2 P_2(\cos\theta)\right\}\right] dr^2 \\ & + r^2\left[1 + 2k_2 P_2(\cos\theta)\right]\left[d\theta^2 + \sin^2\theta\left(d\phi - \omega dt\right)^2\right], \end{aligned} \tag{4.24}$$

where $\omega(r,\theta)$ represents the local angular velocity of a rotating star, and $h_0(r)$, $h_2(r)$, $m_0(r)$, $m_2(r)$, and $k_2(r)$ are the second order perturbative terms with respect to the angular velocity Ω, where Ω is the angular velocity observed far from the neutron star. The second order Legendre polynomial is given as $P_2(\cos\theta) = \frac{1}{2}(3\cos^2\theta - 1)$. Up to second order of Ω, the Hartle equations are employed, which are explicitly given in Appendix E.

In the zeroth order of Ω, usual TOV equations are employed :

$$\frac{dp_0}{dr} = -\frac{\left(M_0 + 4\pi p_0 r^3\right)\left(\varepsilon_0 + p_0\right)}{r\left(r - 2M_0\right)}, \tag{4.25}$$

$$\frac{dM_0}{dr} = 4\pi r^2 \varepsilon_0, \tag{4.26}$$

where energy density ε_0 and pressure p_0 are calculated by the RMF theory as functions of baryon density. The radius R of a neutron star is so determined that pressure $p_0(R) = 0$ after solving TOV equations. Then the total mass is given using an additional mass $m_0(R)$ as

$$M = M_0(R) + m_0(R). \tag{4.27}$$

4.7 Magnetic field

For the magnetic field, we use the following $B(\rho)$.

$$B(\rho) = B_s + B_0\Big(1 - \exp\Big\{-\alpha\left(\frac{\rho}{\rho_0}\right)^{\gamma}\Big\}\Big) \tag{4.28}$$

Here, B_s indicates the magnetic field at the surface and B_0 indicates the magnetic field near the center of the neutron star. Here, $\alpha = 0.05$ and $\gamma = 2$ are adopted [70].

Mangnetic fields strength $B(\rho)$ as a function of baryon number density ρ is shown in Figure 4.1.

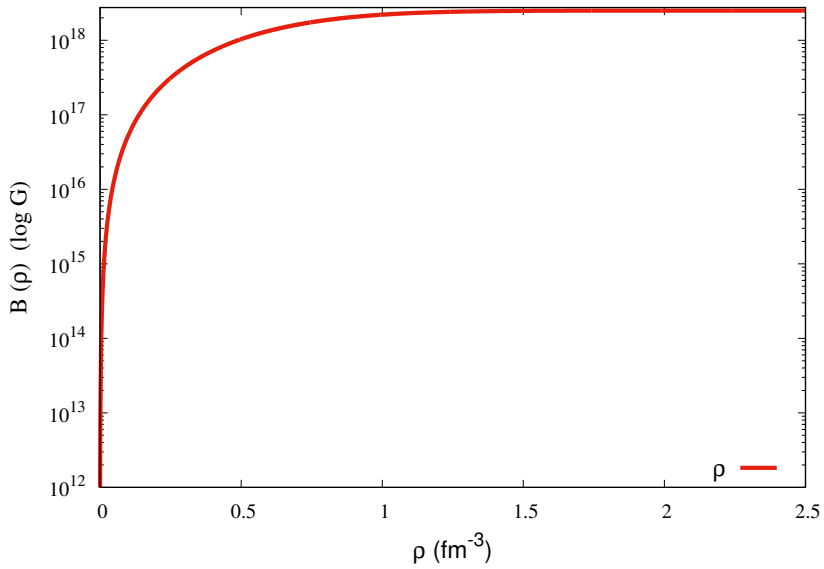

Figure 4.1: Magnetic field strengths $B(\rho)$ as a function of baryon number density ρ (fm $^{-3}$). Here, $\alpha = 0.05$ and $\gamma = 2$ are adopted.

In this thesis, we have used spherically symmetric magnetic pressure (SSMP) (Figure 4.2, left). This magnetic field has spherically symmetric magnetic field, so that there is no directions of magnetic field and it is spherical.

Since Equation (4.28) does not satisfy div B = 0 in general, this form of the magnetic fields must be used with caution as a simple way to implement magnetic fields in an NS. With this problem in mind, however, it should be emphasized that for particles in a very small region of an NS, they feel almost a constant magnetic field, for which div B = 0 is practically satisfied. For more realistic magnetic fields, different equations might be used [71].

Even if one assumes the form of Equation (4.28), one has free parameters α, γ, and B_0. In our work [72], we arbitrarily change α and γ to investigate their effects on the radii and masses of NSs. In this thesis, we discuss more about changing α and γ in Sect. 6.6.

On the other hand, in our work [73], we use poloidal magnetic fields (PMF) (Figure 4.2, right). PMF is a magnetic field with dipole magnetic field. The shape of neutron star in PMF is deformed due to strong magnetic fields.

4.7.1 EoS of hadronic matter with magnetic fields

Here, spherically symmetric magnetic pressure (SSMP) to add magnetic fields to neutron star. The energy density ε and the pressure p of hadronic matter in the presence of the magnetic fields are given as

$$\varepsilon = \varepsilon_m + B^2/2, \tag{4.29}$$
$$p = p_m + B^2/2, \tag{4.30}$$

respectively, where ε_m is the energy density and p_m is the pressure of hadrons where the contribution $B^2/2$ from the magnetic fields are neglected. However, it should be noted that without $B^2/2$ the effects of the magnetic fields to ε_m and p_m are included through particles ' magnetic moments. All the details are given in the Appendix of Ref. [16].

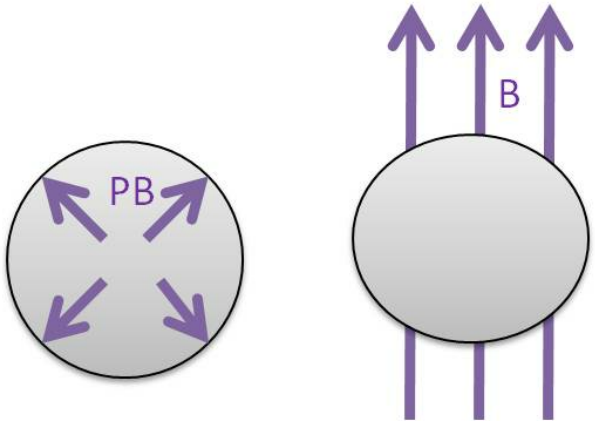

Figure 4.2: Magnetic fields in spherically symmetric magnetic pressure (SSMP) on the left, poloidal magnetic fields (PMF) on the right.

4.7.2 Landau diamagnetism

We pursue the energy levels of a charged particle with mass m, electric charge q in a constant magnetic field $\mathbf{B} = (0, 0, B)$. We choose the gauge of $\mathbf{A} = (0, B_x, 0)$. Then we can write the hamiltonian as follows. We take a non-relativistic formalism in cgs units.

$$\hat{H} = \frac{1}{2m}\left[\hat{p}_x^2 + \left(\hat{p}_y - \frac{qB}{c}\hat{x}\right)^2 + \hat{p}_z^2\right]. \tag{4.31}$$

Now, the expectation of $\hat{p}_y$ and $\hat{p}_z$, p_y and p_z are conserved quantities because,

$$\left[\hat{p}_y, \hat{H}\right] = \left[\hat{p}_z, \hat{H}\right] = 0. \tag{4.32}$$

So, we can write the hamiltonian for the eigen-state of $\hat{p}_y$ and $\hat{p}_z$ as,

$$\begin{aligned}\hat{H} &= \frac{1}{2m}\left[\hat{p}_x^2 + \left(p_y - \frac{qB}{c}\hat{x}\right)^2 + p_z^2\right] \\ &= \frac{1}{2m}\hat{p}_x^2 + \frac{m}{2}\left(\frac{qB}{mc}\right)^2\left(\hat{x} - \frac{cp_y}{qB}\right)^2 + \frac{1}{2m}p_z^2, \end{aligned} \tag{4.33}$$

$$E = \hbar\omega_c\left(n + \frac{1}{2}\right) + \frac{\hbar^2 k_z^2}{2m}. \tag{4.34}$$

Here, $n = 0, 1, 2, \cdots$, and $\omega_c = \frac{qB}{mc}$. These discrete energy levels are called Landau levels. We obtain similar energy levels in a relativistic treatment. See Appendix B and F.

4.8 Eccentricity of neutron star

First we discuss on eccentricity of the neutron star. The eccentricity e is given by Hartle & Thorn (1968) [61],

$$e(r) = e = \left[\frac{{R_e}^2}{{R_p}^2} - 1\right]^{1/2} \tag{4.35}$$

$$= \left[-3(\upsilon_2 - h_2 + \xi_2/r)\right]^{1/2}, \tag{4.36}$$

where R_e is the radius at equator and R_p is polar radius and ξ_2 is defined as follows,

$$\xi_2 = -p_2^* \frac{(E+P)}{(dP/dr)}, \tag{4.37}$$

$$p_2^* = -h_2 - \frac{1}{3}r^2 e^{-\nu}\varpi^2. \tag{4.38}$$

From equation (4.35), we can write down as

$$\begin{aligned}\frac{{R_e}^2}{{R_p}^2} &= e^2 + 1, \\ R_e &= \sqrt{e^2+1} \times R_p. \end{aligned} \tag{4.39}$$

Chapter 5

Results

In this thesis, we employ 12 different hadronic EoSs, namely, GM1, GM3, TM1-a, TM1-b, TM2$\omega\rho$-a, TM2$\omega\rho$-b, NL3-a, NL3-b, NL3$\omega\rho$-a, NL3$\omega\rho$-b, DDME2-a and DDME2-b [23, 25], all of which include hyperons in addition to nucleons as components. These EoSs depend on the different coupling constants between baryons and mesons and having similar saturation properties at nuclear saturation density.

The mass and radius relation (MR relation) of each EoS is compared with GM1 EoS as a reference. TM1 and TM2 are different concerning the slope parameter L, where L is closely related to the radius of a neutron star. The NL3 parametrization is fitted to the ground-state properties of both stable and unstable nuclei. This parametrization predicts very large, purely nucleonic neutron star maximum masses, but a symmetry energy slope parameter L is too large. Thus, we also consider the parametrization NL3$\omega\rho$ with a softer density dependence of the symmetry energy due to the inclusion of the nonlinear $\omega\rho$ term. The GM3 EoS leads to neutron star with compactness smaller than GM1 EoS. In this work, we use various values of the incompressibility K (240 – 300 MeV), and from this point of view, we can check how K affects neutron star structure.

5.1 MR relations of EoSs

First, we calculate MR relations of 12 EoSs without considering internal magnetic fields or rotation of a neutron star. Figure 5.1 shows the total mass M ($M_\odot$) as a function of its radius (km) (MR relation) without magnetic fields or rotation. The unstable region ($\frac{\partial M(\varepsilon_c)}{\partial \varepsilon_c} < 0$, where ε_c is the energy density at the center) is not shown for each EoS in the figure. It is seen that NL3-a, NL3-b, NL3$\omega\rho$-a, NL3$\omega\rho$-b, DDME2-a and DDME2-b EoSs surpass twice the solar mass and these EoSs have masses more than 2.072 $M_\odot$. For each EoS the maximum mass (M_{max}), the radius at $M = 1.4\ M_\odot$, and radius at $M = 2.072\ M_\odot$ are shown in Table 5.1. The observed upper limit of the radius at $M = 1.4\ M_\odot$ is 13.76 km [20] and maximum mass is 2.072 $M_\odot$.

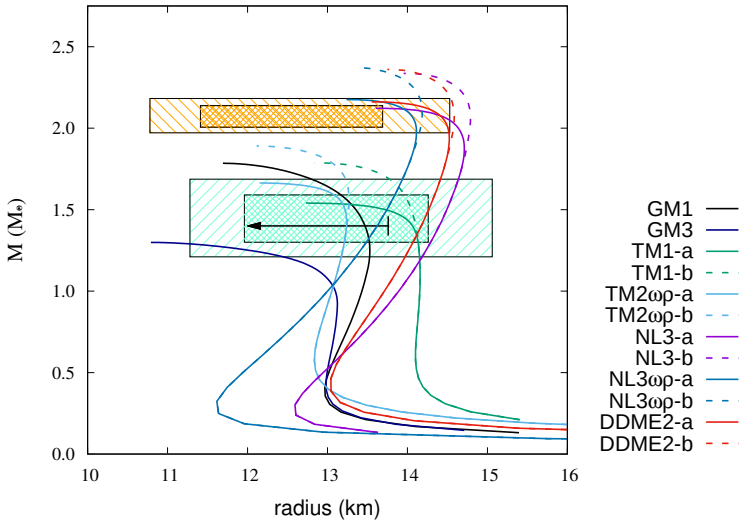

Figure 5.1: MR relations of 12 EoSs without rotation and magnetic fields. The unstable region in each EoS is not shown. The orange and light green dashed areas indicate pulsars PSR J0740 + 6620 and PSR J0030 + 0451 (68% (thick) and 90% (thin) credibility), respectively. The arrow indicates the upper limit of radius for 1.4 $M_\odot$ from the gravitational wave event GW170817. The colored lines represent the following: black (solid line), GM1 EoS; green (solid line), TM1-a EoS; green (dashed line), TM1-b EoS; light blue (solid line), TM2$\omega\rho$-a EoS; light blue (dashed line), TM2$\omega\rho$-b EoS; purple (solid line), NL3-a EoS; purple (dashed line), NL3-b EoS; dark blue (solid line), NL3$\omega\rho$-a EoS; dark blue (dashed line), NL3$\omega\rho$-b EoS; red (solid line), DDME2-a EoS; red (dashed line), DDME2-b EoS.

Table 5.1: Maximum masses (M_{max}), radius at $M = 1.4\ M_\odot$ ($R_{1.4M_\odot}$), and radius at $M = 2.072\ M_\odot$($R_{2.072_{M_\odot}}$) for 12 EoSs without rotation or magnetic fields. The bar indicates no solution.

EoS	M_{max} ($M_\odot$)	$R_{1.4M_\odot}$ (km)	$R_{2.072M_\odot}$ (km)
GM1	1.784	13.49	—
GM3	1.299	—	—
TM1-a	1.540	14.07	—
TM1-b	1.787	14.10	—
TM2$\omega\rho$-a	1.663	13.24	—
TM2$\omega\rho$-b	1.891	13.23	—
NL3-a	2.122	14.37	14.45
NL3-b	2.336	14.37	14.79
NL3$\omega\rho$-a	2.175	13.49	14.05
NL3$\omega\rho$-b	2.372	13.49	14.18
DDME-a	2.161	14.08	14.44
DDME-b	2.360	14.08	14.58

5.2 MR relation of EoS with rotation

Next, we consider rotation of a neutron star and calculate MR relations of 12 EoSs. Here rotation is considered perturbatively by solving Hartle equations, which is explained in detail in Appendix E. Figure 5.2 shows the MR relations of the rotating neutron stars. Here, Ω is taken as 6×10^3 Hz ($\Omega = 0.02$ km^{-1} in gravitational unit), corresponding to the fastest possible neutron star. This frequency corresponds roughly to the Kepler frequency Ω_K [23, 74] :

$$\Omega_K \approx 24 \left(\frac{M/M_\odot}{(R/\mathrm{km})^3} \right)^{1/2} \times 10^4 \ \mathrm{s}^{-1}. \tag{5.1}$$

If we put $M = 1.4\ M_\odot$ and $R = 13$ km as a typical neutron star in eq. (5.1), Ω_K is about 6×10^3 Hz.

A slight increase of mass is seen in all cases as shown in Fig. 5.2 and in Table 5.2. NL3-a, NL3-b, NL3$\omega\rho$-a, NL3$\omega\rho$-b, DDME2-a and DDME2-b EoSs surpass twice the solar mass. In this rotating case, the neutron star is axially deformed. The equatorial radius at $M = 1.4 M_\odot$ is denoted as $R^e_{1.4M_\odot}$, the polar radius at $M = 1.4\ M_\odot$, as $R^p_{1.4M_\odot}$ [59, 60, 61, 62], and the eccentricity e is defined by [61, 62]

$$e = \sqrt{\left(\frac{R_e}{R_p} \right)^2 - 1}. \tag{5.2}$$

Here we indicates the eccentricity at 1.4 $M_\odot$ as $e_{1.4}$. It is found that rotation has a small effect on mass even with the Kepler frequency (6×10^3 Hz).

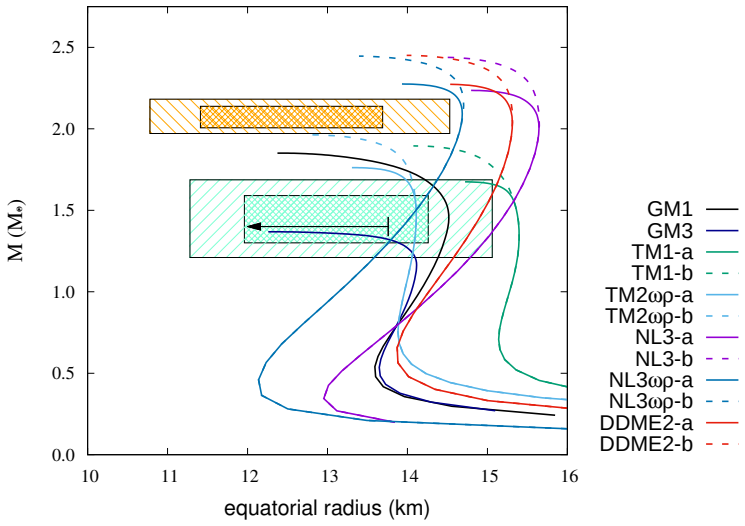

Figure 5.2: Same as Fig. 5.1, but with rotation ($\Omega = 6 \times 10^3$ Hz).

Table 5.2: Maximum mass ($M_{\max}$) of a rotating neutron star in unit of $M_\odot$, equatorial radius at $M = 2.072\ M_\odot$ ($R^e_{2.072M_\odot}$), polar radius ($R^p_{1.4M_\odot}$) and equatorial radius ($R^e_{1.4M_\odot}$) at $M = 1.4M_\odot$, and eccentricity at 1.4 $M_\odot$ ($e_{1.4}$), respectively, at $\Omega = 6 \times 10^3$ Hz ($\Omega = 0.02$ km^{-1} in gravitational unit).

EoS	M_{max} ($M_\odot$)	$R^e_{2.072M_\odot}$ (km)	$R^p_{1.4M_\odot}$ (km)	$R^e_{1.4M_\odot}$ (km)	$e_{1.4}$
GM1	1.851	—	12.43	14.51	0.86
GM3	1.368	—	—	—	—
TM1-a	1.675	—	12.79	15.39	0.83
TM1-b	1.895	—	12.79	15.39	0.83
TM2$\omega\rho$-a	1.762	—	12.12	14.10	0.86
TM2$\omega\rho$-b	1.964	—	12.12	14.10	0.86
NL3-a	2.236	15.63	13.05	15.10	0.86
NL3-b	2.439	15.65	13.05	15.10	0.86
NL3$\omega\rho$-a	2.275	14.68	12.43	13.78	0.90
NL3$\omega\rho$-b	2.446	14.67	12.43	13.78	0.90
DDME2-a	2.273	15.31	12.82	14.78	0.87
DDME2-b	2.450	15.31	12.82	14.78	0.87

The MR relations for 12 EoSs in case with rotation at $\Omega = 6\times10^2$ Hz ($\Omega = 0.002$ km^{-1} in gravitational unit) is shown in Fig. 5.3. Maximum masses ($M_\odot$), equatorial radii at 2.072 $M_\odot$ (km), polar radii at 1.4 $M_\odot$ (km), equatorial radii at 1.4 $M_\odot$ (km), and eccentricities at 1.4 $M_\odot$ with rotation ($\Omega = 6 \times 10^2$ Hz) are shown in Table 5.3. In Fig. 5.3 and Table 5.3, there is a little increase in comparison with the no rotational case (Fig. 5.1, Table 5.1). The most rapid frequency of observed pulsar is $\Omega = 716$ Hz [40], so that $\Omega = 6 \times 10^2$ Hz is a realistic value for rotating neutron star. For NL3-a, NL3-b, NL3$\omega\rho$-a, NL3$\omega\rho$-b, DDME2-a, and DDME2-b EoSs, their masses are over $2\,M_\odot$. As for TM2$\omega\rho$-a, TM2$\omega\rho$-b, NL3$\omega\rho$-a and NL3$\omega\rho$-b EoSs, equatorial radius ($R^e_{1.4M_\odot}$) at $M = 1.4\ M_\odot$ is below 13.76 km.

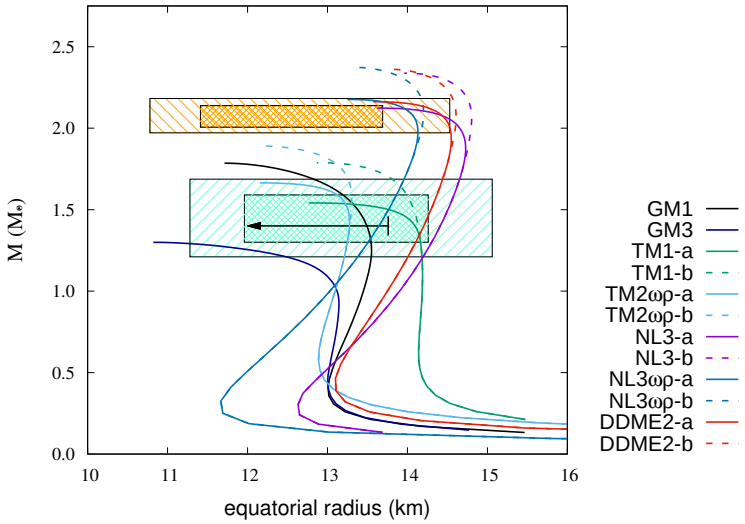

Figure 5.3: Same as Fig. 5.1, but with rotation ($\Omega = 6 \times 10^2$ Hz).

Table 5.3: Same as Table 5.2, but with rotation ($\Omega = 6 \times 10^2$ Hz).

EoS	M_{max} $(M_\odot)$	$R^e_{2.072M_\odot}$ (km)	$R^p_{1.4M_\odot}$ (km)	$R^e_{1.4M_\odot}$ (km)	$e_{1.4}$
GM1	1.785	—	13.46	13.51	0.997
GM3	1.300	—	—	—	—
TM1-a	1.541	—	14.03	14.09	0.996
TM1-b	1.788	—	14.07	14.13	0.996
TM2$\omega\rho$-a	1.664	—	13.20	13.28	0.994
TM2$\omega\rho$-b	1.891	—	13.19	13.27	0.994
NL3-a	2.123	14.46	14.34	14.37	0.998
NL3-b	2.337	14.80	14.34	14.37	0.998
NL3$\omega\rho$-a	2.176	14.06	13.46	13.52	0.996
NL3$\omega\rho$-b	2.372	14.20	13.46	13.52	0.996
DDME2-a	2.162	14.45	14.04	14.12	0.995
DDME2-b	2.361	14.61	14.04	14.12	0.995

5.3 MR relations of EoSs with internal magnetic fields

Next, we calculate MR relations of 12 EoSs with magnetic fields. Next, magnetic fields $-\frac{1}{4}F^{\mu\nu}F_{\mu\nu}$ in Eq. (4.7) are considered for 12 EoSs. In Fig. 5.4 – 5.7, we show MR relations with magnetic fields with different magnetic fields strength at the center of a neutron star $B_0 = 2.5 \times 10^{18}$ G and $B_0 = 3 \times 10^{18}$ G, and different magnetic fields strength at the surface $B_s = 10^{12}$ G and $B_s = 10^{15}$ G.

In Fig. 5.4 – 5.5 and Table 5.4 – 5.5, the strength of magnetic field at the center

is adopted as $B_0 = 2.5 \times 10^{18}$ G. As shown in Fig. 5.4 and Table 5.4, $B_s = 10^{12}$ G is employed. EoSs except GM3, TM1-a, and TM2$\omega\rho$-a EoSs give masses above the two-solar-mass. The strength of magnetic fields at surface $B_s = 10^{15}$ G is shown in Fig. 5.5 and Table 5.5. Also, EoSs except GM3, TM1-a, and TM2$\omega\rho$-a EoSs give masses above the two-solar-mass.

Moreover, considering the upper limit of radius $R = 13.76$ km at 1.4 $M_\odot$, TM2$\omega\rho$-b, NL3$\omega\rho$-a and NL3$\omega\rho$-b EoSs are in the range of the observation with respect to radii in both $B_s = 10^{12}$ G and $B_s = 10^{15}$ G cases.

Considering the maximum mass and the radius at 2.072 $M_\odot$, only TM2$\omega\rho$-b EoS is in the range of the observation.

However, NL3-a, NL3-b, NL3$\omega\rho$-a, NL3$\omega\rho$-b, DDME2-a and DDME2-b EoSs are not in the range of the observation with respect to radius, but their masses surpasses twice the two-solar-mass.

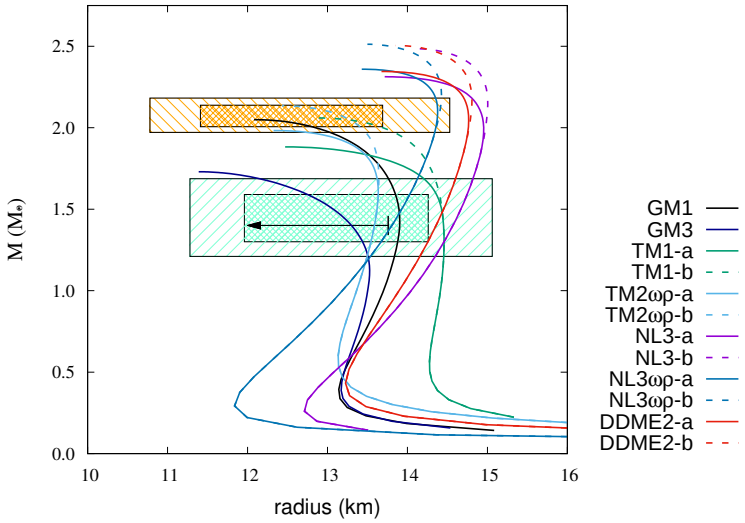

Figure 5.4: Same as Fig. 5.1, but with magnetic fields ($B_0 = 2.5 \times 10^{18}$ G, $B_S = 10^{12}$ G).

Table 5.4: Same as Table 5.1, but with magnetic fields ($B_0 = 2.5 \times 10^{18}$ G, $B_s = 1 \times 10^{12}$ G).

EoS	M_{max} ($M_\odot$)	$R_{2.072M_\odot}$ (km)	$R_{1.4M_\odot}$ (km)
GM1	2.049	—	13.90
GM3	1.730	—	13.32
TM1-a	1.882	—	14.46
TM1-b	2.060	—	14.44
TM2$\omega\rho$-a	1.978	—	13.58
TM2$\omega\rho$-b	2.135	13.17	13.58
NL3-a	2.313	14.93	14.52
NL3-b	2.486	14.99	14.52
NL3$\omega\rho$-a	2.359	14.37	13.69
NL3$\omega\rho$-b	2.512	14.38	13.69
DDME2-a	2.345	14.77	14.26
DDME2-b	2.505	14.79	14.26

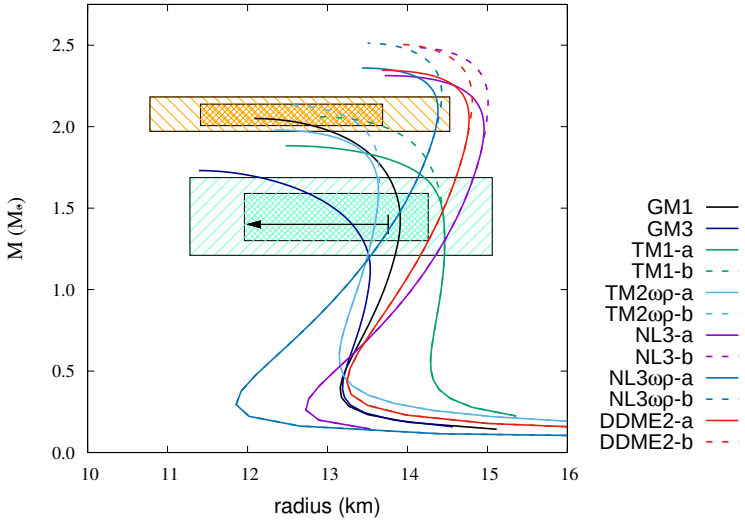

Figure 5.5: Same as Fig. 5.1, but with magnetic fields ($B_0 = 2.5 \times 10^{18}$ G, $B_S = 10^{15}$ G).

Table 5.5: Same as Table 5.1, but with magnetic fields ($B_0 = 2.5 \times 10^{18}$ G, $B_s = 1 \times 10^{15}$ G).

EoS	M_{max} ($M_\odot$)	$R_{2.072M_\odot}$ (km)	$R_{1.4M_\odot}$ (km)
GM1	2.050	—	13.91
GM3	1.731	—	13.32
TM1-a	1.883	—	14.45
TM1-b	2.060	—	14.45
TM2$\omega\rho$-a	1.979	—	13.58
TM2$\omega\rho$-b	2.135	13.17	13.58
NL3-a	2.313	14.93	14.53
NL3-b	2.487	14.99	14.53
NL3$\omega\rho$-a	2.360	14.38	13.70
NL3$\omega\rho$-b	2.513	14.39	13.70
DDME2-a	2.345	14.77	14.27
DDME2-b	2.505	14.80	14.27

MR relations and the details (Maximum masses, radii at 1.4 $M_\odot$, and radii at 2.072 $M_\odot$) with the magnetic field strength $B_0 = 3 \times 10^{18}$ G are shown in Fig. 5.6 – 5.7 and Table 5.6 – 5.7.

In the case of $B_s = 10^{12}$ G are shown in Fig. 5.6 and Table 5.6. All EoSs except GM3 and TM1-a EoSs give masses over the two-solar-mass. Moreover, considering the upper limit of radius $R = 13.76$ km at 1.4 $M_\odot$, TM2$\omega\rho$-a and TM2$\omega\rho$-b EoSs are in the range of the observation concerning radius. Moreover, considering the radius at 2.072 $M_\odot$, TM2$\omega\rho$-a and TM2$\omega\rho$-b EoSs are in the range of the observation concerning radius.

As for the $B_0 = 3 \times 10^{18}$ G and $B_s = 10^{15}$ G case, the results are shown in Fig. 5.7 and Table 5.7. Here, also EoSs except GM3 and TM1-a EoSs give masses over the two-solar-mass. Again, considering the upper limit of radius $R = 13.76$ km at 1.4 $M_\odot$, TM2$\omega\rho$-a and TM2$\omega\rho$-b EoSs are in the range of the observation concerning radius. Moreover, considering the radius at 2.072 $M_\odot$, TM2$\omega\rho$-a and TM2$\omega\rho$-b EoSs are in the range of the observation concerning radius.

However, GM1 and TM1-b EoSs are in the range of the observation concerning radius at 2.072 $M_\odot$ and surpass 2 $M_\odot$.

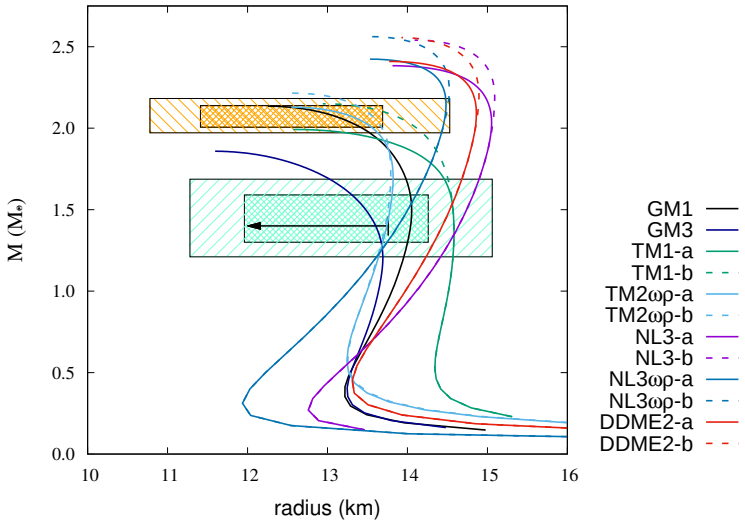

Figure 5.6: Same as Fig. 5.1, but with magnetic fields ($B_0 = 3 \times 10^{18}$ G, $B_S = 10^{12}$ G).

Table 5.6: Same as Table 5.1, but with magnetic fields ($B_0 = 3 \times 10^{18}$ G, $B_s = 1 \times 10^{12}$ G).

EoS	M_{max} ($M_\odot$)	$R_{2.072M_\odot}$ (km)	$R_{1.4M_\odot}$ (km)
GM1	2.135	13.11	14.04
GM3	1.858	—	13.61
TM1-a	1.992	—	14.58
TM1-b	2.149	13.86	14.58
TM2$\omega\rho$-a	2.129	13.32	13.76
TM2$\omega\rho$-b	2.215	13.56	13.72
NL3-a	2.383	15.05	14.69
NL3-b	2.540	15.09	14.68
NL3$\omega\rho$-a	2.424	14.48	13.91
NL3$\omega\rho$-b	2.562	14.45	13.91
DDME2-a	2.410	14.86	14.44
DDME2-b	2.556	14.86	14.44

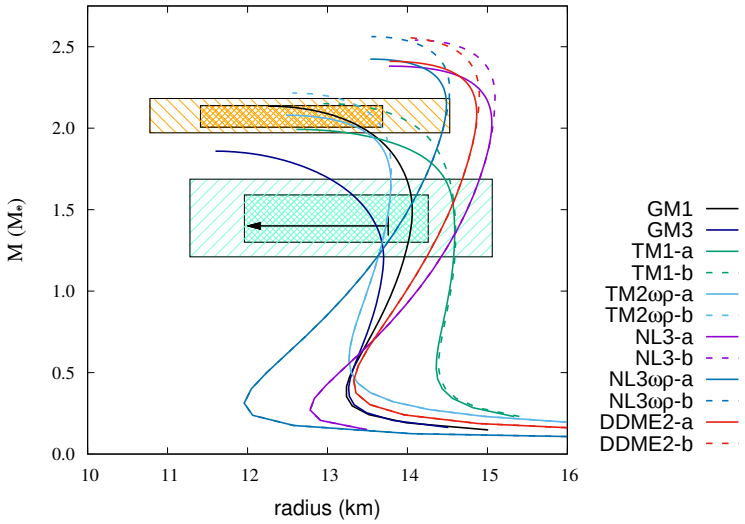

Figure 5.7: Same as Fig. 5.1, but with magnetic fields ($B_0 = 3 \times 10^{18}$ G, $B_S = 10^{15}$ G).

Table 5.7: Same as Table 5.1, but with magnetic fields ($B_0 = 3 \times 10^{18}$ G, $B_s = 1 \times 10^{15}$ G).

EoS	M_{max} ($M_\odot$)	$R_{2.072M_\odot}$ (km)	$R_{1.4M_\odot}$ (km)
GM1	2.135	13.11	14.05
GM3	1.859	—	13.62
TM1-a	1.993	—	14.59
TM1-b	2.150	13.86	14.60
TM2$\omega\rho$-a	2.079	12.76	13.72
TM2$\omega\rho$-b	2.215	13.56	13.72
NL3-a	2.381	15.05	14.69
NL3-b	2.541	15.09	14.69
NL3$\omega\rho$-a	2.424	14.46	13.91
NL3$\omega\rho$-b	2.562	14.45	13.91
DDME2-a	2.410	14.87	14.44
DDME2-b	2.557	14.86	14.44

5.4 MR relation of EoS with rotation and magnetic fields

Finally, the MR relations are calculated in the presence of both rotation and magnetic fields. This case with both rotation and magnetic fields is considered here because of the emergency of a millisecond magnetar in the occasion of a neutron star merger [75], though it is not so common.

The MR relations with rotation ($\Omega = 6 \times 10^2$ Hz) and magnetic fields ($B_0 = 2.5 \times 10^{18}$ G, $B_s = 10^{12}$ G) are shown in Fig. 5.8. Maximum masses of neutron stars, two

kinds of radius and eccentricity with both rotation ($\Omega = 6 \times 10^2$ Hz) and magnetic fields ($B_0 = 2.5 \times 10^{18}$ G, $B_s = 10^{12}$ G) are shown in Table 5.8.

Also, the MR relations with rotation ($\Omega = 6 \times 10^2$ Hz) and magnetic fields ($B_0 = 2.5 \times 10^{18}$ G, $B_s = 10^{15}$ G) are shown in Fig. 5.9. Maximum masses of neutron stars, two kinds of radius and eccentricity with both rotation ($\Omega = 6 \times 10^2$ Hz) and magnetic fields ($B_0 = 2.5 \times 10^{18}$ G, $B_s = 10^{15}$ G) are shown in Table 5.9.

EoSs except GM3, TM1-a, and TM2$\omega\rho$-a EoSs give masses over twice the solar mass in the presence of both rotation and magnetic fields (in the case of both $B_s = 10^{12}$ G and $B_s = 10^{15}$). For TM2$\omega\rho$-b, NL3$\omega\rho$-a and NL3$\omega\rho$-b EoSs, surpasses 2.072 $M_\odot$ and meet the observation with respect to radius ($R \leq 13.76$ km in 1.4 $M_\odot$) in both case of $B_s = 10^{12}$ G and $B_s = 10^{15}$ G. Moreover, considering the radius at 2.072 $M_\odot$, only TM2$\omega\rho$-b EoS is in the range of the observation concerning radius.

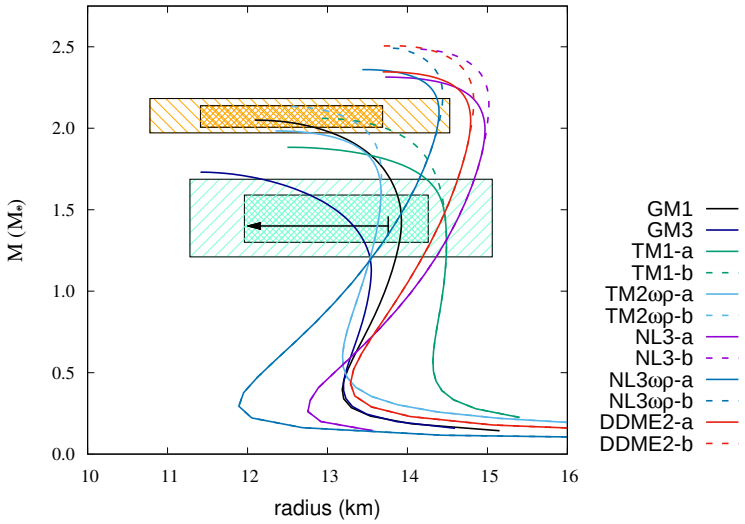

Figure 5.8: Same as Fig. 5.1, but with both rotation (6×10^2 Hz) and magnetic fields ($B_0 = 2.5 \times 10^{18}$ G, $B_S = 10^{12}$ G).

Table 5.8: Same as Table 5.2, but with both rotation ($\Omega = 6 \times 10^2$ Hz) and magnetic fields ($B_0 = 2.5 \times 10^{18}$ G, $B_S = 10^{12}$ G).

EoS	M_{max} ($M_\odot$)	$R^e_{2.072M_\odot}$ (km)	$R^p_{1.4M_\odot}$ (km)	$R^e_{1.4M_\odot}$ (km)	$e_{1.4}$
GM1	2.050	—	13.88	13.92	0.997
GM3	1.730	—	13.29	13.34	0.996
TM1-a	1.883	—	14.41	14.47	0.996
TM1-b	2.061	—	14.41	14.47	0.996
TM2$\omega\rho$-a	1.979	—	13.53	13.61	0.994
TM2$\omega\rho$-b	2.135	13.19	13.53	13.61	0.994
NL3-a	2.314	14.94	14.50	14.54	0.998
NL3-b	2.487	15.00	14.50	14.54	0.998
NL3$\omega\rho$-a	2.360	14.39	13.66	13.72	0.996
NL3$\omega\rho$-b	2.513	14.40	13.66	13.72	0.996
DDME2-a	2.346	14.79	14.23	14.30	0.995
DDME2-b	2.505	14.82	14.23	14.30	0.995

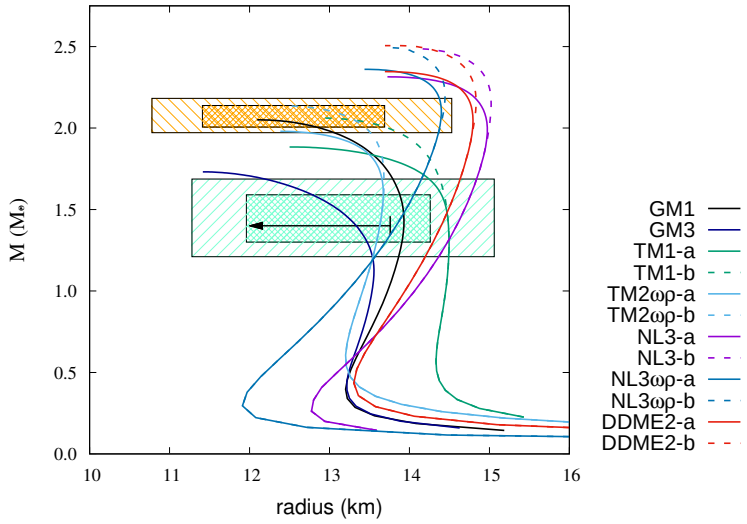

Figure 5.9: Same as Fig. 5.1, but with both rotation (6×10^2 Hz) and magnetic fields ($B_0 = 2.5 \times 10^{18}$ G, $B_S = 10^{15}$ G).

Table 5.9: Same as Table 5.2, but with both rotation ($\Omega = 6 \times 10^2$ Hz) and magnetic fields ($B_0 = 2.5 \times 10^{18}$ G, $B_S = 10^{15}$ G).

EoS	M_{max} ($M_\odot$)	$R^e_{2.072M_\odot}$ (km)	$R^p_{1.4M_\odot}$ (km)	$R^e_{1.4M_\odot}$ (km)	$e_{1.4}$
GM1	2.050	—	13.89	13.93	0.997
GM3	1.731	—	13.29	13.34	0.996
TM1-a	1.884	—	14.42	14.48	0.996
TM1-b	2.061	—	14.42	14.48	0.996
TM2$\omega\rho$-a	1.980	—	13.54	13.62	0.994
TM2$\omega\rho$-b	2.136	13.19	13.54	13.62	0.994
NL3-a	2.314	14.95	14.51	14.54	0.998
NL3-b	2.487	14.96	14.51	14.54	0.998
NL3$\omega\rho$-a	2.360	14.34	13.67	13.73	0.996
NL3$\omega\rho$-b	2.513	14.41	13.67	13.73	0.996
DDME2-a	2.346	14.79	14.23	14.31	0.995
DDME2-b	2.506	14.82	14.23	14.31	0.995

Chapter 6

Discussion

6.1 Two-solar-mass problem

In Chapter 5, MR relations have been calculated for the 12 EoSs. Calculated maximum masses ($M_\odot$) are shown in Table 6.1. Maximum masses for NL3-a, NL3-b, NL3$\omega\rho$-a, NL3$\omega\rho$-b, DDME2-a and DDME2-b EoSs are over twice the solar mass with neither rotation nor magnetic fields.

Masses calculated by GM1, TM1-b and TM2$\omega\rho$-b EoSs with magnetic fields ($B_0 = 2.5 \times 10^{18}$ G and $B_0 = 3 \times 10^{18}$ G) become over twice the solar mass. In Ref. [76], MR relations were calculated with magnetic fields of $B_0 = 3.1 \times 10^{18}$ G. Using GM1 EoS, they obtained a mass of over twice the solar mass. Their results are consistent with ours. Masses are calculated by all 12 EoSs with rotation of $\Omega = 6 \times 10^2$ Hz ($\Omega = 0.002\,\mathrm{km}^{-1}$ in gravitational unit), for which about 0.001 $M_\odot$ increase is seen.

Table 6.1: Maximum masses ($M_\odot$) for 12 EoSs with neither rotation nor magnetic fields (M), with only rotation (M_{rot}; $\Omega = 6 \times 10^2$ Hz), with only magnetic fields ($M_{mag_{2.5}}$; $B_0 = 2.5 \times 10^{18}$ G, $B_s = 10^{12}$ G), with only strong magnetic fields (M_{mag_3}; $B_0 = 3 \times 10^{18}$ G, $B_s = 10^{12}$ G), and rotation ($M_{rot,mag_{2.5}}$; $\Omega = 6 \times 10^2$ Hz) and magnetic fields ($B_0 = 2.5 \times 10^{18}$ G, $B_s = 10^{12}$ G).

EoS	M	M_{rot}	$M_{mag_{2.5}}$	M_{mag_3}	$M_{rot,mag_{2.5}}$
GM1	1.784	1.785	2.049	2.135	2.050
GM3	1.299	1.300	1.730	1.858	1.730
TM1-a	1.540	1.541	1.882	1.992	1.883
TM1-b	1.787	1.788	2.060	2.149	2.061
TM2$\omega\rho$-a	1.663	1.664	1.978	2.129	1.979
TM2$\omega\rho$-b	1.891	1.891	2.135	2.215	2.135
NL3a	2.122	2.123	2.313	2.383	2.314
NL3b	2.336	2.337	2.486	2.540	2.487
NL3$\omega\rho$-a	2.175	2.176	2.359	2.424	2.360
NL3$\omega\rho$-b	2.372	2.372	2.512	2.562	2.513
DDME2-a	2.161	2.162	2.345	2.410	2.346
DDME2-b	2.360	2.361	2.505	2.556	2.505

6.2 Radius at 1.4 $M_\odot$

The upper limit radius at 1.4 $M_\odot$ is determined by the observation of the GW170817 gravitational wave event. The obtained radius at $M = 1.4\ M_\odot$ is 13.6 km [19], and also another source reports the upper limit radius as 13.76 km [20]. In this thesis, the largest radius at 1.4 $M_\odot$ (13.76 km) is taken into account. The radius of the pulsar observed by NICER observations is $13.02^{+1.24}_{-1.06}$ km at $M = 1.44^{+0.15}_{-0.14}\ M_\odot$ [22]. Also, the radius of the pulsar observed by NICER and XMM-Newton observations is $12.39^{+1.30}_{-0.98}$ at $M = 2.072^{+0.067}_{-0.066}\ M_\odot$ [14, 15, 50, 51].

The validity of each EoS in this respect is discussed here. The neutron star radii at 1.4 $M_\odot$ are summarized in Table 6.2, which shows that radii predicted by TM1-a, TM1-b, NL3-a, NL3-b, DDME2-a and DDME2-b EoSs are over 13.76 km in any case. For the GM1 EoS, the radius becomes smaller than 13.76 km only in the case of no magnetic fields. For the GM3 EoS, there are no solution in the case with only rotation, but the radius is smaller than 13.76 km in the case with magnetic fields. As for TM2$\omega\rho$-a and TM2$\omega\rho$-b EoSs, radii become smaller than 13.76 km in all the cases. For NL3$\omega\rho$-a and NL3$\omega\rho$-b EoSs, radii are in the range of observation in the case except with strong magnetic fields ($B_0 = 3 \times 10^{18}$ G).

Considering the observed maximum mass 2.072 $M_\odot$ and the upper limit of the radius 13.76 km at 1.4 $M_\odot$, TM2$\omega\rho$-a and TM2$\omega\rho$-b EoSs are the most suitable of the 12 EoSs in the case with magnetic fields or with both rotation and magnetic fields. Also, NL3$\omega\rho$-a and NL3$\omega\rho$-b EoSs without strong magnetic fields ($B_0 = 3 \times 10^{18}$ G) meet the requirements of observations.

Table 6.2: Radius at M=1.4 $M_\odot$ for each EoS. Each row indicates as follows, $R_{1.4}$; radius without rotation or magnetic fields, $R^e_{1.4rot}$; equator radius with rotation (6×10^2 Hz), $R_{1.4mag2.5}$; radius with magnetic fields ($B_0 = 2.5 \times 10^{18}$ G, $B_S = 10^{12}$ G), $R_{1.4mag3}$; radius with magnetic fields ($B_0 = 3 \times 10^{18}$ G, $B_S = 10^{12}$ G), and $R^e_{1.4rot\&mag}$; equator radius with both rotation ($\Omega = 0.002$ km^{-1}) and magnetic fields ($B_0 = 2.5 \times 10^{18}$ G) for each EoS.

EoS	R **1.4**	R^e **1.4 rot**	R **1.4 mag2.5**	R **1.4 mag3**	R^e **1.4 rot&mag**
GM1	13.49	13.51	13.90	14.04	13.92
GM3	—	—	13.32	13.61	13.34
TM1-a	14.07	14.09	14.46	14.58	14.47
TM1-b	14.10	14.13	14.46	14.58	14.47
TM2$\omega\rho$-a	13.24	13.28	13.58	13.76	13.61
TM2$\omega\rho$-b	13.23	13.27	13.58	13.72	13.61
NL3-a	14.35	14.37	14.52	14.69	14.54
NL3-b	14.35	14.37	14.52	14.68	14.54
NL3$\omega\rho$-a	13.49	13.52	13.69	13.91	13.72
NL3$\omega\rho$-b	13.49	13.52	13.69	13.91	13.72
DDME2-a	14.08	14.12	14.26	14.44	14.30
DDME2-b	14.08	14.12	14.26	14.44	14.30

6.3 Radius at 2.072 $M_\odot$

The radius of the pulsar observed by NICER and XMM-Newton observations is $12.39^{+1.30}_{-0.98}$ km at $M = 2.072^{+0.067}_{-0.066}$ $M_\odot$ [15]. This pulsar is the heaviest observed one and the radius is known by observations. Here, we discuss the radius at 2.072 $M_\odot$.

The radii calculated by 12 EoSs are shown in Table 6.3. From the observation, the radii should be in the range of 11.41 km $\leq R \leq$ 13.69 km. For GM3, TM1-a, TM1-b, NL3-a, NL3-b, NL3$\omega\rho$-a, NL3$\omega\rho$-b, DDME2-a and DDME2-b EoSs, there are no corresponding radii within the range. As for GM1 and TM2$\omega\rho$-a EoSs, the radii become smaller in the case with strong magnetic fields ($B_0 = 3 \times 10^{18}$ G). For TM2$\omega\rho$-b EoS, the radius becomes smaller in the case with magnetic fields, or with both rotation and magnetic fields.

Considering the observed maximum mass 2.072 $M_\odot$, the upper limit of the radius 13.76 km at 1.4 $M_\odot$, and radius $12.39^{+1.30}_{-0.98}$ km at 2.072 $M_\odot$, TM2$\omega\rho$-a EoS with strong magnetic fields ($B_0 = 3 \times 10^{18}$ G), and TM2$\omega\rho$-b EoS with magnetic fields or with both rotation and magnetic fields meet the requirements of observations.

Table 6.3: Radius at M=2.072 $M_\odot$ for each EoS. Each row indicates as follows, $R_{2.072}$; radius without rotation or magnetic fields, $R^e_{2.072rot}$; equator radius with rotation ($\Omega = 6 \times 10^2$ Hz), $R_{2.072mag2.5}$; radius with magnetic fields ($B_0 = 2.5 \times 10^{18}$ G, $B_S = 10^{12}$ G), $R_{2.072mag3}$; radius with magnetic fields ($B_0 = 3 \times 10^{18}$ G, $B_S = 10^{12}$ G), and $R^e_{2.072rot\&mag}$; equator radius with both rotation ($\Omega = 6 \times 10^2$ Hz) and magnetic fields ($B_0 = 2.5 \times 10^{18}$ G) for each EoS.

EoS	R **2.072**	R^e **2.072 rot**	R **2.072 mag2.5**	R **2.072 mag3**	R^e **2.072 rot&mag**
GM1	—	—	—	13.11	—
GM3	—	—	—	—	—
TM1-a	—	—	—	—	—
TM1-b	—	—	—	13.86	—
TM2$\omega\rho$-a	—	—	—	13.32	—
TM2$\omega\rho$-b	—	—	13.17	13.56	13.19
NL3-a	14.45	14.46	14.93	15.05	14.94
NL3-b	14.79	14.80	14.99	15.09	15.00
NL3$\omega\rho$-a	14.05	14.06	14.37	14.48	14.39
NL3$\omega\rho$-b	14.18	14.20	14.38	14.45	14.40
DDME2-a	14.44	14.45	14.77	14.86	14.79
DDME2-b	14.58	14.61	14.79	14.86	14.82

6.4 Constraining masses and radii from two observed pulsars

In this Sect. 6.4, we discuss two observed pulsars, namely. PSR J0030 + 0451 and PSR J0740 + 6620. The radius of the pulsar PSR J0030 + 0451 observed by NICER observations is $13.02^{+1.24}_{-1.06}$ km at $M = 1.44^{+0.15}_{-0.14}$ $M_\odot$ [22]. Also, the radius of the pulsar PSR J0740 + 6620 observed by NICER and XMM-Newton observations is $12.39^{+1.30}_{-0.98}$ at $M = 2.072^{+0.067}_{-0.066}$ $M_\odot$ [15].

The following EoSs go through 68% credibility with respect to the range of masses and radii from observation of PSR J0740 + 6620 and PSR J0030 + 0451.

In the case with magnetic fields ($B_0 = 2.5 \times 10^{18}$ G, $B_s = 10^{12}$ G), GM1 and TM2$\omega\rho$-b EoSs are in the range from the limit of observations. Also in the case with magnetic fields ($B_0 = 2.5 \times 10^{18}$ G, $B_s = 10^{15}$ G), GM1 and TM2$\omega\rho$-b EoSs are in the range from the limit of observations.

For the case with magnetic fields ($B_0 = 3 \times 10^{18}$ G, $B_s = 10^{12}$ G), GM1, TM2$\omega\rho$-a, and TM2$\omega\rho$-b EoSs are in the range from the limit of observations. As for the case with magnetic fields ($B_0 = 3 \times 10^{18}$ G, $B_s = 10^{15}$ G), also, GM1, TM2$\omega\rho$-a, and TM2$\omega\rho$-b EoSs are in the range of observations.

Considering the results, the magnetic fields are necessary to go through the limit of observations.

6.5 Comparison of the case with/without hyperons with magnetic fields

Here, we compare the case without or with hyperons for GM1 EoS [23]. Fig. 6.1 shows the comparison of MR relations for GM1 EoS with hyperons (purple line) and without ones (black line), and MR relations including magnetic fields (dashed lines) or not (solid lines) with the magnetic field. Here, $B_0 = 2.5 \times 10^{18}$ G and $B_s = 10^{12}$ G are employed. The free parameter of magnetic fields is taken as $\alpha = 0.05$ and $\gamma = 2$, whose values are standard in the literature [70]. The orange and light green dashed areas indicate pulsars PSR J0740+6620 and PSR J0030+0451, respectively. The thick area shows the one within 68% credibility and the thinner area shows the one within 90% credibility. Each EoS curve must go through these areas if they satisfy the observational constraints. The arrow indicates the upper limit of radius for $1.4\,M_\odot$ from the gravitational wave event GW170817. The effect of a strong magnetic field is obviously seen in Figure 6.1. The strong magnetic field makes mass larger irrespective of hyperon-inclusion or not. However, inclusion of hyperons makes mass smaller; this is the hyperon puzzle. The maximum masses and the radii at $1.4\,M_\odot$ with or without magnetic fields for GM1 EoS are tabulated in Table 6.4. The GM1 EoS with only nucleons gives mass more than $2\,M_\odot$, regardless of the presence of magnetic fields. The GM1 EoS with hyperons gives mass over $2\,M_\odot$ in the case a strong magnetic field. The radii without magnetic fields are within the observed range, regardless of the case whether hyperons are included or not, while radii with magnetic fields are larger than those allowed by the observation. The maximum mass becomes smaller in the case where hyperons are included. The maximum mass increases in the case where the magnetic field is included in both the case of only nucleons and the case of hyperons included. The average radius decreases in the case where hyperons are included. It increases in the case where a strong magnetic field is included.

Table 6.4: Maximum masses without magnetic fields (M), maximum masses with magnetic fields (M_{mag}) radii at $1.4M_\odot$ without magnetic fields (R) and radii at $1.4M_\odot$ with magnetic fields (R_{mag}) for GM1 EoS with/without hyperons.

EoS	$M(M_\odot)$	$M_{mag}(M_\odot)$	R(km)	R_{mag}(km)
GM1 (without hyperons)	2.38	2.47	13.7	14.0
GM1 (with hyperons)	1.78	2.05	13.5	13.9

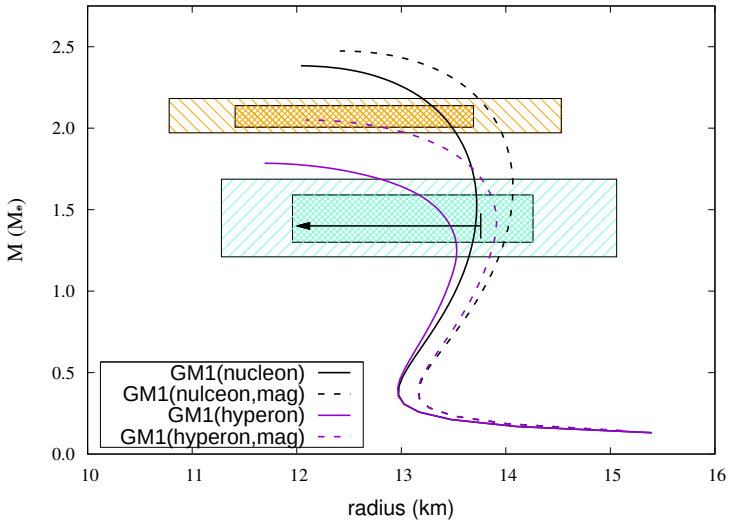

Figure 6.1: MR relations of only nucleons (purple solid line) and those including hyperons (black solid line) for GM1 EoS. Each dashed line indicates the case with the magnetic field strength ($B_0 = 2.5 \times 10^{18}$ G, $\alpha = 0.05$ and $\gamma = 2$). The unstable region in each EoS is not shown. The orange and light green dashed areas indicate pulsars PSR J0740+6620 and PSR J0030+0451 (68% (thick) and 90% (thin) credibility), respectively. The arrow indicates the upper limit of radius for $1.4\,M_\odot$ from the gravitational wave event GW170817.

6.6 Magnetic fields with different forms

In this section, we discuss free parameters α and γ of magnetic fields. First, we consider the case of changing free parameters α and γ of magnetic fields of GM1 EoSto see how it affects mass and radius in Sect. 6.6.1. Next in Sect. 6.6.2, we discuss searching optimum α and γ of the magnetic field for 12 EoSs.

6.6.1 Change of α and γ in magnetic fields

In this Sect. 6.6.1 and Sect. 6.6.2, $B(\rho)$ in Eq. (4.28) is also employed for magnetic fields, but this time α and γ parameters are changed as free parameters.

We consider GM1 EoS in this Sect. 6.6.1. First, we change α parameters and next change γ to see how it works on mass and radius of a neutron star.

The $B(\rho)$ as a function of baryon number density ρ for various α parameters is shown in Fig. 6.2. Each line indicates a magnetic field with $B_0 = 2.5 \times 10^{18}$ G, $B_s = 10^{12}$ G, and $\gamma = 2$. In Fig. 6.2, as α becomes larger, the strength of the magnetic field B changes more abruptly. The MR relation for GM1 EoS by changing the α parameter is shown in Fig. 6.3. As α is increased, the maximum mass increases monotonically. For $\alpha > 0.06$, the maximum mass surpasses the observed neutron star maximum mass ($2.072\,M_\odot$). It

is evident from the figure that as α is made larger, the maximum mass of MR relation gets larger. Furthermore, the radius at $1.4\,M_\odot$ gets larger in the case where α gets larger.

Next, the magnetic field $B(\rho)$ as a function of baryon number density ρ for various γ parameters is shown in Figure 6.4. Each line indicates a magnetic field with $B_0 = 2.5\times10^{18}$ G and $\alpha = 0.05$. For $\rho > 0.3$ fm^{-3}, $B(\rho)$ is almost constant $B_0 = 2.5 \times 10^{18}$ G. Here, magnetic field strengths at saturation density ρ_0 are given as $B(\rho_0) = 1.23 \times 10^{17}$ G for any value of γ. Magnetic field strengths $B(\rho_0)$ at saturation density ρ_0 are shown in Table 6.7.

The maximum mass, radius at $1.4\,M_\odot$, and radius at $2.072\,M_\odot$ by changing α and γ in Eq.(4.28) are shown in Tables G.3–G.2 for each EoSs. The MR relations by changing α and γ are given in Figures G.3–G.2 for those EoSs with various incompressibility, which satisfy the observational constraints.

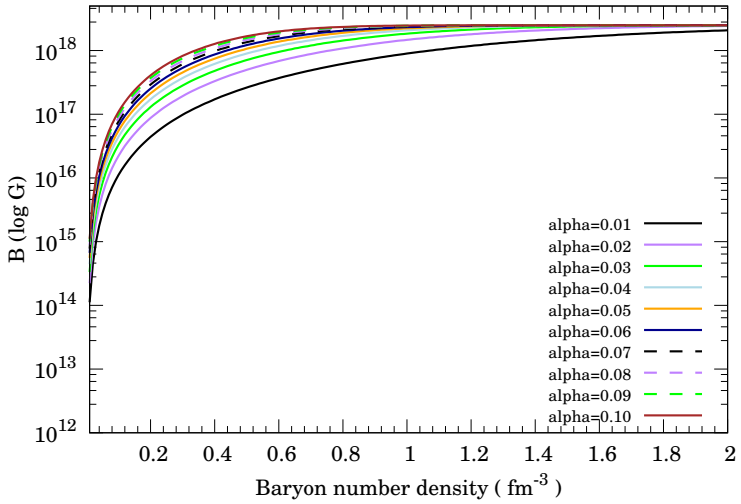

Figure 6.2: B(ρ) as a function of α with $B_0 = 2.5\times10^{18}$ G and $\gamma = 2$. The colored lines represent the following: black (solid line); magnetic fields $B(\rho)$ with $\alpha = 0.01$, purple (solid line); magnetic fields $B(\rho)$ with $\alpha = 0.02$, green (solid line); magnetic fields $B(\rho)$ with $\alpha = 0.03$, light blue (solid line); magnetic fields $B(\rho)$ with $\alpha = 0.04$, orange (solid line); magnetic fields $B(\rho)$ with $\alpha = 0.05$, dark blue (solid line); magnetic fields $B(\rho)$ with $\alpha = 0.06$, black (dashed line); magnetic fields $B(\rho)$ with $\alpha = 0.07$, purple (dashed line); magnetic fields $B(\rho)$ with $\alpha = 0.08$, green (dashed line); magnetic fields $B(\rho)$ with $\alpha = 0.09$, brown (solid line); magnetic fields $B(\rho)$ with $\alpha = 0.10$.

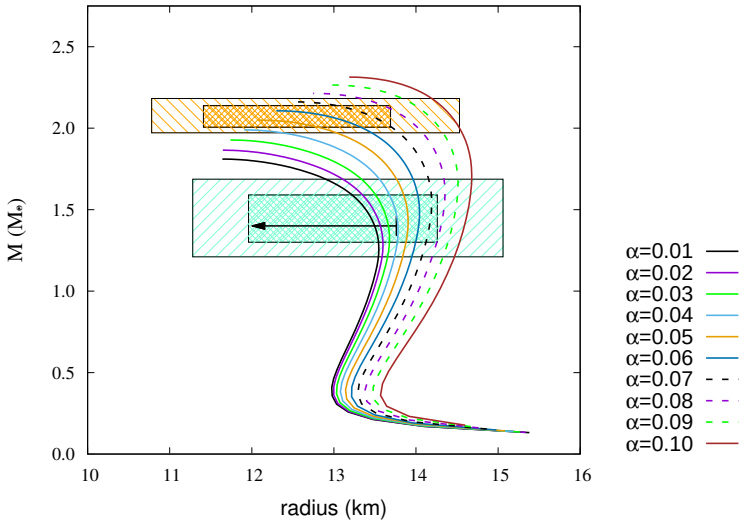

Figure 6.3: MR relation for GM1 EoS of changing α in magnetic fields. The colored lines of MR relations are the same as in Fig. 6.3. Each line indicates an inclusion of the magnetic field ($B_0 = 2.5 \times 10^{18}$ G, $B_s = 10^{12}$ G). Here, $\gamma = 2$ is employed. The arrow and colored hatched areas are the same as in Figure 6.1.

Table 6.5: Maximum mass M_{mag} ($M_\odot$), radius of 1.4 $M_\odot$ $R_{1.4M_\odot}$ (km), and radius of 1.4 $M_\odot$ $R_{2.072M_\odot}$ (km) by changing γ in the magnetic field for GM1 EoS.

α	M_{max} ($M_\odot$)	$R_{1.4M_\odot}$ (km)	$R_{2.072M_\odot}$ (km)
0.01	1.810	13.50	—
0.02	1.867	13.57	—
0.03	1.927	13.66	—
0.04	1.989	13.78	—
0.05	2.049	13.90	—
0.06	2.107	14.03	12.93
0.07	2.161	14.16	13.47
0.08	2.214	14.30	13.85
0.09	2.265	14.44	14.16
0.10	2.313	14.59	14.43

Next, the magnetic field $B(\rho)$ as a function of baryon number density ρ_B for various γ parameters is shown in Fig. 6.4. For $\rho > 0.3$ fm^{-3}, $B(\rho)$ is almost constant $B_0 = 2.5 \times 10^{18}$ G. Here magnetic field strengths at saturation density ρ_0 is given as $B(\rho_0) = 1.23 \times 10^{17}$ G for any value of γ.

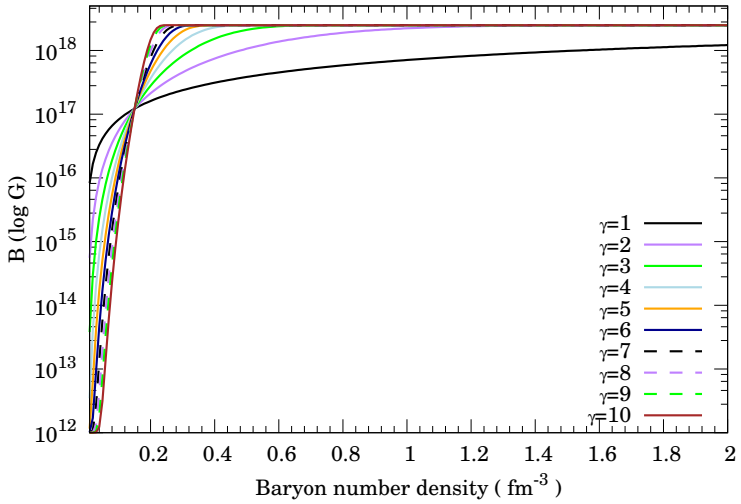

Figure 6.4: $B(\rho)$ as a function of γ with $\alpha = 0.03$, $B_0 = 2.5 \times 10^{18}$ G and $B_s = 10^{12}$ G. The colored lines represent the following: black (solid line); magnetic fields $B(\rho)$ with $\gamma = 1$, purple (solid line); magnetic fields $B(\rho)$ with $\gamma = 2$, green (solid line); magnetic fields $B(\rho)$ with $\gamma = 3$, light blue (solid line); magnetic fields $B(\rho)$ with $\gamma = 4$, orange (solid line); magnetic fields $B(\rho)$ with $\gamma = 5$, yellow (solid line); magnetic fields $B(\rho)$ with $\gamma = 6$, dark blue (solid line); magnetic fields $B(\rho)$ with $\gamma = 7$, red (solid line); magnetic fields $B(\rho)$ with $\gamma = 8$, purple (dashed line); magnetic fields $B(\rho)$ with $\gamma = 9$, brown (solid line); magnetic fields $B(\rho)$ with $\gamma = 10$.

Figure 6.5 shows the MR relations for the GM1 EoS by changing γ parameter in the magnetic field. Here, $\alpha = 0.05$ is employed. The unstable region in each EoS is not shown. The orange and light green dashed areas indicate pulsars PSR J0740+6620 and PSR J0030+0451 (68% (thick) and 90% (thin) credibility), respectively. The arrow indicates the upper limit of radius for $1.4\,M_\odot$ from the gravitational wave event GW170817. Each line indicates an inclusion of the magnetic field ($B_0 = 2.5 \times 10^{18}$ G, $B_s = 10^{12}$ G). As γ is increased, the maximum mass increases up to $3.5\,M_\odot$ approximately at $\gamma = 10$. For $\gamma > 3$ the maximus surpasses the observed maximum masses ($2.072\,M_\odot$).

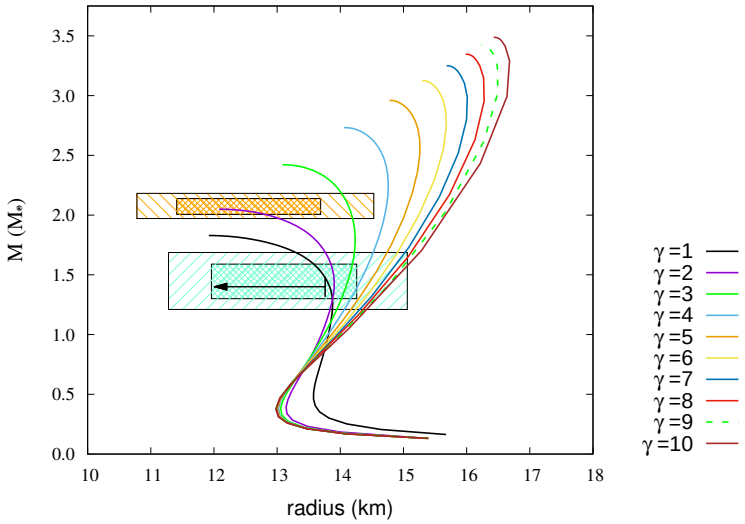

Figure 6.5: MR relations for GM1 EoS by changing γ in magnetic fields with magnetic fields ($B_0 = 2.5 \times 10^{18}$ G, $B_s = 10^{12}$ G, and $\alpha = 0.05$). The colors of the line of MR relations are the same as in Fig. 6.4. The arrow and colored hatched areas are the same as in Fig. 6.1.

The maximum masses ($M_\odot$), radii (km) at average mass (1.4 $M_\odot$) and radii (km) at 2.072 $M_\odot$ by changing γ in the magnetic field for GM1 EoS is shown in Table 6.6. Here, $B_0 = 2.5 \times 10^{18}$ G, $B_s = 10^{12}$ G, and $\alpha = 0.02$ are adopted. For the cases of $\gamma < 2$, the maximum mass increases monotonically and surpasses twice the solar mass by changing γ. Due to observation of GW170817, radius should be below 13.76 km. For GM1 EoS, none of the radius is within the range of the observation by changing γ in the magnetic field.

Table 6.6: Maximum mass M_{max} ($M_\odot$), radius of 1.4 $M_\odot$ ($R_{1.4M_\odot}$) (km), and radius of 2.072 $M_\odot$ ($R_{2.072M_\odot}$) (km) by changing γ in the magnetic field of GM1 EoS. Here, $\alpha = 0.05$ is adopted.

γ	M_{max} ($M_\odot$)	$R_{1.4M_\odot}$ (km)	$R_{2.072M_\odot}$ (km)
1	1.829	13.83	—
2	2.049	13.90	—
3	2.421	14.09	14.13
4	2.732	14.27	14.73
5	2.960	14.42	15.07
6	3.125	14.53	15.31
7	3.250	14.62	15.49
8	3.346	14.69	15.62
9	3.424	14.74	15.72
10	3.488	14.79	15.80

Table 6.7: Strengths of the magnetic field at saturation density $\rho_0 = 0.153$ fm^{-3} ($B(\rho_0)$ in unit of Gauss) for 12 EoSs with $B_0 = 2.5 \times 10^{18}$ G and $\gamma = 2$.

α	$B(\rho_0)$
0.01	2.59×10^{16}
0.02	5.05×10^{16}
0.03	7.79×10^{16}
0.04	9.90×10^{16}
0.05	1.23×10^{17}
0.06	1.47×10^{17}
0.07	1.70×10^{17}
0.08	1.93×10^{17}
0.09	2.16×10^{17}

6.6.2 Searching optimum α and γ in magnetic fields for each EoS

In this Sect. 6.6.2, we solve the Tolman–Oppenheimer–Volkov (TOV) equations to obtain masses and radii for 12 EoSs by changing α (0.01 – 0.10) and γ (1 – 10) parameters of magnetic fields freely. First, we show and discuss the results of MR relations with magnetic fields, which is $B_0 = 2.5 \times 10^{18}$ G and $B_s = 10^{12}$ G (pulsar). Next, we show and discuss the results of MR relations with magnetic fields, which is $B_0 = 2.5 \times 10^{18}$ G and $B_s = 10^{15}$ G (magnetar). For both $B_s = 10^{12}$ G and $B_s = 10^{15}$ G case, we consider two pattern of condition given by observations. In case (1), the MR relations are verified with respect to the constraints that maximum masses are within the range of observed masses over maximum mass 2.072 $M_\odot$ and the radii at 1.4 solar mass are less than 13.76 km. And in the case (2), the MR relations are verified with respect to the constraints that go through 68% credibility with respect to the range of masses and radii from observation of PSR J0740 + 6620 and PSR J0030 + 0451.

In the case without magnetic fields, only three EoSs (NL3a, NL3$\omega\rho$-a, and DDME2-a) barely satisfy the MR constraints (within 90% credibility for the maximum mass), but among them, only NL3$\omega\rho$-a satisfies the radius constraint at $1.4\,M_\odot$ ($K = 250.1$ MeV). It should be noted that DDME2 is a relatively soft EoS at nuclear saturation density, but it becomes harder in a higher density region.

As general features, the maximum mass becomes smaller when hyperons are included, but the maximum mass increases when the magnetic field is imposed in both the cases with only nucleons and with hyperons included. The average radius decreases when hyperons are included. It increases when a strong magnetic field is implemented.

(1) Changing α and γ ($B_s = 10^{12}$ G ; pulsar)

Here, we compare the case with magnetic fields ($B_0 = 2.5 \times 10^{18}$ G and $B_s = 10^{12}$ G). See Appendix G for Figures and Tables.

The MR relations of each EoSs with magnetic fields are shown in Fig. G.1 – G.12. For each EoS the maximum masses ($M_{\max}$), the radii at M=1.4 $M_\odot$, and radii at M = 2.072 $M_\odot$ are shown in Table G.1 – G.12.

(1-1) Considering M_{max}, $R_{2.072M_\odot}$, and $R_{1.4M_\odot}$

Considering the observed maximum mass 2.072 $M_\odot$, the upper limit of the radius 13.76 km at 1.4 $M_\odot$, and the radius at 2.072 $M_\odot$, the following EoSs with α and γ satisfied the limits above are shown in Table 6.8. Here, 4 EoSs (GM1, GM3, TM2$\omega\rho$-a, and TM2$\omega\rho$-b) are satisfying the limits from the observations.

Table 6.8: Free parameter γ, α, and reference of Figure and Table for each EoS satisfying the limits ($M_{max} \geq 2.072$, $R_{1.4M_\odot} < 13.76$, and in the range of $R_{2.072M_\odot}$) with $B_0 = 2.5 \times 10^{18}$ G and $B_s = 10^{12}$ G.

EoS	γ	α	Figure & Table
GM1	3	0.02	Figure G.3, Table G.3
	4	0.01	
GM3	3	0.04	Figure G.4, Table G.4
	4	0.02	
TM2$\omega\rho$-a	3	0.02	Figure G.11, Table G.11
	4	0.01	
TM2$\omega\rho$-b	2	0.04	Figure G.12, Table G.12
	2	0.05	
	2	0.06	
	3	0.02	
	3	0.03	
	4	0.01	

(1-2) Considering two observed pulsars

Next, we consider the limit from two pulsars that the masses and radii are observed. EoSs go through 68% credibility with respect to the range of masses and radii from observation of PSR J0740 + 6620 and PSR J0030 + 0451 are shown in Table 6.9. Here, 6 EoSs (DDME2-a, GM1, GM3, NL3$\omega\rho$-a, TM2$\omega\rho$-a, and TM2$\omega\rho$-b) are satisfying the limits from the observations.

Table 6.9: Free parametar γ, α, and the reference of Figure and Table for each EoS which a limit of the observation of two pulsars contains ($B_0 = 2.5\times10^{18}$ G, $B_s = 10^{12}$ G).

EoS	γ	α	Figures & Tables
DDME2-a	1	0.01	Figure G.1, Table G.1
	1	0.02	
	1	0.03	
	2	0.01	
GM1	2	0.05	Figure G.3, Table G.3
	2	0.06	
	2	0.07	
	3	0.02	
	3	0.03	
	3	0.04	
	4	0.01	
GM3	2	0.09	Figure G.4, Table G.4
	3	0.03	
	3	0.04	
	3	0.05	
	4	0.01	
	4	0.02	
	5	0.01	
NL3$\omega\rho$-a	1	0.01	Figure G.7, Table G.7
	2	0.01	
TM2$\omega\rho$-a	2	0.05	Figure G.11, Table G.11
	2	0.06	
	3	0.02	
	3	0.03	
	3	0.04	
	4	0.01	
TM2$\omega\rho$-b	2	0.03	Figure G.12, Table G.12
	2	0.04	
	2	0.05	
	2	0.06	
	2	0.07	
	3	0.01	
	3	0.02	
	3	0.03	
	4	0.01	

(2) changing α and γ ($B_s = 10^{15}$ G ; magnetar)

Here are the results of 12 EoSs with magnetic fields ($B_0 = 2.5 \times 10^{18}$ G, $B_s = 10^{15}$ G). We consider the difference from (i) the case of $B_s = 10^{12}$ G. See Appendix H for Figures and Tables.

The MR relations of each EoSs with magnetic fields are shown in Figures. H.1 – H.12. For each EoS the maximum mass ($M_{\rm max}$), the radius at $M = 1.4M_\odot$, and radius at $M = 2.072\,M_\odot$ are shown in Tables H.1 – H.12.

(2-1) Considering M_{max}, $R_{2.072M_\odot}$, and $R_{1.4M_\odot}$

Considering the observed maximum mass 2.072 $M_\odot$, the upper limit of the radius 13.76 km at 1.4 $M_\odot$, and the radius at 2.072 $M_\odot$, the following EoSs with α and γ satisfied the limits above are shown in Table 6.10. Here, 4 EoSs (GM1, GM3, TM2$\omega\rho$-a, and TM2$\omega\rho$-b) are satisfying the limits from the observations. These EoSs are same as Table 6.8, but additional case ($\gamma = 3$, $\alpha = 0.03$ for TM2$\omega\rho$-a EoS). This suggests that the parameter sets, α and γ, within the range of the condition of the observation changes by changing the surface of magnetic fields.

Table 6.10: Free parameter γ, α, and reference of Figure and Table for each EoS satisfying the limits ($M_{max} \geq 2.072$, $R_{1.4M_\odot} < 13.76$, and in the range of $R_{2.072M_\odot}$) with $B_0 = 2.5 \times 10^{18}$ G and $B_s = 10^{15}$ G.

EoS	γ	α	Figure & Table
GM1	3	0.02	Figure H.3, Table H.3
	4	0.01	
GM3	3	0.04	Figure H.4, Table H.4
	4	0.02	
TM2$\omega\rho$-a	3	0.02	Figure H.11, Table H.11
	3	0.03	
	4	0.01	
TM2$\omega\rho$-b	2	0.04	Figure H.12, Table H.12
	2	0.05	
	2	0.06	
	3	0.02	
	3	0.03	
	4	0.01	

(2-2) Considering two observed pulsars

Next, we consider the limit from two pulsars that the masses and radii are observed. EoSs go through 68% credibility with respect to the range of masses and radii from observation of PSR J0740 + 6620 and PSR J0030 + 0451 are shown in Table 6.11 with

$B_0 = 2.5 \times 10^{18}$ G, $B_s = 10^{15}$ G. Here, 6 EoSs (DDME2-a, GM1, GM3, NL3$\omega\rho$-a, TM2$\omega\rho$-a, and TM2$\omega\rho$-b) are satisfying the limits from the observations.

Table 6.11: Free parameter γ, α, and the reference of Figure and Table for each EoS which a limit of the observation of two pulsars contains ($B_0 = 2.5 \times 10^{18}$ G, $B_s = 10^{15}$ G).

EoS	γ	α	Figures & Tables
DDME2-a	1	0.01	Figure H.1, Table H.1
	1	0.02	
	1	0.03	
	2	0.01	
GM1	2	0.05	Figure H.3, Table H.3
	2	0.06	
	2	0.07	
	3	0.02	
	3	0.03	
	4	0.01	
GM3	2	0.09	Figure H.4, Table H.4
	3	0.04	
	3	0.05	
	4	0.01	
	4	0.02	
	5	0.01	
NL3$\omega\rho$-a	1	0.01	Figure H.7, Table H.7
TM1-b	3	0.02	Figure H.10, Table H.10
	4	0.01	
TM2$\omega\rho$-a	2	0.06	Figure H.11, Table H.11
	3	0.02	
	3	0.03	
	3	0.04	
	4	0.01	
TM2$\omega\rho$-b	2	0.03	Figure H.12, Table H.12
	2	0.04	
	2	0.05	
	2	0.06	
	2	0.07	
	3	0.01	
	3	0.02	
	3	0.03	
	4	0.01	

6.7 Particle populations of neutron star with magnetic fields

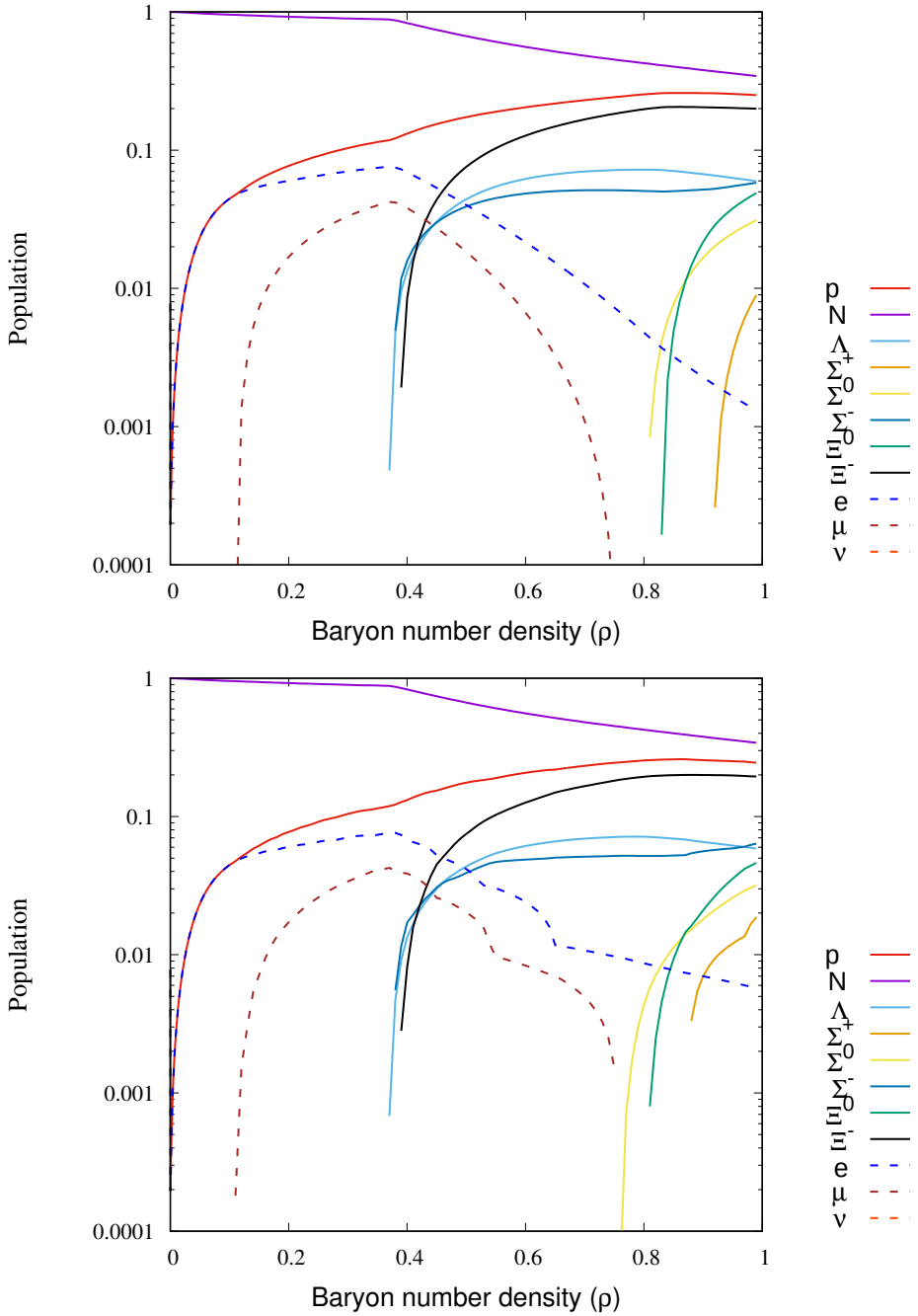

Figure 6.6: Population as a function of baryon number density ρ for TM2$\omega\rho$-b EoS without magnetic fields (top), with magnetic fields ($\alpha = 0.05, \gamma = 2$; bottom). Here, magnetic field strengths of center is $B_0 = 2.5 \times 10^{18}$ G and surface is $B_s = 10^{12}$ G. The colored lines represent the following particles: red (solid line) ; proton, purple (solid line); neutron, light blue (solid line); Λ, orange (solid line); Σ^+, yellow (solid line); Σ^0, dark blue (solid line); Σ^-, green (solid line); Ξ^0, black (solid line); Ξ^-, blue (dashed line); electron, brown (dashed line); muon, orange red (dashed line); tau.

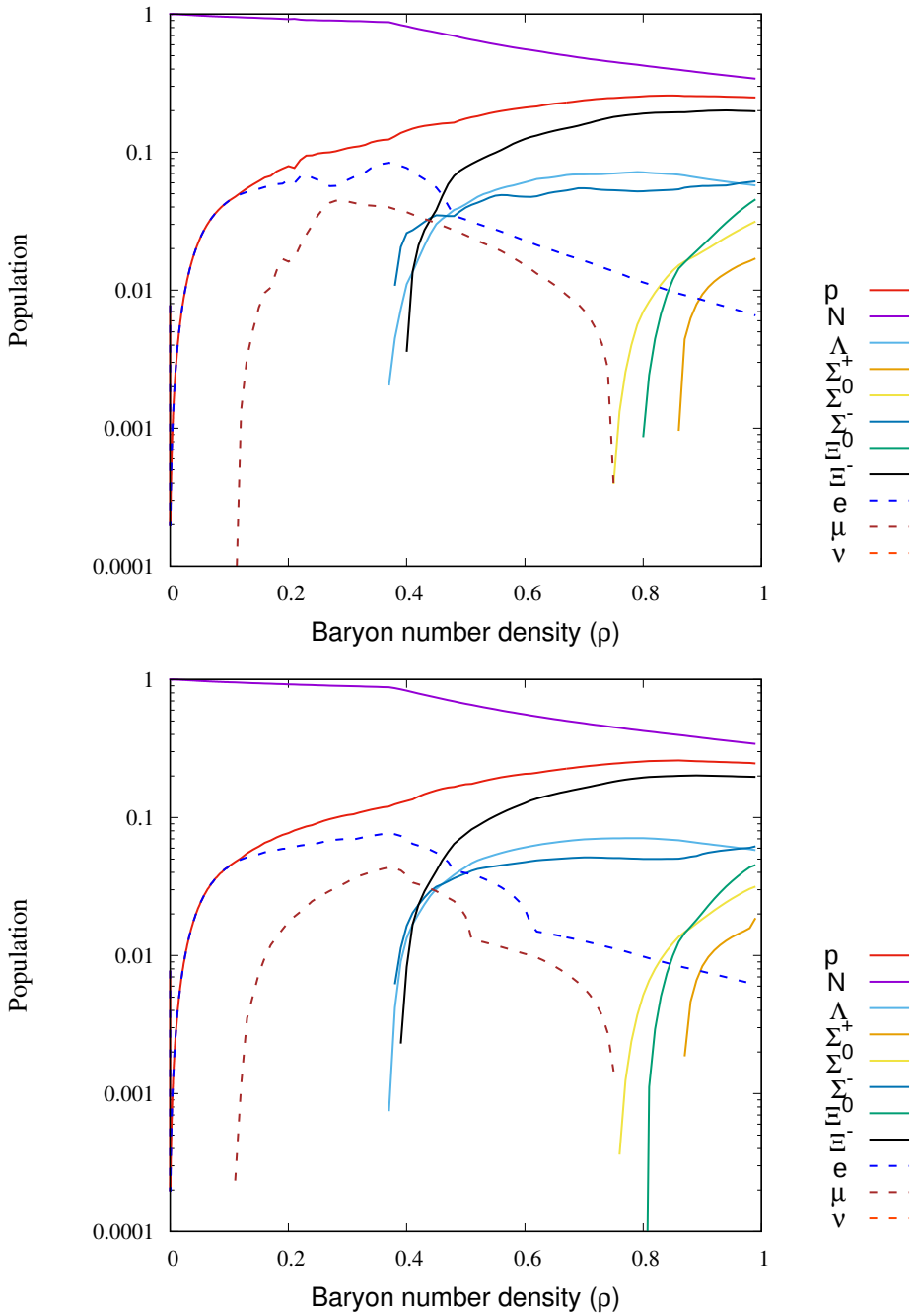

Figure 6.7: Population as a function of baryon number density ρ for TM2$\omega\rho$-b EoS with magnetic fields ($\alpha = 0.05, \gamma = 7$; top), with magnetic fields ($\alpha = 0.07, \gamma = 2$; bottom). Here, magnetic field strengths of center is $B_0 = 2.5 \times 10^{18}$ G and surface is $B_s = 10^{12}$ G. The colored lines is same as Fig. 6.6.

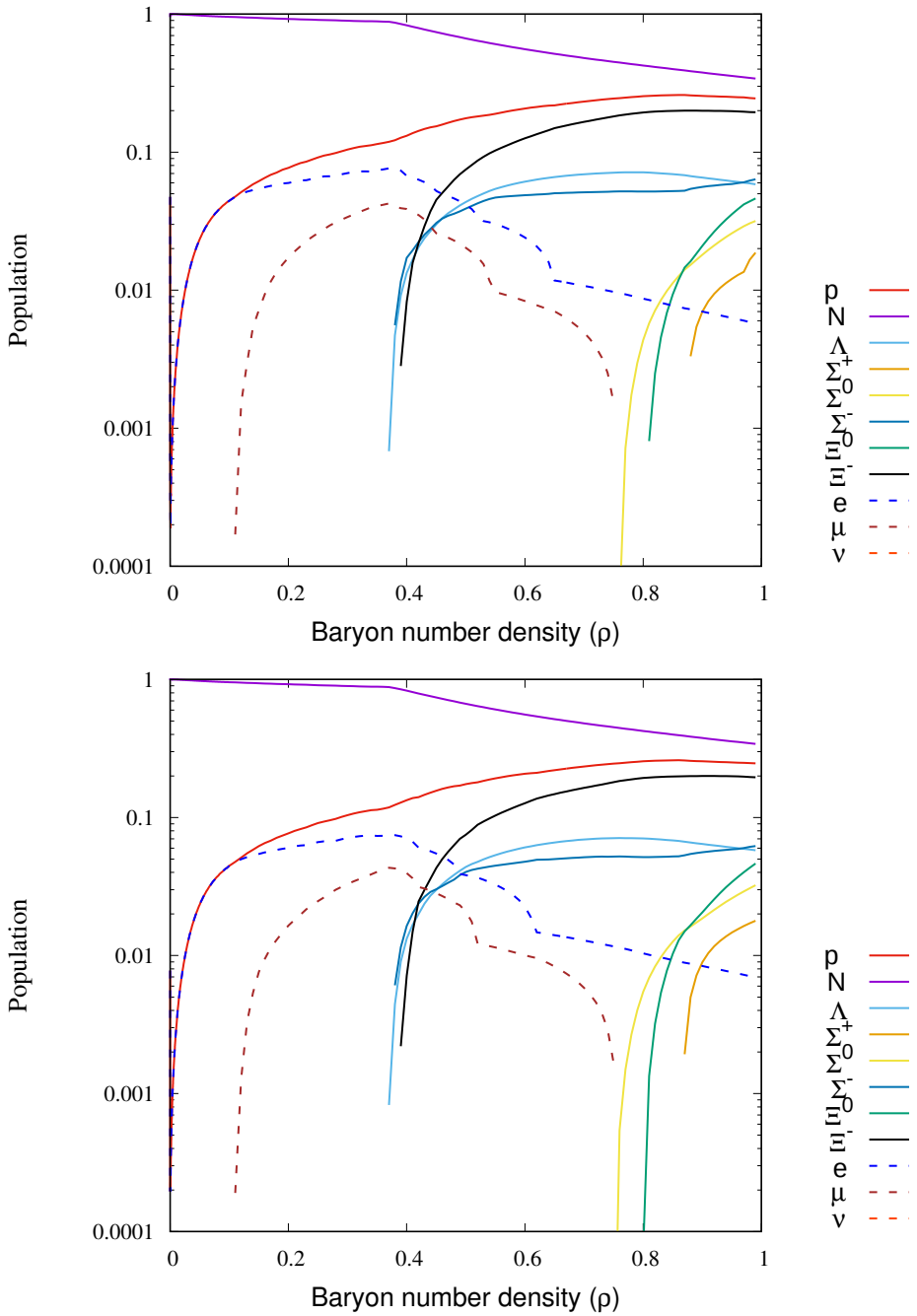

Figure 6.8: Population as a function of baryon number density ρ for TM2$\omega\rho$-b EoS with magnetic fields ($B_0 = 2.5 \times 10^{18}$ G, $B_s = 10^{15}$ G ; top), with magnetic fields $B_0 = 3 \times 10^{18}$ G, $B_s = 10^{12}$ G; bottom). Here, $\alpha = 0.05$ and $\gamma = 2$ are adopted. The colored lines is same as Fig. 6.6.

Figure 6.6 – 6.8 show the population as a function of baryon number density ρ. Here, we employ TM2$\omega\rho$-b EoS, because TM2$\omega\rho$-b EoS is the only EoS that meet the requirements of observations with magnetic fields ($B_0 = 2.5 \times 10^{18}$ G, $B_s = 10^{12}$ G, $\alpha = 0.05$, and $\gamma = 2$).

In Fig. 6.6, population for TM2$\omega\rho$-b EoS without magnetic fields (top) and with magnetic fields ($\alpha = 0.05, \gamma = 2$; bottom) are shown. Here, magnetic field strengths of center is $B_0 = 2.5 \times 10^{18}$ G and surface is $B_s = 10^{12}$ G. We can see that two figures are not so different, but $\sim 0.4 - 0.6$ of baryon number density, electrons and muons are straggling in bottom figure. (with magnetic fields case).

In Fig. 6.7, population for TM2$\omega\rho$-b EoS with magnetic fields ($\alpha = 0.05, \gamma = 7$; top) and with magnetic fields ($\alpha = 0.07, \gamma = 2$; bottom) are shown. Here, magnetic field strengths of center is $B_0 = 2.5 \times 10^{18}$ G and surface is $B_s = 10^{12}$ G. From the figures, leptons (electron, muon) are struggling quicker (rho=0.2-0.5) and some baryons are struggling in the case of large γ. In addition, in the case of large alpha of Fig 6.7(bottom), there is no such difference from Fig. 6.6 (bottom).

In Fig. 6.8, population for TM2$\omega\rho$-b EoS with magnetic fields ($B_0 = 2.5 \times 10^{18}$ G, $B_s = 10^{15}$ G; top) and with magnetic fields ($B_0 = 3 \times 10^{18}$ G, $B_s = 10^{12}$ G; bottom) are shown. Here, free parameter $\alpha = 0.05$ and $\gamma = 2$ are adopted. From the figures, compared with magnetic fields ($B_0 = 2.5 \times 10^{18}$ G, $B_s = 10^{12}$ G; Fig. 6.6; bottom), the is no such difference, but some baryons, Σ^+, Σ^0, and Ξ^0, to begin to appear at low populations. Especially Σ^+ is increase rapidly in case of strong central magnetic field strengths $B_0 = 3 \times 10^{18}$ G than in case of $B_0 = 2.5 \times 10^{18}$ G.

Chapter 7

Summary

7.1 Searching EoS in rotating magnetized neutron star

The mass-radius relations have been calculated for magnetized and rotating neutron stars using 12 EoSs, which include hyperons in addition to nucleons as components.

For TM2$\omega\rho$-a EoS with strong magnetic fields ($B_0 = 3 \times 10^{18}$ G), and TM2$\omega\rho$-b EoS with magnetic fields or with both rotation and magnetic fields, masses over the observed maximum mass of $2.072\,M_\odot$ are obtained, and predicted radii are in the range of $R \leq 13.76\,\mathrm{km}$ at $1.4\,M_\odot$, and also predicted radii are in the range of $12.39^{+1.30}_{-0.98}$ km at $2.072\ M_\odot$.

For NL3$\omega\rho$-a and NL3$\omega\rho$-b EoSs, masses over the observed maximum mass of $2.072\,M_\odot$ are obtained and predicted radii are in the range of $R \leq 13.76\,\mathrm{km}$ at $1.4\,M_\odot$ without rotation or magnetic fields. Calculated maximum masses of NL3-a, NL3-b, DDME2-a and DDME2-b EoSs are over the observed maximum mass of $2.072\,M_\odot$ without rotation and magnetic fields. As for TM2$\omega\rho$-a EoS, masses around twice the solar mass in the case with magnetic fields and over twice the solar mass in the case with strong magnetic fields ($B_0 = 3 \times 10^{18}$ G). Masses calculated by GM1, TM1-b and TM2$\omega\rho$-b EoSs with magnetic fields ($B_0 = 2.5 \times 10^{18}$ G and $B_0 = 3 \times 10^{18}\,\mathrm{G}$) become over twice the solar mass.

However, radii are not in the range of the observation of $R \leq 13.76\,\mathrm{km}$ at $1.4\,M_\odot$. For GM1 and TM1-b EoSs, masses more than $2.072\,M_\odot$ are obtained in the strong magnetic field of 3×10^{18} G at the center. Also, for GM1 and TM1-b EoSs, masses over $2\,M_\odot$ are obtained both with the magnetic field of 2.5×10^{18} G and 3×10^{18} G at the center or with the magnetic field of 2.5×10^{18} G in the center and the rotation of 6×10^2 Hz. From the observed radius, the central magnetic field strength should be smaller than $B_0 = 3 \times 10^{18}\,\mathrm{G}$.

Considering both the observed maximum mass $2.072\,M_\odot$ and the upper limit of the radius from the gravitational wave event, two suitable EoSs, TM2$\omega\rho$-a (with strong magnetic fields of 3×10^{18} G at the center) and TM2$\omega\rho$-b (with magnetic fields of $2.5{\times}10^{18}$ G or $3{\times}10^{18}$ G at the center) among 12 EoSs are found to meet the requirements of observations. This result also suggests that most EoSs need a stiffer matter in the

core of a neutron star, such as quark matter, especially in the case with both rotation and magnetic fields.

GM1 and TM2$\omega\rho$-b EoSs with magnetic fields ($B_0 = 2.5\times10^{18}$ G) and GM1, TM2$\omega\rho$-a, and TM2$\omega\rho$-b EoSs with magnetic fields ($B_0 = 3\times10^{18}$ G) go through 68% credibility with respect to the range of masses and radii from observation of PSR J0740 + 6620 and PSR J0030 + 0451.

7.2 Searching α and γ of magnetic fields

Comparing the case of GM1 EoS with hyperons or only nucleons, there is about 0.5 – 0.6 $M_\odot$ decrease in mass with hyperons. For the radius of 1.4 $M_\odot$, there is small difference (about 0.1 – 0.2 km). The values of masses and radii at 1.4 $M_\odot$ are increasing in the case of with magnetic fields in both with hyperons or without hyperons.

Change of α and γ parameters as free parameters for magnetic fields, we search how the shapes of the magnetic field changes and affects MR relations. When α increases, the magnetic field increases gradually, and mass and radius increase accordingly to α. When γ increases, the shape of the magnetic fields becomes rapid, and the mass and radius suddenly change.

We considered changing α and γ with magnetic fields with (1) $B_0 = 2.5\times10^{18}$ G, $B_s = 10^{12}$ G, and (2) $B_0 = 2.5\times10^{18}$ G, $B_s = 10^{15}$ G,

Moreover, to limit the EoS, we considered limits of 3 constraints ($M_{max} \geq 2.072\ M_\odot$, $R_{1.4M_\odot} < 13.76$ km, and $R_{2.072M_\odot} = 12.39^{+1.30}_{-0.98}$ km) and 2 pulsars (observed masses and radii of PSR J0740 + 6620 and PSR J0030 + 0451). Table 7.1 shows the EoSs satisfing each limit by changing α and γ.

As for the EoSs with magnetic fields, MR relations meet the requirements from the observation not only by changing a α and γ parameters, but also by changing B_0 and B_s of the magnetic fields.

7.3 Summary of summary

To summarize, in this thesis, we have searched for optimum EoSs that provide us masses and radii in the range of observed values w/o internal magnetic fields. Without magnetic fields, only a few EoSs meet the requirements from observation, but with strong internal magnetic fields a considerable number of EoSs satisfy the constraints from observations.

Table 7.1: Changing the free parameter γ and α in magnetic fields. Here, $B_0 = 2.5 \times 10^{18}$ G. There are the case (1) $B_s = 10^{12}$ G and the case (2) $B_s = 10^{15}$ G. 3 constraints indicate the limits ($M_{max} \geq 2.072$, $R_{1.4M_\odot} < 13.76$, and $R_{2.072M_\odot} = 12.39^{+1.30}_{-0.98}$) and 2 pulsars indicate the limits respect to the range of masses and radii from observation of PSR J0740 + 6620 and PSR J0030 + 0451.

	(1) 3 constraints		(1) 2 pulsars		(2) 3 constraints		(2) 2 pulsars	
EoS	γ	α	γ	α	γ	α	γ	α
DDME2-a	—	—	1	0.01	—	—	1	0.01
			1	0.02			1	0.02
			1	0.03			1	0.03
			2	0.01			2	0.01
GM1	3	0.02	2	0.05	3	0.02	2	0.05
	4	0.01	2	0.06	4	0.01	2	0.06
			2	0.07			2	0.07
			3	0.02			3	0.02
			3	0.03			3	0.03
			4	0.01			4	0.01
GM3	3	0.04	2	0.09	3	0.04	2	0.09
	4	0.02	3	0.03	4	0.02	3	0.04
			3	0.04			3	0.05
			3	0.05			4	0.01
			4	0.01			4	0.02
			4	0.02			5	0.01
			5	0.01				
NL3$\omega\rho$-a	—	—	1	0.01	—	—	1	0.01
			2	0.01				
TM1-b	—	—	—	—	—	—	3	0.02
							4	0.01
TM2$\omega\rho$-a	3	0.02	2	0.03	3	0.02	2	0.06
	4	0.01	2	0.04	3	0.03	3	0.02
			3	0.02	4	0.01	3	0.03
			3	0.03			3	0.04
			3	0.04			4	0.01
			4	0.01				
TM2$\omega\rho$-b	2	0.04	2	0.03	2	0.04	2	
	2	0.05	2	0.04	2	0.05	2	0.04
	2	0.06	2	0.05	2	0.06	2	0.05
	3	0.02	2	0.06	3	0.02	2	0.06
	3	0.03	2	0.07	3	0.03	2	0.07
	4	0.01	3	0.01	4	0.01	3	0.01
			3	0.02			3	0.02
			3	0.03			3	0.03
			4	0.01			4	0.01

Acknowledgment

First, I would like to thank my supervisor, Professor N. Yoshinaga, for research. Next, I appreciate Associate Professors Y. Terada, K. Sato and Assistant Professor S. Ebata for judging this thesis and its study.

I also thank Professor Constança Providência in Universidade de Coimbra and Professor Débora Peres Menezes in Universidade Federal de Santa Catarina for supporting me on research.

Furthermore, I thank everyone in Nuclear Theory Group, supporting me in nuclear theory group. I thank all the people for having spent a great time. I would like to thank everyone who ha s supported my academic days.

Finally, I thank my family for supporting me every day.

References

[1] T. Takuji, and T. Shigeyama, "Enrichment history of r-process elements shaped by a merger of neutron star pairs.", *Astronomy & Astrophysics* **565**, L5 (2014).

[2] B. P. Abbott, R. Abbott, T. D. Abbott, M. R. Abernathy, F. Acernese, K. Ackley, C. Adams, T. Adams, P. Addesso, R. X. Adhikari et al. (LIGO Scientific Collaboration and Virgo Collaboration), "Observation of Gravitational Waves from a Binary Black Hole Merger.", Phys. Rev. Lett. **116**, 061102 (2016).

[3] B. P. Abbott, R. Abbott, T. D. Abbott, F. Acernese, K. Ackley, C. Adams, T. Adams, P. Addesso, R. X. Adhikari, V. B. Adya et al. (LIGO Scientific Collaboration and Virgo Collaboration), "GW170817: Observation of Gravitational Waves from a Binary Neutron Star Inspiral.", Phys. Rev. Lett. **119**, 161101 (2017).

[4] B. P. Abbott, R. Abbott, T. D. Abbott, F. Acernese, K. Ackley, C. Adams, T. Adams, P. Addesso, R. X. Adhikari, V. B. Adya et al. (LIGO Scientific Collaboration and Virgo Collaboration, Fermi Gamma-ray Burst Monitor, and INTEGRAL), "Gravitational Waves and Gamma-Rays from a Binary Neutron Star Merger: GW170817 and GRB 170817A.", The Astrophysical Journal Letters **848**:L13, 27 (2017).

[5] W. Baade and F. Zwicky, "Remarks on super-novae and cosmic rays.", Phys. Rev. **46**, Number 1, 76 (1934).

[6] A. G. Cameron, "Neutron Star Models.", Astrophysical Journal **139**, 884 (1959).

[7] M. Baldo, I. Bombaci, and G. F. Burgio, "Microscopic nuclear equation of state with three-body forces and neutron star structure." , *Astronomy & Astrophysics* **328**, 274-282 (1997).

[8] G. F. Burgio, A. Figura, H.-J. Schulze, and J.-B.Wei, "Constraints from the GW170817 merger event on thenuclear matter equation of state", *Proceedings of XIII Quark Confinement and the Hadron Spectrum — PoS(Confinement2018)* **336**, 203 (2019).

[9] Z. A. Aghbolaghi and M. Bigdeli, "Argonne family potentials and neutron star matter equation of state.", Eur. Phys. J. Plus **134**, 430 (2019).

[10] H. A. Bethe and G. E. Brown, "Observational Constraints on the Maximum Neutron Star Mass. ", *Astrophys. J.* **1995**, *445*, L129 (1995).

[11] T. Muto, T. Maruyama, and T. Tatsumi, "Effects of three-baryon forces on kaon condensation in hyperon-mixed matter.", *Phys. Lett. B* **2021**, *820*, 136587 (2021).

[12] P. B. Demorest, T. Pennucci, S. M. Ransom, M. S. E. Roberts, and J. W. T. Hessels, "A two-solar-mass neutron star measured using Shapiro delay.", Nature **467**, 1081-1083 (2010).

[13] J. Antoniadis, P.C.C. Freire, N. Wex, T. M. Tauris, R. S. Lynch, M. H. van Kerkwijk, M. Kramer, C. Bassa, V. S. Dhillon, T. Driebe et al., "A massive pulsar in a compact relativistic binary.", *Science* **2013**, *340*, 1233232 (2013).

[14] H. T. Cromartie, E. Fonseca, and W. W. Zhu et al., "Relativistic Shapiro delay measurements of an extremely massive millisecond pulsar.", Nature Astronomy **4**, 72–76 (2020).

[15] T. E. Riley, A. L. Watts, P. S. Ray, S. Bogdanov, S. Guillot, S. M. Morsink, A. V. Bilous, Z. Arzoumanian, D. Choudhury, J. S. Deneva et al., "A NICER View of the Massive Pulsar PSR J0740+6620 Informed by Radio Timing and XMM-Newton Spectroscopy.", *Astrop. J. Lett.* **2021**, *918*, L27 (2021).

[16] C. Watanabe, K. Yanase, and N. Yoshinaga, "Searching optimum equations of state of neutron star matter in strong magnetic fields with rotation.", *Prog. Theor. Exp. Phys.* **2020**, *10*. 103E04 (2020).

[17] S. A. Olausen and V. M. Kaspi, "The McGill Magnetar Catalog", The Astrophysical Journal Supplement Series, **212:6**, 22pp (2014).

[18] McGill Online Magnetar Catalog, http://www.physics.mcgill.ca/ pulsar/magnetar/main.html, McGill Pulsar Group (2020).

[19] E. Annala, T. Gorda, A. Kurkela, and A. Vuorinen, "Gravitational-wave constraints on the neutron-star-matter Equation of State.", Phys. Rev. Lett. **120**, 172703 (2018).

[20] F. J. Fattoyev, J. Piekarewicz, and C. J. Horowitz, "Neutron skins and neutron stars in the multimessenger era.", Phys. Rev. Lett. **120**, Number 17, 172702, (2018).

[21] A. Bauswein, O. Just, H.-T. Janka, and N. Stergioulas, "Neutron-star radius constraints from GW170817 and future detections.", *Astrop. Jour. Lett.* **2017**, *850*, L34 (2017).

[22] M. C. Miller, F. K. Lamb, A. J. Dittmann, S. Bogdanov, Z. Arzoumanian, K. C. Gendreau, S. Guillot, A. K. Harding, W. C. G. Ho, J. M. Lattimer et al., "PSR J0030+0451 Mass and Radius from NICER Data and Implications for the Properties of Neutron Star Matter", Astrophys. J. Lett. **887**, L24 (2019).

[23] N. K. Glendenning, *Compact Stars*, (Springer Science & Business Media, 2012).

[24] N. K. Glendenning and S. A. Moszkowski, "Reconciliation of neutron-star masses and binding of the Λ in hypernuclei.", Phy. Rev. Letter **67**, Number 18, 2414 (1991).

[25] M. Fortin, S. S. Avancini, C. Providência, and I. Vidaña, "Hypernuclei and massive neutron stars.", Phy. Rev. C **95**, Number 6, 065803 (2017).

[26] G. A. Lalazissis, J. König, and P. Ring, "New parametrization for the Lagrangian density of relativistic mean field theory.", Phy. Rev. C **55**, Number 1, 540 (1997).

[27] G. A. Lalazissis, T. Nikšić, D. Vretenar, and P. Ring, "New relativistic mean-field interaction with density-dependent meson-nucleon couplings." Phy. Rev. C **71**, Number 2, 024312 (2005).

[28] N. Takigawa, "*Nuclear Physics*", Asakura Syoten (2013).

[29] I. Bombaci and U. Lombardo, "Asymmetric nuclear matter equation of state.", Phys. Rev. C **44**, 1892 (1991).

[30] B.-A. Li and M. Magno, "Curvature-slope correlation of nuclear symmetry energy and its imprints on the crust-core transition, radius, and tidal deformability of canonical neutron stars.", Phy. Rev. C **102**, Number 4, 045807 (2020).

[31] L.-W. Chen, C. M. Ko, and B.-A. Li, "Nuclear matter symmetry energy and the neutron skin thickness of heavy nuclei.", Phy. Rev. C **72**, Number 6, 064309 (2005).

[32] D. D. Ivanenko and D. F. Kurdgelaidze, "HYPOTHESIS CONCERNING QUARK STARS.", Astrofizika, **1**, Number 4, pp. 479-482 (1965).

[33] R. K .Bhaduri, "Model of the nucleon: from quarks to soliton", inspirehep.net (1988).

[34] D. P. Menezes and C. Providência, "Warm stellar matter with deconfinement: Application to compact stars.", Phy. Rev. C **68**, 035804 (2003).

[35] S. Chakrabarty, "Quark matter in a strong magnetic field.", Phys. Rev. D **54**, Number 2, 1306 (1996).

[36] P. K. Panda, D. P. Menezes and C. Providência, "Hybrid stars in the quark-meson coupling model with superconducting quark matter.", Phys. Rev. C **69**, Number 2, 025207 (2004).

[37] K. Itokazu, K. Yanase, and N. Yoshinaga, "Quark Star in a Strong Magnetic Field.", JPS Conf. Proc.**23**, 013003 (2018).

[38] F. Özel and P. Freire, "Masses, radii, and the equation of state of neutron stars.", Annual Review of Astronomy and Astrophysics **54**, 401-440 (2016).

[39] "ATNF Pulsar Catalogue" (http://www.atnf.csiro.au/people/pulsar/psrcat/)

[40] J. W. Hessels, S. M. Ransom, I. H. Stairs, P. C. C. Freire, V. M. Kaspi, and F. Camilo, "A radio pulsar spinning at 716 Hz.", Science **311**, Issue 5769, 1901-1904 (2005).

[41] S. A. Olausen and V. M. Kaspi, "The McGill magnetar catalog.", The Astrophysical Journal Supplement Series, 212:6 (2014).

[42] B.P. Abbott, R. Abbott, T. D. Abbott, M. R. Abernathy, F. Acernese, K. Ackley, C. Adams, T. Adams, P. Addesso, R. X. Adhikari et al., (LIGO Scientific Collaboration and Virgo Collaboration), "Observation of Gravitational Waves from a Binary Black Hole Merger.", Phys. Rev. Lett. **116**, 061102 (2016).

[43] B. P. Abbott, R. Abbott, T. D. Abbott, M. R. Abernathy, F. Acernese, K. Ackley, C. Adams, T. Adams, P. Addesso, R. X. Adhikari et al. (LIGO Scientific Collaboration and Virgo Collaboration), "GW151226: Observation of Gravitational Waves from a 22-Solar-Mass Binary Black Hole Coalescence.", Phys. Rev. Lett. **116**, 241103 (2016).

[44] B.P. Abbott, R. Abbott, T. D. Abbott, F. Acernese, K. Ackley, C. Adams, T. Adams, P. Addesso, R. X. Adhikari, V. B. Adya et al., (LIGO Scientific and Virgo Collaboration), "GW170104: observation of a 50-solar-mass binary black hole coalescence at redshift 0.2.", Phys. Rev. Lett. **118**, Number 22, 221101 (2017).

[45] B.P. Abbott, R. Abbott, T. D. Abbott, F. Acernese, K. Ackley, C. Adams, T. Adams, P. Addesso, R. X. Adhikari, V. B. Adya et al. (LIGO Scientific Collaboration and Virgo Collaboration), "GW170608: observation of a 19 solar-mass binary black hole coalescence.", The Astrophysical Journal Letters **851**, L35 (2017).

[46] B.P. Abbott, R. Abbott, T. D. Abbott, F. Acernese, K. Ackley, C. Adams, T. Adams, P. Addesso, R. X. Adhikari, V. B. Adya et al., (LIGO Scientific Collaboration and Virgo Collaboration), "GW170814: a three-detector observation of gravitational waves from a binary black hole coalescence.", Phys. Rev. Lett. **119**, Number 14, 141101 (2017).

[47] B. P. Abbott, R. Abbott, T. D. Abbott, F. Acernese, K. Ackley, C. Adams, T. Adams, P. Addesso, R. X. Adhikari, V. B. Adya et al. (LIGO Scientific Collaboration and Virgo Collaboration), "Properties of the Binary Neutron Star Merger GW170817.", Phy. Rev. X **9**, 011001 (2019).

[48] M. Tanaka and K. Hotokezaka, "Radiative transfer simulations of neutron star merger ejecta.", The Astrophysical Journal **775**, Number 2, 113 (2013).

[49] M. Tanaka, Y. Utsumi, P. A. Mazzali, N. Tominaga, M. Yoshida, Y. Sekiguchi, T. Morokuma, K. Motohara, K. Ohta, K. S. Kawabata et al., "Kilonova from post-merger ejecta as an optical and near-Infrared counterpart of GW170817.", Publications of the Astronomical Society of Japan **69**, Issue 6, 102 (2017).

[50] E. Fonseca, H. T. Cromartie, T. T. Pennucci, P. S. Ray, A. Y. Kirichenko, S. M. Ransom, P. B. Demorest, I. H. Stairs, Z. Arzoumanian, L. Guillemot et al., "Refined Mass and Geometric Measurements of the High-Mass PSR J0740+6620.", *arXiv* **2021**, arXiv:2104.00880v2.

[51] M. C. Miller, F. K. Lamb, A. J. Dittmann, S. Bogdanov, Z. Arzoumanian, K. C. Gendreau, S. Guillot, W. C. G. Ho, J. M. Lattimer, M. Loewenstein et al. , "THE RADIUS OF PSR J0740+6620 FROM NICER AND XMM-NEWTON DATA.", *arXiv* **2021**, arXiv:2105.06979v1.

[52] S. Guillot, M. Servillat, N. A. Webb, and R. E. Rutledge, "Measurement of the radius of neutron stars with high signal-to-noise quiescent low-mass X-ray binaries in globular clusters.", The Astrophysical Journal **772**, Number 1, 7 (2013).

[53] M. Zamfir, C. Andrew, and D. K. Galloway, "CONSTRAINTS ON NEUTRON STAR MASS AND RADIUS IN GS 1826 − 24 FROM SUB-EDDINGTON X-RAY BURSTS.", The Astrophysical Journal **749**, Issue 1, 69 (2012).

[54] I. Waki, H. Inoue, K. Koyama, M. Matsuoka, T. Murakami, Y. Ogawara, T. Ohashi, and Y. Tanaka, "Discovery of Absorption Lines in X-Ray Burst Spectra from X1636-536.", Publ. Astron. Soc. Japan **36**, 819-830 (1984).

[55] T. Güver, D. Psaltis, and F. Özel, "Systematic uncertainties in the spectroscopic measurements of neutron-star masses and radii from thermonuclear X-ray bursts. I. Apparent radii.", The Astrophysical Journal **747**, Number 1, 76 (2012).

[56] W. H. G. Lewin, J. V. Paradus, and R.E.Taam, "*X-Ray bursts*", springer, (1993).

[57] S. Abrahamyan, Z. Ahmed, H. Albataineh, K. Aniol, D. S. Armstrong, W. Armstrong, T. Averett, B. Babineau, A. Barbieri, V. Bellini et al. (PREX Collaboration), "Measurement of the Neutron Radius of ^{208}Pb through Parity Violation in Electron Scattering.", Phys. Rev. Lett. **108**, Number 11, 112502 (2012).

[58] C. J. Horowitz, Z. Ahmed, C.-M. Jen, A. Rakhman, P. A. Souder, M. M. Dalton, N. Liyanage, K. D. Paschke, K. Saenboonruang, R. Silwal et al., "Weak charge form factor and radius of ^{208}Pb through parity violation in electron scattering.", Phys. Rev. C **85**, 032501(R) (2012).

[59] J. B. Hartle, "Slowly rotating relativistic stars. I. Equations of structure.", The Astrophysical Journal **150**, p.1005 (1967).

[60] J. B Hartle and D. H Sharp, "Variational principle for the equilibrium of a relativistic, rotating star.", The Astrophysical Journal **147**, p.317 (1967).

[61] J. B. Hartle and K. S. Thorne, "Slowly rotating relativistic stars. II. Models for neutron stars and supermassive stars.", The Astrophysical Journal **153**, p. 807 (1968).

[62] S. Chandrasekhar and J. C. Miller, "On slowly rotating homogeneous masses in general relativity.", Monthly Notices of the Royal Astronomical Society **167**, Number 1, p.63-80 (1974).

[63] "The Review of Particle Physics" (http://pdg.lbl.gov/).

[64] C. Providência and A. Rabhi, "Interplay between the symmetry energy and the strangeness content of neutron stars.", Phys. Rev. C **87**, Number 5, 055801 (2013).

[65] Y. Sugahara and H. Toki, "Relativistic mean-field theory for unstable nuclei with non-linear σ and ω terms.", Nuclear Physics A **579**, 557-572 (1994).

[66] G. Baym, C. Pethick, and P. Sutherland, "The ground state of matter at high densities: equation of state and stellar models.", The Astrophysical Journal **170**, p. 299 (1971).

[67] G. Audi1, M. Wang, A.H. Wapstra, F.G. Kondev, M. MacCormick, X. Xu, and B. Pfeiffer, "The Ame2012 atomic mass evaluation." Chinese physics C **36**, No.12, p.1287 (2012).

[68] M. Wang, G. Audi, A.H. Wapstra, F.G. Kondev, M. MacCormick, X. Xu, and B. Pfeiffer, Wang, Meng, et al. "The Ame2012 atomic mass evaluation.", Chinese Physics C **36**, No.12, p.1603 (2012).

[69] S. Goriely, N. Chamel, and J. M. Pearson, "Further explorations of Skyrme-Hartree-Fock-Bogoliubov mass formulas. XIII. The 2012 atomic mass evaluation and the symmetry coefficient.", Phy. Rev. C **88**, Number 2, p.024308 (2013).

[70] R. H. Casali, L. B. Castro and D. P. Menezes, "Hadronic and hybrid stars subject to density-dependent magnetic fields.", Phy. Rev. C **89**, No.1, 015805 (2014).

[71] D. P. Menezes and M. D. Alloy, "Maxwell equation violation by density dependent magnetic fields in neutron stars.", *arXiv* **2016**, arXiv:1607.07687.

[72] C.Watanabe, N. Yoshinaga, and S. Ebata, "Equations of State for Hadronic Matter and Mass-Radius Relations of Neutron Stars with Strong Magnetic Fields.", *Universe* 8.1, 48 (2022).

[73] K. Yanase, N. Yoshinaga, E. Nakano, and C. Watanabe, "Deformation of neutron stars due to poloidal magnetic fields.", *Prog. Theor. Exp. Phys.* **2019**, *8*. 083E01 (2019).

[74] P. Haensel, M. Salgado, and S. Bonazzola, "Equation of state of dense matter and maximum rotation frequency of neutron stars.", *Astronomy & Astrophysics* **296**, 745-751 (1995).

[75] Y.-Z. Fan and D. Xu, "The X-ray afterglow flat segment in short GRB 051221A: Energy injection from a millisecond magnetar?.", Monthly Notices of the Royal Astronomical Society: Letters **372**, p.L19–L22 (2006).

[76] L. L. Lopes and D. P. Menezes, "The influence of hyperons and strong magnetic field in neutron star properties.", Brazilian Journal of Physics **42**, No.5, 428-436 (2012).

[77] A. Rabhi, H. Pais, P.K. Panda, and C. Providência, "Quark–hadron phase transition in a neutron star under strong magnetic fields.", Journal of Physics G: Nuclear and Particle Physics **36**, Number 11, 115204 (2009).

[78] A. Rabhi, C. Providência, and J. Da Providência, "Stellar matter with strong magnetic field within density dependent relativistic models.", Journal of Physics G: Nuclear and Particle Physics **35**, Number 12, 125201 (2008).

[79] C. Y. Ryu, K. S. Kim, and M.-K. Cheoun, "Medium effects of magnetic moments of baryons on neutron stars under strong magnetic fields.", Phys. Rev. C **82**, Number 2, 025804 (2010).

[80] D. P. Menezes and L. L. Lopes, "Quark matter under strong magnetic fields.", The European Physical Journal A **52** : 17, (2016).

Appendices

Appendix A

Relativistic mean field

A.1 RMF without and with magnetic fields

The potential is defined as (cf. Rabhi, Providência, and Providência (2009) [77])

$$U = \frac{1}{3} b m_n (g_\sigma \sigma)^3 + \frac{1}{4} c (g_\sigma \sigma)^4. \tag{A.1}$$

The meson equations are when $g_{\sigma b} = g_\sigma x_{\sigma b}$, it is given by

$$m_\sigma^2 \sigma + \frac{\partial U}{\partial \sigma} = \sum_b g_{\sigma b} \rho_b^s = g_\sigma \sum_b x_{\sigma b} \rho_b^s, \tag{A.2}$$

$$m_\omega^2 \omega^0 = \sum_b g_{\omega b} \rho_b^v = g_\omega \sum_b x_{\omega b} \rho_b^v, \tag{A.3}$$

$$m_\rho^2 \rho^0 = \sum_b g_{\rho b} I_{3b} \rho_b^v = g_\rho \sum_b x_{\rho b} I_{3b} \rho_b^v. \tag{A.4}$$

where I_{3b} is a projection operator of isospin. The effective mass is given by

$$m_b^* = m_b - g_\sigma \sigma. \tag{A.5}$$

From the chemical potential and the charge neutrality,

$$\mu_b = \mu_n - q_b \mu_e, \quad \mu_\mu = \mu_e, \tag{A.6}$$

$$0 = \sum_b q_b \rho_b^\nu + \sum_l q_l p_l^\nu. \tag{A.7}$$

The effective mass of charged baryon is

$$\overline{m}_{b\nu s}^c = \sqrt{(m_b^*)^2 + 2\nu |q_b| B} - s \mu_N \kappa_b B. \tag{A.8}$$

And scalar and vector charged baryon densities are

$$\rho_b^s = \frac{|q_b|\,Bm_b^*}{2\pi^2}\sum_s\sum_{\nu_{\min}(s)}^{\nu_{\max}(s)}\frac{\bar{m}_{b\nu s}^c}{\sqrt{\left(m_b^*\right)^2+2\nu\,|q_b|\,B}}\ln\left|\frac{k_{F,\nu s}^b+E_F^b}{\bar{m}_{b\nu s}^c}\right|, \tag{A.9}$$

$$\rho_b^v = \frac{|q_b|\,B}{2\pi^2}\sum_s\sum_{\nu_{\min}(s)}^{\nu_{\max}(s)}k_{F,\nu s}^b. \tag{A.10}$$

Baryon Fermi wave numbers of charged baryon and neutral baryon are

$$\left(k_{F,\nu s}^b\right)^2 = \left(E_F^b\right)^2-(\bar{m}_{b\nu s}^c)^2, \tag{A.11}$$

$$\left(k_{F,s}^b\right)^2 = \left(E_F^b\right)^2-\left(\overline{m}_{bs}\right)^2. \tag{A.12}$$

The effective mass of neutral baryon is

$$\bar{m}_{bs} = m_b^* - s\mu_N\kappa_p B. \tag{A.13}$$

Scolar and vector density of neutral baryon is

$$\rho_b^s = \frac{m_b^*}{4\pi^2}\sum_s\left[E_F^bk_{F,s}^b-(\bar{m}_{bs})^2\ln\left|\frac{k_{F,s}^b+E_F^b}{\bar{m}_{bs}}\right|\right], \tag{A.14}$$

$$\rho_b^v = \frac{1}{2\pi^2}\sum_s\left[\frac{1}{3}\left(k_{F,s}^b\right)^3-\frac{1}{2}s\mu_N\kappa_bB\left(\bar{m}_{bs}k_{F,s}^b+\left(E_F^b\right)^2\left(\sin^{-1}\left(\frac{\bar{m}_{bs}}{E_F^b}\right)-\frac{\pi}{2}\right)\right)\right]. \tag{A.15}$$

Vector density of Lepton is

$$\rho_l^\nu = \frac{|q_l|B}{2\pi^2}\sum_s\sum_{V_{min}(s)}^{V_{max}(s)}k_{F,\nu}^l. \tag{A.16}$$

The wave numbers do not depend on spin, so

$$\rho_l^\nu = \frac{|q_l|B}{2\pi^2}\left(2\sum_{\nu=1}^{\nu_{max}}k_{F,\nu}^l+k_{F,0}^l\right) \tag{A.17}$$

Leptons are all charged and

$$(k_{F,\nu}^l)^2 = (E_F^l)^2-(\overline{m}_{l\nu})^2, \tag{A.18}$$

$$(\overline{m}_{l\nu})^2 = (m_l)^2+2\nu|q_l|B. \tag{A.19}$$

where Eq. (A.18) means that mass of lepton is independent to s, and Eq.(A.19) means that effective mass depends on ν. The maximum ν is

$$\nu_{\max} = \left[\frac{\left(E_F^\ell\right)^2-\left(m_\ell\right)^2}{2\,|q_\ell|\,B}\right]. \tag{A.20}$$

And the maximum of charged baryon is

$$\nu_{\max} = \left[\frac{\left(E_F^b + s\mu_N \kappa_b B\right)^2 - (m_b^*)^2}{2\left|q_b\right| B} \right]. \tag{A.21}$$

On the other hand, the minimum of ν is $\nu = n + \frac{1}{2} - \mathrm{sqn(q)}\frac{\mathrm{s}}{2}$. When it is positive charged particle, in the case of spin down ($s = -1$) will start from $\nu = 1$. When it is negative charged particle, in the case of spin up ($s = -1$) will start from $\nu = 1$. In the other case, it will start from $\nu = 0$.

The relation of the chemical potential and Fermi energy is

$$\mu_b = E_F^b + g_{\omega b}\omega^0 + g_{\rho b} I_{3b} \rho^0, \tag{A.22}$$

$$\mu_l = E_F^l. \tag{A.23}$$

The energy density without magnetic field

$$\varepsilon_m = \sum_b \varepsilon_b + \sum_\ell \varepsilon_\ell + \frac{1}{2} m_\sigma^2 \sigma^2 + U(\sigma) + \frac{1}{2} m_\omega^2 \left(\omega^0\right)^2 + \frac{1}{2} m_\rho^2 \left(\rho^0\right)^2, \tag{A.24}$$

where charged baryon ε_b^c, neutral baryon ε_b^n, and lepton ε_l is as follows.

$$\varepsilon_b^c = \frac{\left|q_b\right| B}{4\pi^2} \sum_s \sum_{\nu_{\min}(s)}^{\nu_{\max}(s)} \left[k_{F,\nu s}^b E_F^b + \left(\bar{m}_{b\nu s}^c\right)^2 \ln \left| \frac{k_{F,\nu s}^b + E_F^b}{\bar{m}_{b\nu s}^c} \right| \right], \tag{A.25}$$

$$\begin{aligned} \varepsilon_b^n = {} & \frac{1}{4\pi^2} \sum_s \left[\frac{1}{2} k_{F,s}^b \left(E_F^b\right)^3 - \frac{2}{3} s\mu_N \kappa_b B \left(E_F^b\right)^3 \left(\sin^{-1}\left(\frac{\bar{m}_{bs}}{E_F^b}\right) - \frac{\pi}{2} \right) \right. \\ & \left. - \left(\frac{1}{3} s\mu_N \kappa_b B + \frac{1}{4} \bar{m}_{bs} \right) \left(\bar{m}_{bs} k_{F,s}^b E_F^b + \left(\bar{m}_{bs}\right)^3 \ln \left| \frac{k_{F,s}^b + E_F^b}{\bar{m}_{bs}} \right| \right) \right], \end{aligned} \tag{A.26}$$

$$\varepsilon_\ell = \frac{\left|q_\ell\right| B}{4\pi^2} \sum_s \sum_{\nu_{\min}(s)}^{\nu_{\max}} \left[k_{F,\nu}^\ell E_F^\ell + \left(\bar{m}_{\ell\nu}\right)^2 \ln \left| \frac{k_{F,\nu}^\ell + E_F^\ell}{\bar{m}_{\ell\nu}} \right| \right]. \tag{A.27}$$

As same as wave number,

$$\varepsilon_\ell = \frac{\left|q_\ell\right| B}{4\pi^2} \left\{ 2 \sum_{\nu=1}^{\nu_{\max}} \left(k_{F,\nu}^\ell E_F^\ell + \left(\bar{m}_{\ell\nu}\right)^2 \ln \left| \frac{k_{F,\nu}^\ell + E_F^\ell}{\bar{m}_{\ell\nu}} \right| \right) + k_{F,0}^\ell E_F^\ell + \left(\bar{m}_{\ell 0}\right)^2 \ln \left| \frac{k_{F,0}^\ell + E_F^\ell}{\bar{m}_{\ell 0}} \right| \right\}. \tag{A.28}$$

The pressure is

$$p_m = \sum_i \mu_i \rho_i^v - \varepsilon_m = \mu_n \sum_b \rho_b^v - \varepsilon_m. \tag{A.29}$$

To derivation this, we use $q_\ell = -1$ and charge neutrality $0 = \sum_b q_b \rho_b^v + \sum_\ell q_\ell \rho_\ell^v$.

$$\begin{aligned}\sum_i \mu_i \rho_i^v &= \sum_b \mu_b \rho_b^v + \sum_\ell \mu_\ell \rho_\ell^v \\ &= \sum_b \left(\mu_n - q_b \mu_e\right) \rho_b^v + \mu_e \sum_\ell \rho_\ell^v \\ &= \mu_n \sum_b \rho_b^v - \mu_e \sum_b q_b \rho_b^v - \mu_e \sum_\ell q_\ell \rho_\ell^v \\ &= \mu_n \sum_b \rho_b^v. \end{aligned} \tag{A.30}$$

The definition of pressure (partical pressure) is given by (cf. Glendenning (2012)[23])

$$p_i = {\rho_i}^2 \frac{d\left(\varepsilon_i/\rho_i\right)}{d\rho_i}. \tag{A.31}$$

The definition of chemical potential is

$$\mu_i = \frac{d\varepsilon_i}{d\rho_i}, \tag{A.32}$$

$$p_i = {\rho_i}^2 \frac{d\left(\varepsilon_i/\rho_i\right)}{d\rho_i} = \rho_i \left(\frac{d\varepsilon_i}{d\rho_i} - \frac{\varepsilon_i}{\rho_i}\right) = \rho_i \mu - \varepsilon_i. \tag{A.33}$$

The total pressure is

$$p = \sum_i p_i = \sum_i \left(\rho_i \mu_i - \varepsilon_i\right), \tag{A.34}$$

where we can derivation the above equation changing ρ_i to ρ_i^v.

In the case of energy density and pressure with magnetic field is

$$\varepsilon = \varepsilon_m + \frac{B^2}{2}, \tag{A.35}$$

$$p = p_m + \frac{B^2}{2}. \tag{A.36}$$

What is the effect of magnetized $\vec{M}$?

To translate cgs units (Gauss) from natural units, we need to via SI units (Tesla), since

$$\frac{1}{4\pi\varepsilon_0} = 1, \quad \text{(cgs units)}$$
$$\varepsilon_0 = \mu_0 = 1. \quad \text{(natural units)}$$

The pressure of magnetic field in natural units is $\frac{B^2}{2}$, because the pressure of magnetic field is $\frac{B^2}{2\mu_0}$ in SI units.

Appendix B

Landau level

B.1 Zero temperature

In the case of temperature is 0, as for all the levels of n satisfying the following equation (B.1) , a charged particle is contract and if it is not satisfying, the level will be completely empty.

$$E_F \geq \hbar\omega_c\left(n+\frac{1}{2}\right)+\frac{\hbar^2 k_z^2}{2m}. \tag{B.1}$$

At this time, the state density for a certain k_z is given by

$$D(E)=\frac{mL^2}{2\pi\hbar^2}=\xi\ (constant), \tag{B.2}$$

where L is the one side of length of system.

$$\begin{aligned}\delta E_1=\delta E_2&=\int_0^{\Delta} ED(E)dE\\&=\xi\frac{\Delta^2}{2}\\&\equiv\delta E.\end{aligned} \tag{B.3}$$

Δ is takes the number from 0 to $\hbar\omega_c/2=\mu_B B$, so the average is

$$\delta E\ =\frac{1}{\mu_B B}\int_0^{\mu_B B}\delta E d\Delta=\xi\frac{(\mu_B B)^2}{6}. \tag{B.4}$$

Here, $\mu_B=q\hbar/2mc$ is Bohr magneton. Integral equation (B.4) about k_z and get,

$$\begin{aligned}\Delta E_{total}&=2L\int_{-k_F}^{k_F}dk_z\xi\frac{(\mu_B B)^2}{6}\\&=\eta(E_F)\frac{(\mu_B B)^2}{3},\end{aligned} \tag{B.5}$$

where $\eta(E)$ is state density. From this equation, the magnetic susceptibility is as follows.

$$\chi = -2\eta(E_F)\frac{\mu_B}{3}, \tag{B.6}$$

which we called Landau diamagnetism. The energy level becomes the Landau level when we add a magnetic field to the system including charged particle, and we get in more total energy. This suggests that an equation of state becomes stiffer because of the magnetic field.

B.2 BPS with magnetic fields

The energy spectra for charged baryons, neutral baryons, and leptons are derived from the Dirac equation and given by

$$E^b_{\nu,s} = \sqrt{(k^b_z)^2 + \left(\overline{m}^c_b\right)^2} + g_{\omega b}\omega^0 + \tau_{3b}g_{\rho b}\rho^{03}, \tag{B.7}$$

$$E^b_s = \sqrt{(k^b_z)^2 + (\overline{m}_b)^2} + g_{\omega b}\omega^0 + \tau_{3b}g_{\rho b}\rho^{03}, \tag{B.8}$$

$$E^l_\nu = \sqrt{(k^l_z)^2 + (\overline{m}_l)^2}, \tag{B.9}$$

respectively. Here, we define the effective masses

$$\overline{m}^c_b = \sqrt{m^{*2}_b + 2\nu|q_b|B} - s\mu_N\kappa_b B, \tag{B.10}$$

$$\overline{m}_b = m^*_b - s\mu_N\kappa_b B, \tag{B.11}$$

$$\overline{m}_l = \sqrt{m^2_l + 2\nu|q_l|B}, \tag{B.12}$$

for charged baryons, neutral baryons, and leptons, respectively, where

$$m^*_b = m_b - g_{\sigma b}\sigma. \tag{B.13}$$

The ν represents the Landau levels

$$\nu = n + \frac{1}{2} - \mathrm{sgn}(q_b)\frac{s}{2} = 0, 1, 2, \cdots, \nu_{\max}, \tag{B.14}$$

where n implies any integer greater than or equal to zero, and $s = +1$ for spin-up and $s = -1$ for spin-down, respectively. Namely, we should take differently the lowest values of ν, which takes 0 or 1, depending on the signs of charges and the spin third components. The maximum values of the Landau levels are given by

$$\nu_{\max} = \frac{(E^b_{\mathrm{F}} + s\mu_N\kappa_b B)^2 - m^{*2}_b}{2|q_b|B}, \tag{B.15}$$

$$\nu_{\max} = \frac{(E^l_{\mathrm{F}})^2 - m^2_l}{2|q_l|B}. \tag{B.16}$$

The Fermi wave numbers $k^b_{F,\nu,s}$, $k^b_{F,s}$, and $k^l_{F,\nu}$ are given by usual relations

$$(E^b_F)^2 = \begin{cases} (k^b_{F,\nu,s})^2 + (\overline{m}^c_b)^2 \\ \\ (k^b_{F,s})^2 + (\overline{m}_b)^2 \end{cases}, \tag{B.17}$$

for baryons, and

$$(E^l_{\rm F})^2 = (k^l_{{\rm F},\nu})^2 + \overline{m}^2_l \tag{B.18}$$

for leptons. We then obtain the scalar density and the vector density

$$\rho^s_b = \frac{|q_b|Bm^*_b}{2\pi^2} \sum_s \sum_\nu^{\nu_{\max}} \frac{\overline{m}^c_b}{\sqrt{m^{*2}_b + 2\nu|q_b|B}} \ln \left| \frac{k^b_{F,\nu,s} + E^b_F}{\overline{m}^c_b} \right|, \tag{B.19}$$

$$\rho^v_b = \frac{|q_b|B}{2\pi^2} \sum_s \sum_\nu^{\nu_{\max}} k^b_{F,\nu,s}, \tag{B.20}$$

for charged baryons,

$$\rho^s_b = \frac{m^*_b}{4\pi^2} \sum_s \left[E^b_F k^b_{F,s} - \overline{m}^2_b \ln \left| \frac{k^b_{F,s} + E^b_F}{\overline{m}_b} \right| \right], \tag{B.21}$$

$$\rho^v_b = \frac{1}{2\pi^2} \sum_s \left[\frac{1}{3} \left(k^b_{F,s} \right)^3 - \frac{1}{2} s \mu_N \kappa_b B \left\{ \overline{m}_b k^b_{F,s} + \left(E^b_F \right)^2 \left(\arcsin \left(\frac{\overline{m}_b}{E^b_F} \right) - \frac{\pi}{2} \right) \right\} \right], \tag{B.22}$$

for neutral baryons, and

$$\rho^v_l = \frac{|q_l|B}{2\pi^2} \sum_s \sum_\nu^{\nu_{\max}} k^l_{{\rm F},\nu}, \tag{B.23}$$

for leptons, respectively.

Appendix C

TOV equation

C.1 Derivation of TOV equation

Here, we introduce the differential equations so that structure of the relativistic star of the spherical symmetry can be calculated in the rest frame. In the outside domain of the star, the vanishment of the Einstein tensor is equal to extinction of rich tensors or the scalar curvature. This is not a case inside stars. Both the rich tensor and scalar curvature are necessary to constitute the Einstein tensor. The general formulae of a stationary homolytic space-time measurement are as follows.

$$\begin{aligned} &g_{00} = e^{2\nu(r)}, \quad g_{11} = e^{2\lambda(r)}, \quad g_{22} = -r^2, \quad g_{33} = -r^2\sin^2\theta, \\ &g_{\mu\nu} = g^{\mu\nu} = 0 \quad (\mu \neq \nu). \end{aligned} \tag{C.1}$$

From metric in static isotropic spacetime, we find the scalar curvature,

$$\begin{aligned} R &= g^{\mu\nu}R_{\mu\nu} \\ &= e^{-2\nu}R_{00} - e^{-2\lambda}R_{11} - \frac{2}{r^2}R_{22} \\ &= e^{-2\lambda}\left\{-2\nu'' + 2\lambda'\nu' - 2\nu'^2 - \frac{2}{r^2} + 4\frac{\lambda'}{r} - 4\frac{\nu'}{r}\right\} + \frac{2}{r^2}/ \end{aligned} \tag{C.2}$$

Here we can find that the components of Einstein tensor are

$$\begin{aligned} r^2{G_0}^0 \equiv e^{-2\lambda}\left(1 - 2r\lambda'\right) - 1 = -\frac{d}{dr}\left[r\left(1 - e^{-2\lambda}\right)\right], \\ r^2{G_1}^1 \equiv e^{-2\lambda}\left(1 + 2r\lambda'\right) - 1, \\ {G_2}^2 \equiv e^{-2\lambda}\left(\nu'' + \nu'^2 - \lambda'\nu' + \frac{\nu' - \lambda'}{r}\right), \\ {G_3}^3 = {G_2}^2. \end{aligned} \tag{C.3}$$

Assume the star is static, the three-velocity of every fluid element is zero, so

$$u^\mu = 0 \ (\mu \neq 0), \quad u^0 = 1/\sqrt{g_{00}}, \tag{C.4}$$

For the energy-momentum tensor expressed as a mixed tensor, we have the nonzero components in the present metric,

$$T_0{}^0 = \varepsilon, \quad T_\mu{}^\mu = -p \ (\mu \neq 0). \tag{C.5}$$

The (00) component of Einstein equations gives

$$\begin{aligned} r^2 G_0{}^0 &= -\frac{d}{dr}\left\{ r\left(1 - e^{-2\lambda(r)}\right)\right\} \\ &= kr^2 T_0{}^0 \\ &= kr^2 \varepsilon(r). \end{aligned} \tag{C.6}$$

This can be integrated immediately to yield $e^{-2\lambda(r)}$ and define $M(r)$,

$$e^{-2\lambda(r)} = 1 + \frac{k}{r}\int_0^r \varepsilon(r) r^2 dr. \tag{C.7}$$

$$M(r) \equiv 4\pi \int_0^r \varepsilon(r) r^2 dr. \tag{C.8}$$

To obtain Newtonian limit, we must choose,

$$k = -8\pi G. \tag{C.9}$$

Einstein's field equations can now be written

$$G^{\mu\nu} = -8\pi G T^{\mu\nu}. \tag{C.10}$$

From the above, we have found so far that

$$\begin{aligned} g_{11}(r) &= -e^{-2\lambda(r)} \\ &= -\left(1 - \frac{2GM(r)}{r}\right)^{-1}, \end{aligned} \tag{C.11}$$

From the constant of proportionality in Einstein's equations C.10, writing out the field equations for a spherically symmetric static star, the differential equations from C.3 are

$$G_0{}^0 \equiv e^{-2\lambda}\left(\frac{1}{r^2} - \frac{2\lambda'}{r}\right) - \frac{1}{r^2} = -8\pi G\varepsilon(r), \tag{C.12}$$

$$G_1{}^1 \equiv e^{-2\lambda}\left(\frac{1}{r^2} + \frac{2\mu'}{r}\right) - \frac{1}{r^2} = 8\pi G p(r), \tag{C.13}$$

$$G_2{}^2 \equiv e^{-2\lambda}\left(\nu'' + \nu'^2 - \lambda'\nu' + \frac{\nu' - \lambda'}{r}\right) = 8\pi G p(r), \tag{C.14}$$

$$G_3{}^3 = G_2{}^2 = 8\pi G p(r). \tag{C.15}$$

To simplify notation, choose units so that $G = c = 1$. Solve equation C.12 and equation C.13 to find

$$-2r\lambda' = (1 - 8\pi r^2\varepsilon)e^{2\lambda} - 1, \tag{C.16}$$

$$2r\nu' = (1 + 8\pi r^2 p)e^{2\lambda} - 1, \tag{C.17}$$

Take the derivative of equation C.17 and then multiply by r:

$$2r\nu' + 2r^2\nu'' = \Big[2r\lambda'(1 + 8\pi r^2 p) + (16\pi r^2 p + 8\pi r^3 p')\Big]e^{2\lambda}, \tag{C.18}$$

$$2r^2\nu'' = 1 + (16\pi r^2 p + 8\pi r^3 p')e^{2\lambda} - (1 + 8\pi r^2 p)(1 - 8\pi r^2\varepsilon)e^{4\lambda} \tag{C.19}$$

Square equation C.17 to obtain the result

$$2r^2\nu'^2 = \frac{1}{2}(1 + 8\pi r^2 p)^2 e^{4\lambda} - (1 + 8\pi r^2 p)e^{2\lambda} + \frac{1}{2}. \tag{C.20}$$

From above and equation C.14, we emerge with the result

$$\frac{dp}{dr} = -\frac{\big[p(r) + \varepsilon(r)\big]\big[M(r) + 4\pi r^3 p(r)\big]}{r\,\big[r - 2M(r)\big]}. \tag{C.21}$$

And when we take the derivative of equation C.8, we get,

$$\frac{dM}{dr} = 4\pi\varepsilon(r)r^2 \tag{C.22}$$

So from the above calculations, here we have the following equation, which is so-called Tolman Oppenheimer-Volkoff (TOV) equation,

$$\frac{dp}{dr} = -\frac{\big[p(r) + \varepsilon(r)\big]\big[M(r) + 4\pi r^3 p(r)\big]}{r\,\big[r - 2M(r)\big]}, \tag{C.23}$$

$$\frac{dM}{dr} = 4\pi\varepsilon(r)r^2. \tag{C.24}$$

Appendix D

Units

D.1 Gravitational unit and Natural unit

D.1.1 Gravitational unit

For calculating TOV equation, we use gravitational unit. It is useful, not only because they facilitate computation, but also our equations are not burdened with the appearance of c, G, and $\hbar$. We start with gravitational units:

$$1 = c = 2.9979 \times 10^{10}\ \mathrm{cm/s}, \tag{D.1}$$

$$1 = G = 6.6720 \times 10^{-8}\ \mathrm{cm^3 g^{-1} s^{-2}}, \tag{D.2}$$

$$1 = k = 1.3807 \times 10^{-16}\ \mathrm{erg/K}, \tag{D.3}$$

where k is the Boltzmann constant and K denotes temperature in degrees Kelvin. These definitions can be treated as equations so that we have for example, shown in Table D.1.

Table D.1: Example values for gravitational units.(1)

SI units	Gravitational units
1 s	2.9979×10^{10} cm
1.0×10^{-3}kg	7.4237×10^{-29} cm
1K	1.3807×10^{-16} erg
$1\mathrm{s}^{-2}$	$1.4988 \times 10^{7}\mathrm{g/cm^3}$
1erg $(= 1 \times 10^{-7}\mathrm{kg \cdot m^2 s^{-2}})$	8.2601×10^{-50} cm
$1\mathrm{g/cm^3}(=10^3\ \mathrm{kg/m^3})$	$7.4237 \times 10^{-19}\ \mathrm{km^{-2}}$

Table D.2: Example values for gravitational units.(2)

	SI units	Gravitational units
1MeV	$1.602 \times 10^{-20}\mathrm{kg \cdot m^2 \cdot s^{-2}}$	$1.3234 \times 10^{55}\mathrm{cm}$
$\hbar$c	$3.162 \times 10^{-33}\mathrm{kg \cdot m^3 \cdot s^{-2}}$	197.33 MeV
$B^2/2\mu_0$	$1.259 \times 10^{-37}\mathrm{fm^{-4}}$	

D.1.2 Natural unit

It is useful in nuclear and particle physics to use natural units. Natural units is $\hbar$=c=1. Then from the value of $\hbar c$, we obtain by dividing by fm^4

$$1/\mathrm{fm}^4 = 197.33\,\mathrm{MeV/fm}^3, \tag{D.4}$$
$$= 3.5178 \times 10^{14}\,\mathrm{g/cm}^3, \tag{D.5}$$
$$= 2.6115 \times 10^{-4}\,/\mathrm{km}^2. \tag{D.6}$$

Mixed units are obtained by combining Eq. (D.4) with value MeV in cm,

$$\mathrm{MeV/fm}^3 = 1.3234 \times 10^{-6}\,/\mathrm{km}^2. \tag{D.7}$$

This can be compared with the solar mass,

$$\mathrm{M}_\odot = 1.4766\,\mathrm{km}, \tag{D.8}$$
$$= 1.116 \times 10^{60}\,\mathrm{MeV}. \tag{D.9}$$

Appendix E

Hartle equations

In this paper Hartle equations are employed to calculate the additional mass m_0 and the equatorial and polar radii for a rotating neutron star [59, 60, 61, 62]. The Hartle equations are coupled ordinary differential equations for the metric parameters $h_0(r)$, $h_2(r)$, $m_0(r)$, $m_2(r)$, and $k_2(r)$ with respect to r, which refers to the distance from the center of a neutron star :

$$\frac{1}{r^3}\frac{d}{dr}\left(r^4 j\frac{d\varpi}{dr}\right)+4\frac{dj}{dr}\varpi=0, \tag{E.1}$$

$$\begin{aligned}&-\frac{d}{dr}\delta P_0+\frac{1}{3}\frac{d}{dr}\left(r^2e^{-2\nu_0}\varpi^2\right)\\&=m_0e^{4\lambda_0}\left(\frac{1}{r^2}+8\pi p_0\right)-\frac{1}{12}e^{2\lambda_0}r^3j^2\left(\frac{d\varpi}{dr}\right)^2\\&\quad+4\pi re^{2\lambda_0}\left(\varepsilon_0+p_0\right)\delta P_0,\end{aligned} \tag{E.2}$$

$$\begin{aligned}\frac{dm_0}{dr}&=4\pi r^2\left(\varepsilon_0+p_0\right)\frac{d\varepsilon}{dp}\delta P_0+\frac{1}{12}r^4j^2\left(\frac{d\varpi}{dr}\right)^2\\&\quad-\frac{1}{3}r^3\varpi^2\frac{dj^2}{dr},\end{aligned} \tag{E.3}$$

$$\begin{aligned}\frac{dv_2}{dr}&=-2\frac{d\nu_0}{dr}h_2\\&\quad+\left(\frac{1}{r}+\frac{d\nu_0}{dr}\right)\left[\frac{1}{6}r^4j^2\left(\frac{d\varpi}{dr}\right)^2-\frac{1}{3}r^3\varpi^2\frac{dj^2}{dr}\right],\end{aligned} \tag{E.4}$$

$$\begin{aligned}\frac{dh_2}{dr} &= -\frac{2v_2}{r(r-2M)d\nu_0/dr} \\ &+ \left\{-2\frac{d\nu_0}{dr} + \frac{r}{2(r-2M)d\nu_0/dr}\left[8\pi\left(\varepsilon_0+p_0\right) - \frac{4M}{r^3}\right]\right\}h_2 \\ &+ \frac{1}{6}\left[r\frac{d\nu_0}{dr} - \frac{1}{2(r-2M)d\nu_0/dr}\right]r^3j^2\left(\frac{d\varpi}{dr}\right)^2 \\ &- \frac{2}{3}\left[r\frac{d\nu_0}{dr} + \frac{1}{2(r-2M)d\nu_0/dr}\right]r^2\varpi^2\frac{dj^2}{dr}. \end{aligned} \tag{E.5}$$

Here, one has the following relations:

$$e^{2\lambda_0} = \frac{r}{r-2M}, \tag{E.6}$$

$$M = M(r) = 4\pi\int_0^r \varepsilon_0 r^2 dr. \tag{E.7}$$

From Ref. [62], one has

$$2\frac{d\nu_0}{dr} + \frac{1}{r} = re^{2\lambda_0}\left(\frac{1}{r^2} + 8\pi p_0\right), \tag{E.8}$$

$$\frac{dp_0}{dr} = -(\varepsilon_0 + p_0)\frac{d\nu_0}{dr}, \tag{E.9}$$

$$\varpi = \Omega - \omega, \tag{E.10}$$

$$j = e^{-(\lambda_0+\nu_0)}, \tag{E.11}$$

$$v_2 = h_2 + k_2. \tag{E.12}$$

By differentiating Eq. (E.7), one has

$$\frac{dM}{dr} = 4\pi\varepsilon_0 r^2. \tag{E.13}$$

The Eq. (E.8) is transformed as,

$$\frac{d\nu_0}{dr} = \frac{\left(4\pi p_0 r^3 + M\right)}{r\left(r-2M\right)}. \tag{E.14}$$

By differentiating Eq. (E.11), one has

$$\frac{dj}{dr} = -j\left(\frac{d\lambda_0}{dr} + \frac{d\nu_0}{dr}\right), \tag{E.15}$$

By differentiating $r^4 j\frac{d\varpi}{dr}$, one has

$$\frac{d}{dr}\left(r^4 j\frac{d\varpi}{dr}\right) = \left(4r^3 j\frac{d\varpi}{dr} + r^4\frac{dj}{dr}\frac{d\varpi}{dr} + r^4 j\frac{d}{dr}\frac{d\varpi}{dr}\right). \tag{E.16}$$

Here, assuming

$$\frac{d\varpi}{dr} = g, \tag{E.17}$$

Eq. (E.16) is written as

$$\begin{aligned}\frac{d}{dr}g &= -\frac{1}{r^4 j}\left(4\frac{dj}{dr}\varpi r^3 + 4r^3 jg + r^4\frac{dj}{dr}g\right) \\ &= -\frac{4}{rj}\frac{dj}{dr}\varpi - \frac{4}{r}g - \frac{1}{j}\frac{dj}{dr}g.\end{aligned} \tag{E.18}$$

Eq. (E.2) is transformed as,

$$\begin{aligned}\frac{d}{dr}\delta P_0 = &\frac{1}{3}\frac{d}{dr}\left(r^2 e^{-2\nu_0}\varpi^2\right) - m_0 e^{4\lambda_0}\left(\frac{1}{r^2} + 8\pi p_0\right) \\ &+ \frac{1}{12}e^{2\lambda_0} r^3 j^2\left(\frac{d\varpi}{dr}\right)^2 \\ &- 4\pi r e^{2\lambda_0}\left(\varepsilon_0 + p_0\right)\delta P_0,\end{aligned}$$

Therefore, one has

$$\begin{aligned}\frac{d}{dr}\delta P_0 = &\frac{2}{3}rj^2 e^{2\lambda_0}\varpi^2 + \frac{2}{3}r^2 j\frac{dj}{dr}e^{2\lambda_0}\varpi^2 \\ &- \frac{1}{3}r^2 j^2\frac{2M}{(r-2M)^2}\varpi^2 + \frac{2}{3}r^2 j^2 e^{2\lambda_0}\varpi\frac{d\varpi}{dr} \\ &- m_0 e^{4\lambda_0}\left(\frac{1}{r^2} + 8\pi p_0\right) \\ &+ \frac{1}{12}e^{2\lambda_0} r^3 j^2\left(\frac{d\varpi}{dr}\right)^2 \\ &- 4\pi r e^{2\lambda_0}\left(\varepsilon_0 + p_0\right)\delta P_0.\end{aligned} \tag{E.19}$$

From Eq.(E.3), one has

$$\begin{aligned}\frac{dm_0}{dr} = &4\pi r^2\left(\varepsilon_0 + p_0\right)\frac{d\varepsilon}{dp}\delta P_0 \\ &+ \frac{1}{12}r^4 j^2\left(\frac{d\varpi}{dr}\right)^2 - \frac{2}{3}jr^3\varpi^2\frac{dj}{dr}.\end{aligned} \tag{E.20}$$

From Eq.(E.4), one has

$$\begin{aligned}\frac{dv_2}{dr} = &-2\frac{d\nu_0}{dr}h_2 \\ &+ \left(\frac{1}{r} + \frac{d\nu_0}{dr}\right)\left[\frac{1}{6}r^4 j^2\left(\frac{d\varpi}{dr}\right)^2 - \frac{2}{3}r^3\varpi^2 j\frac{dj}{dr}\right].\end{aligned} \tag{E.21}$$

From above equations, 9 nonlinear equations are obtained (Eqs. (E.5), (E.9), (E.13), (E.15), (E.17), (E.18), (E.19), (E.20), and (E.21)) with respect to 9 variables (M, p_0, j, g, ϖ, δP_0, m_0, v_2, and h_2). The equations are solved from $r = 0$. The initial value of the central density is given as ε_c where $\varepsilon_c = \varepsilon(r = 0)$. In addition, the pressure of the center $p_c = p(\varepsilon_c)$ is determined from the equation of state. The initial value of other variables are 0 except for j and ϖ. Here the initial value of j is taken as 1.

Appendix F

Energy levels in a strong magnetic field

Energy levels of a relativistic particle in a strong magnetic field were calculated in various references [70, 76, 77, 78, 79, 80]. Here we summarize the formula used in this paper. The energy spectra for charged baryons ($E^b_{\nu,s}$), neutral baryons (E^b_s), and leptons (E^l_ν) in a strong magnetic field in z-direction are derived from Dirac equation and given by

$$E^b_{\nu,s} = \sqrt{(k^b_z)^2 + \left(\overline{m}^c_{b,s}\right)^2} + g_{\omega b}\omega^0 + \tau_{3b} g_{\rho b}\rho^{03}, \tag{F.1}$$

$$E^b_s = \sqrt{(k^b_z)^2 + (\overline{m}_{b,s})^2} + g_{\omega b}\omega^0 + \tau_{3b} g_{\rho b}\rho^{03}, \tag{F.2}$$

$$E^l_\nu = \sqrt{(k^l_z)^2 + (\overline{m}_l)^2}, \tag{F.3}$$

respectively, where k^i_z is the wave-number of particle i in z-direction. Here, for simplicity, only σ, ω, and ρ mesons are treated. σ, ω^0 and ρ^{03} are expectation values of mesons in vacuum. Here effective masses are given by

$$\overline{m}^c_{b,s} = \sqrt{m^{*2}_b + 2\nu|q_b|B} - s\mu_N\kappa_b B, \tag{F.4}$$

$$\overline{m}_{b,s} = m^*_b - s\mu_N\kappa_b B, \tag{F.5}$$

$$\overline{m}_l = \sqrt{m^2_l + 2\nu|q_l|B}, \tag{F.6}$$

for charged baryons ($\overline{m}^c_{b,s}$), neutral baryons ($\overline{m}_{b,s}$), and leptons ($\overline{m}_l$), respectively. Here B indicates the strength of the magnetic field. q_i is charge of particle i and s $(= +1, -1)$ indicates its spin. κ_b is the anomalous magnetic moment of baryon b. Here the reduced mass is

$$m^*_b = m_b - g_{\sigma b}\sigma, \tag{F.7}$$

where m_b is the original baryon mass. The integer ν represents the Landau levels

$$\nu = n + \frac{1}{2} - \mathrm{sgn}(q_b)\frac{s}{2} = 0, 1, 2, \cdots, \nu_{\max}, \tag{F.8}$$

where n implies any integer greater than or equal to zero, and $s = +1$ for spin-up and $s = -1$ for spin-down, respectively. Namely, we should take differently the lowest values of ν, which takes 0 or 1, depending on the signs of charges and the spin third components. The maximum values of the Landau levels are given by

$$\nu_{\max} = \frac{(E_{\rm F}^b + s\mu_N\kappa_b B)^2 - m_b^{*2}}{2|q_b|B}, \tag{F.9}$$

$$\nu_{\max} = \frac{(E_{\rm F}^l)^2 - m_l^2}{2|q_l|B}, \tag{F.10}$$

for baryons and leptons, respectively. The Fermi wave numbers $k^b_{F,\nu,s}$, $k^b_{F,s}$, and $k^l_{F,\nu}$ are related with the Fermi energy (E_F) by

$$(E_F^b)^2 = \begin{cases} (k^b_{F,\nu,s})^2 + \left(\overline{m}^c_{b,s}\right)^2 \\ \\ (k^b_{F,s})^2 + \left(\overline{m}_{b,s}\right)^2 \end{cases}, \tag{F.11}$$

for charged baryons and neutral baryons, respectively, and

$$(E_F^l)^2 = (k^l_{F,\nu})^2 + \overline{m}_l^2 \tag{F.12}$$

for leptons. The vector number density is

$$\rho_b^v = \frac{|q_b|B}{2\pi^2}\sum_s\sum_\nu^{\nu_{\max}} k^b_{F,\nu,s}, \tag{F.13}$$

for charged baryons, and

$$\rho_b^v = \frac{1}{2\pi^2}\sum_s\left[\frac{1}{3}\left(k^b_{F,s}\right)^3 - \frac{1}{2}s\mu_N\kappa_b B \times\left\{\overline{m}_b k^b_{F,s} + \left(E_F^b\right)^2\left(\arcsin\left(\frac{\overline{m}_b}{E_F^b}\right) - \frac{\pi}{2}\right)\right\}\right], \tag{F.14}$$

for neutral baryons, and

$$\rho_l^v = \frac{|q_l|B}{2\pi^2}\sum_s\sum_\nu^{\nu_{\max}} k^l_{{\rm F},\nu}, \tag{F.15}$$

for leptons, respectively.

Then the total energy density for the matter is

$$\varepsilon_m = \sum_b \varepsilon_b + \sum_\ell \varepsilon_\ell + \frac{1}{2}m_\sigma^2\sigma^2 + U(\sigma) + \frac{1}{2}m_\omega^2\left(\omega^0\right)^2 + \frac{1}{2}m_\rho^2\left(\rho^{03}\right)^2, \tag{F.16}$$

where $U(\sigma) = \frac{1}{3}bm_n(g_\sigma\sigma)^2 + \frac{1}{4}c(g_\sigma\sigma)^4$. Here

$$\varepsilon_b^c = \frac{|q_b|\,B}{4\pi^2}\sum_s \sum_{\nu_{\min}(s)}^{\nu_{\max}(s)} \left[k_{F,\nu s}^b E_F^b + (\bar{m}_{b\nu s}^c)^2 \ln\left| \frac{k_{F,\nu s}^b + E_F^b}{\bar{m}_{b\nu s}^c} \right| \right], \tag{F.17}$$

for charged baryons, and

$$\begin{aligned}\varepsilon_b^n = \frac{1}{4\pi^2}\sum_s \Bigg[&\frac{1}{2}k_{F,s}^b \Big(E_F^b\Big)^3 - \frac{2}{3}s\mu_N\kappa_b B\Big(E_F^b\Big)^3 \left(\sin^{-1}\left(\frac{\bar{m}_{bs}}{E_F^b}\right) - \frac{\pi}{2}\right) \\ &- \left(\frac{1}{3}s\mu_N\kappa_b B + \frac{1}{4}\bar{m}_{bs}\right)\left(\bar{m}_{bs}k_{F,s}^b E_F^b + (\bar{m}_{bs})^3 \ln\left| \frac{k_{F,s}^b + E_F^b}{\bar{m}}_{bs} \right|\right)\Bigg],\end{aligned} \tag{F.18}$$

for neutral baryons, and

$$\varepsilon_\ell = \frac{|q_\ell|\,B}{4\pi^2}\sum_s \sum_{\nu_{\min}(s)}^{\nu_{\max}} \left[k_{F,\nu}^\ell E_F^\ell + (\bar{m}_{\ell\nu})^2 \ln\left| \frac{k_{F,\nu}^\ell + E_F^\ell}{\bar{m}_{\ell\nu}} \right| \right], \tag{F.19}$$

for leptons, respectively. Then the pressure for the matter is given by

$$p_m = \sum_i \mu_i \rho_i^v - \varepsilon_m, \tag{F.20}$$

where μ_i is the chemical potential of particle i. Including self-energy of the magnetic fields, the energy density ε and the pressure p in the presence of the magnetic fields are

$$\varepsilon = \varepsilon_m + \frac{B^2}{2}, \tag{F.21}$$

$$p = p_m + \frac{B^2}{2}, \tag{F.22}$$

respectively, which gives an EoS for a specific relativistic mean field theory.

Appendix G

Original results by changing α and γ for neutron star with magnetic fields ($B_s = 10^{12}$ G)

Here, the MR relations and Tables are given by calculations of changing α and γ for neutron star with magnetic fields ($B_s = 10^{12}$ G, $B_0 = 2.5 \times 10^{18}$ G). Tables show the values of maximum mass ($M_\odot$), radius (km) at $M = 1.4M_\odot$, and radius (km) at $M = 2.072M_\odot$ for each EoSs.

The MR relations of each EoSs with magnetic fields are shown in Fig. G.1 – G.12 (DDME2-a EoS; in Fig. G.1, DDME2-b EoS; in Fig. G.2, GM1 EoS; in Fig. G.3, GM3 EoS; in Fig. G.4, NL3-a EoS; in Fig. G.5, NL3-b EoS; in Fig. G.6, NL3$\omega\rho$-a EoS; in Fig. G.7, NL3$\omega\rho$-b EoS; in Fig. G.8, TM1-a EoS; in Fig. G.9, TM1-b EoS; in Fig. G.10, TM2$\omega\rho$-a EoS; in Fig. G.11, TM2$\omega\rho$-b EoS; in Fig. G.12). The colored lines of MR relations represent the following: dark blue (solid line); magnetic fields $B(\rho)$ with $\alpha = 0.01$, green (solid line); magnetic fields $B(\rho)$ with $\alpha = 0.02$, light blue (solid line); magnetic fields $B(\rho)$ with $\alpha = 0.03$, purple (solid line); magnetic fields $B(\rho)$ with $\alpha = 0.04$, red (solid line); magnetic fields $B(\rho)$ with $\alpha = 0.05$, dark blue (dashed line); magnetic fields $B(\rho)$ with $\alpha = 0.06$, green (dashed line); magnetic fields $B(\rho)$ with $\alpha = 0.07$, light blue (dashed line); magnetic fields $B(\rho)$ with $\alpha = 0.08$, purple (dashed line); magnetic fields $B(\rho)$ with $\alpha = 0.09$, red (dashed line); magnetic fields $B(\rho)$ with $\alpha = 0.10$.

For each EoS the maximum masses ($M_{\rm max}$), the radii at M=1.4 $M_\odot$, and radii at M = 2.072 $M_\odot$ are shown in Table G.1 – G.12 (DDME2-a EoS; in Table G.1, DDME2-b EoS; in Table G.2, GM1 EoS; in Table G.3, GM3 EoS; in Table G.4, NL3-a EoS; in Table G.5, NL3-b EoS; in Table G.6, NL3$\omega\rho$-a EoS; in Table G.7, NL3$\omega\rho$-b EoS; in Table G.8, TM1-a EoS; in Table G.9, TM1-b EoS; in Table G.10, TM2$\omega\rho$-a EoS; in Table G.11, TM2$\omega\rho$-b EoS; in Table G.12).

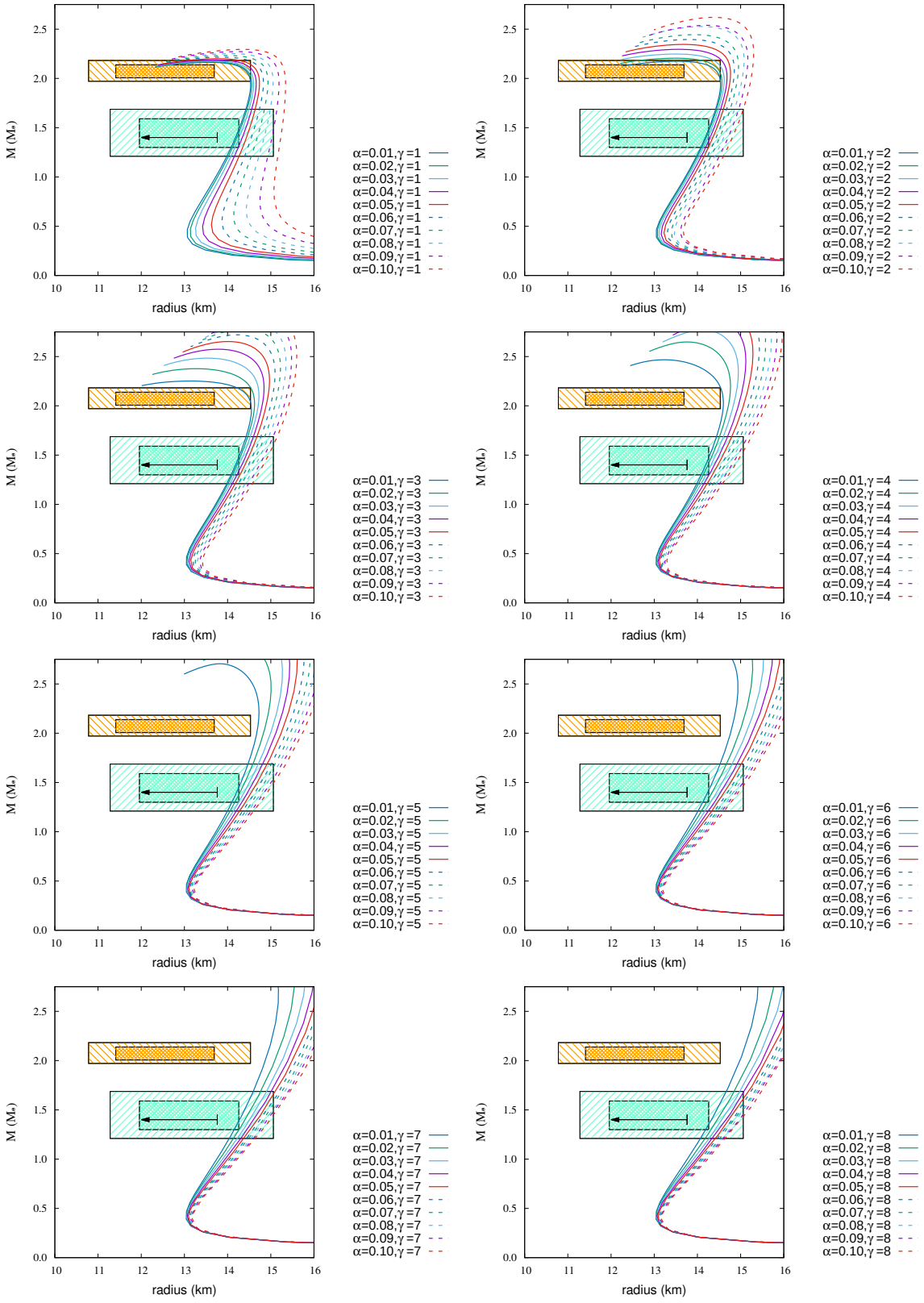

Figure G.1: MR relations of DDME2-a EoS with magnetic fields. The strength of surface magnetic field strength B_s is 10^{12} G, and the central magnetic field strength B_0 is 2.5×10^{18} G. The colored areas are the same as in Fig 6.1.

Table G.1: Maximum mass ($M_{\max}$) in unit of $M_\odot$ and radius (km) at $M = 1.4M_\odot$ ($R_{1.4M_\odot}$) and radius (km) at $M = 2.072M_\odot$ ($R_{2.072M_\odot}$) for DDME2-a EoS with magnetic fields ($B_0 = 2.5 \times 10^{18}$ G, $B_s = 10^{12}$ G).

$\gamma = 1$				$\gamma = 2$			
α	$M_{\max}$	$R_{1.4M_\odot}$	$R_{2.072M_\odot}$	α	$M_{\max}$	$R_{1.4M_\odot}$	$R_{2.072M_\odot}$
0.01	2.163	14.18	14.43	0.01	2.174	14.18	14.45
0.02	2.168	14.22	14.47	0.02	2.205	14.21	14.51
0.03	2.176	14.27	14.52	0.03	2.247	14.24	14.59
0.04	2.187	14.34	14.59	0.04	2.295	14.30	14.68
0.05	2.200	14.44	14.68	0.05	2.345	14.36	14.76
0.06	2.215	14.55	14.78	0.06	2.395	14.43	14.86
0.07	2.233	14.69	14.90	0.07	2.444	14.52	14.95
0.08	2.252	14.85	15.02	0.08	2.527	14.61	15.06
0.09	2.272	15.03	15.16	0.09	2.539	14.71	15.15
0.10	2.295	15.23	15.31	0.10	2.620	14.81	15.27
$\gamma = 3$				$\gamma = 4$			
α	$M_{\max}$	$R_{1.4M_\odot}$	$R_{2.072M_\odot}$	α	$M_{\max}$	$R_{1.4M_\odot}$	$R_{2.072M_\odot}$
0.01	2.251	14.18	14.50	0.01	2.467	14.19	14.60
0.02	2.377	14.22	14.62	0.02	2.648	14.25	14.74
0.03	2.484	14.27	14.72	0.03	2.770	14.32	14.87
0.04	2.574	14.33	14.83	0.04	2.862	14.39	14.99
0.05	2.652	14.40	14.93	0.05	2.935	14.48	15.12
0.06	2.721	14.48	15.03	0.06	2.995	14.56	15.23
0.07	2.781	14.56	15.13	0.07	3.046	14.64	15.35
0.08	2.835	14.65	15.24	0.08	3.091	14.72	15.45
0.09	2.885	14.74	15.35	0.09	3.130	14.80	15.55
0.10	2.929	14.83	15.46	0.10	3.166	14.88	15.65
$\gamma =5$				$\gamma =6$			
α	$M_{\max}$	$R_{1.4M_\odot}$	$R_{2.072M_\odot}$	α	$M_{\max}$	$R_{1.4M_\odot}$	$R_{2.072M_\odot}$
0.01	2.705	14.21	14.70	0.01	2.900	14.24	14.81
0.02	2.884	14.29	14.88	0.02	3.055	14.35	15.02
0.03	3.010	14.39	15.05	0.03	3.145	14.45	15.19
0.04	3.069	14.47	15.17	0.04	3.209	14.54	15.34
0.05	3.128	14.55	15.30	0.05	3.259	14.63	15.46
0.05	3.177	14.64	15.42	0.06	3.301	14.71	15.57
0.07	3.219	14.72	15.52	0.07	3.337	14.78	15.67
0.08	3.256	14.79	15.62	0.08	3.370	14.84	15.76
0.09	3.289	14.86	15.71	0.09	3.399	14.90	15.84
0.10	3.331	14.93	15.81	0.10	3.425	14.96	15.91
$\gamma =7$				$\gamma =8$			
α	$M_{\max}$	$R_{1.4M_\odot}$	$R_{2.072M_\odot}$	α	$M_{\max}$	$R_{1.4M_\odot}$	$R_{2.072M_\odot}$
0.01	3.046	14.28	14.93	0.01	3.153	14.33	15.05
0.02	3.176	14.41	15.16	0.02	3.267	14.47	15.29
0.03	3.253	14.52	15.34	0.03	3.337	14.58	15.46
0.04	3.310	14.61	15.47	0.04	3.390	14.67	15.59
0.05	3.355	14.69	15.59	0.05	3.433	14.75	15.69
0.06	3.394	14.77	15.69	0.06	3.469	14.81	15.79
0.07	3.427	14.83	15.78	0.07	3.501	14.86	15.87
0.08	3.457	14.88	15.86	0.08	3.528	14.92	15.94
0.09	3.484	14.94	15.93	0.09	3.553	14.97	16.01
0.10	3.509	15.00	16.00	0.10	3.575	15.01	16.07

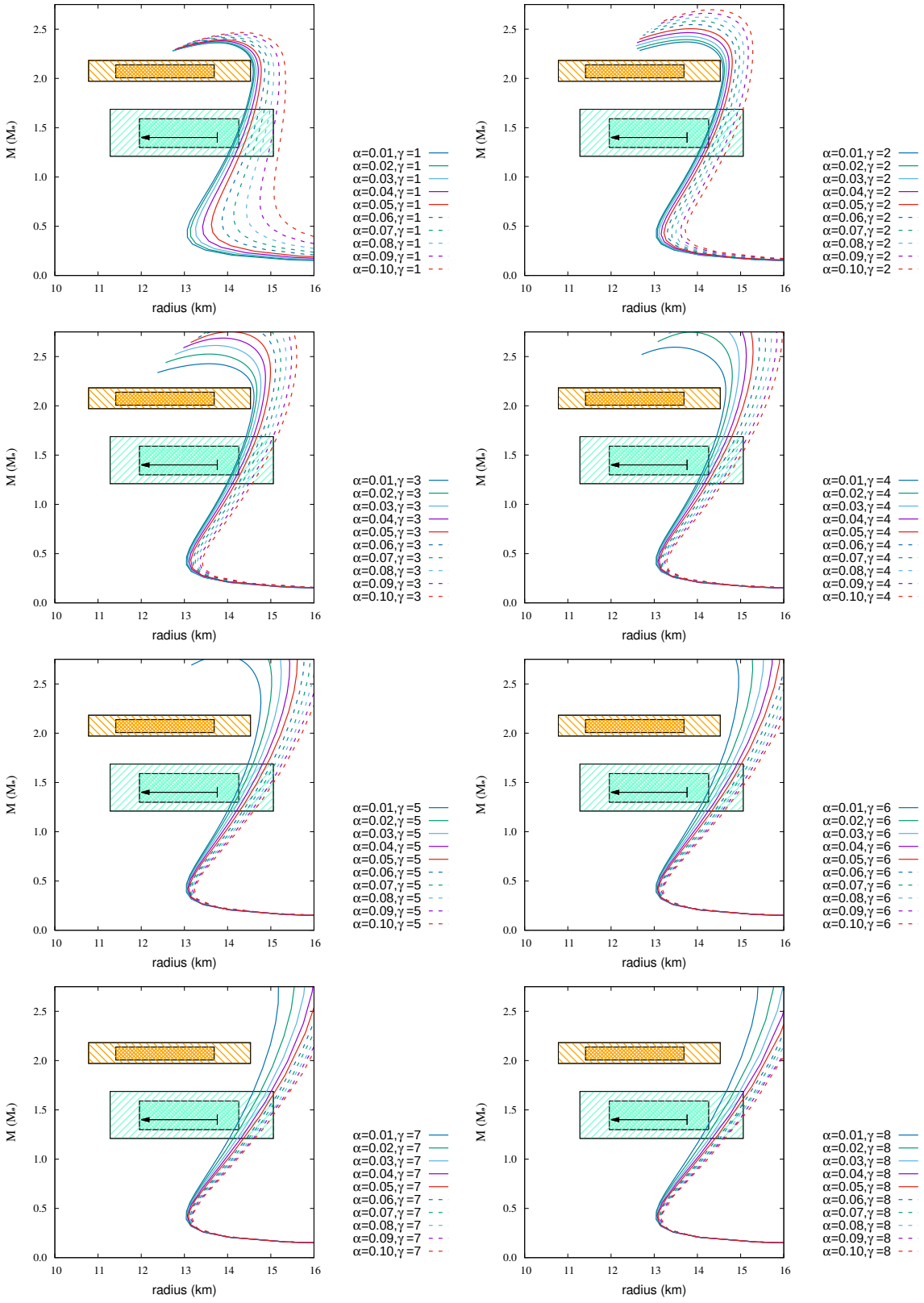

Figure G.2: Same as Fig. G.1, but for DDME2-b EoS ($B_s = 10^{12}\,G$).

Table G.2: Same as Table G.1, but for DDME2-b EoS ($B_s = 10^{12}\,G$).

γ =1				γ =2			
α	$M_{\max}$	$R_{1.4M_\odot}$	$R_{2.072M_\odot}$	α	$M_{\max}$	$R_{1.4M_\odot}$	$R_{2.072M_\odot}$
0.01	2.362	14.18	14.59	0.01	2.370	14.18	14.60
0.02	2.366	14.22	14.62	0.02	2.394	14.21	14.62
0.03	2.372	14.27	14.66	0.03	2.427	14.24	14.67
0.04	2.381	14.34	14.71	0.04	2.465	14.30	14.73
0.05	2.391	14.44	14.78	0.05	2.505	14.36	14.79
0.06	2.403	14.55	14.86	0.06	2.547	14.43	14.87
0.07	2.417	14.69	14.96	0.07	2.584	14.52	14.95
0.08	2.432	14.85	15.07	0.08	2.622	14.61	15.05
0.09	2.449	15.03	15.19	0.09	2.661	14.71	15.15
0.10	2.466	15.23	15.34	0.10	2.697	14.81	15.25
γ =3				γ =4			
α	$M_{\max}$	$R_{1.4M_\odot}$	$R_{2.072M_\odot}$	α	$M_{\max}$	$R_{1.4M_\odot}$	$R_{2.072M_\odot}$
0.01	2.427	14.18	14.61	0.01	2.595	14.19	14.64
0.02	2.525	14.22	14.67	0.02	2.748	14.25	14.75
0.03	2.612	14.27	14.74	0.03	2.849	14.32	14.87
0.04	2.687	14.33	14.83	0.04	2.926	14.39	14.99
0.05	2.752	14.40	14.93	0.05	2.987	14.48	15.12
0.06	2.807	14.48	15.03	0.06	3.040	14.56	15.23
0.07	2.859	14.56	15.13	0.07	3.084	14.64	15.35
0.08	2.906	14.65	15.24	0.08	3.124	14.72	15.45
0.09	2.947	14.74	15.35	0.09	3.159	14.80	15.55
0.10	2.983	14.83	15.46	0.10	3.191	14.88	15.65
γ =5				γ =6			
α	$M_{\max}$	$R_{1.4M_\odot}$	$R_{2.072M_\odot}$	α	$M_{\max}$	$R_{1.4M_\odot}$	$R_{2.072M_\odot}$
0.01	2.793	14.21	14.71	0.01	2.958	14.24	14.81
0.02	2.944	14.29	14.88	0.02	3.091	14.35	15.02
0.03	3.037	14.38	15.03	0.03	3.168	14.45	15.19
0.04	3.103	14.47	15.17	0.04	3.226	14.54	15.34
0.05	3.155	14.55	15.30	0.05	3.273	14.63	15.46
0.05	3.198	14.64	15.42	0.06	3.313	14.71	15.57
0.07	3.237	14.72	15.52	0.07	3.347	14.78	15.67
0.08	3.271	14.79	15.62	0.08	3.378	14.84	15.76
0.09	3.302	14.86	15.71	0.09	3.406	14.90	15.84
0.10	3.331	14.92	15.80	0.10	3.432	14.96	15.91
γ =7				γ =8			
α	$M_{\max}$	$R_{1.4M_\odot}$	$R_{2.072M_\odot}$	α	$M_{\max}$	$R_{1.4M_\odot}$	$R_{2.072M_\odot}$
0.01	3.082	14.28	14.93	0.01	3.173	14.33	15.05
0.02	3.196	14.41	15.16	0.02	3.280	14.47	15.29
0.03	3.267	14.52	15.34	0.03	3.347	14.58	15.46
0.04	3.321	14.61	15.47	0.04	3.398	14.67	15.59
0.05	3.364	14.69	15.59	0.05	3.440	14.75	15.69
0.06	3.402	14.77	15.69	0.06	3.475	14.81	15.79
0.07	3.434	14.83	15.78	0.07	3.506	14.86	15.87
0.08	3.463	14.88	15.86	0.08	3.533	14.92	15.94
0.09	3.490	14.94	15.93	0.09	3.557	14.97	16.01
0.10	3.514	15.00	16.00	0.10	3.579	15.01	16.07

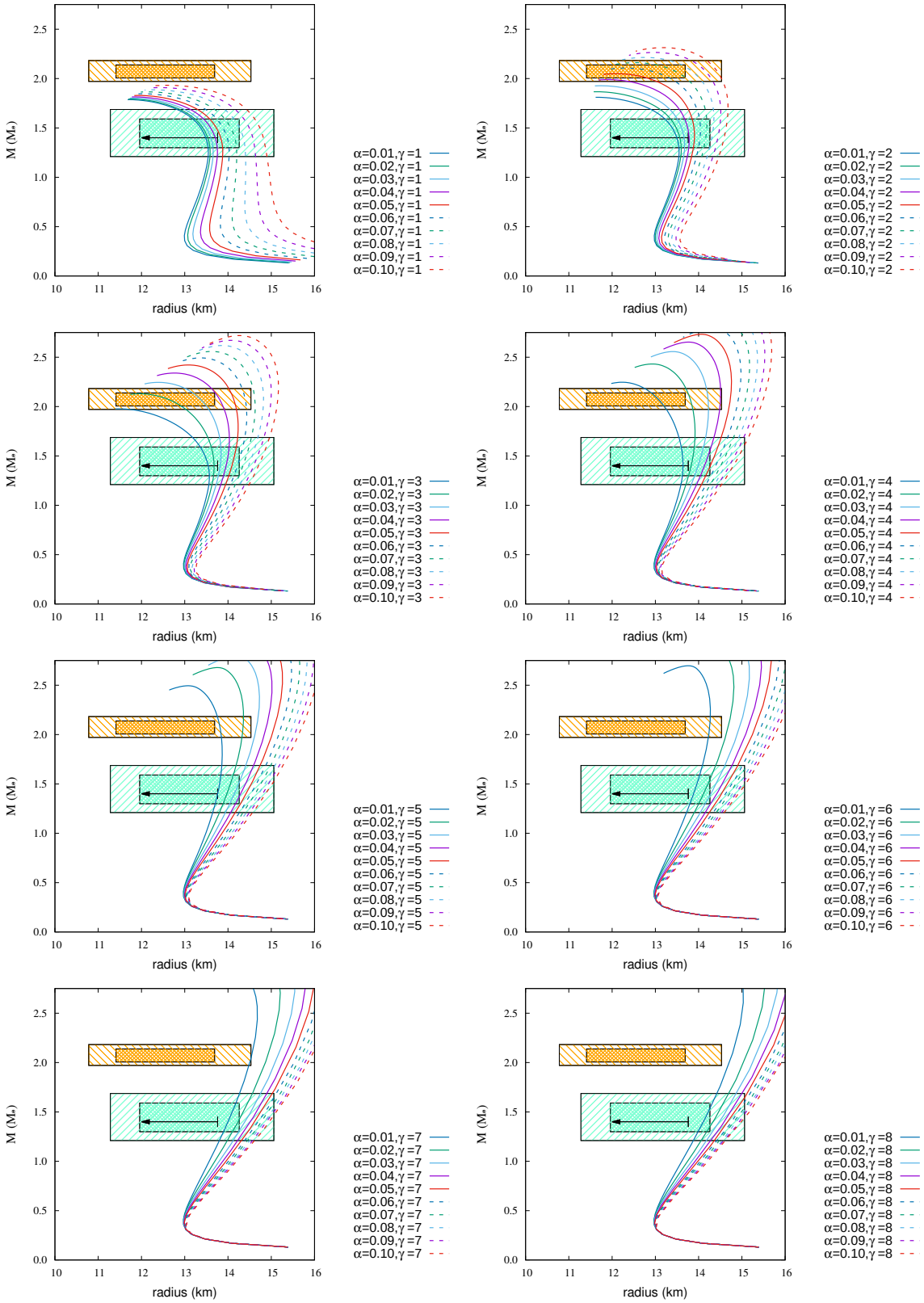

Figure G.3: Same as Fig. G.1, but for GM1 EoS ($B_s = 10^{12}\,G$).

Table G.3: Same as Table G.1, but for GM1 EoS ($B_s = 10^{12}\,G$).

γ =1				γ =2			
α	$M_{\max}$	$R_{1.4M_\odot}$	$R_{2.072M_\odot}$	α	$M_{\max}$	$R_{1.4M_\odot}$	$R_{2.072M_\odot}$
0.01	1.786	13.49	—	0.01	1.810	13.50	—
0.02	1.792	13.53	—	0.02	1.867	13.57	—
0.03	1.802	13.60	—	0.03	1.927	13.66	—
0.04	1.814	13.70	—	0.04	1.989	13.78	—
0.05	1.829	13.83	—	0.05	2.049	13.90	—
0.06	1.846	13.98	—	0.06	2.107	14.03	12.93
0.07	1.865	14.16	—	0.07	2.161	14.16	13.47
0.08	1.886	14.35	—	0.08	2.214	14.30	13.85
0.09	1.908	14.57	—	0.09	2.265	14.44	14.16
0.10	1.932	14.82	—	0.10	2.313	14.59	14.43
γ =3				γ =4			
α	$M_{\max}$	$R_{1.4M_\odot}$	$R_{2.072M_\odot}$	α	$M_{\max}$	$R_{1.4M_\odot}$	$R_{2.072M_\odot}$
0.01	1.977	13.54	—	0.01	2.247	13.64	13.07
0.02	2.130	13.68	12.62	0.02	2.431	13.83	13.81
0.03	2.245	13.82	13.37	0.03	2.557	13.99	14.22
0.04	2.339	13.96	13.81	0.04	2.653	14.14	14.51
0.05	2.421	14.09	14.13	0.05	2.732	14.27	14.73
0.06	2.493	14.22	14.40	0.06	2.800	14.40	14.92
0.07	2.558	14.35	14.62	0.07	2.862	14.51	15.08
0.08	2.619	14.47	14.82	0.08	2.915	14.62	15.23
0.09	2.671	14.59	15.00	0.09	2.962	14.71	15.37
0.10	2.719	14.71	15.15	0.10	3.005	14.81	15.49
γ =5				γ =6			
α	$M_{\max}$	$R_{1.4M_\odot}$	$R_{2.072M_\odot}$	α	$M_{\max}$	$R_{1.4M_\odot}$	$R_{2.072M_\odot}$
0.01	2.494	13.76	13.82	0.01	2.697	13.88	14.25
0.02	2.679	13.98	14.35	0.02	2.873	14.11	14.68
0.03	2.799	14.15	14.66	0.03	2.981	14.28	14.95
0.04	2.889	14.29	14.88	0.04	3.061	14.42	15.15
0.05	2.960	14.42	15.07	0.05	3.125	14.53	15.31
0.05	3.020	14.53	15.23	0.06	3.178	14.63	15.45
0.07	3.072	14.63	15.37	0.07	3.224	14.72	15.57
0.08	3.118	14.72	15.50	0.08	3.265	14.79	15.67
0.09	3.160	14.80	15.61	0.09	3.301	14.86	15.77
0.10	3.197	14.88	15.71	0.10	3.334	14.93	15.86
γ =7				γ =8			
α	$M_{\max}$	$R_{1.4M_\odot}$	$R_{2.072M_\odot}$	α	$M_{\max}$	$R_{1.4M_\odot}$	$R_{2.072M_\odot}$
0.01	2.863	14.00	14.55	0.01	2.993	14.11	14.77
0.02	3.021	14.23	14.92	0.02	3.140	14.33	15.11
0.03	3.120	14.39	15.16	0.03	3.229	14.48	15.33
0.04	3.192	14.52	15.34	0.04	3.295	14.60	15.49
0.05	3.250	14.62	15.49	0.05	3.346	14.69	15.62
0.06	3.297	14.71	15.61	0.06	3.389	14.77	15.73
0.07	3.338	14.78	15.71	0.07	3.426	14.84	15.82
0.08	3.374	14.85	15.80	0.08	3.459	14.90	15.90
0.09	3.406	14.91	15.88	0.09	3.488	14.95	15.97
0.10	3.435	14.97	15.96	0.10	3.514	14.99	16.03

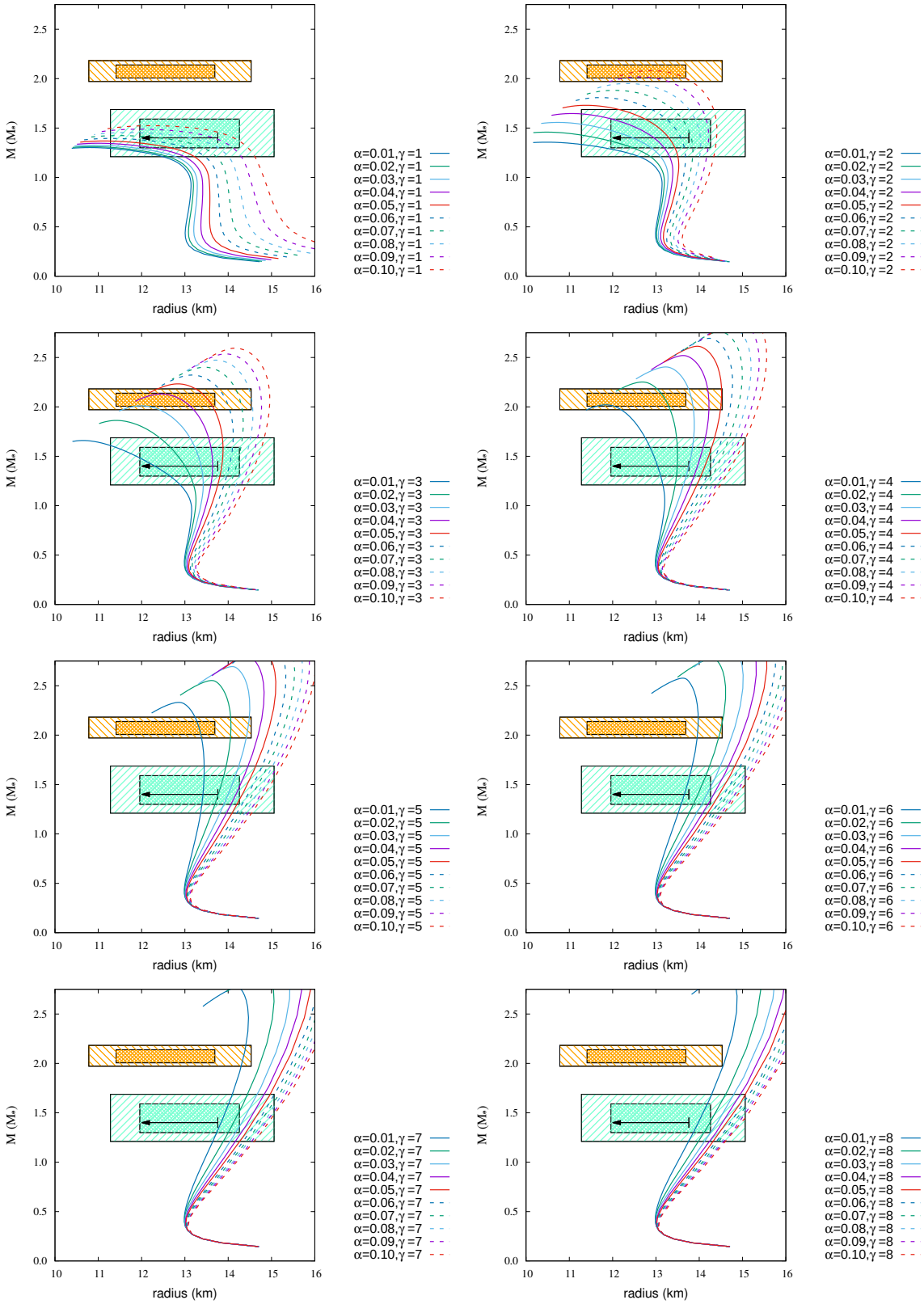

Figure G.4: Same as Fig. G.1, but for GM3 EoS ($B_s = 10^{12}\,G$).

Table G.4: Same as Table G.1, but for GM3 EoS ($B_s = 10^{12}\,G$).

γ =1				γ =2			
α	$M_{\max}$	$R_{1.4M_\odot}$	$R_{2.072M_\odot}$	α	$M_{\max}$	$R_{1.4M_\odot}$	$R_{2.072M_\odot}$
0.01	1.302	—	—	0.01	1.357	—	—
0.02	1.312	—	—	0.02	1.458	11.63	—
0.03	1.327	—	—	0.03	1.557	12.46	—
0.04	1.346	—	—	0.04	1.647	12.95	—
0.05	1.369	—	—	0.05	1.730	13.30	—
0.06	1.395	11.28	—	0.06	1.808	13.58	—
0.07	1.424	12.41	—	0.07	1.881	13.82	—
0.08	1.455	13.13	—	0.08	1.951	14.03	—
0.09	1.488	13.67	—	0.09	2.018	14.22	—
0.10	1.524	14.13	—	0.10	2.081	14.40	13.19
γ =3				γ =4			
α	$M_{\max}$	$R_{1.4M_\odot}$	$R_{2.072M_\odot}$	α	$M_{\max}$	$R_{1.4M_\odot}$	$R_{2.072M_\odot}$
0.01	1.660	12.31	—	0.01	2.021	13.04	—
0.02	1.863	13.00	—	0.02	2.252	13.49	13.22
0.03	2.011	13.38	—	0.03	2.404	13.76	13.83
0.04	2.130	13.64	12.92	0.04	2.520	13.96	14.22
0.05	2.233	13.85	13.54	0.05	2.614	14.13	14.51
0.06	2.322	14.03	13.95	0.06	2.694	14.28	14.74
0.07	2.402	14.19	14.27	0.07	2.763	14.42	14.94
0.08	2.473	14.34	14.54	0.08	2.824	14.54	15.11
0.09	2.536	14.48	14.77	0.09	2.878	14.65	15.26
0.10	2.594	14.61	14.96	0.10	2.927	14.75	15.40
γ =5				γ =6			
α	$M_{\max}$	$R_{1.4M_\odot}$	$R_{2.072M_\odot}$	α	$M_{\max}$	$R_{1.4M_\odot}$	$R_{2.072M_\odot}$
0.01	2.768	13.84	14.36	0.01	2.917	13.98	14.63
0.02	2.949	14.13	14.80	0.02	3.082	14.25	15.02
0.03	3.060	14.31	15.07	0.03	3.180	14.42	15.26
0.04	3.139	14.45	15.27	0.04	3.250	14.55	15.43
0.05	3.201	14.57	15.42	0.05	3.306	14.65	15.57
0.06	3.253	14.66	15.55	0.06	3.353	14.73	15.68
0.07	3.297	14.75	15.66	0.07	3.392	14.81	15.78
0.08	3.336	14.82	15.76	0.08	3.427	14.87	15.86
0.09	3.370	14.89	15.85	0.09	3.458	14.93	15.94
0.10	3.401	14.95	15.93	0.10	3.486	14.98	16.01
γ =7				γ =8			
α	$M_{\max}$	$R_{1.4M_\odot}$	$R_{2.072M_\odot}$	α	$M_{\max}$	$R_{1.4M_\odot}$	$R_{2.072M_\odot}$
0.01	2.331	13.42	13.33	0.01	2.577	13.66	13.97
0.02	2.553	13.77	14.06	0.02	2.779	13.97	14.51
0.03	2.694	14.00	14.46	0.03	2.902	14.18	14.82
0.04	2.796	14.18	14.73	0.04	2.993	14.34	15.04
0.05	2.877	14.33	14.95	0.05	3.065	14.47	15.23
0.06	2.945	14.45	15.13	0.06	3.123	14.58	15.38
0.07	3.005	14.57	15.28	0.07	3.174	14.67	15.51
0.08	3.056	14.66	15.42	0.08	3.218	14.75	15.62
0.09	3.102	14.76	15.54	0.09	3.257	14.83	15.72
0.10	3.143	14.84	15.65	0.10	3.292	14.90	15.82

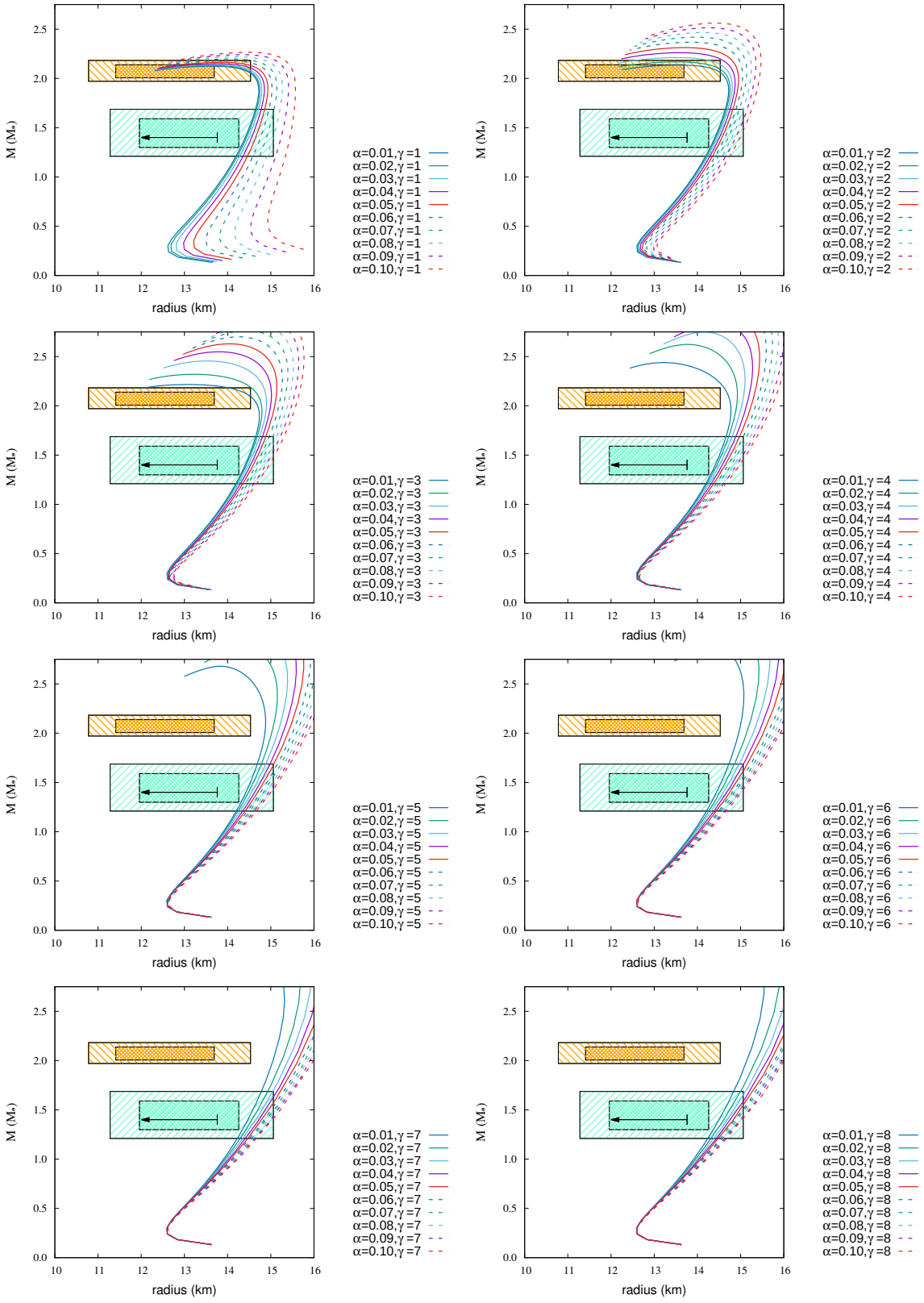

Figure G.5: Same as Fig. G.1, but for NL3-a EoS ($B_s = 10^{12}\,G$).

Table G.5: Same as Table G.1, but for NL3-a EoS ($B_s = 10^{12}\,G$).

γ =1				γ =2			
α	$M_{\max}$	$R_{1.4M_\odot}$	$R_{2.072M_\odot}$	α	$M_{\max}$	$R_{1.4M_\odot}$	$R_{2.072M_\odot}$
0.01	2.124	14.41	14.45	0.01	2.135	14.41	14.49
0.02	2.129	14.44	14.50	0.02	2.167	14.43	14.59
0.03	2.138	14.49	14.58	0.03	2.211	14.46	14.71
0.04	2.149	14.56	14.67	0.04	2.261	14.51	14.82
0.05	2.163	14.65	14.78	0.05	2.313	14.57	14.93
0.06	2.180	14.76	14.91	0.06	2.368	14.64	15.04
0.07	2.198	14.90	15.04	0.07	2.419	14.71	15.14
0.08	2.219	15.06	15.19	0.08	2.466	14.80	15.25
0.09	2.241	15.24	15.34	0.09	2.514	14.89	15.35
0.10	2.265	15.44	15.51	0.10	2.561	14.99	15.46
γ =3				γ =4			
α	$M_{\max}$	$R_{1.4M_\odot}$	$R_{2.072M_\odot}$	α	$M_{\max}$	$R_{1.4M_\odot}$	$R_{2.072M_\odot}$
0.01	2.216	14.41	14.59	0.01	2.438	14.41	14.74
0.02	2.320	14.44	14.74	0.02	2.623	14.46	14.92
0.03	2.455	14.48	14.90	0.03	2.749	14.51	15.06
0.04	2.548	14.53	15.01	0.04	2.845	14.58	15.18
0.05	2.629	14.60	15.12	0.05	2.922	14.64	15.29
0.06	2.700	14.66	15.22	0.06	2.987	14.72	15.40
0.07	2.763	14.73	15.32	0.07	3.042	14.78	15.51
0.08	2.820	14.81	15.43	0.08	3.090	14.85	15.61
0.09	2.872	14.89	15.53	0.09	3.133	14.92	15.71
0.10	2.919	14.96	15.63	0.10	3.171	14.98	15.80
γ =5				γ =6			
α	$M_{\max}$	$R_{1.4M_\odot}$	$R_{2.072M_\odot}$	α	$M_{\max}$	$R_{1.4M_\odot}$	$R_{2.072M_\odot}$
0.01	2.680	14.43	14.88	0.01	2.881	14.44	14.99
0.02	2.866	14.49	15.06	0.02	3.049	14.52	15.19
0.03	2.981	14.56	15.21	0.03	3.147	14.61	15.35
0.04	3.065	14.63	15.34	0.04	3.217	14.68	15.49
0.05	3.129	14.70	15.46	0.05	3.271	14.75	15.60
0.06	3.183	14.77	15.57	0.06	3.328	14.82	15.71
0.07	3.228	14.83	15.67	0.07	3.356	14.87	15.79
0.08	3.268	14.89	15.76	0.08	3.390	14.93	15.87
0.09	3.303	14.95	15.84	0.09	3.421	14.98	15.95
0.10	3.335	15.01	15.92	0.10	3.448	15.03	16.02
γ =7				γ =8			
α	$M_{\max}$	$R_{1.4M_\odot}$	$R_{2.072M_\odot}$	α	$M_{\max}$	$R_{1.4M_\odot}$	$R_{2.072M_\odot}$
0.01	3.038	14.47	15.10	0.01	3.156	14.50	15.21
0.02	3.182	14.57	15.32	0.02	3.280	14.61	15.44
0.03	3.265	14.65	15.48	0.03	3.356	14.70	15.59
0.04	3.326	14.73	15.61	0.04	3.411	14.77	15.71
0.05	3.375	14.80	15.71	0.05	3.455	14.83	15.81
0.06	3.415	14.86	15.81	0.06	3.492	14.89	15.89
0.07	3.450	14.91	15.89	0.07	3.524	14.94	15.96
0.08	3.481	14.96	15.96	0.08	3.553	14.98	16.03
0.09	3.508	15.01	16.03	0.09	3.578	15.02	16.09
0.10	3.534	15.05	16.09	0.10	3.601	15.06	16.14

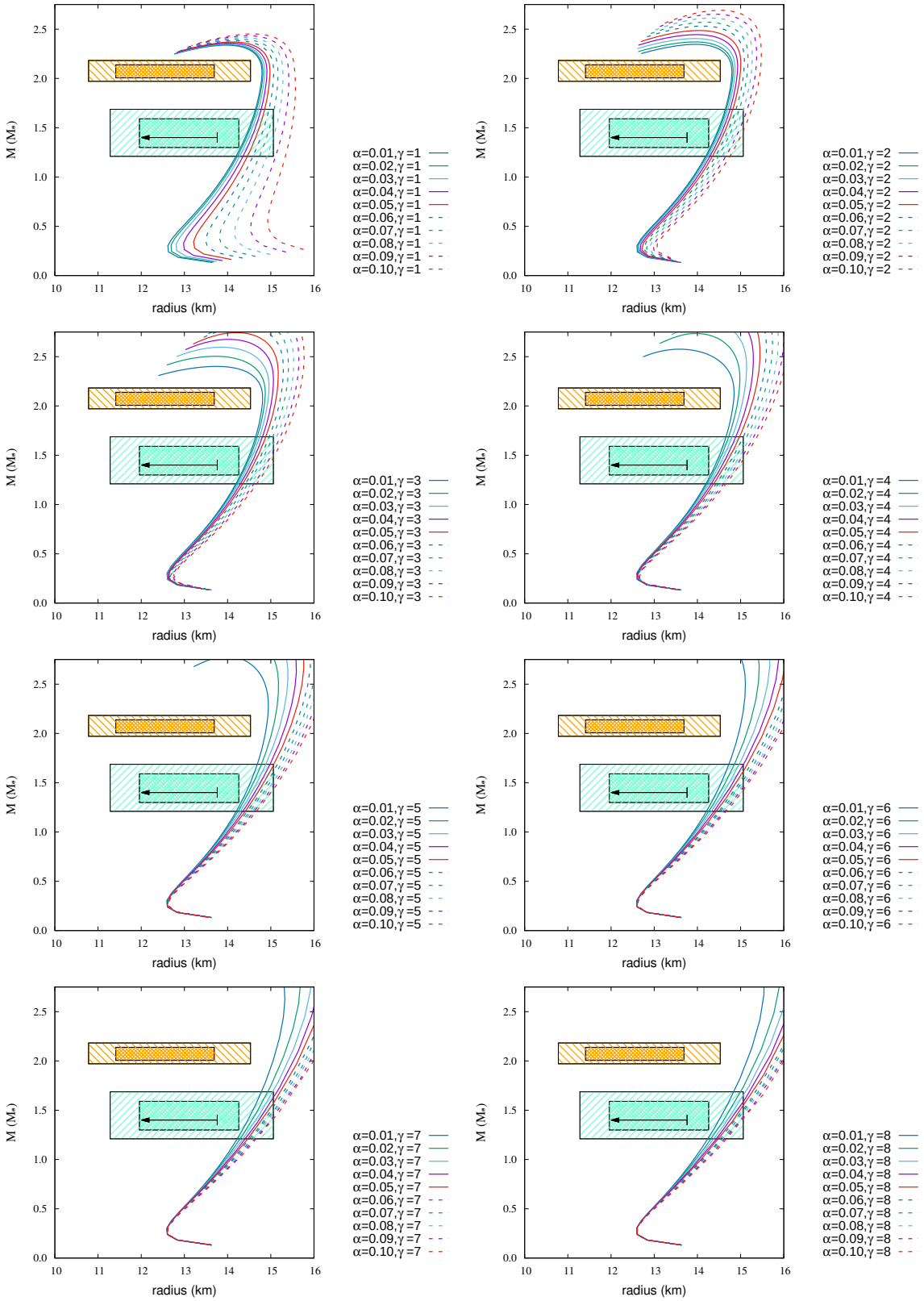

Figure G.6: Same as Fig. G.1, but for NL3-b EoS ($B_s = 10^{12}\,G$).

Table G.6: Same as Table G.1, but for NL3-b EoS ($B_s = 10^{12}\,G$).

γ =1				γ =2			
α	$M_{\max}$	$R_{1.4M_\odot}$	$R_{2.072M_\odot}$	α	$M_{\max}$	$R_{1.4M_\odot}$	$R_{2.072M_\odot}$
0.01	2.338	14.41	14.80	0.01	2.346	14.41	14.80
0.02	2.342	14.44	14.82	0.02	2.371	14.43	14.83
0.03	2.349	14.49	14.86	0.03	2.405	14.46	14.87
0.04	2.358	14.56	14.91	0.04	2.444	14.51	14.93
0.05	2.370	14.65	14.98	0.05	2.486	14.57	15.00
0.06	2.383	14.76	15.07	0.06	2.531	14.64	15.08
0.07	2.398	14.90	15.17	0.07	2.571	14.71	15.16
0.08	2.415	15.06	15.28	0.08	2.612	14.80	15.25
0.09	2.433	15.24	15.41	0.09	2.652	14.89	15.35
0.10	2.452	15.44	15.56	0.10	2.691	14.99	15.46
γ =3				γ =4			
α	$M_{\max}$	$R_{1.4M_\odot}$	$R_{2.072M_\odot}$	α	$M_{\max}$	$R_{1.4M_\odot}$	$R_{2.072M_\odot}$
0.01	2.401	14.41	14.81	0.01	2.576	14.41	14.84
0.02	2.504	14.44	14.87	0.02	2.735	14.46	14.94
0.03	2.596	14.48	14.94	0.03	2.844	14.51	15.06
0.04	2.675	14.53	15.03	0.04	2.927	14.58	15.18
0.05	2.743	14.60	15.12	0.05	2.992	14.64	15.29
0.06	2.804	14.66	15.22	0.06	3.047	14.72	15.40
0.07	2.857	14.73	15.32	0.07	3.094	14.78	15.51
0.08	2.906	14.81	15.43	0.08	3.136	14.85	15.61
0.09	2.951	14.89	15.53	0.09	3.173	14.92	15.71
0.10	2.992	14.96	15.63	0.10	3.207	14.98	15.80
γ =5				γ =6			
α	$M_{\max}$	$R_{1.4M_\odot}$	$R_{2.072M_\odot}$	α	$M_{\max}$	$R_{1.4M_\odot}$	$R_{2.072M_\odot}$
0.01	2.784	14.43	14.90	0.01	2.957	14.44	14.99
0.02	2.944	14.49	15.06	0.02	3.099	14.52	15.19
0.03	3.042	14.56	15.21	0.03	3.182	14.61	15.35
0.04	3.113	14.63	15.34	0.04	3.242	14.68	15.49
0.05	3.169	14.70	15.46	0.05	3.291	14.75	15.60
0.06	3.215	14.77	15.57	0.06	3.338	14.82	15.71
0.07	3.254	14.83	15.67	0.07	3.370	14.87	15.79
0.08	3.290	14.89	15.76	0.08	3.402	14.93	15.87
0.09	3.321	14.95	15.84	0.09	3.431	14.98	15.95
0.10	3.351	15.01	15.92	0.10	3.458	15.03	16.02
γ =7				γ =8			
α	$M_{\max}$	$R_{1.4M_\odot}$	$R_{2.072M_\odot}$	α	$M_{\max}$	$R_{1.4M_\odot}$	$R_{2.072M_\odot}$
0.01	3.090	14.47	15.10	0.01	3.186	14.50	15.21
0.02	3.210	14.57	15.32	0.02	3.298	14.61	15.44
0.03	3.284	14.65	15.48	0.03	3.369	14.70	15.59
0.04	3.341	14.73	15.61	0.04	3.422	14.77	15.71
0.05	3.387	14.80	15.71	0.05	3.465	14.83	15.81
0.06	3.426	14.86	15.81	0.06	3.501	14.89	15.89
0.07	3.459	14.91	15.89	0.07	3.532	14.94	15.96
0.08	3.489	14.96	15.96	0.08	3.559	14.98	16.03
0.09	3.516	15.01	16.03	0.09	3.584	15.02	16.09
0.10	3.540	15.05	16.09	0.10	3.607	15.06	16.14

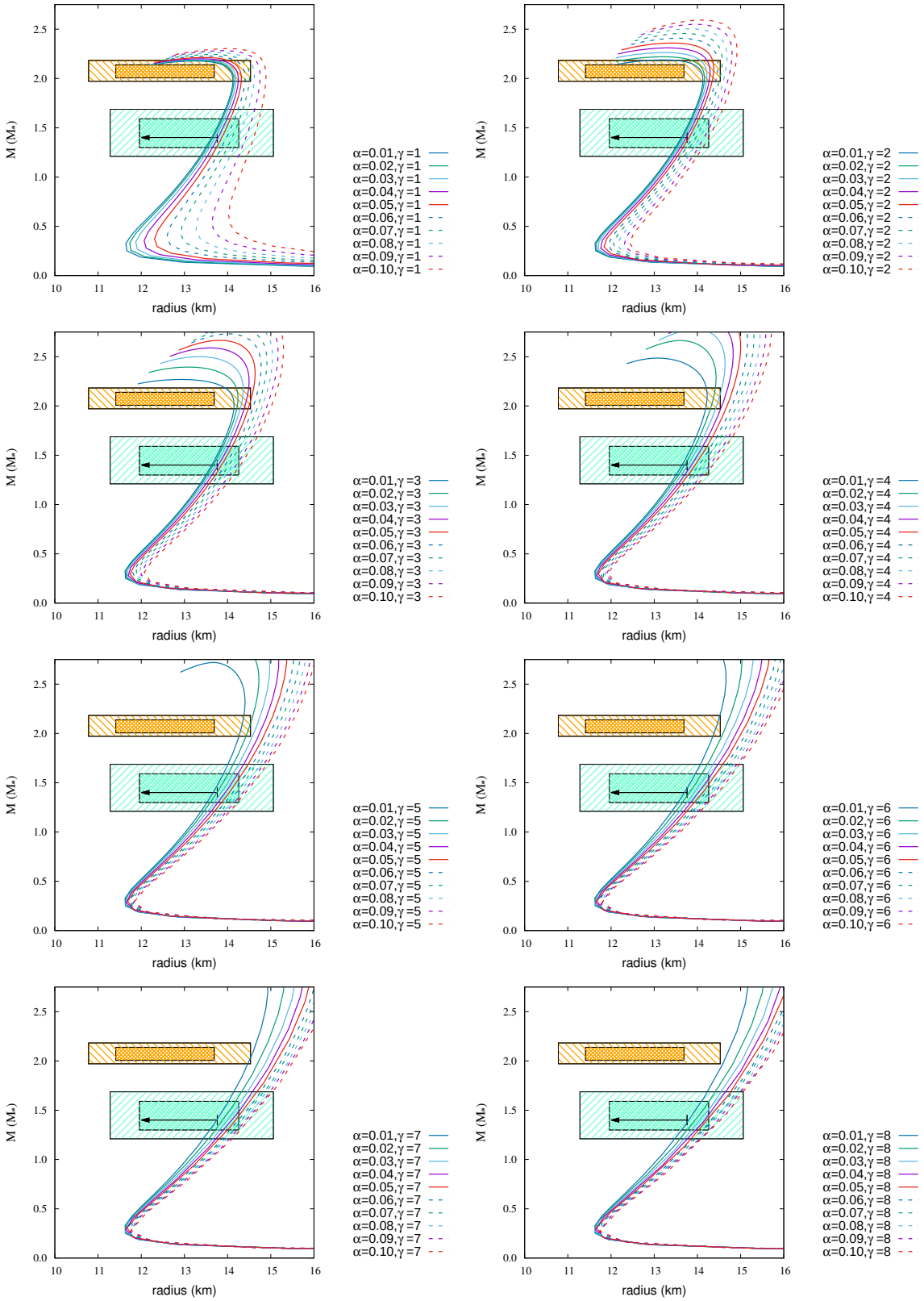

Figure G.7: Same as Fig. G.1, but for NL3$\omega\rho$-a EoS ($B_s = 10^{12}\,G$).

Table G.7: Same as Table G.1, but for NL3$\omega\rho$-a EoS ($B_s = 10^{12}\,G$).

γ =1				γ =2			
α	$M_{\rm max}$	$R_{1.4M_\odot}$	$R_{2.072M_\odot}$	α	$M_{\rm max}$	$R_{1.4M_\odot}$	$R_{2.072M_\odot}$
0.01	2.177	13.63	14.07	0.01	2.188	13.63	14.08
0.02	2.182	13.66	14.10	0.02	2.220	13.65	14.14
0.03	2.190	13.71	14.15	0.03	2.262	13.69	14.21
0.04	2.200	13.78	14.21	0.04	2.310	13.74	14.29
0.05	2.212	13.87	14.29	0.05	2.359	13.81	14.38
0.06	2.227	13.98	14.39	0.06	2.409	13.88	14.47
0.07	2.244	14.10	14.49	0.07	2.457	13.96	14.55
0.08	2.262	14.25	14.61	0.08	2.503	14.05	14.65
0.09	2.282	14.42	14.75	0.09	2.549	14.16	14.75
0.10	2.303	14.61	14.88	0.10	2.592	14.26	14.86
γ =3				γ =4			
α	$M_{\rm max}$	$R_{1.4M_\odot}$	$R_{2.072M_\odot}$	α	$M_{\rm max}$	$R_{1.4M_\odot}$	$R_{2.072M_\odot}$
0.01	2.268	13.63	14.13	0.01	2.485	13.64	14.22
0.02	2.394	13.67	14.24	0.02	2.664	13.70	14.37
0.03	2.500	13.72	14.34	0.03	2.782	13.78	14.50
0.04	2.589	13.79	14.44	0.04	2.869	13.86	14.63
0.05	2.665	13.86	14.55	0.05	2.939	13.95	14.75
0.06	2.731	13.94	14.65	0.06	2.997	14.04	14.87
0.07	2.789	14.03	14.76	0.07	3.047	14.12	14.98
0.08	2.841	14.12	14.87	0.08	3.089	14.21	15.09
0.09	2.887	14.21	14.97	0.09	3.127	14.29	15.19
0.10	2.930	14.30	15.08	0.10	3.161	14.37	15.29
γ =5				γ =6			
α	$M_{\rm max}$	$R_{1.4M_\odot}$	$R_{2.072M_\odot}$	α	$M_{\rm max}$	$R_{1.4M_\odot}$	$R_{2.072M_\odot}$
0.01	2.720	13.67	14.33	0.01	2.909	13.70	14.44
0.02	2.892	13.76	14.51	0.02	3.056	13.82	14.67
0.03	2.996	13.85	14.67	0.03	3.141	13.93	14.84
0.04	3.069	13.95	14.82	0.04	3.203	14.03	14.99
0.05	3.125	14.04	14.95	0.05	3.252	14.12	15.11
0.05	3.172	14.13	15.06	0.06	3.293	14.21	15.22
0.07	3.213	14.21	15.17	0.07	3.329	14.28	15.32
0.08	3.248	14.29	15.27	0.08	3.362	14.35	15.41
0.09	3.280	14.36	15.37	0.09	3.391	14.42	15.50
0.10	3.310	14.43	15.45	0.10	3.417	14.48	15.57
γ =7				γ =8			
α	$M_{\rm max}$	$R_{1.4M_\odot}$	$R_{2.072M_\odot}$	α	$M_{\rm max}$	$R_{1.4M_\odot}$	$R_{2.072M_\odot}$
0.01	3.047	13.75	14.57	0.01	3.148	13.81	14.70
0.02	3.171	13.89	14.81	0.02	3.261	13.96	14.95
0.03	3.247	14.01	14.99	0.03	3.331	14.08	15.12
0.04	3.303	14.11	15.13	0.04	3.384	14.17	15.25
0.05	3.348	14.20	15.25	0.05	3.426	14.26	15.36
0.06	3.387	14.28	15.35	0.06	3.461	14.33	15.45
0.07	3.420	14.35	15.44	0.07	3.492	14.38	15.53
0.08	3.449	14.40	15.52	0.08	3.519	14.44	15.61
0.09	3.476	14.46	15.59	0.09	3.544	14.50	15.67
0.10	3.500	14.52	15.66	0.10	3.566	14.55	15.73

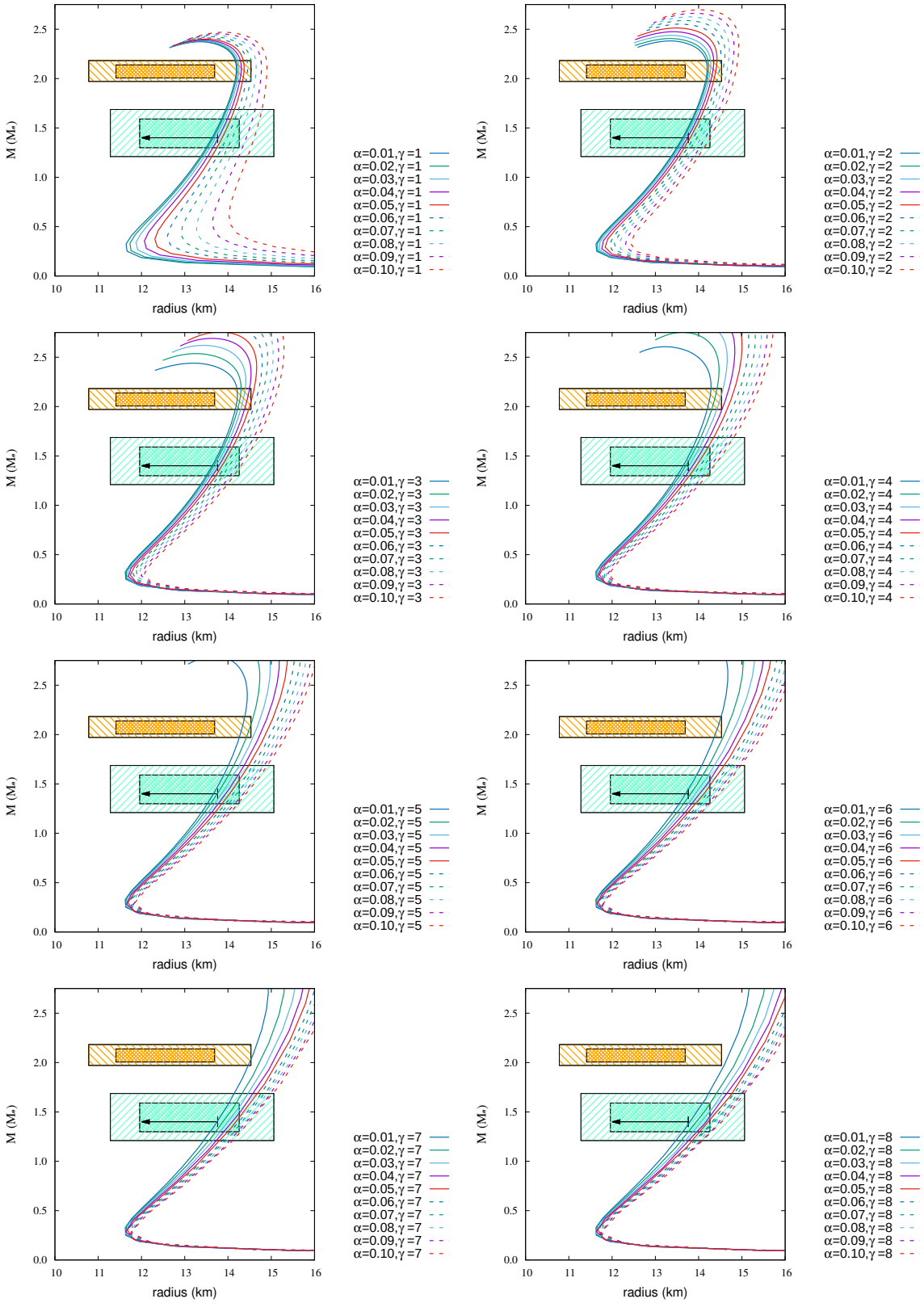

Figure G.8: Same as Fig. G.1, but for NL3$\omega\rho$-b EoS ($B_s = 10^{12}\,G$).

Table G.8: Same as Table G.1, but for NL3$\omega\rho$-b EoS ($B_s = 10^{12}\,G$).

γ =1				γ =2			
α	$M_{\rm max}$	$R_{1.4M_\odot}$	$R_{2.072M_\odot}$	α	$M_{\rm max}$	$R_{1.4M_\odot}$	$R_{2.072M_\odot}$
0.01	2.373	13.63	14.19	0.01	2.381	13.63	14.19
0.02	2.377	13.66	14.21	0.02	2.405	13.65	14.23
0.03	2.383	13.71	14.25	0.03	2.438	13.69	14.27
0.04	2.390	13.78	14.30	0.04	2.475	13.74	14.33
0.05	2.400	13.87	14.37	0.05	2.512	13.81	14.39
0.06	2.411	13.98	14.45	0.06	2.551	13.88	14.47
0.07	2.424	14.10	14.54	0.07	2.588	13.96	14.56
0.08	2.438	14.25	14.65	0.08	2.625	14.05	14.65
0.09	2.453	14.42	14.77	0.09	2.661	14.16	14.75
0.10	2.469	14.61	14.90	0.10	2.696	14.26	14.86
γ =3				γ =4			
α	$M_{\rm max}$	$R_{1.4M_\odot}$	$R_{2.072M_\odot}$	α	$M_{\rm max}$	$R_{1.4M_\odot}$	$R_{2.072M_\odot}$
0.01	2.440	13.63	14.21	0.01	2.606	13.64	14.25
0.02	2.536	13.67	14.27	0.02	2.751	13.70	14.37
0.03	2.620	13.72	14.35	0.03	2.848	13.78	14.50
0.04	2.691	13.79	14.45	0.04	2.924	13.86	14.63
0.05	2.754	13.86	14.55	0.05	2.984	13.95	14.75
0.06	2.808	13.94	14.65	0.06	3.033	14.04	14.87
0.07	2.855	14.03	14.76	0.07	3.076	14.12	14.98
0.08	2.900	14.12	14.87	0.08	3.114	14.21	15.09
0.09	2.940	14.21	14.97	0.09	3.149	14.29	15.19
0.10	2.977	14.30	15.08	0.10	3.180	14.37	15.29
γ =5				γ =6			
α	$M_{\rm max}$	$R_{1.4M_\odot}$	$R_{2.072M_\odot}$	α	$M_{\rm max}$	$R_{1.4M_\odot}$	$R_{2.072M_\odot}$
0.01	2.796	13.67	14.33	0.01	2.956	13.70	14.44
0.02	2.943	13.76	14.51	0.02	3.083	13.82	14.67
0.03	3.030	13.85	14.67	0.03	3.159	13.93	14.84
0.04	3.095	13.95	14.82	0.04	3.216	14.03	14.99
0.05	3.146	14.04	14.95	0.05	3.263	14.12	15.11
0.05	3.189	14.13	15.06	0.06	3.303	14.21	15.22
0.07	3.226	14.21	15.17	0.07	3.337	14.28	15.32
0.08	3.260	14.29	15.27	0.08	3.368	14.35	15.41
0.09	3.290	14.36	15.37	0.09	3.397	14.42	15.50
0.10	3.318	14.43	15.45	0.10	3.422	14.48	15.57
γ =7				γ =8			
α	$M_{\rm max}$	$R_{1.4M_\odot}$	$R_{2.072M_\odot}$	α	$M_{\rm max}$	$R_{1.4M_\odot}$	$R_{2.072M_\odot}$
0.01	3.074	13.75	14.57	0.01	3.165	13.81	14.70
0.02	3.186	13.89	14.81	0.02	3.271	13.96	14.95
0.03	3.258	14.01	14.99	0.03	3.339	14.08	15.12
0.04	3.312	14.11	15.13	0.04	3.390	14.17	15.25
0.05	3.356	14.20	15.25	0.05	3.431	14.26	15.36
0.06	3.393	14.28	15.35	0.06	3.466	14.33	15.45
0.07	3.425	14.35	15.44	0.07	3.496	14.38	15.53
0.08	3.454	14.40	15.52	0.08	3.522	14.44	15.61
0.09	3.480	14.46	15.59	0.09	3.546	14.50	15.67
0.10	3.503	14.52	15.66	0.10	3.568	14.55	15.73

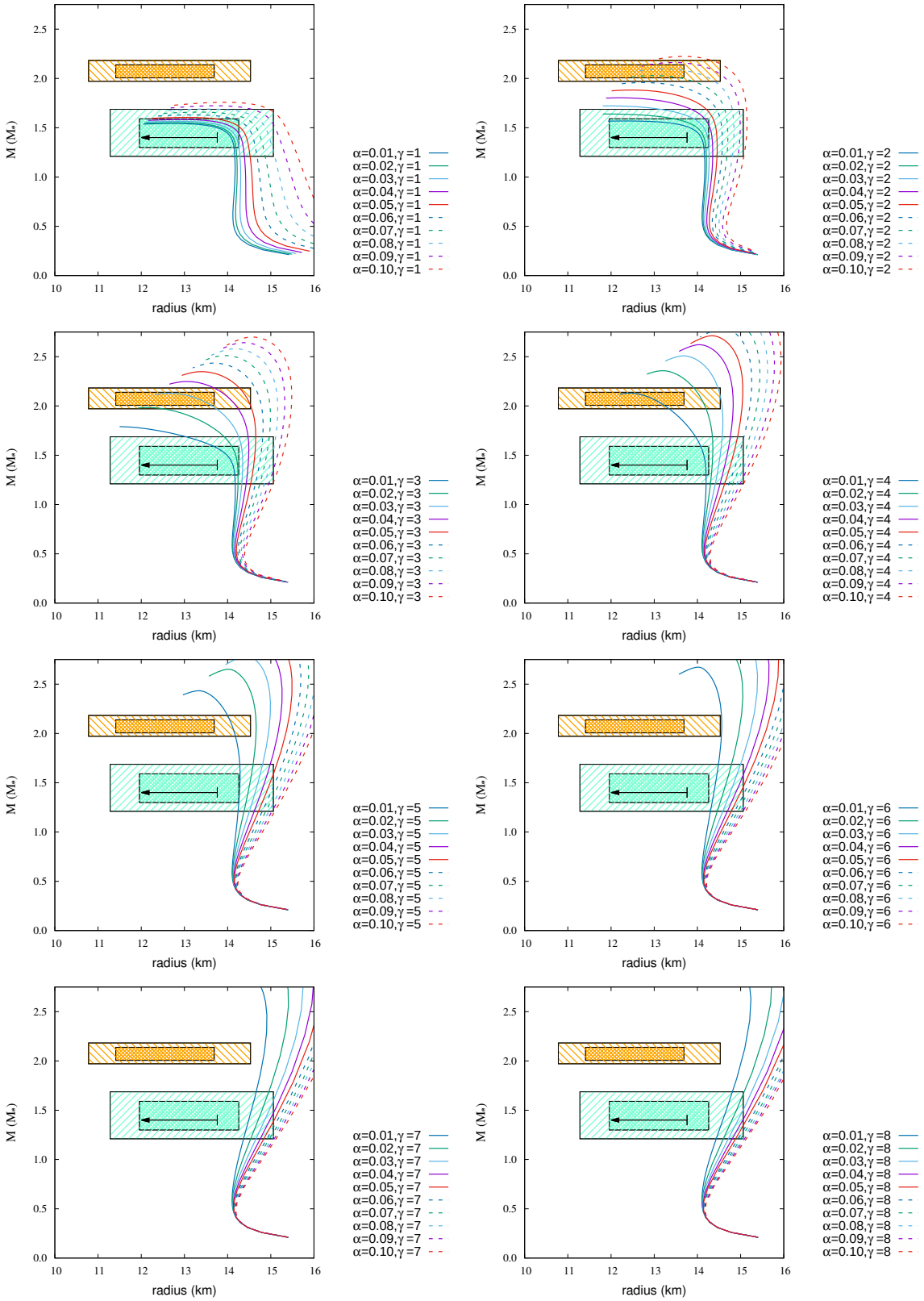

Figure G.9: Same as Fig. G.1, but for TM1-a EoS ($B_s = 10^{12}\,G$).

Table G.9: Same as Table G.1, but for TM1-a EoS ($B_s = 10^{12}\,G$).

γ =1				γ =2			
α	$M_{\max}$	$R_{1.4M_\odot}$	$R_{2.072M_\odot}$	α	$M_{\max}$	$R_{1.4M_\odot}$	$R_{2.072M_\odot}$
0.01	1.543	14.08	—	0.01	1.569	14.09	—
0.02	1.552	14.13	—	0.02	1.639	14.15	—
0.03	1.565	14.21	—	0.03	1.722	14.24	—
0.04	1.583	14.31	—	0.04	1.804	14.34	—
0.05	1.605	14.44	—	0.05	1.882	14.45	—
0.06	1.630	14.59	—	0.06	1.958	14.58	—
0.07	1.658	14.77	—	0.07	2.029	14.70	12.99
0.08	1.690	14.97	—	0.08	2.097	14.84	13.81
0.09	1.723	15.19	—	0.09	2.162	14.98	14.42
0.10	1.758	15.45	—	0.10	2.224	15.13	14.79
γ =3				γ =4			
α	$M_{\max}$	$R_{1.4M_\odot}$	$R_{2.072M_\odot}$	α	$M_{\max}$	$R_{1.4M_\odot}$	$R_{2.072M_\odot}$
0.01	1.790	1.414	—	0.01	2.130	14.19	12.96
0.02	1.984	14.23	—	0.02	2.357	14.34	14.09
0.03	2.129	14.35	13.32	0.03	2.508	14.49	14.54
0.04	2.248	14.48	14.05	0.04	2.621	14.64	14.83
0.05	2.348	14.61	14.46	0.05	2.712	14.77	15.05
0.06	2.435	14.73	14.74	0.06	2.788	14.89	15.24
0.07	2.511	14.86	14.96	0.07	2.853	15.00	15.41
0.08	2.580	14.98	15.15	0.08	2.909	15.10	15.56
0.09	2.642	15.09	15.32	0.09	2.960	15.19	15.70
0.10	2.699	15.20	15.49	0.10	3.006	15.28	15.82
γ =5				γ =6			
α	$M_{\max}$	$R_{1.4M_\odot}$	$R_{2.072M_\odot}$	α	$M_{\max}$	$R_{1.4M_\odot}$	$R_{2.072M_\odot}$
0.01	2.433	14.28	14.11	0.01	2.672	14.38	14.56
0.02	2.651	14.47	14.66	0.02	2.865	14.60	14.98
0.03	2.785	14.64	14.97	0.03	2.980	14.76	15.26
0.04	2.882	14.78	15.20	0.04	3.062	14.89	15.46
0.05	2.958	14.90	15.39	0.05	3.127	15.00	15.62
0.06	3.021	15.00	15.55	0.05	3.182	15.09	15.76
0.07	3.074	15.10	15.69	0.07	3.229	15.18	15.88
0.08	3.122	15.19	15.81	0.08	3.270	15.25	15.98
0.09	3.164	15.27	15.93	0.09	3.307	15.32	16.08
0.10	3.202	15.34	16.03	0.10	3.340	15.38	16.16
γ =7				γ =8			
α	$M_{\max}$	$R_{1.4M_\odot}$	$R_{2.072M_\odot}$	α	$M_{\max}$	$R_{1.4M_\odot}$	$R_{2.072M_\odot}$
0.01	2.854	14.49	14.85	0.01	2.991	14.59	15.07
0.02	3.021	14.71	15.23	0.02	3.141	14.80	15.42
0.03	3.121	14.86	15.47	0.03	3.232	14.94	15.63
0.04	3.195	14.98	15.65	0.04	3.299	15.05	15.79
0.05	3.254	15.08	15.79	0.05	3.351	15.14	15.92
0.06	3.302	15.16	15.91	0.06	3.395	15.21	16.03
0.07	3.344	15.23	16.01	0.07	3.434	15.28	16.12
0.08	3.380	15.30	16.11	0.08	3.466	15.34	16.20
0.09	3.413	15.36	16.19	0.09	3.497	15.39	16.27
0.10	3.443	15.41	16.26	0.10	3.523	15.43	16.33

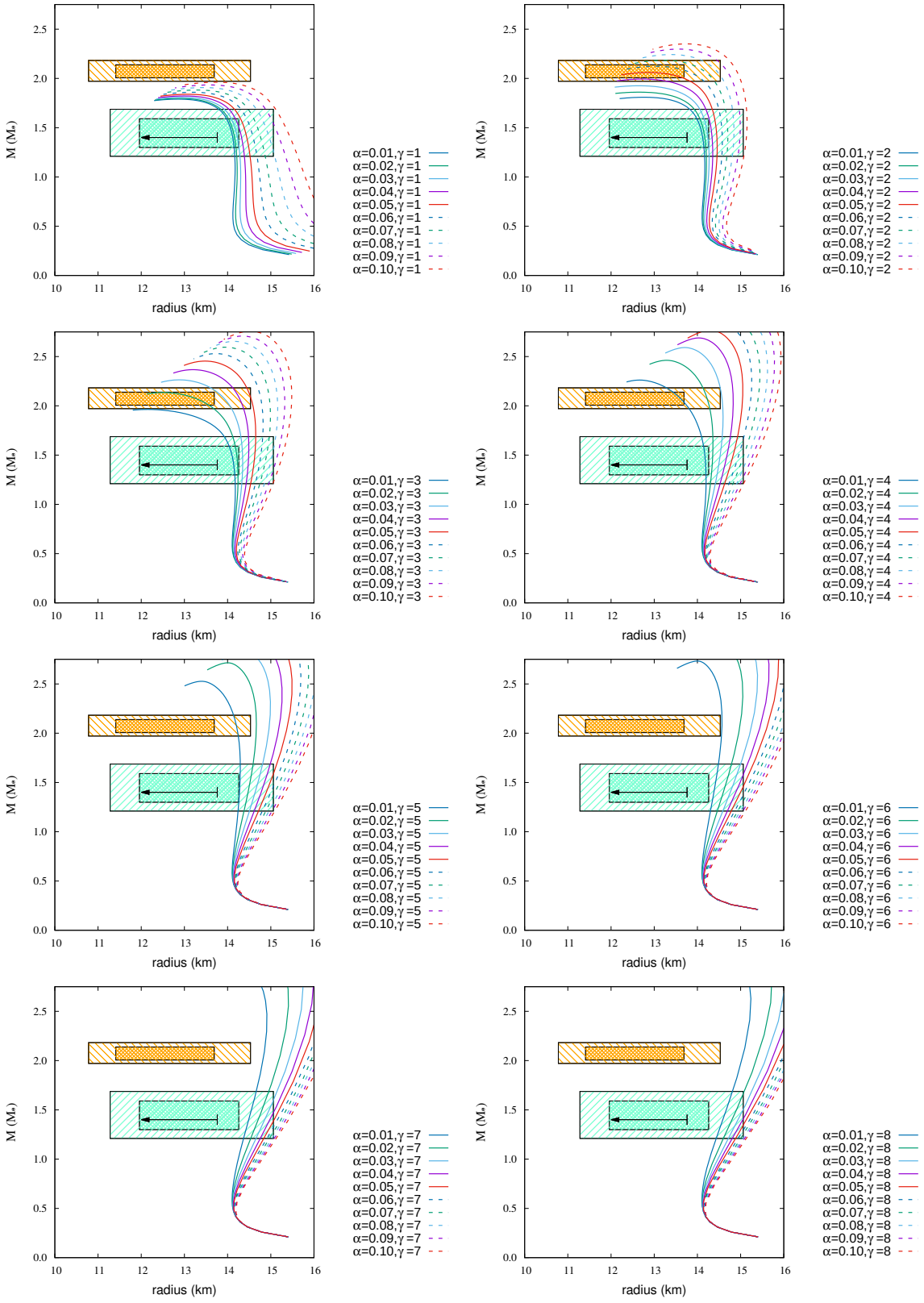

Figure G.10: Same as Fig. G.1, but for TM1-b EoS ($B_s = 10^{12}\,G$).

Table G.10: Same as Table G.1, but for TM1-b EoS ($B_s = 10^{12}\,G$)..

γ =1				γ =2			
α	$M_{\max}$	$R_{1.4M_\odot}$	$R_{2.072M_\odot}$	α	$M_{\max}$	$R_{1.4M_\odot}$	$R_{2.072M_\odot}$
0.01	1.790	14.12	—	0.01	1.809	14.12	—
0.02	1.796	14.16	—	0.02	1.861	14.17	—
0.03	1.807	14.23	—	0.03	1.925	14.24	—
0.04	1.822	14.32	—	0.04	1.993	14.34	—
0.05	1.839	14.44	—	0.05	2.060	14.45	12.86
0.06	1.860	14.59	—	0.06	2.124	14.58	13.77
0.07	1.882	14.77	—	0.07	2.184	14.70	14.17
0.08	1.907	14.97	—	0.08	2.242	14.84	14.45
0.09	1.934	15.19	—	0.09	2.297	14.98	14.69
0.10	1.962	15.45	—	0.10	2.351	15.13	14.91
γ =3				γ =4			
α	$M_{\max}$	$R_{1.4M_\odot}$	$R_{2.072M_\odot}$	α	$M_{\max}$	$R_{1.4M_\odot}$	$R_{2.072M_\odot}$
0.01	1.963	14.14	—	0.01	2.261	14.19	13.61
0.02	2.135	14.23	13.27	0.02	2.462	14.34	14.23
0.03	2.263	14.35	13.93	0.03	2.591	14.49	14.57
0.04	2.367	14.48	14.28	0.04	2.689	14.64	14.83
0.05	2.454	14.61	14.54	0.05	2.768	14.77	15.05
0.06	2.530	14.73	14.77	0.06	2.834	14.89	15.24
0.07	2.595	14.86	14.97	0.07	2.891	15.00	15.41
0.08	2.654	14.98	15.15	0.08	2.942	15.10	15.56
0.09	2.708	15.09	15.32	0.09	2.988	15.19	15.70
0.10	2.757	15.20	15.49	0.10	3.030	15.28	15.82
γ =5				γ =6			
α	$M_{\max}$	$R_{1.4M_\odot}$	$R_{2.072M_\odot}$	α	$M_{\max}$	$R_{1.4M_\odot}$	$R_{2.072M_\odot}$
0.01	2.527	14.28	14.21	0.01	2.732	14.38	14.57
0.02	2.714	14.47	14.67	0.02	2.900	14.60	14.98
0.03	2.830	14.64	14.97	0.03	3.003	14.76	15.25
0.04	2.916	14.78	15.20	0.04	3.079	14.89	15.46
0.05	2.984	14.90	15.39	0.05	3.141	15.00	15.62
0.05	3.042	15.00	15.55	0.06	3.193	15.09	15.76
0.07	3.091	15.10	15.69	0.07	3.239	15.18	15.88
0.08	3.136	15.19	15.81	0.08	3.279	15.25	15.98
0.09	3.176	15.27	15.93	0.09	3.314	15.32	16.08
0.10	3.213	15.34	16.03	0.10	3.347	15.38	16.16
γ =7				γ =8			
α	$M_{\max}$	$R_{1.4M_\odot}$	$R_{2.072M_\odot}$	α	$M_{\max}$	$R_{1.4M_\odot}$	$R_{2.072M_\odot}$
0.01	2.889	14.49	14.85	0.01	3.012	14.59	15.07
0.02	3.040	14.71	15.23	0.02	3.154	14.80	15.42
0.03	3.136	14.86	15.47	0.03	3.242	14.94	15.63
0.04	3.206	14.98	15.65	0.04	3.306	15.05	15.79
0.05	3.263	15.08	15.79	0.05	3.358	15.14	15.92
0.06	3.310	15.16	15.91	0.06	3.401	15.21	16.03
0.07	3.350	15.23	16.01	0.07	3.438	15.28	16.12
0.08	3.386	15.30	16.11	0.08	3.470	15.34	16.20
0.09	3.418	15.36	16.19	0.09	3.500	15.39	16.27
0.10	3.447	15.41	16.26	0.10	3.525	15.43	16.33

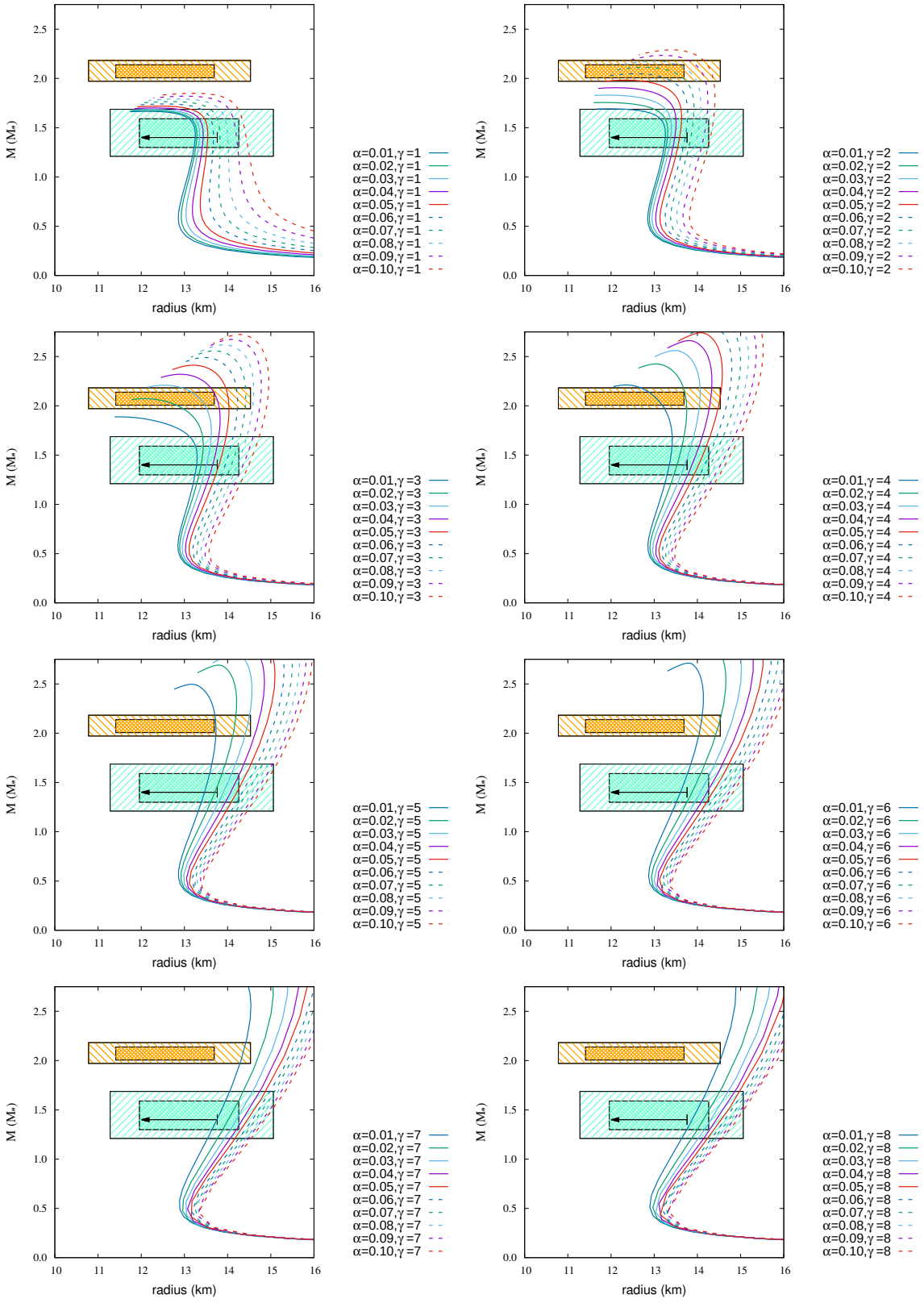

Figure G.11: Same as Fig. G.1, but for TM2$\omega\rho$-a EoS ($B_s = 10^{12}\,G$).

Table G.11: Same as Table G.1, but for TM2$\omega\rho$-a EoS ($B_s = 10^{12}\,G$).

γ =1				γ =2			
α	$M_{\max}$	$R_{1.4M_\odot}$	$R_{2.072M_\odot}$	α	$M_{\max}$	$R_{1.4M_\odot}$	$R_{2.072M_\odot}$
0.01	1.666	13.25	—	0.01	1.692	13.26	—
0.02	1.673	13.29	—	0.02	1.756	13.31	—
0.03	1.685	13.35	—	0.03	1.831	13.38	—
0.04	1.701	13.43	—	0.04	1.906	13.47	—
0.05	1.719	13.54	—	0.05	1.983	13.59	—
0.06	1.741	13.67	—	0.06	2.048	13.71	12.56
0.07	1.765	13.82	—	0.07	2.113	13.85	13.40
0.08	1.791	14.00	—	0.08	2.175	13.99	13.81
0.09	1.820	14.21	—	0.09	2.234	14.15	14.09
0.10	1.849	14.43	—	0.10	2.289	14.30	14.31
γ =3				γ =4			
α	$M_{\max}$	$R_{1.4M_\odot}$	$R_{2.072M_\odot}$	α	$M_{\max}$	$R_{1.4M_\odot}$	$R_{2.072M_\odot}$
0.01	1.888	13.28	—	0.01	2.212	13.35	13.06
0.02	2.072	13.38	12.12	0.02	2.425	13.53	13.73
0.03	2.210	13.51	13.35	0.03	2.561	13.71	14.06
0.04	2.320	13.65	13.75	0.04	2.662	13.88	14.31
0.05	2.412	13.80	14.02	0.05	2.741	14.03	14.52
0.06	2.490	13.95	14.23	0.06	2.808	14.17	14.71
0.07	2.558	14.09	14.42	0.07	2.864	14.30	14.89
0.08	2.619	14.23	14.60	0.08	2.914	14.42	15.04
0.09	2.674	14.36	14.77	0.09	2.961	14.54	15.19
0.10	2.724	14.49	14.93	0.10	3.001	14.65	15.33
γ =5				γ =6			
α	$M_{\max}$	$R_{1.4M_\odot}$	$R_{2.072M_\odot}$	α	$M_{\max}$	$R_{1.4M_\odot}$	$R_{2.072M_\odot}$
0.01	2.497	13.46	13.73	0.01	2.711	13.61	14.08
0.02	2.691	13.71	14.16	0.02	2.877	13.88	14.49
0.03	2.807	13.90	14.46	0.03	2.978	14.07	14.76
0.04	2.891	14.07	14.69	0.04	3.053	14.23	14.98
0.05	2.958	14.22	14.89	0.05	3.113	14.36	15.15
0.05	3.014	14.34	15.06	0.06	3.163	14.47	15.30
0.07	3.063	14.46	15.20	0.07	3.207	14.58	15.42
0.08	3.106	14.57	15.34	0.08	3.245	14.67	15.54
0.09	3.145	14.66	15.46	0.09	3.280	14.75	15.64
0.10	3.180	14.75	15.57	0.10	3.312	14.83	15.73
γ =7				γ =8			
α	$M_{\max}$	$R_{1.4M_\odot}$	$R_{2.072M_\odot}$	α	$M_{\max}$	$R_{1.4M_\odot}$	$R_{2.072M_\odot}$
0.01	2.869	13.75	14.36	0.01	2.989	13.88	14.59
0.02	3.016	14.02	14.75	0.02	3.127	14.14	14.95
0.03	3.108	14.21	15.00	0.03	3.213	14.32	15.18
0.04	3.177	14.35	15.19	0.04	3.275	14.44	15.35
0.05	3.232	14.46	15.34	0.05	3.325	14.57	15.49
0.06	3.277	14.58	15.47	0.06	3.367	14.64	15.60
0.07	3.317	14.65	15.58	0.07	3.403	14.74	15.70
0.08	3.351	14.74	15.68	0.08	3.434	14.83	15.78
0.09	3.382	14.82	15.77	0.09	3.462	14.88	15.86
0.10	3.411	14.88	15.85	0.10	3.488	14.92	15.94

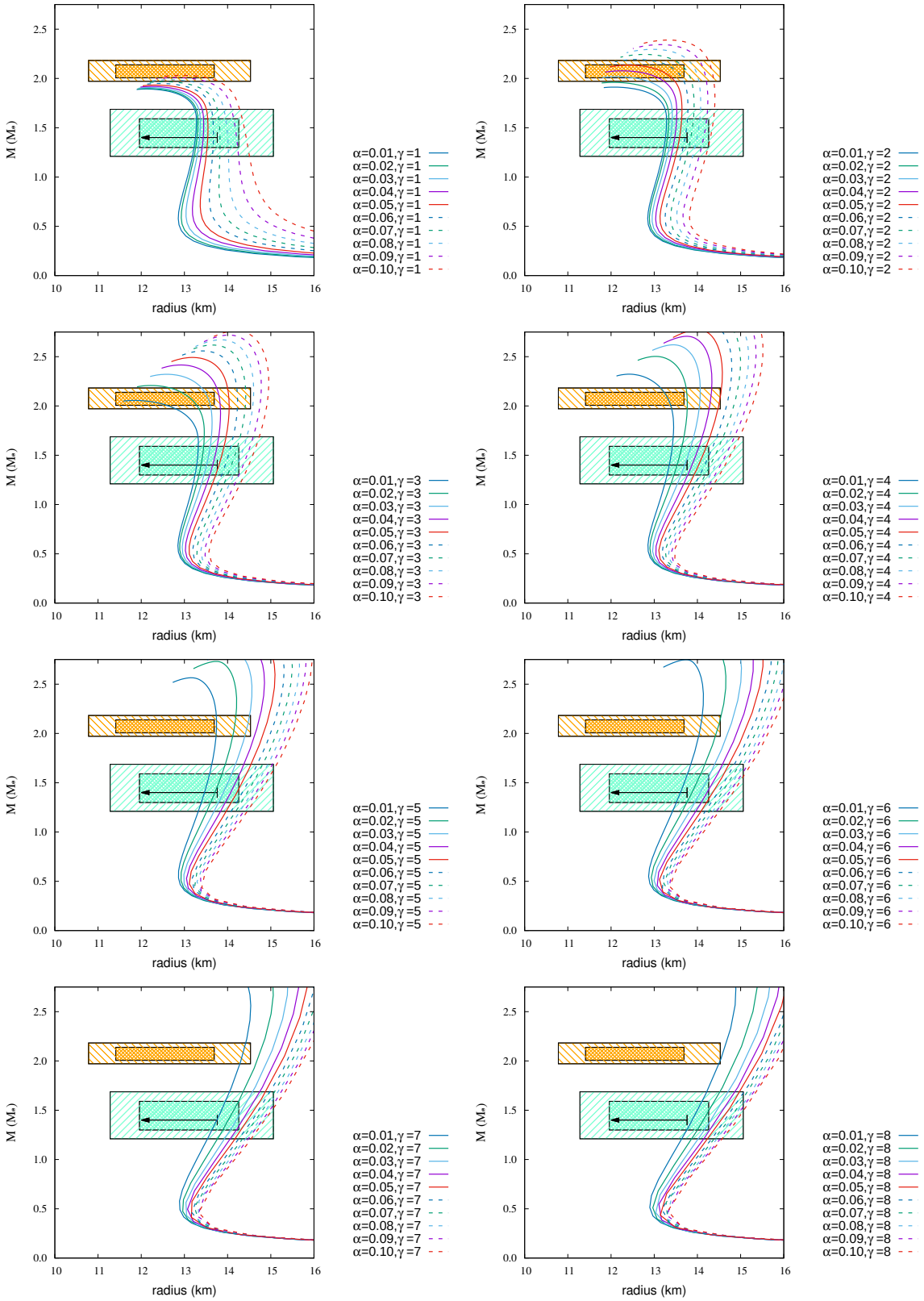

Figure G.12: Same as Fig. G.1, but for TM2$\omega\rho$-b EoS ($B_s = 10^{12}\,G$).

Table G.12: Same as Table G.1, but for TM2$\omega\rho$-b EoS ($B_s = 10^{12}\,G$).

γ =1				γ =2			
α	$M_{\max}$	$R_{1.4M_\odot}$	$R_{2.072M_\odot}$	α	$M_{\max}$	$R_{1.4M_\odot}$	$R_{2.072M_\odot}$
0.01	1.892	13.26	—	0.01	1.912	13.26	—
0.02	1.898	13.29	—	0.02	1.960	13.31	—
0.03	1.907	13.35	—	0.03	2.018	13.38	—
0.04	1.919	13.44	—	0.04	2.077	13.47	12.51
0.05	1.933	13.54	—	0.05	2.135	13.59	13.18
0.06	1.949	13.67	—	0.06	2.192	13.71	13.52
0.07	1.967	13.82	—	0.07	2.244	13.85	13.76
0.08	1.987	14.00	—	0.08	2.295	13.99	13.97
0.09	2.009	14.21	—	0.09	2.343	14.15	14.16
0.10	2.031	14.43	—	0.10	2.389	14.30	14.34
γ =3				γ =4			
α	$M_{\max}$	$R_{1.4M_\odot}$	$R_{2.072M_\odot}$	α	$M_{\max}$	$R_{1.4M_\odot}$	$R_{2.072M_\odot}$
0.01	2.056	13.28	—	0.01	2.322	13.35	13.32
0.02	2.207	13.38	13.15	0.02	2.503	13.53	13.76
0.03	2.321	13.51	13.55	0.03	2.620	13.71	14.06
0.04	2.416	13.65	13.81	0.04	2.707	13.88	14.31
0.05	2.492	13.80	14.03	0.05	2.776	14.03	14.52
0.06	2.558	13.95	14.23	0.06	2.836	14.17	14.71
0.07	2.618	14.09	14.42	0.07	2.887	14.30	14.89
0.08	2.671	14.23	14.60	0.08	2.933	14.42	15.04
0.09	2.719	14.36	14.77	0.09	2.975	14.54	15.19
0.10	2.763	14.49	14.93	0.10	3.013	14.64	15.32
γ =5				γ =6			
α	$M_{\max}$	$R_{1.4M_\odot}$	$R_{2.072M_\odot}$	α	$M_{\max}$	$R_{1.4M_\odot}$	$R_{2.072M_\odot}$
0.01	2.565	13.46	13.74	0.01	2.748	13.61	14.08
0.02	2.731	13.71	14.16	0.02	2.897	13.88	14.49
0.03	2.834	13.90	14.46	0.03	2.992	14.07	14.76
0.04	2.911	14.07	14.69	0.04	3.064	14.23	14.98
0.05	2.973	14.22	14.89	0.05	3.122	14.36	15.15
0.05	3.026	14.34	15.06	0.06	3.170	14.47	15.30
0.07	3.073	14.46	15.20	0.07	3.213	14.58	15.42
0.08	3.115	14.57	15.34	0.08	3.250	14.67	15.54
0.09	3.152	14.66	15.46	0.09	3.284	14.75	15.64
0.10	3.187	14.75	15.57	0.10	3.315	14.83	15.73
γ =7				γ =8			
α	$M_{\max}$	$R_{1.4M_\odot}$	$R_{2.072M_\odot}$	α	$M_{\max}$	$R_{1.4M_\odot}$	$R_{2.072M_\odot}$
0.01	2.888	13.75	14.36	0.01	3.003	13.88	14.59
0.02	3.028	14.02	14.75	0.02	3.136	14.14	14.95
0.03	3.118	14.21	15.00	0.03	3.219	14.32	15.18
0.04	3.184	14.35	15.19	0.04	3.280	14.44	15.35
0.05	3.237	14.46	15.34	0.05	3.329	14.57	15.49
0.06	3.282	14.58	15.47	0.06	3.370	14.64	15.60
0.07	3.320	14.65	15.58	0.07	3.405	14.74	15.70
0.08	3.354	14.74	15.68	0.08	3.436	14.83	15.78
0.09	3.385	14.82	15.77	0.09	3.463	14.88	15.86
0.10	3.412	14.88	15.85	0.10	3.488	14.92	15.94

Appendix H

Original resutls by changing α and γ for neutron star with magnetic fields ($B_s = 10^{15}$ G)

Here, the MR relations and Tables are given by calculations of changing α and γ for neutron star with magnetic fields ($B_s = 10^{15}$ G, $B_0 = 2.5 \times 10^{18}$ G). Tables show the values of maximum mass ($M_\odot$), radius (km) at $M = 1.4M_\odot$, and radius (km) at $M = 2.072M_\odot$ for each EoSs.

The MR relations of each EoSs with magnetic fields are shown in Figures. H.1 – H.12 (DDME2-a EoS; in Fig. H.1, DDME2-b EoS; in Fig. H.2, GM1 EoS; in Fig. H.3, GM3 EoS; in Fig. H.4, NL3-a EoS; in Fig. H.5, NL3-b EoS; in Fig. H.6, NL3$\omega\rho$-a EoS; in Fig. H.7, NL3$\omega\rho$-b EoS; in Fig. H.8, TM1-a EoS; in Fig. H.9, TM1-b EoS; in Fig. H.10, TM2$\omega\rho$-a EoS; in Fig. H.11, TM2$\omega\rho$-b EoS; in Fig. H.12). The colored lines of MR relations represent the following : dark blue (solid line); magnetic fields $B(\rho)$ with $\alpha = 0.01$, green (solid line); magnetic fields $B(\rho)$ with $\alpha = 0.02$, light blue (solid line); magnetic fields $B(\rho)$ with $\alpha = 0.03$, purple (solid line); magnetic fields $B(\rho)$ with $\alpha = 0.04$, red (solid line); magnetic fields $B(\rho)$ with $\alpha = 0.05$, dark blue (dashed line); magnetic fields $B(\rho)$ with $\alpha = 0.06$, green (dashed line); magnetic fields $B(\rho)$ with $\alpha = 0.07$, light blue (dashed line); magnetic fields $B(\rho)$ with $\alpha = 0.08$, purple (dashed line); magnetic fields $B(\rho)$ with $\alpha = 0.09$, red (dashed line); magnetic fields $B(\rho)$ with $\alpha = 0.10$.

For each EoS the maximum mass ($M_{\rm max}$), the radius at $M = 1.4M_\odot$, and radius at $M = 2.072\,M_\odot$ are shown in Tables H.1 – H.12 (DDME2-a EoS; in Table H.1, DDME2-b EoS; in Table H.2, GM1 EoS; in Table H.3, GM3 EoS; in Table H.4, NL3-a EoS; in Table H.5, NL3-b EoS; in Table H.6, NL3$\omega\rho$-a EoS; in Table H.7, NL3$\omega\rho$-b EoS; in Table H.8, TM1-a EoS; in Table H.9, TM1-b EoS; in Table H.10, TM2$\omega\rho$-a EoS; in Table H.11, TM2$\omega\rho$-b EoS; in Table H.12).

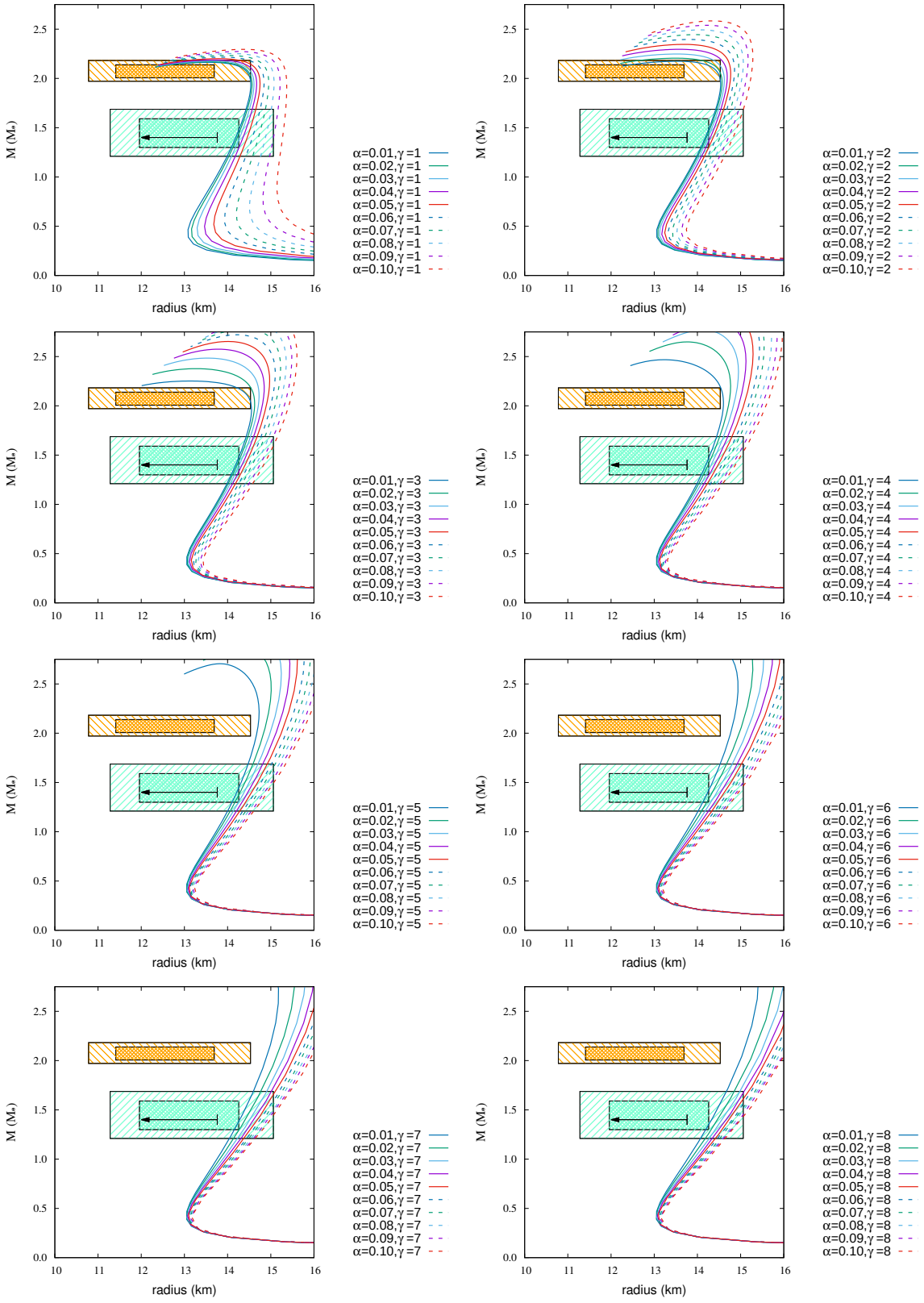

Figure H.1: MR relations of DDME2-a EoS with magnetic fields. The strength of surface magnetic field strenge B_s is 10^{15} G, and the centeral magnetic field strength B_0 is 2.5×10^{18} G. The colored areas are the same as in Fig. 6.1.

Table H.1: Maximum mass ($M_{\max}$) in unit of $M_\odot$ and radius (km) at $M = 1.4M_\odot$ ($R_{1.4M_\odot}$) and radius (km) at $M = 2.072M_\odot$ ($R_{2.072M_\odot}$) for DDME2-a EoS with magnetic fields ($B_0 = 2.5 \times 10^{18}$ G, $B_s = 10^{15}$ G).

γ =1				γ =2			
α	$M_{\max}$	$R_{1.4M_\odot}$	$R_{2.072M_\odot}$	α	$M_{\max}$	$R_{1.4M_\odot}$	$R_{2.072M_\odot}$
0.01	2.163	14.19	14.44	0.01	2.174	14.18	14.45
0.02	2.168	14.22	14.47	0.02	2.205	14.21	14.51
0.03	2.176	14.28	14.53	0.03	2.248	14.25	14.59
0.04	2.187	14.36	14.60	0.04	2.296	14.30	14.68
0.05	2.200	14.45	14.69	0.05	2.346	14.36	14.77
0.06	2.216	14.57	14.80	0.06	2.396	14.44	14.86
0.07	2.233	14.71	14.91	0.07	2.445	14.52	14.95
0.08	2.252	14.88	15.04	0.08	2.493	14.62	15.05
0.09	2.273	15.06	15.18	0.09	2.539	14.72	15.16
0.10	2.295	15.27	15.34	0.10	2.584	14.82	15.26
γ =3				γ =4			
α	$M_{\max}$	$R_{1.4M_\odot}$	$R_{2.072M_\odot}$	α	$M_{\max}$	$R_{1.4M_\odot}$	$R_{2.072M_\odot}$
0.01	2.252	14.19	14.50	0.01	2.468	14.20	14.60
0.02	2.377	14.22	14.62	0.02	2.648	14.25	14.75
0.03	2.484	14.27	14.73	0.03	2.771	14.32	14.87
0.04	2.575	14.33	14.83	0.04	2.863	14.40	15.00
0.05	2.653	14.41	14.93	0.05	2.936	14.48	15.12
0.06	2.721	14.49	15.03	0.06	2.995	14.56	15.24
0.07	2.781	14.57	15.14	0.07	3.025	14.64	15.33
0.08	2.836	14.66	15.25	0.08	3.091	14.73	15.46
0.09	2.885	14.75	15.36	0.09	3.131	14.81	15.56
0.10	2.929	14.84	15.46	0.10	3.167	14.88	15.65
γ =5				γ =6			
α	$M_{\max}$	$R_{1.4M_\odot}$	$R_{2.072M_\odot}$	α	$M_{\max}$	$R_{1.4M_\odot}$	$R_{2.072M_\odot}$
0.01	2.705	14.21	14.71	0.01	2.900	14.24	14.81
0.02	2.884	14.29	14.88	0.02	3.056	14.35	15.02
0.03	2.992	14.38	15.04	0.03	3.145	14.45	15.20
0.04	3.069	14.47	15.18	0.04	3.209	14.55	15.34
0.05	3.129	14.56	15.31	0.05	3.259	14.63	15.46
0.05	3.178	14.64	15.42	0.06	3.301	14.71	15.57
0.07	3.219	14.72	15.53	0.07	3.338	14.78	15.67
0.08	3.256	14.79	15.63	0.08	3.370	14.85	15.76
0.09	3.289	14.86	15.72	0.09	3.399	14.91	15.84
0.10	3.318	14.93	15.80	0.10	3.426	14.97	15.92
γ =7				γ =8			
α	$M_{\max}$	$R_{1.4M_\odot}$	$R_{2.072M_\odot}$	α	$M_{\max}$	$R_{1.4M_\odot}$	$R_{2.072M_\odot}$
0.01	3.047	14.28	14.93	0.01	3.153	14.33	15.05
0.02	3.177	14.41	15.17	0.02	3.267	14.47	15.29
0.03	3.254	14.52	15.34	0.03	3.338	14.58	15.46
0.04	3.310	14.61	15.48	0.04	3.391	14.67	15.59
0.05	3.356	14.69	15.59	0.05	3.434	14.75	15.70
0.06	3.394	14.77	15.69	0.06	3.470	14.81	15.79
0.07	3.428	14.83	15.78	0.07	3.501	14.86	15.87
0.08	3.458	14.89	15.86	0.08	3.528	14.92	15.94
0.09	3.485	14.95	15.94	0.09	3.553	14.98	16.01
0.10	3.509	15.00	16.00	0.10	3.576	15.02	16.07

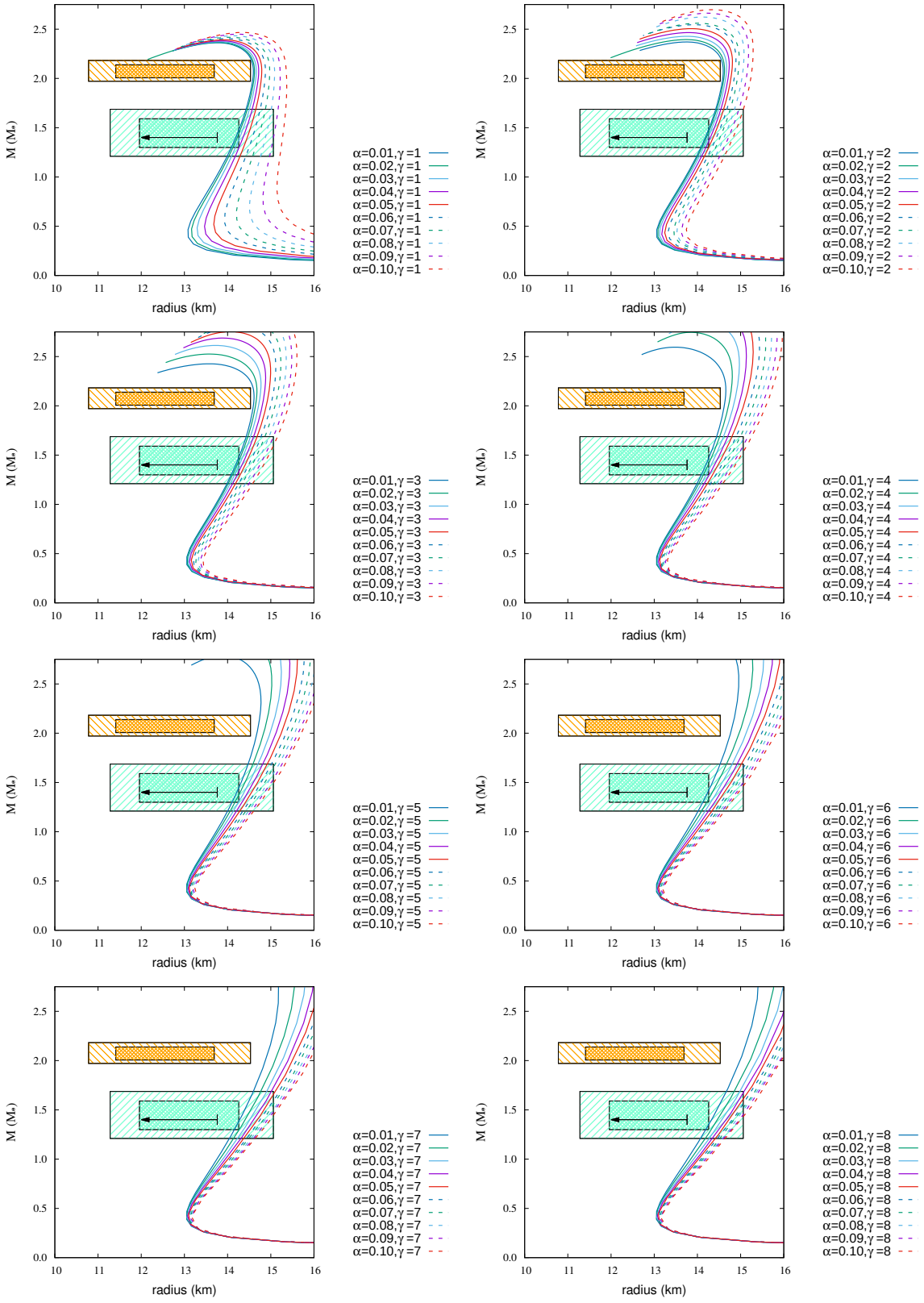

Figure H.2: Same as Fig. H.1, but for DDME2-b EoS ($B_s = 10^{15}\,G$).

Table H.2: Same as Table H.1, but for DDME2-b EoS ($B_s = 10^{15}\,G$).

γ =1				γ =2			
α	$M_{\rm max}$	$R_{1.4M_\odot}$	$R_{2.072M_\odot}$	α	$M_{\rm max}$	$R_{1.4M_\odot}$	$R_{2.072M_\odot}$
0.01	2.362	14.19	14.60	0.01	2.370	14.18	14.60
0.02	2.366	14.22	14.62	0.02	2.394	14.21	14.63
0.03	2.372	14.28	14.66	0.03	2.427	14.25	14.67
0.04	2.381	14.36	14.72	0.04	2.465	14.30	14.73
0.05	2.391	14.45	14.79	0.05	2.505	14.36	14.80
0.06	2.404	14.57	14.88	0.06	2.545	14.44	14.87
0.07	2.417	14.71	14.97	0.07	2.560	14.52	14.95
0.08	2.433	14.88	15.09	0.08	2.623	14.62	15.05
0.09	2.449	15.06	15.22	0.09	2.662	14.72	15.16
0.10	2.467	15.27	15.36	0.10	2.697	14.82	15.26
γ =3				γ =4			
α	$M_{\rm max}$	$R_{1.4M_\odot}$	$R_{2.072M_\odot}$	α	$M_{\rm max}$	$R_{1.4M_\odot}$	$R_{2.072M_\odot}$
0.01	2.426	14.19	14.61	0.01	2.595	14.20	14.65
0.02	2.525	14.22	14.67	0.02	2.746	14.25	14.75
0.03	2.613	14.27	14.74	0.03	2.849	14.32	14.87
0.04	2.688	14.33	14.83	0.04	2.926	14.40	15.00
0.05	2.752	14.41	14.93	0.05	2.988	14.48	15.12
0.06	2.808	14.49	15.03	0.06	3.040	14.56	15.24
0.07	2.859	14.57	15.14	0.07	3.085	14.65	15.35
0.08	2.906	14.66	15.25	0.08	3.124	14.73	15.46
0.09	2.947	14.75	15.36	0.09	3.159	14.81	15.56
0.10	2.983	14.84	15.46	0.10	3.191	14.88	15.65
γ =5				γ =6			
α	$M_{\rm max}$	$R_{1.4M_\odot}$	$R_{2.072M_\odot}$	α	$M_{\rm max}$	$R_{1.4M_\odot}$	$R_{2.072M_\odot}$
0.01	2.793	14.21	14.71	0.01	2.959	14.24	14.81
0.02	2.944	14.29	14.88	0.02	3.091	14.35	15.02
0.03	3.037	14.38	15.04	0.03	3.168	14.45	15.20
0.04	3.104	14.47	15.18	0.04	3.227	14.55	15.34
0.05	3.155	14.56	15.31	0.05	3.273	14.63	15.46
0.05	3.199	14.64	15.42	0.06	3.313	14.71	15.57
0.07	3.237	14.72	15.53	0.07	3.348	14.78	15.67
0.08	3.272	14.79	15.63	0.08	3.379	14.85	15.76
0.09	3.302	14.86	15.72	0.09	3.407	14.91	15.84
0.10	3.319	14.92	15.79	0.10	3.433	14.97	15.92
γ =7				γ =8			
α	$M_{\rm max}$	$R_{1.4M_\odot}$	$R_{2.072M_\odot}$	α	$M_{\rm max}$	$R_{1.4M_\odot}$	$R_{2.072M_\odot}$
0.01	3.082	14.28	14.93	0.01	3.174	14.33	15.05
0.02	3.196	14.41	15.17	0.02	3.280	14.47	15.29
0.03	3.267	14.52	15.34	0.03	3.348	14.58	15.46
0.04	3.321	14.61	15.48	0.04	3.399	14.67	15.59
0.05	3.365	14.69	15.59	0.05	3.440	14.75	15.70
0.06	3.402	14.77	15.69	0.06	3.476	14.81	15.79
0.07	3.435	14.83	15.78	0.07	3.506	14.86	15.87
0.08	3.464	14.89	15.86	0.08	3.533	14.92	15.94
0.09	3.490	14.95	15.94	0.09	3.557	14.98	16.01
0.10	3.514	15.00	16.00	0.10	3.579	15.02	16.07

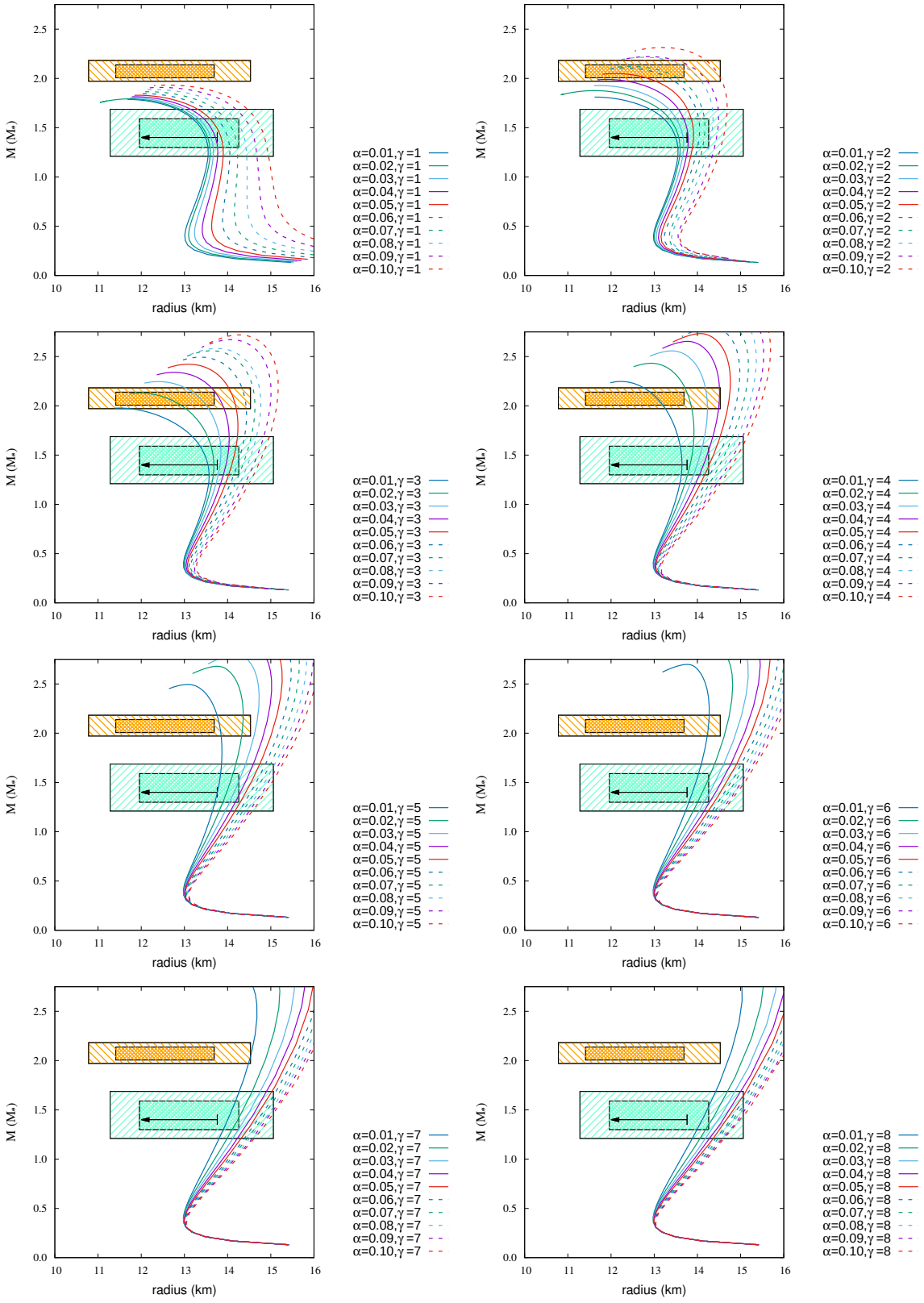

Figure H.3: Same as Fig. H.1, but for GM1 EoS ($B_s = 10^{15}\,G$).

Table H.3: Same as Table H.1, but for GM1 EoS ($B_s = 10^{15}\,G$).

γ =1				γ =2			
α	$M_{\max}$	$R_{1.4M_\odot}$	$R_{2.072M_\odot}$	α	$M_{\max}$	$R_{1.4M_\odot}$	$R_{2.072M_\odot}$
0.01	1.787	13.49	—	0.01	1.811	13.50	—
0.02	1.793	13.54	—	0.02	1.876	13.57	—
0.03	1.802	13.62	—	0.03	1.928	13.67	—
0.04	1.814	13.72	—	0.04	1.990	13.79	—
0.05	1.829	13.85	—	0.05	2.050	13.91	—
0.06	1.846	14.00	—	0.06	2.107	14.04	12.94
0.07	1.865	14.18	—	0.07	2.122	14.16	13.20
0.08	1.886	14.38	—	0.08	2.214	14.31	13.86
0.09	1.909	14.61	—	0.09	2.221	14.44	14.01
0.10	1.932	14.86	—	0.10	2.314	14.60	14.44
γ =3				γ =4			
α	$M_{\max}$	$R_{1.4M_\odot}$	$R_{2.072M_\odot}$	α	$M_{\max}$	$R_{1.4M_\odot}$	$R_{2.072M_\odot}$
0.01	1.977	13.54	—	0.01	2.247	13.64	13.08
0.02	2.130	13.68	12.63	0.02	2.432	13.83	13.81
0.03	2.246	13.82	13.37	0.03	2.558	13.99	14.22
0.04	2.340	13.96	13.81	0.04	2.654	14.14	14.51
0.05	2.422	14.10	14.14	0.05	2.733	14.28	14.74
0.06	2.494	14.23	14.40	0.06	2.801	14.40	14.92
0.07	2.559	14.35	14.63	0.07	2.862	14.52	15.09
0.08	2.583	14.46	14.77	0.08	2.915	14.62	15.24
0.09	2.672	14.60	15.00	0.09	2.962	14.72	15.37
0.10	2.720	14.71	15.16	0.10	3.005	14.81	15.50
γ =5				γ =6			
α	$M_{\max}$	$R_{1.4M_\odot}$	$R_{2.072M_\odot}$	α	$M_{\max}$	$R_{1.4M_\odot}$	$R_{2.072M_\odot}$
0.01	2.495	13.76	13.82	0.01	2.698	13.89	14.26
0.02	2.679	13.98	14.35	0.02	2.874	14.12	14.68
0.03	2.800	14.15	14.66	0.03	2.981	14.29	14.95
0.04	2.890	14.30	14.89	0.04	3.062	14.42	15.15
0.05	2.961	14.42	15.07	0.05	3.126	14.54	15.31
0.05	3.020	14.53	15.23	0.06	3.179	14.63	15.45
0.07	3.073	14.63	15.37	0.07	3.225	14.72	15.57
0.08	3.119	14.72	15.50	0.08	3.266	14.80	15.68
0.09	3.160	14.80	15.61	0.09	3.302	14.87	15.77
0.10	3.198	14.88	15.72	0.10	3.335	14.93	15.86
γ =7				γ =8			
α	$M_{\max}$	$R_{1.4M_\odot}$	$R_{2.072M_\odot}$	α	$M_{\max}$	$R_{1.4M_\odot}$	$R_{2.072M_\odot}$
0.01	2.863	14.00	14.55	0.01	2.993	14.11	14.77
0.02	3.022	14.24	14.93	0.02	3.140	14.34	15.12
0.03	3.121	14.40	15.17	0.03	3.230	14.49	15.33
0.04	3.193	14.52	15.35	0.04	3.295	14.60	15.49
0.05	3.250	14.62	15.49	0.05	3.347	14.69	15.62
0.06	3.298	14.71	15.61	0.06	3.390	14.77	15.73
0.07	3.339	14.79	15.71	0.07	3.427	14.84	15.82
0.08	3.375	14.85	15.81	0.08	3.459	14.90	15.90
0.09	3.407	14.92	15.89	0.09	3.489	14.95	15.97
0.10	3.436	14.97	15.96	0.10	3.515	15.00	16.04

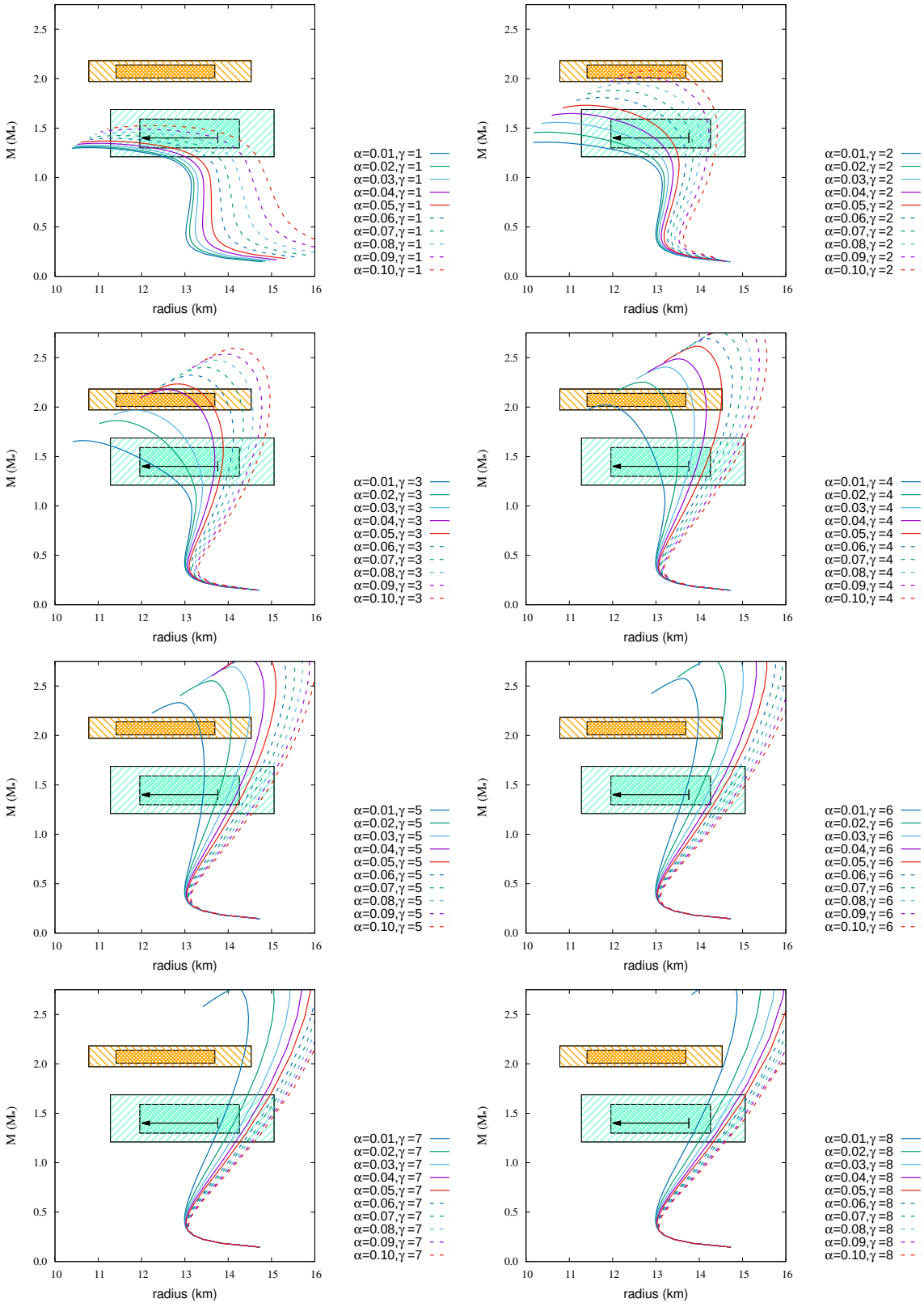

Figure H.4: Same as Fig. H.1, but for GM3 EoS ($B_s = 10^{15}\,G$).

Table H.4: Same as Table H.1, but for GM3 EoS ($B_s = 10^{15}\,G$).

γ =1				γ =2			
α	$M_{\max}$	$R_{1.4M_\odot}$	$R_{2.072M_\odot}$	α	$M_{\max}$	$R_{1.4M_\odot}$	$R_{2.072M_\odot}$
0.01	1.302	—	—	0.01	1.357	—	—
0.02	1.312	—	—	0.02	1.459	11.64	—
0.03	1.327	—	—	0.03	1.557	12.47	—
0.04	1.346	—	—	0.04	1.647	12.96	—
0.05	1.369	11.14	—	0.05	1.731	13.31	—
0.06	1.395	11.30	—	0.06	1.809	13.59	—
0.07	1.424	12.45	—	0.07	1.882	13.83	—
0.08	1.456	13.16	—	0.08	1.951	14.04	—
0.09	1.489	13.71	—	0.09	2.019	14.23	—
0.10	1.525	14.17	—	0.10	2.082	14.41	13.21
γ =3				γ =4			
α	$M_{\max}$	$R_{1.4M_\odot}$	$R_{2.072M_\odot}$	α	$M_{\max}$	$R_{1.4M_\odot}$	$R_{2.072M_\odot}$
0.01	1.660	12.31	—	0.01	2.021	13.04	—
0.02	1.863	13.01	—	0.02	2.252	13.50	13.22
0.03	1.967	13.33	—	0.03	2.405	13.76	13.83
0.04	2.176	13.69	13.17	0.04	2.487	13.94	14.15
0.05	2.234	13.86	13.54	0.05	2.615	14.14	14.52
0.06	2.323	14.03	13.95	0.06	2.692	14.29	14.74
0.07	2.403	14.19	14.28	0.07	2.761	14.42	14.94
0.08	2.474	14.35	14.55	0.08	2.825	14.54	15.11
0.09	2.537	14.49	14.77	0.09	2.878	14.65	15.27
0.10	2.595	14.62	14.97	0.10	2.928	14.76	15.41
γ =5				γ =6			
α	$M_{\max}$	$R_{1.4M_\odot}$	$R_{2.072M_\odot}$	α	$M_{\max}$	$R_{1.4M_\odot}$	$R_{2.072M_\odot}$
0.01	2.332	13.42	13.33	0.01	2.577	13.66	13.97
0.02	2.553	13.77	14.07	0.02	2.780	13.97	14.51
0.03	2.694	14.00	14.46	0.03	2.903	14.18	14.82
0.04	2.797	14.18	14.73	0.04	2.994	14.34	15.05
0.05	2.878	14.33	14.95	0.05	3.065	14.47	15.23
0.06	2.946	14.46	15.13	0.06	3.124	14.58	15.38
0.07	3.005	14.57	15.29	0.07	3.174	14.67	15.51
0.08	3.057	14.67	15.42	0.08	3.218	14.76	15.62
0.09	3.103	14.76	15.55	0.09	3.258	14.84	15.73
0.10	3.144	14.84	15.66	0.10	3.293	14.91	15.82
γ =7				γ =8			
α	$M_{\max}$	$R_{1.4M_\odot}$	$R_{2.072M_\odot}$	α	$M_{\max}$	$R_{1.4M_\odot}$	$R_{2.072M_\odot}$
0.01	2.769	13.84	14.36	0.01	2.918	13.98	14.63
0.02	2.950	14.13	14.80	0.02	3.082	14.25	15.02
0.03	3.061	14.32	15.07	0.03	3.180	14.42	15.26
0.04	3.140	14.46	15.27	0.04	3.251	14.55	15.43
0.05	3.202	14.57	15.43	0.05	3.307	14.65	15.57
0.06	3.254	14.67	15.56	0.06	3.353	14.74	15.68
0.07	3.298	14.75	15.67	0.07	3.393	14.81	15.78
0.08	3.336	14.82	15.76	0.08	3.428	14.88	15.87
0.09	3.371	14.89	15.85	0.09	3.459	14.93	15.94
0.10	3.402	14.95	15.93	0.10	3.486	14.98	16.01

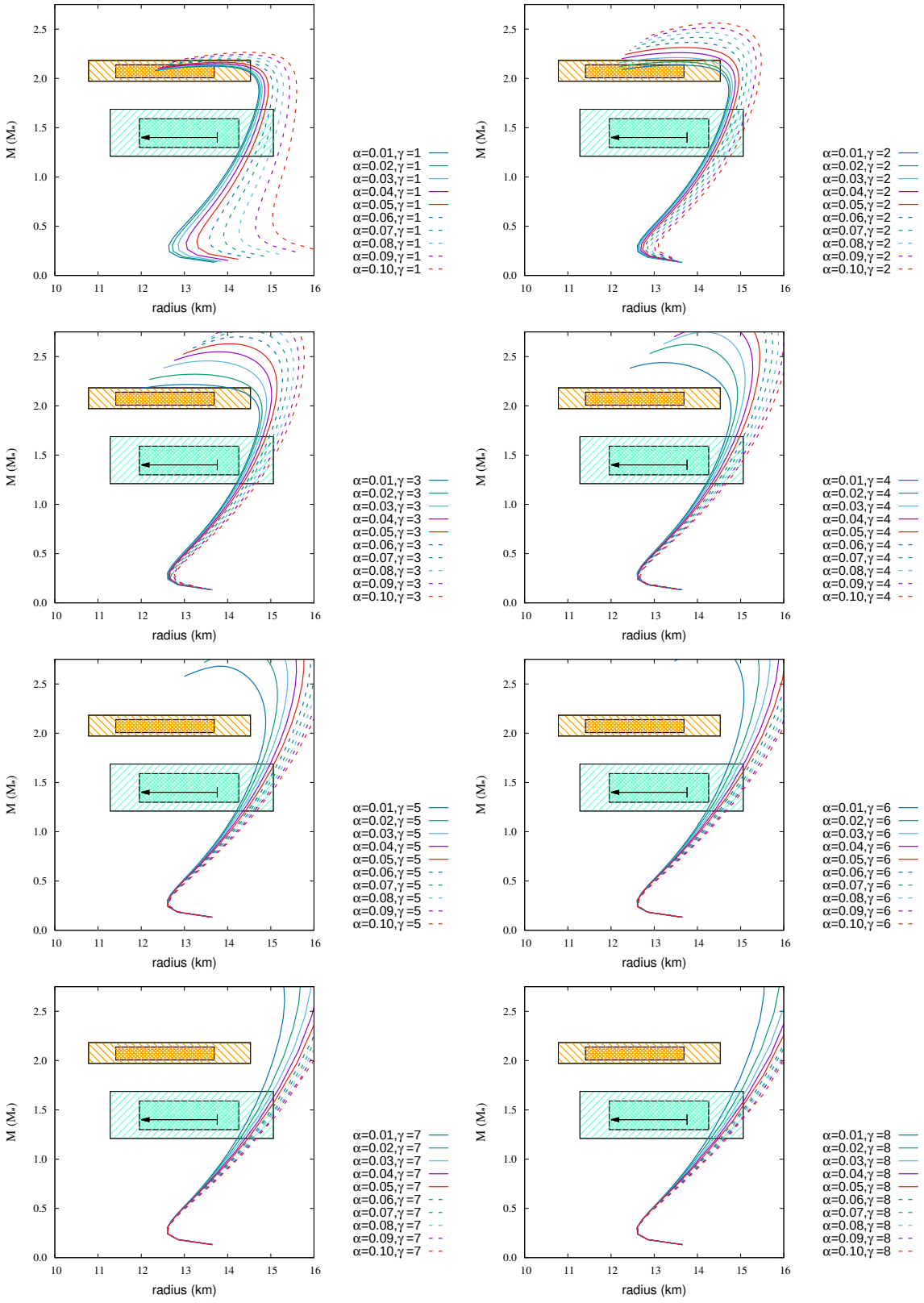

Figure H.5: Same as Fig. H.1, but for NL3-a EoS ($B_s = 10^{15}\,G$).

Table H.5: Same as Table H.1, but for NL3-a EoS ($B_s = 10^{15}\,G$).

γ =1				γ =2			
α	$M_{\max}$	$R_{1.4M_\odot}$	$R_{2.072M_\odot}$	α	$M_{\max}$	$R_{1.4M_\odot}$	$R_{2.072M_\odot}$
0.01	2.124	14.41	14.46	0.01	2.135	14.41	14.49
0.02	2.130	14.44	14.51	0.02	2.168	14.43	14.60
0.03	2.138	14.50	14.58	0.03	2.212	14.47	14.71
0.04	2.150	14.57	14.68	0.04	2.261	14.52	14.83
0.05	2.164	14.67	14.79	0.05	2.313	14.58	14.94
0.06	2.180	14.79	14.92	0.06	2.365	14.64	15.04
0.07	2.199	14.93	15.06	0.07	2.416	14.72	15.15
0.08	2.219	15.09	15.21	0.08	2.467	14.81	15.25
0.09	2.242	15.28	15.37	0.09	2.515	14.90	15.35
0.10	2.265	15.48	15.54	0.10	2.562	15.00	15.46
γ =3				γ =4			
α	$M_{\max}$	$R_{1.4M_\odot}$	$R_{2.072M_\odot}$	α	$M_{\max}$	$R_{1.4M_\odot}$	$R_{2.072M_\odot}$
0.01	2.217	14.41	14.59	0.01	2.439	14.42	14.74
0.02	2.320	14.44	14.74	0.02	2.623	14.46	14.93
0.03	2.456	14.48	14.90	0.03	2.750	14.52	15.06
0.04	2.549	14.54	15.02	0.04	2.845	14.58	15.18
0.05	2.630	14.60	15.12	0.05	2.923	14.65	15.30
0.06	2.701	14.67	15.23	0.06	2.987	14.72	15.41
0.07	2.764	14.74	15.33	0.07	3.043	14.79	15.51
0.08	2.821	14.82	15.43	0.08	3.091	14.86	15.61
0.09	2.872	14.89	15.53	0.09	3.133	14.92	15.71
0.10	2.920	14.97	15.63	0.10	3.172	14.99	15.80
γ =5				γ =6			
α	$M_{\max}$	$R_{1.4M_\odot}$	$R_{2.072M_\odot}$	α	$M_{\max}$	$R_{1.4M_\odot}$	$R_{2.072M_\odot}$
0.01	2.680	14.43	14.88	0.01	2.882	14.45	15.00
0.02	2.866	14.49	15.06	0.02	3.049	14.53	15.20
0.03	2.982	14.56	15.21	0.03	3.148	14.61	15.36
0.04	3.065	14.63	15.34	0.04	3.217	14.68	15.49
0.05	3.130	14.70	15.46	0.05	3.272	14.75	15.60
0.05	3.183	14.77	15.57	0.06	3.305	14.81	15.69
0.07	3.229	14.84	15.67	0.07	3.356	14.88	15.79
0.08	3.268	14.90	15.76	0.08	3.390	14.93	15.88
0.09	3.303	14.96	15.85	0.09	3.421	14.99	15.95
0.10	3.335	15.01	15.93	0.10	3.449	15.03	16.02
γ =7				γ =8			
α	$M_{\max}$	$R_{1.4M_\odot}$	$R_{2.072M_\odot}$	α	$M_{\max}$	$R_{1.4M_\odot}$	$R_{2.072M_\odot}$
0.01	3.038	14.47	15.11	0.01	3.156	14.51	15.21
0.02	3.182	14.57	15.32	0.02	3.281	14.61	15.44
0.03	3.266	14.66	15.48	0.03	3.356	14.70	15.59
0.04	3.327	14.73	15.61	0.04	3.411	14.77	15.71
0.05	3.375	14.80	15.72	0.05	3.456	14.84	15.81
0.06	3.415	14.86	15.81	0.06	3.493	14.89	15.89
0.07	3.450	14.91	15.89	0.07	3.525	14.94	15.96
0.08	3.481	14.96	15.96	0.08	3.553	14.99	16.03
0.09	3.509	15.01	16.03	0.09	3.579	15.03	16.09
0.10	3.534	15.05	16.09	0.10	3.602	15.07	16.14

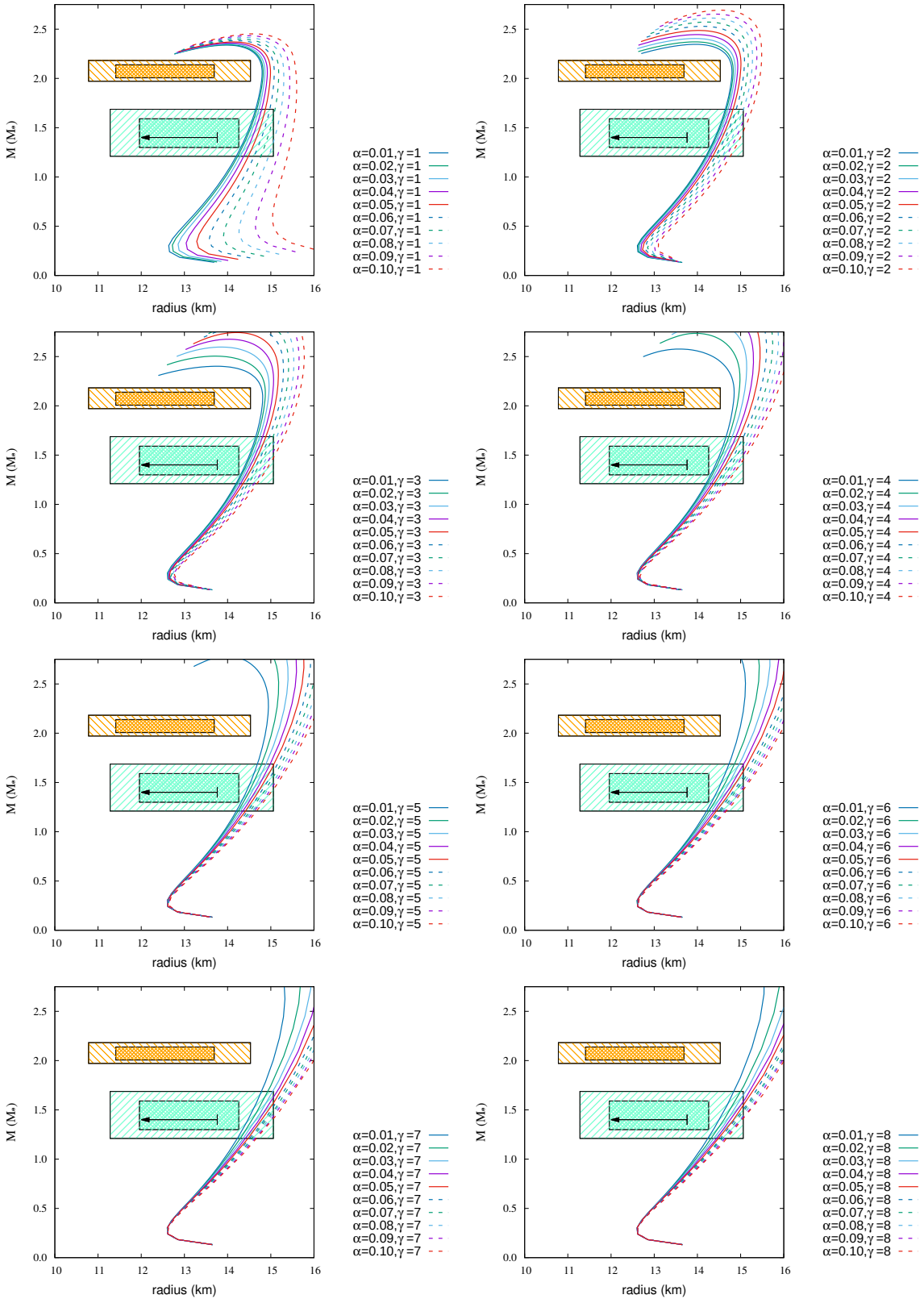

Figure H.6: Same as Fig. H.1, but for NL3-b EoS ($B_s = 10^{15}\,G$).

Table H.6: Same as Table H.1, but for NL3-b EoS ($B_s = 10^{15}\,G$).

γ =1				γ =2			
α	$M_{\max}$	$R_{1.4M_\odot}$	$R_{2.072M_\odot}$	α	$M_{\max}$	$R_{1.4M_\odot}$	$R_{2.072M_\odot}$
0.01	2.338	14.41	14.80	0.01	2.346	14.41	14.80
0.02	2.342	14.44	14.82	0.02	2.371	14.43	14.83
0.03	2.349	14.50	14.86	0.03	2.405	14.47	14.87
0.04	2.359	14.57	14.92	0.04	2.445	14.52	14.93
0.05	2.370	14.67	14.99	0.05	2.487	14.58	15.00
0.06	2.384	14.79	15.08	0.06	2.529	14.64	15.08
0.07	2.399	14.93	15.18	0.07	2.572	14.72	15.16
0.08	2.415	15.09	15.30	0.08	2.613	14.81	15.26
0.09	2.433	15.28	15.43	0.09	2.653	14.90	15.36
0.10	2.452	15.48	15.58	0.10	2.693	15.00	15.47
γ =3				γ =4			
α	$M_{\max}$	$R_{1.4M_\odot}$	$R_{2.072M_\odot}$	α	$M_{\max}$	$R_{1.4M_\odot}$	$R_{2.072M_\odot}$
0.01	2.402	14.41	14.81	0.01	2.576	14.42	14.84
0.02	2.504	14.44	14.87	0.02	2.736	14.46	14.95
0.03	2.596	14.48	14.94	0.03	2.845	14.52	15.06
0.04	2.676	14.54	15.03	0.04	2.927	14.58	15.18
0.05	2.744	14.60	15.13	0.05	2.993	14.65	15.30
0.06	2.804	14.67	15.23	0.06	3.047	14.72	15.41
0.07	2.858	14.74	15.33	0.07	3.094	14.79	15.51
0.08	2.906	14.82	15.43	0.08	3.137	14.86	15.61
0.09	2.952	14.89	15.53	0.09	3.174	14.92	15.71
0.10	2.993	14.97	15.63	0.10	3.208	14.99	15.80
γ =5				γ =6			
α	$M_{\max}$	$R_{1.4M_\odot}$	$R_{2.072M_\odot}$	α	$M_{\max}$	$R_{1.4M_\odot}$	$R_{2.072M_\odot}$
0.01	2.784	14.43	14.90	0.01	2.958	14.45	15.00
0.02	2.944	14.49	15.06	0.02	3.099	14.53	15.20
0.03	3.042	14.56	15.21	0.03	3.183	14.61	15.36
0.04	3.114	14.63	15.34	0.04	3.243	14.68	15.49
0.05	3.169	14.70	15.46	0.05	3.291	14.75	15.60
0.06	3.215	14.77	15.57	0.06	3.338	14.83	15.72
0.07	3.255	14.84	15.67	0.07	3.370	14.88	15.79
0.08	3.290	14.90	15.76	0.08	3.402	14.93	15.88
0.09	3.322	14.96	15.85	0.09	3.432	14.99	15.95
0.10	3.351	15.01	15.93	0.10	3.458	15.03	16.02
γ =7				γ =8			
α	$M_{\max}$	$R_{1.4M_\odot}$	$R_{2.072M_\odot}$	α	$M_{\max}$	$R_{1.4M_\odot}$	$R_{2.072M_\odot}$
0.01	3.090	14.47	15.11	0.01	3.187	14.51	15.21
0.02	3.210	14.57	15.32	0.02	3.298	14.61	15.44
0.03	3.285	14.66	15.48	0.03	3.369	14.70	15.59
0.04	3.342	14.73	15.61	0.04	3.422	14.77	15.71
0.05	3.388	14.80	15.72	0.05	3.465	14.84	15.81
0.06	3.426	14.86	15.81	0.06	3.501	14.89	15.89
0.07	3.460	14.91	15.89	0.07	3.532	14.94	15.96
0.08	3.490	14.96	15.96	0.08	3.560	14.99	16.03
0.09	3.516	15.01	16.03	0.09	3.584	15.03	16.09
0.10	3.541	15.05	16.09	0.10	3.607	15.07	16.14

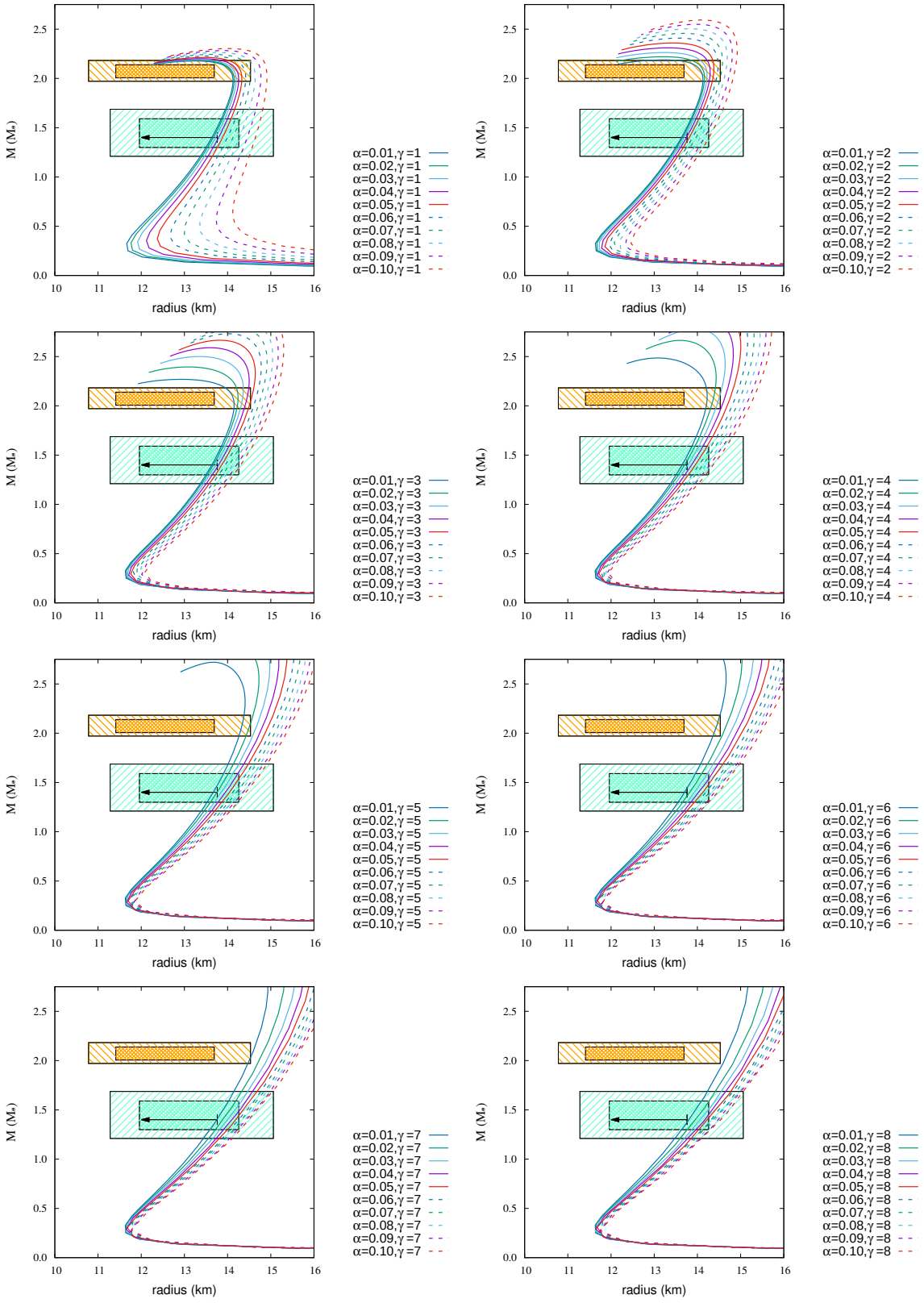

Figure H.7: Same as Fig. H.1, but for NL3$\omega\rho$-a EoS ($B_s = 10^{15}\,G$).

Table H.7: Same as Table H.1, but for NL3$\omega\rho$-a EoS ($B_s = 10^{15}\,G$).

γ =1				γ =2			
α	$M_{\rm max}$	$R_{1.4M_\odot}$	$R_{2.072M_\odot}$	α	$M_{\rm max}$	$R_{1.4M_\odot}$	$R_{2.072M_\odot}$
0.01	2.177	13.64	14.07	0.01	2.188	13.63	14.08
0.02	2.182	13.67	14.10	0.02	2.220	13.66	14.14
0.03	2.190	13.72	14.16	0.03	2.263	13.70	14.21
0.04	2.200	13.79	14.22	0.04	2.310	13.75	14.30
0.05	2.213	13.88	14.30	0.05	2.360	13.81	14.38
0.06	2.227	14.00	14.40	0.06	2.409	13.89	14.47
0.07	2.244	14.13	14.51	0.07	2.457	13.97	14.56
0.08	2.262	14.28	14.63	0.08	2.504	14.06	14.66
0.09	2.282	14.46	14.76	0.09	2.550	14.16	14.76
0.10	2.303	14.64	14.90	0.10	2.593	14.27	14.86
γ =3				γ =4			
α	$M_{\rm max}$	$R_{1.4M_\odot}$	$R_{2.072M_\odot}$	α	$M_{\rm max}$	$R_{1.4M_\odot}$	$R_{2.072M_\odot}$
0.01	2.269	13.64	14.13	0.01	2.485	13.65	14.22
0.02	2.394	13.67	14.24	0.02	2.664	13.71	14.37
0.03	2.500	13.72	14.35	0.03	2.782	13.78	14.50
0.04	2.589	13.79	14.45	0.04	2.870	13.87	14.63
0.05	2.666	13.87	14.55	0.05	2.940	13.95	14.75
0.06	2.732	13.95	14.66	0.06	2.998	14.04	14.87
0.07	2.790	14.04	14.76	0.07	3.047	14.13	14.98
0.08	2.841	14.12	14.87	0.08	3.090	14.21	15.09
0.09	2.888	14.21	14.98	0.09	3.128	14.29	15.20
0.10	2.931	14.30	15.08	0.10	3.162	14.37	15.30
γ =5				γ =6			
α	$M_{\rm max}$	$R_{1.4M_\odot}$	$R_{2.072M_\odot}$	α	$M_{\rm max}$	$R_{1.4M_\odot}$	$R_{2.072M_\odot}$
0.01	2.720	13.67	14.33	0.01	2.909	13.70	14.45
0.02	2.892	13.76	14.51	0.02	3.057	13.82	14.67
0.03	2.996	13.86	14.67	0.03	3.142	13.94	14.84
0.04	3.069	13.95	14.82	0.04	3.203	14.04	14.99
0.05	3.126	14.05	14.95	0.05	3.252	14.13	15.12
0.05	3.173	14.13	15.07	0.06	3.294	14.21	15.23
0.07	3.213	14.21	15.18	0.07	3.330	14.29	15.33
0.08	3.249	14.29	15.28	0.08	3.362	14.36	15.42
0.09	3.281	14.36	15.37	0.09	3.371	14.41	15.48
0.10	3.310	14.43	15.46	0.10	3.408	14.48	15.56
γ =7				γ =8			
α	$M_{\rm max}$	$R_{1.4M_\odot}$	$R_{2.072M_\odot}$	α	$M_{\rm max}$	$R_{1.4M_\odot}$	$R_{2.072M_\odot}$
0.01	3.048	13.75	14.57	0.01	3.149	13.81	14.70
0.02	3.172	13.90	14.82	0.02	3.261	13.96	14.95
0.03	3.247	14.01	14.99	0.03	3.332	14.08	15.12
0.04	3.303	14.11	15.13	0.04	3.384	14.18	15.25
0.05	3.349	14.20	15.25	0.05	3.426	14.26	15.36
0.06	3.387	14.28	15.35	0.06	3.462	14.34	15.45
0.07	3.420	14.35	15.44	0.07	3.493	14.38	15.54
0.08	3.450	14.41	15.52	0.08	3.520	14.44	15.61
0.09	3.476	14.47	15.60	0.09	3.544	14.50	15.67
0.10	3.500	14.52	15.66	0.10	3.566	14.55	15.73

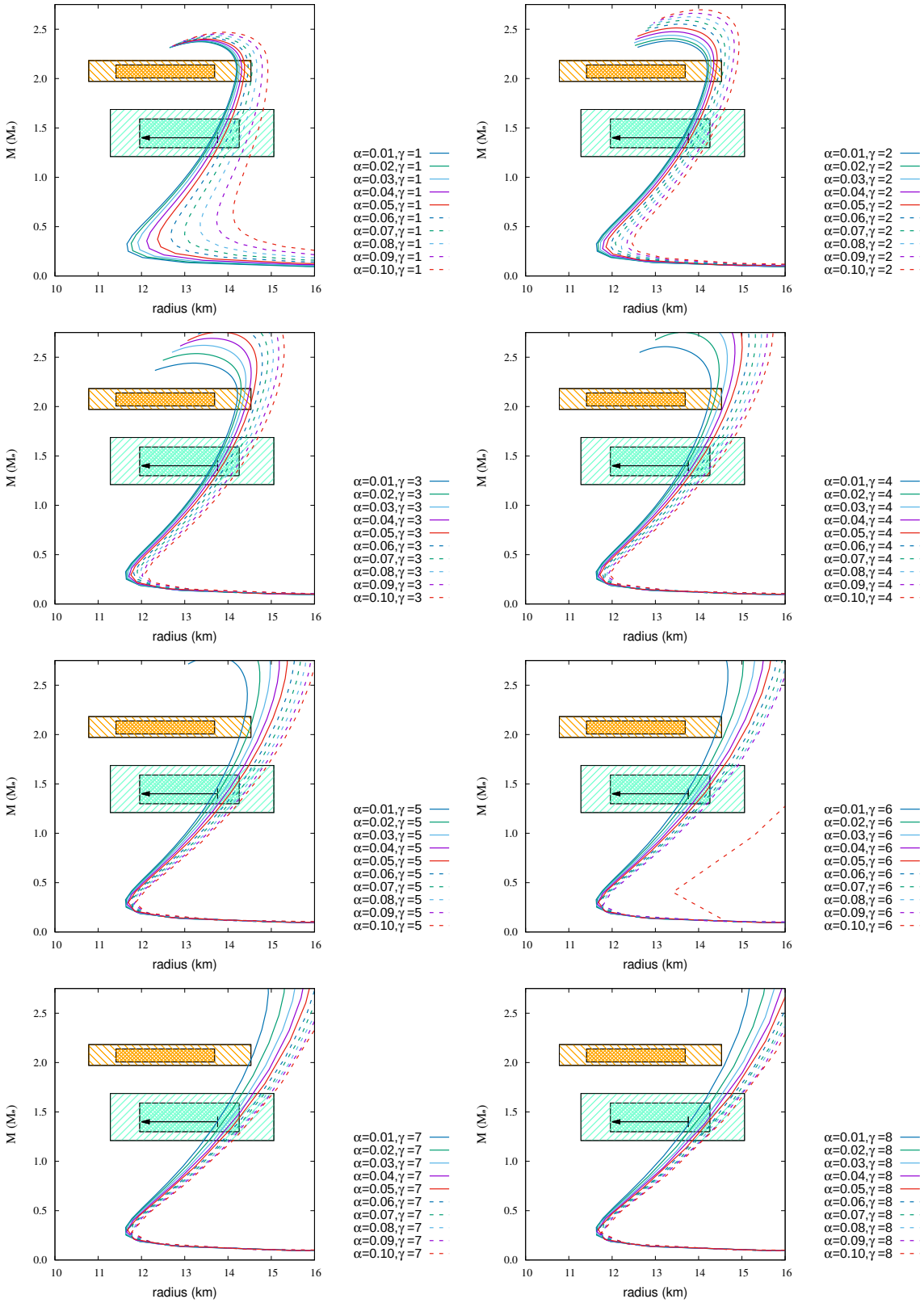

Figure H.8: Same as Fig. H.1, but for NL3$\omega\rho$-b EoS ($B_s = 10^{15}\,G$).

Table H.8: Same as Table H.1, but for NL3$\omega\rho$-b EoS ($B_s = 10^{15}\,G$). .

γ =1				γ =2			
α	$M_{\rm max}$	$R_{1.4M_\odot}$	$R_{2.072M_\odot}$	α	$M_{\rm max}$	$R_{1.4M_\odot}$	$R_{2.072M_\odot}$
0.01	2.373	13.64	14.19	0.01	2.381	13.63	14.20
0.02	2.377	13.67	14.22	0.02	2.406	13.66	14.23
0.03	2.383	13.72	14.26	0.03	2.438	13.70	14.27
0.04	2.391	13.79	14.31	0.04	2.475	13.75	14.33
0.05	2.400	13.88	14.38	0.05	2.513	13.81	14.40
0.06	2.412	14.00	14.46	0.06	2.552	13.89	14.48
0.07	2.424	14.13	14.56	0.07	2.589	13.97	14.56
0.08	2.438	14.28	14.66	0.08	2.625	14.06	14.66
0.09	2.454	14.46	14.79	0.09	2.662	14.16	14.76
0.10	2.469	14.64	14.92	0.10	2.697	14.27	14.87
γ =3				γ =4			
α	$M_{\rm max}$	$R_{1.4M_\odot}$	$R_{2.072M_\odot}$	α	$M_{\rm max}$	$R_{1.4M_\odot}$	$R_{2.072M_\odot}$
0.01	2.440	13.64	14.21	0.01	2.607	13.65	14.25
0.02	2.537	13.67	14.28	0.02	2.751	13.71	14.37
0.03	2.620	13.73	14.36	0.03	2.848	13.78	14.50
0.04	2.691	13.79	14.45	0.04	2.924	13.87	14.63
0.05	2.754	13.87	14.55	0.05	2.984	13.95	14.75
0.06	2.809	13.95	14.66	0.06	3.034	14.04	14.87
0.07	2.856	14.04	14.76	0.07	3.077	14.13	14.98
0.08	2.900	14.12	14.87	0.08	3.115	14.21	15.09
0.09	2.941	14.21	14.98	0.09	3.149	14.29	15.20
0.10	2.978	14.30	15.08	0.10	3.180	14.37	15.30
γ =5				γ =6			
α	$M_{\rm max}$	$R_{1.4M_\odot}$	$R_{2.072M_\odot}$	α	$M_{\rm max}$	$R_{1.4M_\odot}$	$R_{2.072M_\odot}$
0.01	2.796	13.67	14.33	0.01	2.956	13.70	14.45
0.02	2.943	13.76	14.51	0.02	3.083	13.82	14.67
0.03	3.031	13.86	14.67	0.03	3.159	13.94	14.84
0.04	3.095	13.95	14.82	0.04	3.217	14.04	14.99
0.05	3.146	14.05	14.95	0.05	3.263	14.13	15.12
0.05	3.189	14.13	15.07	0.06	3.303	14.21	15.23
0.07	3.226	14.21	15.18	0.07	3.338	14.29	15.33
0.08	3.260	14.29	15.28	0.08	3.369	14.36	15.42
0.09	3.291	14.36	15.37	0.09	3.375	14.41	15.47
0.10	3.319	14.43	15.46	0.10	4.144	16.49	17.78
γ =7				γ =8			
α	$M_{\rm max}$	$R_{1.4M_\odot}$	$R_{2.072M_\odot}$	α	$M_{\rm max}$	$R_{1.4M_\odot}$	$R_{2.072M_\odot}$
0.01	3.075	13.75	14.57	0.01	3.165	13.81	14.70
0.02	3.187	13.90	14.82	0.02	3.272	13.96	14.95
0.03	3.258	14.01	14.99	0.03	3.340	14.08	15.12
0.04	3.312	14.11	15.13	0.04	3.391	14.18	15.25
0.05	3.356	14.20	15.25	0.05	3.432	14.26	15.36
0.06	3.393	14.28	15.35	0.06	3.466	14.34	15.45
0.07	3.426	14.35	15.44	0.07	3.496	14.38	15.53
0.08	3.454	14.41	15.52	0.08	3.523	14.44	15.61
0.09	3.480	14.47	15.60	0.09	3.547	14.50	15.67
0.10	3.504	14.52	15.66	0.10	3.568	14.55	15.73

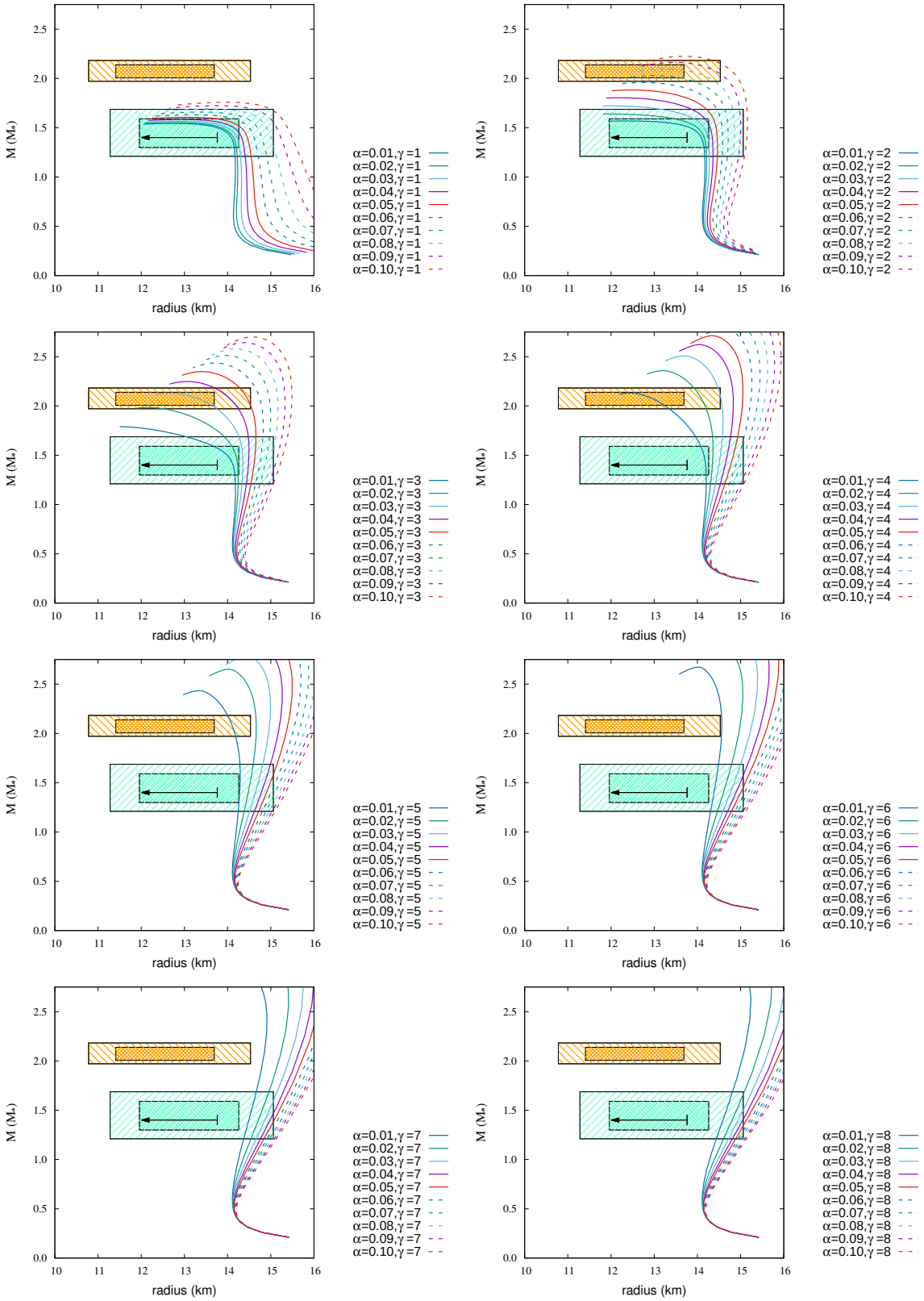

Figure H.9: Same as Fig. H.1, but for TM1-a EoS ($B_s = 10^{15}\,G$).

Table H.9: Same as Table H.1, but for TM1-a EoS ($B_s = 10^{15}\,G$). .

γ =1				γ =2			
α	$M_{\max}$	$R_{1.4M_\odot}$	$R_{2.072M_\odot}$	α	$M_{\max}$	$R_{1.4M_\odot}$	$R_{2.072M_\odot}$
0.01	1.543	14.09	—	0.01	1.569	14.09	—
0.02	1.640	14.16	—	0.02	1.984	14.23	—
0.03	1.722	14.24	—	0.03	2.130	14.35	13.32
0.04	1.804	14.35	—	0.04	2.248	14.48	14.06
0.05	1.883	14.46	—	0.05	2.349	14.61	14.46
0.06	1.958	14.58	—	0.06	2.436	14.74	14.75
0.07	2.030	14.71	—	0.07	2.512	14.86	14.97
0.08	2.098	14.85	13.83	0.08	2.581	14.99	15.16
0.09	2.163	15.00	14.43	0.09	2.643	15.10	15.33
0.10	2.225	15.15	14.80	0.10	2.700	15.21	15.49
γ =3				γ =4			
α	$M_{\max}$	$R_{1.4M_\odot}$	$R_{2.072M_\odot}$	α	$M_{\max}$	$R_{1.4M_\odot}$	$R_{2.072M_\odot}$
0.01	2.131	14.19	12.97	0.01	2.433	14.28	14.11
0.02	2.358	14.35	14.09	0.02	2.651	14.48	14.66
0.03	2.509	14.50	14.55	0.03	2.786	14.64	14.97
0.04	2.622	14.64	14.83	0.04	2.882	14.78	15.20
0.05	2.713	14.77	15.05	0.05	2.959	14.90	15.39
0.06	2.789	14.89	15.24	0.06	3.021	15.01	15.55
0.07	2.853	15.00	15.41	0.07	3.075	15.10	15.69
0.08	2.910	15.10	15.56	0.08	3.122	15.19	15.82
0.09	2.961	15.20	15.70	0.09	3.164	15.27	15.93
0.10	3.007	15.29	15.83	0.10	3.203	15.34	16.03
γ =5				γ =6			
α	$M_{\max}$	$R_{1.4M_\odot}$	$R_{2.072M_\odot}$	α	$M_{\max}$	$R_{1.4M_\odot}$	$R_{2.072M_\odot}$
0.01	2.673	14.38	14.57	0.01	2.854	14.49	14.85
0.02	2.866	14.60	14.99	0.02	3.021	14.71	15.23
0.03	2.980	14.76	15.26	0.03	3.122	14.86	15.47
0.04	3.062	14.89	15.46	0.04	3.196	14.98	15.65
0.05	3.128	15.00	15.62	0.05	3.254	15.08	15.79
0.05	3.183	15.10	15.76	0.06	3.303	15.17	15.91
0.07	3.230	15.18	15.88	0.07	3.344	15.24	16.02
0.08	3.271	15.26	15.99	0.08	3.381	15.30	16.11
0.09	3.308	15.32	16.08	0.09	3.414	15.36	16.19
0.10	3.341	15.39	16.17	0.10	3.443	15.42	16.26
γ =7				γ =8			
α	$M_{\max}$	$R_{1.4M_\odot}$	$R_{2.072M_\odot}$	α	$M_{\max}$	$R_{1.4M_\odot}$	$R_{2.072M_\odot}$
0.01	2.991	14.59	15.07	0.01	3.100	14.68	15.25
0.02	3.141	14.80	15.42	0.02	3.238	14.88	15.57
0.03	3.233	14.95	15.64	0.03	3.321	15.01	15.77
0.04	3.299	15.05	15.80	0.04	3.383	15.11	15.91
0.05	3.352	15.14	15.92	0.05	3.431	15.19	16.02
0.06	3.396	15.22	16.03	0.06	3.471	15.26	16.12
0.07	3.434	15.28	16.12	0.07	3.506	15.32	16.20
0.08	3.467	15.34	16.20	0.08	3.536	15.37	16.27
0.09	3.497	15.39	16.27	0.09	3.562	15.41	16.33
0.10	3.523	15.44	16.34	0.10	3.586	15.45	16.39

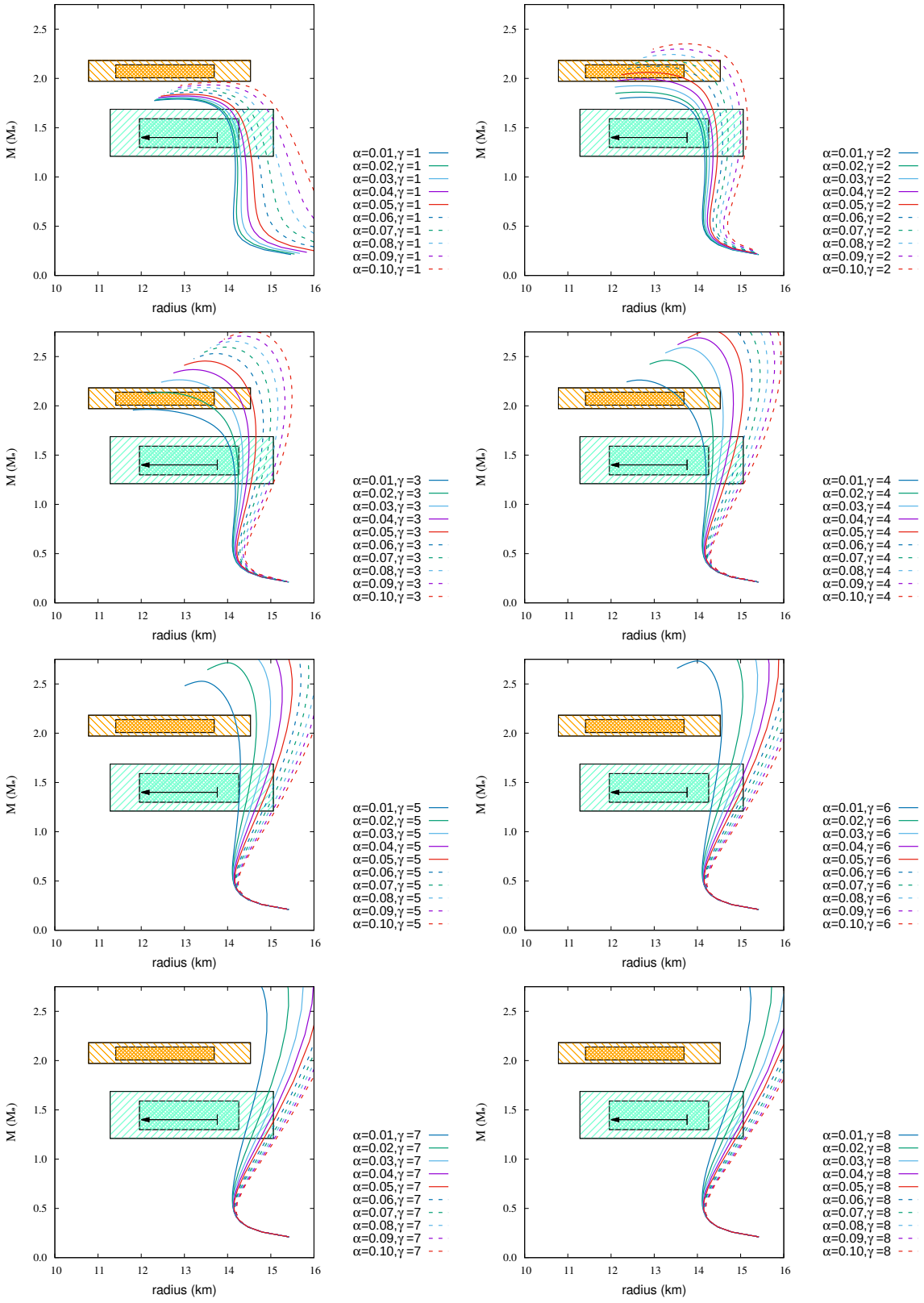

Figure H.10: Same as Fig. H.1, but for TM1-b EoS ($B_s = 10^{15}\,G$).

Table H.10: Same as Table H.1, but for TM1-b EoS ($B_s = 10^{15}\,G$)..

γ =1				γ =2			
α	$M_{\max}$	$R_{1.4M_\odot}$	$R_{2.072M_\odot}$	α	$M_{\max}$	$R_{1.4M_\odot}$	$R_{2.072M_\odot}$
0.01	1.790	14.12	—	0.01	1.809	14.13	—
0.02	1.797	14.17	—	0.02	1.861	14.18	—
0.03	1.808	14.24	—	0.03	1.926	14.25	—
0.04	1.822	14.34	—	0.04	1.994	14.35	—
0.05	1.839	14.46	—	0.05	2.060	14.46	—
0.06	1.860	14.62	—	0.06	2.124	14.58	13.78
0.07	1.883	14.79	—	0.07	2.185	14.71	14.17
0.08	1.908	15.00	—	0.08	2.243	14.85	14.46
0.09	1.934	15.23	—	0.09	2.298	15.00	14.70
0.10	1.962	15.49	—	0.10	2.351	15.15	14.92
γ =3				γ =4			
α	$M_{\max}$	$R_{1.4M_\odot}$	$R_{2.072M_\odot}$	α	$M_{\max}$	$R_{1.4M_\odot}$	$R_{2.072M_\odot}$
0.01	1.963	14.15	—	0.01	2.262	14.19	13.62
0.02	2.135	14.24	13.28	0.02	2.462	14.35	14.23
0.03	2.264	14.35	13.93	0.03	2.592	14.50	14.57
0.04	2.367	14.48	14.28	0.04	2.689	14.64	14.83
0.05	2.454	14.61	14.55	0.05	2.769	14.77	15.05
0.06	2.530	14.74	14.77	0.06	2.834	14.89	15.24
0.07	2.596	14.86	14.97	0.07	2.892	15.00	15.41
0.08	2.655	14.99	15.16	0.08	2.943	15.10	15.56
0.09	2.709	15.10	15.33	0.09	2.988	15.20	15.70
0.10	2.758	15.21	15.49	0.10	3.030	15.29	15.83
γ =5				γ =6			
α	$M_{\max}$	$R_{1.4M_\odot}$	$R_{2.072M_\odot}$	α	$M_{\max}$	$R_{1.4M_\odot}$	$R_{2.072M_\odot}$
0.01	2.527	14.28	14.21	0.01	2.733	14.38	14.57
0.02	2.715	14.48	14.67	0.02	2.900	14.60	14.99
0.03	2.831	14.64	14.97	0.03	3.003	14.76	15.26
0.04	2.916	14.78	15.20	0.04	3.080	14.89	15.46
0.05	2.985	14.90	15.39	0.05	3.141	15.00	15.62
0.05	3.042	15.01	15.55	0.06	3.194	15.10	15.76
0.07	3.092	15.10	15.69	0.07	3.239	15.18	15.88
0.08	3.136	15.19	15.82	0.08	3.279	15.26	15.99
0.09	3.176	15.27	15.93	0.09	3.315	15.32	16.08
0.10	3.213	15.34	16.03	0.10	3.347	15.39	16.17
γ =7				γ =8			
α	$M_{\max}$	$R_{1.4M_\odot}$	$R_{2.072M_\odot}$	α	$M_{\max}$	$R_{1.4M_\odot}$	$R_{2.072M_\odot}$
0.01	2.889	14.49	14.85	0.01	3.013	14.59	15.07
0.02	3.041	14.71	15.23	0.02	3.155	14.80	15.42
0.03	3.136	14.86	15.47	0.03	3.243	14.95	15.64
0.04	3.207	14.98	15.65	0.04	3.307	15.05	15.80
0.05	3.263	15.08	15.79	0.05	3.358	15.14	15.92
0.06	3.310	15.17	15.91	0.06	3.401	15.22	16.03
0.07	3.351	15.24	16.02	0.07	3.438	15.28	16.12
0.08	3.386	15.30	16.11	0.08	3.471	15.34	16.20
0.09	3.418	15.36	16.19	0.09	3.500	15.39	16.27
0.10	3.447	15.42	16.26	0.10	3.526	15.44	16.34

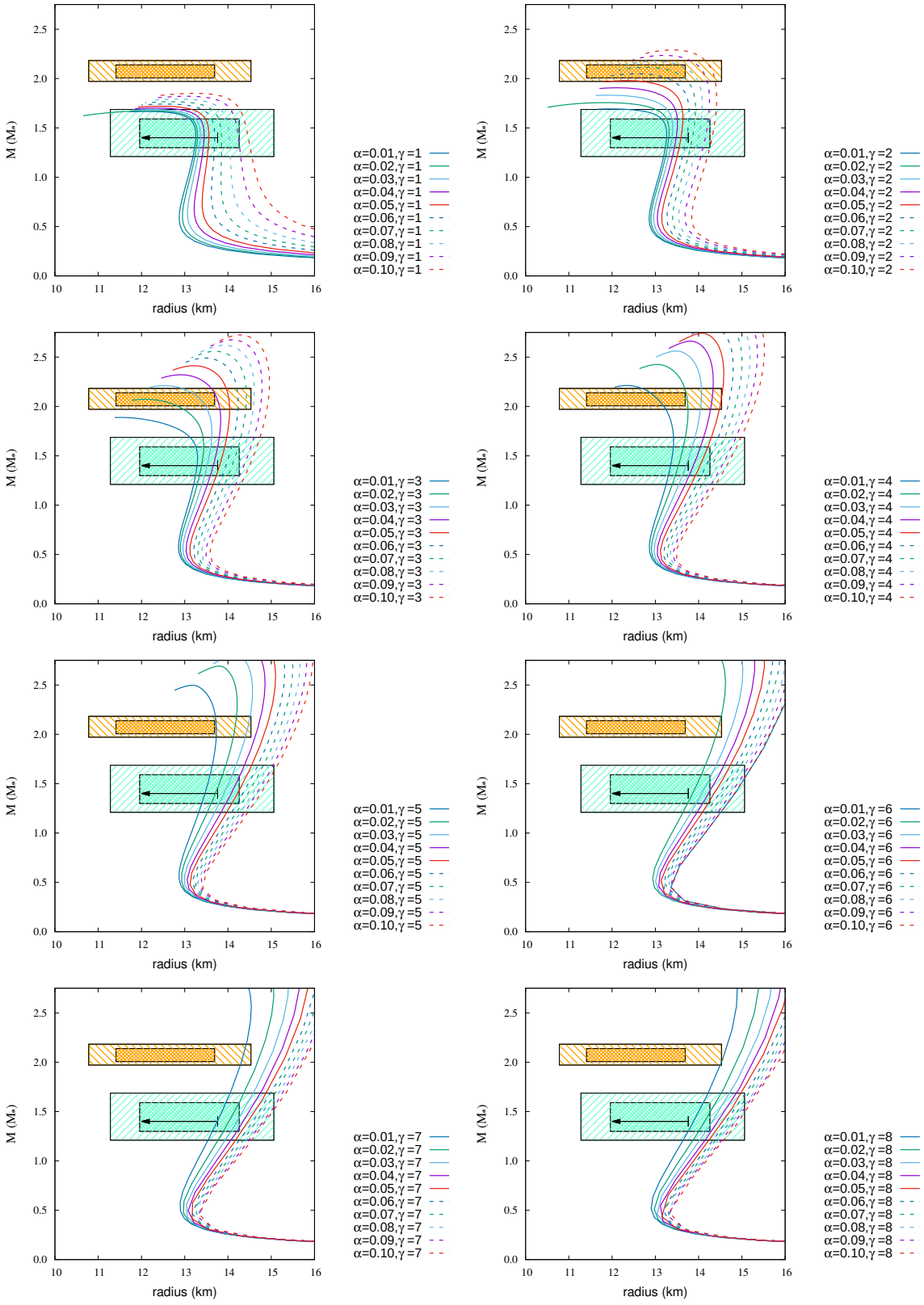

Figure H.11: Same as Fig. H.1, but for TM2$\omega\rho$-a EoS ($B_s = 10^{15}\,G$).

Table H.11: Same as Table H.1, but for TM2$\omega\rho$-a EoS ($B_s = 10^{15}\,G$).

γ =1				γ =2			
α	$M_{\max}$	$R_{1.4M_\odot}$	$R_{2.072M_\odot}$	α	$M_{\max}$	$R_{1.4M_\odot}$	$R_{2.072M_\odot}$
0.01	1.666	13.26	—	0.01	1.692	13.26	—
0.02	1.674	13.30	—	0.02	1.756	13.31	—
0.03	1.685	13.36	—	0.03	1.831	13.38	—
0.04	1.701	13.45	—	0.04	1.906	13.48	—
0.05	1.719	13.56	—	0.05	1.979	13.59	—
0.06	1.741	13.69	—	0.06	2.049	13.72	—
0.07	1.765	13.85	—	0.07	2.114	13.86	13.41
0.08	1.792	14.03	—	0.08	2.175	14.00	13.82
0.09	1.820	14.24	—	0.09	2.235	14.16	14.10
0.10	1.850	14.47	—	0.10	2.290	14.31	14.32
γ =3				γ =4			
α	$M_{\max}$	$R_{1.4M_\odot}$	$R_{2.072M_\odot}$	α	$M_{\max}$	$R_{1.4M_\odot}$	$R_{2.072M_\odot}$
0.01	1.888	13.29	—	0.01	2.213	13.35	13.06
0.02	2.073	13.39	12.16	0.02	2.425	13.53	13.74
0.03	2.210	13.52	13.36	0.03	2.562	13.71	14.06
0.04	2.321	13.66	13.76	0.04	2.662	13.88	14.31
0.05	2.413	13.81	14.02	0.05	2.742	14.03	14.53
0.06	2.491	13.95	14.23	0.06	2.808	14.18	14.72
0.07	2.559	14.10	14.42	0.07	2.865	14.31	14.89
0.08	2.620	14.23	14.60	0.08	2.915	14.43	15.05
0.09	2.675	14.37	14.77	0.09	2.959	14.54	15.19
0.10	2.725	14.50	14.94	0.10	3.000	14.65	15.33
γ =5				γ =6			
α	$M_{\max}$	$R_{1.4M_\odot}$	$R_{2.072M_\odot}$	α	$M_{\max}$	$R_{1.4M_\odot}$	$R_{2.072M_\odot}$
0.01	2.497	13.47	13.73	0.01	3.331	14.84	15.75
0.02	2.692	13.71	14.17	0.02	2.862	13.86	14.46
0.03	2.808	13.91	14.46	0.03	2.978	14.08	14.77
0.04	2.892	14.08	14.70	0.04	3.053	14.23	14.98
0.05	2.959	14.22	14.89	0.05	3.113	14.37	15.15
0.05	3.015	14.35	15.06	0.06	3.164	14.48	15.30
0.07	3.063	14.47	15.21	0.07	3.207	14.58	15.43
0.08	3.107	14.57	15.34	0.08	3.246	14.67	15.54
0.09	3.146	14.67	15.46	0.09	3.281	14.75	15.64
0.10	3.181	14.76	15.57	0.10	3.312	14.83	15.74
γ =7				γ =8			
α	$M_{\max}$	$R_{1.4M_\odot}$	$R_{2.072M_\odot}$	α	$M_{\max}$	$R_{1.4M_\odot}$	$R_{2.072M_\odot}$
0.01	2.868	13.76	14.36	0.01	2.990	13.89	14.59
0.02	3.017	14.03	14.75	0.02	3.128	14.15	14.95
0.03	3.109	14.21	15.00	0.03	3.213	14.32	15.18
0.04	3.177	14.36	15.19	0.04	3.276	14.44	15.36
0.05	3.232	14.47	15.34	0.05	3.326	14.57	15.49
0.06	3.278	14.58	15.47	0.06	3.367	14.65	15.61
0.07	3.317	14.66	15.59	0.07	3.403	14.75	15.70
0.08	3.352	14.74	15.69	0.08	3.435	14.84	15.79
0.09	3.392	14.84	15.78	0.09	3.463	14.88	15.87
0.10	3.417	14.89	15.86	0.10	3.488	14.93	15.94

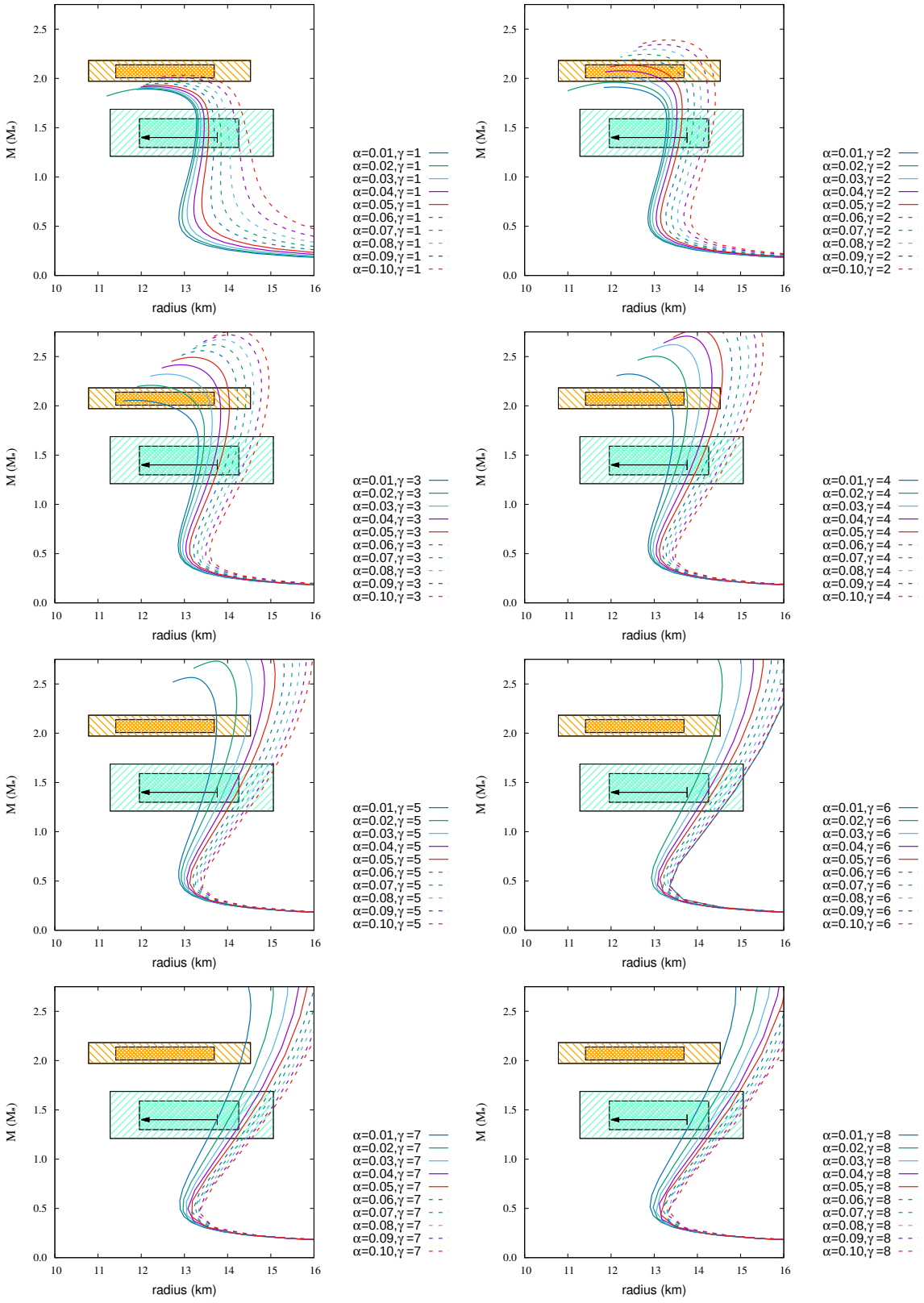

Figure H.12: Same as Fig. H.1, but for TM2$\omega\rho$-b EoS ($B_s = 10^{15}\,G$).

Table H.12: Same as Table H.1, but for TM2$\omega\rho$-b EoS ($B_s = 10^{15}\,G$).

γ =1				γ =2			
α	$M_{\max}$	$R_{1.4M_\odot}$	$R_{2.072M_\odot}$	α	$M_{\max}$	$R_{1.4M_\odot}$	$R_{2.072M_\odot}$
0.01	1.893	13.26	—	0.01	1.912	13.26	—
0.02	1.898	13.30	—	0.02	1.960	13.31	—
0.03	1.907	13.36	—	0.03	2.018	13.39	—
0.04	1.919	13.45	—	0.04	2.078	13.48	12.52
0.05	1.933	13.56	—	0.05	2.135	13.59	13.19
0.06	1.949	13.69	—	0.06	2.192	13.72	13.53
0.07	1.968	13.85	—	0.07	2.244	13.86	13.77
0.08	1.988	14.03	—	0.08	2.296	14.00	13.97
0.09	2.009	14.24	—	0.09	2.344	14.16	14.17
0.10	2.032	14.47	—	0.10	2.390	14.31	14.35
γ =3				γ =4			
α	$M_{\max}$	$R_{1.4M_\odot}$	$R_{2.072M_\odot}$	α	$M_{\max}$	$R_{1.4M_\odot}$	$R_{2.072M_\odot}$
0.01	2.056	13.29	—	0.01	2.323	13.35	13.32
0.02	2.208	13.39	13.16	0.02	2.503	13.53	13.77
0.03	2.322	13.52	13.56	0.03	2.621	13.71	14.06
0.04	2.416	13.66	13.82	0.04	2.707	13.88	14.31
0.05	2.492	13.81	14.03	0.05	2.777	14.03	14.53
0.06	2.559	13.95	14.24	0.06	2.836	14.18	14.72
0.07	2.618	14.10	14.42	0.07	2.888	14.31	14.89
0.08	2.672	14.23	14.60	0.08	2.934	14.43	15.05
0.09	2.720	14.37	14.77	0.09	2.975	14.54	15.19
0.10	2.764	14.50	14.94	0.10	3.013	14.65	15.33
γ =5				γ =6			
α	$M_{\max}$	$R_{1.4M_\odot}$	$R_{2.072M_\odot}$	α	$M_{\max}$	$R_{1.4M_\odot}$	$R_{2.072M_\odot}$
0.01	2.565	13.47	13.75	0.01	3.334	14.84	15.75
0.02	2.731	13.71	14.17	0.02	2.868	13.85	14.43
0.03	2.835	13.91	14.46	0.03	2.992	14.08	14.77
0.04	2.912	14.08	14.70	0.04	3.064	14.23	14.98
0.05	2.974	14.22	14.89	0.05	3.122	14.37	15.15
0.05	3.027	14.35	15.06	0.06	3.171	14.48	15.30
0.07	3.074	14.47	15.21	0.07	3.213	14.58	15.43
0.08	3.115	14.57	15.34	0.08	3.251	14.67	15.54
0.09	3.153	14.67	15.46	0.09	3.285	14.75	15.64
0.10	3.187	14.76	15.57	0.10	3.316	14.83	15.74
γ =7				γ =8			
α	$M_{\max}$	$R_{1.4M_\odot}$	$R_{2.072M_\odot}$	α	$M_{\max}$	$R_{1.4M_\odot}$	$R_{2.072M_\odot}$
0.01	2.888	13.76	14.36	0.01	3.003	13.89	14.59
0.02	3.029	14.03	14.75	0.02	3.136	14.15	14.95
0.03	3.118	14.21	15.00	0.03	3.219	14.32	15.18
0.04	3.184	14.36	15.19	0.04	3.280	14.44	15.36
0.05	3.238	14.47	15.34	0.05	3.329	14.57	15.49
0.06	3.282	14.58	15.47	0.06	3.370	14.65	15.61
0.07	3.321	14.66	15.59	0.07	3.405	14.75	15.70
0.08	3.355	14.74	15.69	0.08	3.436	14.84	15.79
0.09	3.394	14.84	15.78	0.09	3.464	14.88	15.87
0.10	3.421	14.89	15.86	0.10	3.489	14.93	15.94